Synthesis and Characterization of Polyimides: Membrane Material for Gas Permeation and Polymer Electrolyte for Fuel Cell

A thesis submitted to the
UNIVERSITY OF PUNE

for the degree of
DOCTOR OF PHILOSOPHY

in

CHEMISTRY

by

Sandeep S. Kothawade

Research Guide
Dr. Ulhas K. Kharul

Polymer Science and Engineering Division
National Chemical Laboratory
Pune 411 008, INDIA

December 2009

Dedicated to

My Family

Their patience, understanding, support and most importantly love has made this possible.

Acknowledgement

I think, I am one of the luckiest and hence thankful to GOD, for being contoured myself in the beautiful and fathomless world of CHEMISTRY, though accidentally. This doctoral work is nothing but my contribution for understanding the myriad intricate in science which may render the living for betterment.

There are so many people, whose support, encouragement and inspiration are very much obligatory to accomplish major achievements in life, especially, if it involves the elements of fulfilling one's cherish dreams. For me, this thesis is such an important destiny and I am indeed indebted to lot of people for their well wishes and blessings for completing this journey.

Among the various people, I would like to take this opportunity first to Dr U. K. Kharul, my research supervisor, whose inspiration, encouragement, and continual guidance and not to forget timely pressurization, has lead me to bring my dream to reality. I owe big gratitude for his guidance and support for some of the past years. Dr. Kharul not only guided me in the scientific problem but also in my personnel life, shaping it for professional as well as personnel matching. Hence I am in debt to him.

I would also like to offer my sincere admiration to Dr. S. P. Vernekar, for all his help, support, suggestion and moral advice during the course of this study. Dr .Vernekar had been my immediate advisor in the initial stages of my research work. Infact, he acted as a window for my entrance in the research. I especially enjoyed his style of mentoring students from which I have benefited tremendously in my personal and professional growth.

I also would like to thank my research co-supervisor Dr. K. Vijaymohanan, whose advice especially in the fuel cell characterization has been valuable during the course of this study.

My thanks are duly acknowledged to CSIR, New Delhi for valuable support in the form of a Senior Research Fellowship.

I wish to place on record my sincere thanks to Dr. S. Sivaram, Director, National Chemical Laboratory for allowing me to carry out my research work at this prestigious Institute. I am grateful to Dr. B. D. Kulkarni, Deputy Director, NCL and Dr. M. G. Kulkarni, Head, PSE Division, for providing the infrastructure and facilities for my research work and allowing me to access the facilities in the division. I am thankful to NMR facility, Elemental Analysis Group, Glass Blowing and Workshop groups for their technical support. I also wish to thank the Library, Administrative and other supporting staff at NCL.

I was really an auspicious student for getting the rare opportunity in the membrane group to interact with all the students working in divergent research areas. I truly enjoyed the valuable discussions with Harshada, Yogesh Chendake, Santosh, Manoj Achalpurkar, Prasad, Sundar, Nazarul, Yogesh Bhole, Pankaj and Anita. I am thankful to Harshada who really put all the possible ways for completing my thesis work, especially in the last stages.

I owe special thanks to Mr. A. S. Patil, who assisted me in an acquirement of experimental skills at my embryonic stage of research career. I am also thankful to Dr. P. P. Wadgoankar, Dr. A. K. Lele, Dr. Guruswamy, Dr. Premanth, Dr. B. B. Idage, Dr. (Mrs.) S. B. Idage, Dr. C. V. Avadhani, Dr. R. P. Singh, Mr. K. G. Raut, Dr.(Mrs.) A. N.

Bote, Dr. S. Shreekumar, Dr. C. V. Rode, Dr. R. S. Khisti, Mr. S. K. Menon, Dr. N. N. Chavan, Dr. S. S. Mahajan, Dr. M. B. Sabne, Dr. S.D. Patil, Dr. Badigar, Dr. (Mrs.) J. P. Jog, Dr. (Mrs.) Garnaik, Mrs. D. A. Dhoble, Dr. B. D. Sarwade, Dr. A. S. Jadhav Dr. B. M. Shinde, Dr. T. P. Mohandas, Dr. P. G. Sukhla, Dr. I. S. Mulla, Dr. C. Ramesh, Mr. Borkar, Mr. Kiran Pandhare and Dr. Saini for their valuable help and cooperation during my research stay in NCL.

Contribution from one of closet friends, Liladhar Bagad and his family can not be forgotten. I feel proud to have friends like Ravi Potrekar, Arvind and Mahesh who motivated at my every stage during this research sojourn. They not only contributed my happiness but also shared sorrows. I can not forget all my lab members Rupesh, Nahire, Alkesh, Ritesh, Manoj Patil, Shubhangi, Mrunal, Soumya, Prerana, Pradnya, Bhavana, Anurag, Kailas and Yogesh with whom I spent nice time and thankful to them for their co-operation. I would like to mention special thanks to Mr. Soraj Singh for his assistance during my work in the membrane group.

I also extend my thank my friends Kannann, Vikas, JP, Wasif, Rakesh, Girish, Hamid, Ravi Sonawane, Ram, Narkhede, Sanjay Desale, Ajit Deore, Prashant Sonar, Mallikarjuna, Vivek, Sony, Arun, Vijay, Pandurang, Anjana, Mukesh, Sunil, Dnyaneshwar, Jadab, Niranjan, Bhaskar, Bhalchandra, Trupti, Harsha, Mahima, Mukta, Vishal, Pinak, Ausutosh and Satish Patil for their support and co-operation.

I find no words to express my feelings for my Father and Mother, whose moral support, love and constant encouragements have helped me to complete this journey. Their patience and sacrifice are always a main source of my inspiration and will remain throughout my life, motivating me to pursue still higher goals. I would like to thanks my Sister, Jijaji, Ashu and little Vedant for their love and prayer. I do not have any word to thank Bapu Mama, Mr. Balasaheb, Shri. Morankar Tatya, Bhushan, Dr. Tushar, Dr. Vivek, Pravin, Nilesh, Nayana, Jeetendra, Mr. Bhamare, sister-in-law, brother-in-law, mother-in-law, father-in-law, Mihir, Abhineet and Shreya for their constant encouragement.

Last, but certainly not least, I would like to acknowledge deep thanks to my wife, Ashwini. She has taken care of every problem, every possible responsibility without a complaint to help me focus on finishing my dissertation. Thank you Ashwini! I am also thankful to my sweet and cute daughter; Anwesha…..! her smiling has really been the catalyst for expediting this doctoral work.

The thesis would be useful, if my efforts are ever to be of any use for the welfare of mankind and the advancement of science.

Finally, I genuflect before the GOD ('Shree Swami Samarth') for giving me an opportunity to have wondered in such a nice world of polymer science.

Sandeep Subhash Kothawade

Certificate of the Guide

Certified that the work incorporated in the thesis entitled "**Synthesis and Characterization of Polyimides: Membrane Material for Gas Permeation and Polymer Electrolyte for Fuel Cell**" submitted by **Sandeep Subhash Kothawade** was carried out under our supervision. Such material as has been obtained from other sources has been duly acknowledged in this thesis.

December, 2009	**Dr. U. K. Kharul**	**Dr. K. Vijayamohanan**
Pune	(Research Guide)	(Research Co-Guide)

Declaration by the Candidate

I declare that the thesis entitled "**Synthesis and Characterization of Polyimides: Membrane Material for Gas Permeation and Polymer Electrolyte for Fuel Cell**" is my own work conducted under the supervision of Dr. U. K. Kharul, at Polymer Science and Engineering Division, National Chemical Laboratory, Pune. I further declare that to the best of my knowledge, this thesis does not contain any part of work, which has been submitted for the award of any degree either of this University or any other University without proper citation.

December 2009 **Research Student**

Pune **(Sandeep S. Kothawade)**

Senior Research Fellow
Polymer Science and Engineering Division
National Chemical Laboratory
Pune – 411 008, India.

Contents

Chapter 2

Monomer synthesis and characterization

Chapter 3

Polyimide synthesis and their characterization

Chapter 4

Structure-gas permeability correlation in polyimides

Chapter 5

Investigation of polyimides towards their applicability as PEM materials

Abstract

The present dissertation constitutes synthesis and characterization of polyimides (PI) having a pendant flexible phenoxy group and their investigations as membrane materials for gas permeation and polymer electrolytes for fuel cell.

Accordingly, monomers (aromatic diamines) were designed in such a fashion that the resultant PIs comprise pendant phenoxy group as a side chain exhibiting improved solubility without sacrificing their thermal properties and became the prime objective of this thesis. Polyimides were prepared from these synthesized aromatic diamines with commercial dianhydrides such as 4,4′-oxydiphthalic dianhydride (ODPA), 4,4′-(hexafluoroisopropylidene)diphthalic anhydride (6FDA), 1,4,5,8-naphthalene tetracarboxylic dianhydride (NTDA), etc. by using single step solution polycondensation and imidization in *meta*-cresol as the solvent.

In ***Chapter 1***, a brief literature survey on synthesis of PIs with an emphasis on polycondensation and applications of PIs are given. Gas permeation in PIs and membrane based gas separation is discussed, followed by theoretical consideration and physical parameters affecting gas permeation. A literature reports on sulfonated PIs with an importance on side-chain-type PIs and other polymers as PEMFC is also discussed. This chapter ends with history and types of fuel cell covering criteria for PEM.

Chapter 2 presents a detailed study on synthesis and characterization of monomers viz., aromatic *meta*-phenylene diamines containing phenoxy group, to be used in the synthesis of polyimides. Diamines were prepared by condensing 1-chloro-2,4-dinitrobenzene with various phenols. In this way, a detailed discussion on synthesis and characterization of dinitro precursors and their corresponding diamines viz., 1-phenoxy-2,4-diamino benzene (PDAB), 2′methyl-1-phenoxy-2,4-diamino benzene (2′MPDAB), 4′-methyl-1-phenoxy-2,4-diamino benzene (4′MPDAB), 2′,6′-dimethyl-1-phenoxy-2,4-diamino benzene (2′,6′DMPDAB), 4’-*t*-butyl-1-phenoxy-2,4-diamino benzene (4′*t*BPDAB) and 4′-sulfonic-1-phenoxy-2,4-diaminobenzene (SPDAB) is given.

Chapter 3 presents a detailed study on synthesis of PIs based on monomers mentioned in Chapter 2, their characterizations by FT-IR, solubility, solution viscosity, thermal properties and WAXD analysis. Preparation and characterization of blend

membranes based on sulfonated polyimide (SPI) with polybenzimidazole is also discussed.

Chapter 4 constitutes investigations towards effects of bulk and site of alkyl substituent on pendant phenoxy group in PIs on their pure gas permeability (using He, H_2, Ar, N_2, O_2, CH_4 and CO_2). Crucial physical properties of these polyimides are correlated with gas permeability. Alkyl substituent on the pendant phenoxy group at *para* position is more effective than at *ortho* substitution for increasing gas permeability in PIs. Structural variation in diamine moiety greatly affects chain packing and gas permeability in ODPA based PIs than that of 6FDA based PIs. SPIs in salt form as well in sulfonic acid form were also evaluated for H_2, O_2 and CO_2 permeation with and without humidifying feed gas. Permeability coefficient for H_2, O_2 and CO_2 were also evaluated for blends membranes.

Chapter 5 describes proton conductivity of SPIs (in imidazolium and triethylammonium sulfonate form as well as in $–SO_3H$ form) and blends of SPI and PBI measured at various temperatures. Physico-chemical properties of SPIs and blend membranes influencing proton conductivity such as water uptake capacity, IEC, hydrolytic stability and oxidative stability were also evaluated. Proton conductivity in humid and anhydrous conditions with varying temperature was also measured. NTDA based SPIs in $–SO_3H$ exhibited higher ion exchange capacity (IECs) and proton conductivity while in salt form hydrolytic and oxidative stability was improved. Detailed investigation on proton conductivity of H_3PO_4 doped blend membranes based on SPI with polybenzimidazole reveals the transportation of proton both by$–SO_3H$ belonging to SPI and H_3PO_4. Detailed analysis done by electrochemical impedance spectroscopy (EIS) of proton conductivity of blends membrane on doping with 12 M H_3PO_4 in anhydrous condition and with 1M H_3PO_4 in humid atmosphere at various temperatures is discussed. While same blend membranes after converting in pure $–SO_3H$ form exhibited comparatively lower proton conductivity as compared with SPIs in 100 % humidification with increase in temperature.

Chapter 6 summarizes the results and describes salient conclusions of the investigations reported in this thesis.

List of Abbreviations

CDNB	1-chloro-2,4-dinitrobenzene
PDNB	1-phenoxy-2,4-dinitrobenzene
PDAB	1-phenoxy-2,4-diaminobenzene
SPDAB	4′-sulfonic-1-phenoxy-2,4-diaminobenzene
2′MPDNB	2′-methyl-1-phenoxy-2,4-dinitro benzene
2′MPDAB	2′methyl-1-phenoxy-2,4-diamino benzene
4′MPDNB	4′-methyl-1-phenoxy-2,4-dinitro benzene
4′MPDAB	4′-methyl-1-phenoxy-2,4-diamino benzene
2′,6′DMPDNB	2′,6′-dimethyl-1-phenoxy-2,4-dinitro benzene
2′,6′DMPDAB	2′,6′-dimethyl-1-phenoxy-2,4-diamino benzene
4′*t*BPDNB	4’-t-butyl-1-phenoxy-2,4-dinitro benzene
4′*t*BPDAB	4’-t-butyl-1-phenoxy-2,4-diamino benzene
ODPA	4,4′-Oxydiphthalic dianhydride
BPDA	3,3′,4,4′-biphenyltetracorboxylic dianhydride
BTDA	3,3′,4,4′-benzophenone tetracarboxylic dianhydride
6FDA	4,4′-(hexafluoroisopropylidene)diphthalic anhydride
PMDA	pyrromellitic dianhydride
NTDA	1,4,5,8-naphthalene tetracarboxylic dianhydride
ODA	4,4′-oxydianiline
DAB	3,3′-diaminobenzedine
IPA	isophthalic acid
BuI	5-*tert*-butyl isophthalic acid
TEA	Triethyl amine
Im	Imidazole
$TEAH^+$	Triethylammonium cation
ImH^+	Imidazolium cation
PI	Polyimide
SPI	Sulfonated polyimide
CPI	Copolyimide
PBI	Polybenzimidazole
PDAB-ODPA	PI based on diamine ‘PDAB’ and dianhydride ‘ODPA’
PDAB-6FDA	PI based on diamine ‘PDAB’ and dianhydride ‘6FDA’
PDAB-BPDA	PI based on diamine ‘PDAB’ and dianhydride ‘BPDA’
PDAB-BTDA	PI based on diamine ‘PDAB’ and dianhydride ‘BTDA’
PDAB-PMDA	PI based on diamine ‘PDAB’ and dianhydride ‘PMDA’
ODA-ODPA	PI based on diamine ‘ODA’ and dianhydride ‘ODPA’
CPI-0595	CPI based on 5 mole% PDAB, 95 mole% ODA with ODPA
CPI-2575	CPI based on 25 mole% PDAB, 75 mole% ODA with ODPA
CPI-5050	CPI based on 50 mole% PDAB, 50 mole% ODA with ODPA
SPDAB•TA-N	SPI based on SPDAB and NTDA in triethylammonium sulfonate salt form

SPDAB•Im-N	SPI based on SPDAB and NTDA in imidazolium sulfonate salt form
$SPDAB_I$-N	SPI based on SPDAB and NTDA in $–SO_3H$ form obtained from SPDAB•TA-N
$SPDAB_{II}$-N	SPI based on SPDAB and NTDA in $–SO_3H$ form obtained from SPDAB•Im-N
SPDAB•TA-O	SPI based on SPDAB and ODPA in triethylammonium sulfonate salt form
SPDAB-O	SPI based on SPDAB and ODPA $–SO_3H$ form obtained from SPDAB•TA-O
PBI-I	Polybenzimidazole based on DAB and IPA
PBI-BuI	Polybenzimidazole based on DAB and BuI
SPI(*TEA*)/PBI-BuI*(a/b)*	Blends with "a" wt% of SPDAB•TA-N and "b" wt% of PBI-BuI, where '*TEA*' denotes SPI in triethylammonium sulfonate salt form
SPI(*H*)/PBI-BuI*(a/b)*	Blends with "a" wt% of SPDAB•TA-N and "b" wt% of PBI-BuI, where '*H*' represents proton form of SPI
SPI(*PA*)/PBI-BuI*(a/b)*	Blends with "a" wt% of SPDAB•TA-N and "b" wt% of PBI-BuI, where '*PA*' denotes acid doping with H_3PO_4
SPI(*SA*)/PBI-BuI*(a/b)*	Blends with "a" wt% of SPDAB•TA-N and "b" wt% of PBI-BuI, where '*SA*' denotes acid doping with H_2SO_4
4′MPDAB-ODPA	PI based on diamine '4′MPDAB' and dianhydride 'ODPA'
4′MPDAB-6FDA	PI based on diamine '4′MPDAB' and dianhydride '6FDA'
2′MPDAB-ODPA	PI based on diamine '2′MPDAB' and dianhydride 'ODPA'
2′MPDAB-6FDA	PI based on diamine '2′MPDAB' and dianhydride '6FDA'
2′,6′DMPDAB-ODPA	PI based on diamine '2′,6′DMPDAB' and dianhydride 'ODPA'
2′,6′DMPDAB - 6FDA	PI based on diamine '2′,6′DMPDAB' and dianhydride '6FDA'
4′*t*BPDAB-ODPA	PI based on diamine '4′*t*BPDAB' and dianhydride 'ODPA'
4′*t*BPDAB-6FDA	PI based on diamine '4′*t*BPDAB' and dianhydride '6FDA'
MEA	Membrane Electrode Assembly
PEMFC	Polymer Electrolyte Membrane Fuel Cell
DSC	Differential Scanning Calorimetry
TGA	Thermo Gravimetric Analysis
IEC	Ion Exchange Capacity
IDT	Initial Decomposition Temperature
SD	Degree of Sulfonation
CTC	Charge transfer complex
WAXD	Wide angle X-ray diffraction

List of Tables

List of Schemes

List of Figures

Chapter 1

Introduction and literature survey

1.1 Polyimides

Polyimides (PIs) are the condensation polymers derived mainly from organic diamines or their derivatives and dianhydrides. They possess heterocyclic five or six membered imide linkage in their chain repeat unit (Figure 1.1).

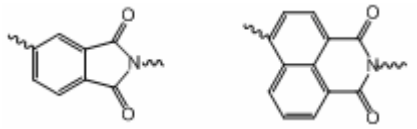

Figure 1.1 General structures of aromatic polyimides

The importance of six membered-imide linkage came in the picture due its relative high chemical stability in acidic environment as compared to five membered analogues in the emerging advanced technology such as polymer electrolyte membrane fuel cells (PEMFC) (Genies, 2001a; Yin, 2006a). The excellence of aromatic PIs as gas separation materials can be credited to their physical properties (Kim, 1988; Stern, 1989; Sroog, 1991; Robeson, 2008). Considerable research has been accelerated towards aromatic PIs for their use in pioneering fields such as aerospace, liquid crystal displays, automotive components, microelectronics, gas separation membrane materials, PEMFC, etc. (Takekoshi 1990; Sroog, 1991; de Abajo, 1999; Ding, 2007; Marestin, 2008).

The present chapter briefly describes history of polyimides, their synthetic routes, physical characterizations, applications and scope of aromatic polyimides as membrane material in gas permeation and PEMFC. Since the invention of aromatic PI was laid on the five-membered imide ring, these PIs will be discussed in the beginning, followed by PIs with six-membered ring.

1.2 A brief history of polyimides

Retrospection in PIs informs their first synthesis in 1908 by Bogert and Renshaw (1908). In their invention, they observed elimination of water instead of melting upon heating the relatively stable organic compound, 4-aminophthalic anhydride and

concluded the formation of "polymolecular imide". The development of modern polyimides can be linked to the outcome of use of the polycarboxylic acids prepared from oxidation of a major petroleum component, polymethyl benzenes. At the embryonic stage of polyimides, aliphatic diamines in salt form were prepared specially for making Nylons (polyamides). Aliphatic diamines were condensed with polycarboxylic acids such as tetracarboxylic aromatic acid or their derivatives; typically pyrromellitic dianhydride (PMDA) (Edward, 1959a and 1959b). The obtained aliphatic-aromatic polyimides could only be melt-processed if aliphatic diamines used had either linear long-chain or relatively shorter branched chain. Later on, implementation of less basic aromatic diamines following two stage synthesis through intermediate poly(amic acid) formation drove the development in polyimides. Commercial polyimides such as Pyralin and Kapton H followed these routes. With the advancement in aromatic PIs, it was further observed that such a fully aromatic system constituted CTC because of the interaction between electron withdrawing cyclic imide rings and electron donating π-cloud of phenyl rings. Such interactions make them densely packed and hence intractable (Chen, 2008; Zhang, 2007). However, excellent mechanical properties, outstanding oxidative stability, extraordinary non-flammability and good electrical properties have made them more useful in advanced technologies (Ghosh, 1996; Li, 2007a) and they emerged as high performance polymers.

1.3 Synthesis of polyimides

Various synthetic methods such as polycondensation via ester derivatives of poly(amic acids), polycondensation of dianhydrides and diisocynates, transition metal catalyzed polycondensation of diamines and polymerization of cycloaddition reaction to prepare polyimides have been explored (Mathew, 2001; Shingte, 2006). Most widely used polycondensation methods are briefly discussed below.

1.3.1 Polycondensation of a diamine and a dianhydride

This is one of the most widely adopted methods for the synthesis of polyimides (Sroog, 1991; Volksen, 1994). It can be carried out in two ways, viz., two-step method via poly(amic acid) intermediate and one-step or one pot method.

1.3.1.1 Two-step method via poly(amic acid) intermediate

A successful route to the synthesis of high molecular weight polyimide was first described by Endrey *et. al.* in 1962 and successively by Du Pont patents (Mathew, 2001; Shingte, 2006). In this method, the synthesis was conducted in two stages in a suitable solvent. First, a soluble poly(amic acid) was prepared; which was then converted to the desired polyimide by imidization as exemplified in Figure 1.2.

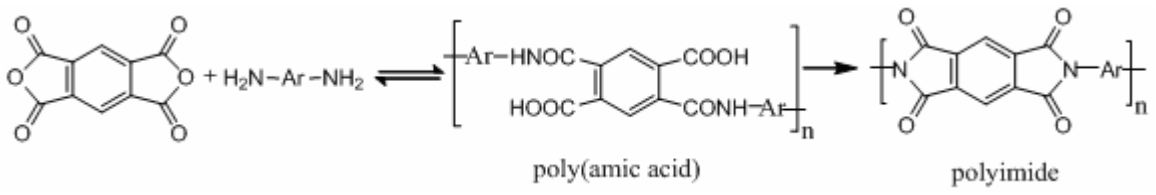

Figure 1.2 Two step synthesis of polyimides

Various factors such as structure of monomers, type of solvent, imidization method, etc. play an important role in the formation of high molecular weight polyimide as described below.

1.3.1.1.a Role of monomers

Poly(amic acid) (PAA) is formed by reversible nucleophilic substitution reaction. Herein, nucleophilic attack of a diamine takes place at one of the carbonyl carbons of an anhydride moiety followed by its opening to carboxylate functionality. This is followed by intra-proton abstraction (-NH_2-) from the attacked diamine leading to the formation of amic acid in the first stage. This reaction is an equilibrium reaction, favored by the high concentration of monomers, reactivity of each monomeric unit, basicity of the solvent and low to moderate temperature (Cassidey, 1982). In general, diamine is dissolved in a solvent at the beginning of polymerization, followed by solid dianhydride addition to the solution of diamine (Dine-Hart, 1967; Johnson, 1972; Kumar, 1981). Since poly(amic acid) formation is a nucleophilic substitution reaction, consequently the major boosters for such a reaction are high nucleophilicity of the amino nitrogen atom of diamine and greater electrophilicity of the carbonyl groups belonging to dianhydride. In other words,

more basic character of the diamine and the enhanced electronic affinity (*EA*) in dianhydride result in a higher reaction rate.

The Lewis acid-base concept can also be well correlated in poly(amic acid) formation. Diamine acts as a Lewis base and dianhydride as a Lewis acid. Consequently, the larger electron pair donation ability of amino group in diamine which is associated with pK_a and the more acceptance nature of the carbonyl group in dianhydride correlating with *EA* should favor higher forward reaction rate of poly(amic acid) formation (Zubkov, 1981). This phenomenon can be exemplified with comparative reactivity of PMDA, BPDA, ODPA and BTDA (Koton, 1984; Cornelius, 2000). Higher *EA* value in BTDA is attributed to the bridged electron withdrawing carbonyl carbon, while the lower *EA* value in ODPA is due to the bridged electron donating ether linkage. BPDA with absence of such bridged functionality demonstrates *EA* between BTDA and ODPA. In addition, placement of such functionality with respective to carbonyl becomes more effective as *para>ortho>meta* (Pine, 1987; Cornelius, 2000). In diamines, similar correlation between pK_a with their reactivity is found (Zubkov, 1981; Cornelius, 2000). Higher values of pK_a show enhanced reactivity, since basicity of these diamines gets increased. Embodiment of electron donating functionality in diamines increases their nucleophilic nature. Such diamines therefore show higher basicity with increased pK_a values executing rapid polymerization for the same period of polymerization as compared with diamines with lower basicity and pK_a values.

Molecular weight of poly(amic acid) is affected by the sequence of monomer addition. This is due to the solubility difference of monomers in polymerization solvent. In general, complete dissolution of diamine is followed by dianhydride addition. Diamine can be rapidly dissolved in the solvent at room temperature, while dianhydride consumes more time for dissolution in diamine solution. This sequential procedure confers high molecular weight of poly(amic acid). Orwoll *et. al.* (1981) attributed this phenomenon to the interfacial condensation of crystalline dianhydride and diamine.

1.3.1.1.b Role of solvent

More polar as well as basic solvents enhance the rate of poly(amic acid) formation (Vygodskii, 1977). Most of the polar aprotic solvents with basic nature such as

DMF, DMAc, NMP etc. are utilized for preparation of poly(amic acid). Such types of solvents have ability to effectively interact as well as solvate the propagating poly(amic acid). In addition, the heat evolved during such acid-base interactions drives the reaction in forward direction. In order to achieve high molecular weight for poly(amic acid), removal of water from the starting monomers as well as reaction medium becomes important. Presence of water in the solvent affects reaction kinetics of poly(amic acid) formation as it can hydrolyze poly(amic acid) (Bower, 1963; Sroog, 1965).

Probability of hydrogen bonding of hydroxyl group belonging to –COOH with neighboring chain of poly(amic acid) leads to increased viscosity of poly(amic acid) solution (Bryant, 2006). As a result, nucleophilic attack of diamine also becomes prominent on the carbonyl carbon of anhydride moiety due to hydrogen bonding with carbonyl oxygen leading to its enhanced electrophilicity. This phenomenon can be considered as autocatalytic type of behavior (Kaas, 1981). However, autocatalysis is not observed in polar aprotic basic solvents (DMF, DMAc) (Kuzenetsove, 2000; Bryant, 2006). This can be attributed to the better solvation and association with acidic carboxyl group of propagating poly(amic acid) by these basic solvents, thus isolating them from interaction with anhydride as well as amic acids (Kuzenetsove, 2000; Bryant, 2006; Hasanain, 2008). Hence benzoic acid is added in such amide type basic solvents in order to enhance the rate of poly(amic acid) formation. Poly(amic acid) can also be prepared in polar protic solvents like *m*-cresol (Mathew, 2001). This enhances the rate of nucleophilic substitution reaction in amide formation. Carbonyl groups of an anhydride become highly electrophilic after their protonation, as a result nucleophilic attack of diamine becomes feasible. High molecular weight polyimide has been synthesized in acidic solvents such as salicylic acid (Hasanain, 2008) and melt of benzoic acid (Kuzenetsove, 2000).

1.3.1.1.c. Transformation of poly(amic acid) to polyimide

Properties of polyimides depend on an extent of imidization of intermediate poly(amic acid) (PAA). Presence of amic acid in PI significantly affects thermal, hydrolytic stability and other properties. Imidization is achieved by cyclodehydration of amic acid, which is accomplished by two methods as described below.

(i) Chemical imidization of poly(amic acid)

Chemical imidization is carried out by external dehydrating agents. Type of solvent, temperature, concentration of amic acid, ratio of dehydrating agent (usually acetic anhydride) to the catalyst organic base, catalyst structure and its base strength influence the chemical imidization process (Endrey, 1965a and 1965b; Kailani, 1998a; Kailani, 1998b). Since the reagent used for dehydration lowers the activation energy for ring closure, transforming poly(amic acid) to polyimide becomes feasible at relatively lower temperature. A combination of external dehydrating agents and a catalyst in dipolar aprotic solvents are also used (Endrey, 1965a). Dehydrating reagents such as acetic anhydride or anhydrides of other acids and the catalysts such as tertiary amines, viz; triethylamine (TEA), pyridine etc. are chosen (Kailani, 1998a; Kailani, 1998b). The advantage of chemical imidization over thermal imidization is that former reveals faster conversion to polyimides. However, in chemical imidization process, imide formation is accompanied by isoimide formation. The presence of water in the solvent also affects the kinetics of imidization (Kailani, 1998a). The chemical structure as well as base strength of the catalyst also plays the dominant role in chemical imidization process. Imidization kinetics is well investigated by various researchers (Dickinson, 1992; Kailani, 1992; 1998a; 1998b; Kim, 1993; Yu, 1997)

(ii) Thermal Imidization of poly(amic acid)

In this process, imidization is accomplished by gradual heating of poly(amic acid) in the solid state to 250-350 °C (Volksen, 1994; Mathew, 2001; Shingate, 2006). In thermal imidization, removal of the condensate produced during cyclodehydration becomes an indispensable step. The simultaneous water removal, which is a byproduct, moves imidization in the forward direction. In the solid state, cyclodehydration of poly(amic acid) is difficult. Hence, high viscous solution of poly(amic acid) is also utilized, as residual solvent plays the significant role. It is said that use of dipolar aprotic solvents speeds up cyclization since they can efficiently solvate poly(amic acid) chains as well as offer favorable conformation of the orthoamic acid to cyclize (Kreuz, 1966; Bryant, 2006). In addition, being weak Lewis bases, they are able to accept protons during cyclization. It is reported that various factors such as film thickness, molecular

mobility, amount of residual solvent, physical state of the poly(amic acid), conformations of each macromolecule, degree of imidization, degradation of poly(amic acid) chains, and curing reaction of intermolecular imide link formation at higher temperature (350 °C) significantly affect the kinetics, in particular for solid phase imidization (Kim, 1993). Use of various aromatic acids is known to accelerate the imidization in solid state (Lavrov, 1977 and 1980).

1.3.1.2 One-step or one pot method

In this process, polymerization is typically carried out in high boiling solvent such as *m*-cresol, *p*-chlorophenol, nitrobenzene, benzonitrile etc.; as well as dipolar aprotic amide solvents or a mixture of these at 180 °C, where imidization proceeds rapidly (Dotcheva, 1994; Mathew, 2001; Bryant, 2006). Those polyimides which are not likely to precipitate out in high boiling polymerizing solvent at higher temperature can only be synthesized by this method. Solvents like toluene, *o*-dichlorobenzene are typically used to eliminate the water formed azeotropically. One of the advantages on following this one step method is that amic acid and isoimide are not present in the formed polymer. Thus, polyimides formed by this method possess different physical properties than that of formed by conventional two-step process. Obstruction in direct processing of polyimides into final end application (films and coatings) due to lower polymerization concentration as well as use of carcinogen solvents and requirement of long polymerization time (> 18 h) are some of the drawbacks of this technique (Hasanain, 2008).

The most favorable solvent used for this high temperature solution polymerization is *m*-cresol, indicating favorable imidization catalysis in acidic media. Kuznetsov *et. al.* (2000) and Hasanain *et. al.* (2008) prepared polyimides by this method in acidic solvents viz; melt of benzoic acid and salicylic acid. Built up of high molecular weight polymer within a short period of time (1-2 h) was demonstrated.

1.4 Properties and applications of polyimides

Polyimides usually have high mechanical properties, excellent thermal stability, high chemical resistance, high T_g and good oxidative stability. These polymers also have film forming properties and low dielectric constant. Owing to these properties, they find

wide applications in different fields such as aerospace, liquid crystal displays (LCD), automotives, gas separation membranes, dielectric, microelectronics, etc. Since the introduction of first commercial polyimides (Kapton) by Du Pont in 1960 (Sroog, 1991; de Abajo, 1999), polyimides have been explored in innumerable fields (Mittal, 2001). Kapton was especially made as the heat resistant polymer for applications in space and military requirements. In microelectronics, a major demand for insulating materials with lower dielectric constants relative to the silicon dioxide (ε = 3.9–4.2) are needed and polyimides containing, in particular, perfluoroalkyl groups are the best suited for this application (de Abajo, 1999). Fluorinated PI in the fully imidized state have also proved better performance in the field of optical waveguides. The presence of fluorine containing linkage such as hexafluoroisopropylidene, in the main chain not only increases the solubility and T_g, but also decreases the chain packing and charge transfer complexes. This is favorable for many applications. The low thermal expansion coefficient, good adhesion property, high modulus and tough ductile mechanical properties of polyimides are also the other driving forces for their implementation as insulators in microelectronics (Hedrick, 1999a and 1999b).

Polyimides possess excellent adhesion to a number of substrates including metals, enabling their composites build-up feasible. Such composites can further raise the mechanical properties to a superior level, which includes high flexural modulus and compressive strength, outstanding dimensional stability under loads, aerodynamic properties, low fatigue, corrosion resistance making useful in the engineering field like aerospace. Polyimides are also used as biomaterials for cardiovascular medical applications (Wang, 2007a). NASA developed the thermoset polyimide PMR-15 for the specific application as a matrix resin for graphite fiber resin composite in the aerospace industry. Later on Ciba-Geigy also developed another type of thermoset PI having end capped allylnorbornenedicarboxyl anhydride (Takekoshi, 1990). Fire retardancy in polyimides can be improved by incorporation of phosphorous containing organic compounds (Lee, 1995). They showed improvement in solubility of these PIs and adhesive strength to titanium. PI coating having excellent heat as well as chemical resistance is of specially interest in electronic devices as the stress buffer of semiconductor and interlayer dielectrics. Fabrication of PI in thin film form has

successfully been applied in organic electroluminescent diode (OLED) as emissive layer and hole transporting layer.

Deposition of metals like Co(II), Pd, Pt, Ag, Au, etc. in the poly(amic acid) stage followed by thermal curing leads to surface conductive polyimide films (Rancourt, 1987; Bergemeister, 1990; Biswas, 1994). PIs have also been used as substrate material of electrode panels in the crystallization of protein under an electric field (Al-Haq, 2007).

Another important application of PI is for separation of gases. PIs with wide structural variations have been studied as membrane material for gas separation. In consistent with present trend, the present thesis also describes synthesis and application of alkyl substituted PIs as membrane material for gas separation. In this context, a brief overview on gas separation is given below.

1.5 Gas Permeation in polyimides

The beauty of aromatic polyimides as membrane material for gas permeation lies in the rigidity of the imide ring, their high mechanical and thermal properties (Koros, 1988; de Abajo, 1999). Several reports are available on structure-gas permeation relation of polyimide, conveying effects of monomer structure modification on gas permeability of resulting PIs (Hirayama, 1996a; Koros 1988; Langsam, 1993; Stern, 1989, 1990 and 1993; Tsujita, 2003; Ding, 2007).

Polyimides exhibit charge transfer complex (CTC) formation (Matsumoto, 1993b) resulting in poor processability and lower gas permeation properties. Hence various efforts on structural modification in PIs leading to improved processability as well as gas permeability have been reported (Stern, 1989; Tanaka, 1992a; Shao, 2005; Xiao, 2007; Qiu, 2006). These include structural variations in the diamine or dianhydride molecule leading to reduced molecular order and torsional mobility (Kim, 1988; Tanaka, 1992b; Matsumoto, 1993a and 1993b). Incorporation of $-C(CF_3)_2-$ linkage in a polyimide is one of the ways to improve solubility of PI in common organic solvents with increase in permeability and appreciable permselectivity. The $-C(CF_3)_2-$ linkage inhibits rotation of the neighbouring phenyl ring leading to increased rigidity of polymer chain, thus enhancing the permselectivity (Chung, 2001). Presence of this linkage in a dianhydride

moiety was shown to be more effective towards governing permeation properties than in the diamine (Matsumoto, 1993b).

To develop a better gas separation material, various approaches comprise designing of proper chemical structure of monomers, facile modifications of either monomers or polymers, embodiment of bulky substituents on the precursor monomers, making *meta*-linked PIs than *para*-linked, lowering of interchain interactions, enhancing rigidity of the PIs, etc. Among these, one of the widely followed efforts is incorporation of voluminous substituent on phenyl rings of PIs. Such substituent if located at *ortho* to an imide linkage not only reduces the interchain interactions by increasing free volume but it also increases T_g and hence chain stiffness by restricting rotation around C-N bond of phenyl and imide rings (Takekoshi, 1990; Tanaka, 1992b; Hsiao, 1998a and 1998b; Liu, 1999; Mittal, 2001; Qiu, 2006). Thus, enhancement in both, permeability due to bulky substituent and permselectivity due to increased stiffness can be accomplished. Structure-property correlations in gas permeation suggests that polymers exhibiting high gas permeability tend to lower the permselectivity or vice versa (Robeson, 2008). Architecture of polymers leading to increased inter-segmental distance with decreased intra-segmental mobility should offer both, high permeability and selectivity. PIs having -$C(CF_3)_2$- linkage in their backbone are typical examples of such behavior (Matsumoto, 1993b; Chung, 2001). Being bulkier, -$C(CF_3)_2$- reduces the interchain interactions with increased free volume and thus cerates spaces for gas diffusion conferring high permeation (Kim, 1988; Tanaka, 1992a; Matsumoto, 1993b). 6FDA based PIs can therefore reveal higher permselectivity and comparable permeability with other polymers, deviating the general trade-off relationship between permeability and permselectivity (Lin, 2000; Liu, 2001). Furthermore, it has been reported that *meta*-isomers of PIs lead to decrease in permeability and an increase in permselectivity as compared with their *para*-isomer analogues due to the difference in the intrasegmental mobility (Stern, 1989; Coleman, 1990; Mi, 1993). This also confers more bent structure in main chain of *meta*-isomers of PIs (Ding, 2007).

Side chain substitution could also be one of the methods for polyimide structural architecture towards enhancement of gas permeation in polyimides. However, embodiment of bulky groups by flexible linkages like C-O-C can be advantageous than

that of by C-C since the former offers more sub-group mobility. In addition, depending on such sub-group mobility, permeability coefficient of gases can be varied. Qiu *et. al.* (2007) prepared PIs by modifying the dianhydride BPDA with substitution of various pendant flexible phenoxy groups and reported increase in permeability than that of PIs based on unsubstituted BPDA. Authors also revealed improvements in gas-separation performance as evidenced by their permeability values lie closer to the Robeson's 1991 upper bound limit (Robeson, 1991).

1.5.1 Application of membrane based gas separation

Application of membranes encompasses separation of H_2 from CO, CH_4 and N_2, acid gas separation from natural gas, gas dehydration, removal of volatile organic compounds (VOC) from air, O_2 or N_2 enrichment of air, etc. Because of simplicity and low capital investment, membrane system competes with adsorptive and cryogenic separations. Monsanto established the first commercial application based on membrane gas separation by separating H_2 from N_2 in ammonia pure gas streams (Baker, 2004; Koros, 2000). Recovery of H_2 gas from waste gases produced at various refinery operations finds major application for hydrogen-selective membrane (Bollinger, 1982). Palladium alloy membrane demonstrated above 99.9% purity of H_2 (McBride, 1965). Today, various polymeric membranes such as polyimides (Ube, Praxair), polyaramide (Medal) or brominated polysulfone (Permea) are used for hydrogen membrane gas separation. Gas separation is well acknowledged in the separation of air into its component, i.e. O_2 or N_2 enrichment. Oxygen separation membranes with a separation factor of 4-6 and oxygen permeability around 250 Barrers is desired for effective commercialization (Koros, 2000). Air containing 30-40% O_2 is useful in enhanced combustion and biochemical processes, while for medical purposes, O_2 enrichment is valuable. Purified N_2 above 90% facilitates inert atmosphere, being useful in blanketing fuel storage tanks and pipelines for diminishing fire hazards. In order to avoid spoilage of food during transport and storage, N_2-enriched air is used. In the recent times, green house effect has built up the tremendous pressure over membrane technologist for separation of CO_2 from effluent streams. Membrane based gas separation is competitive over conventional technologies for CO_2 capture (Scholes, 2008). For the specific

application of CO_2 capture from the flue gas, a CO_2/N_2 selectivity of >70 and a minimum CO_2 permeability of 100 Barrers (a permeance of 1000 GPU) are required for the economic operation (Hirayama, 1999). In the future, market would eventually expand with an economical opportunity for the membrane community.

The following Figure 1.3 represents major breakthroughs in gas separation technology from the year 1850 to 2000.

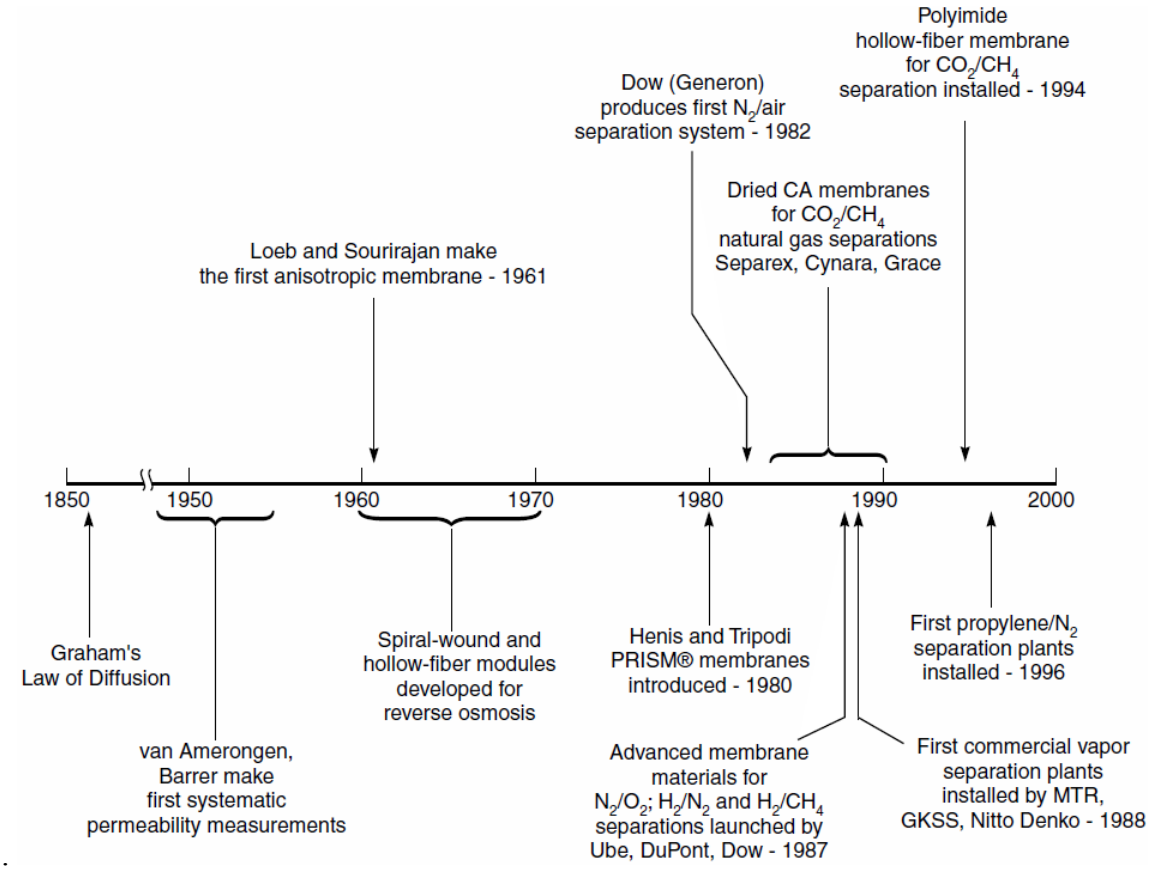

Figure 1.3 Major breakthroughs in membrane based gas separation technology (1850-2000) (Baker, 2000)

1.5.2 Theoretical consideration

Gas permeation in polymeric membranes can take place based on one of the three general transport mechanisms (Koros, 1993): Knudsen-diffusion, molecular sieving or solution-diffusion, which can be schematically represented as shown in Figure 1.4.

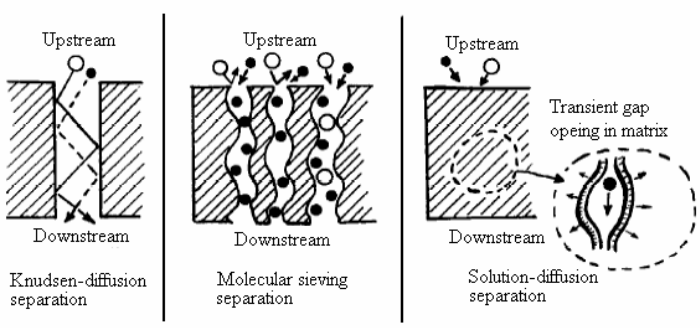

Figure 1.4 Representation of gas permeation mechanisms in polymeric membranes (Koros, 1993)

When gaseous mixture is allowed to diffuse through a porous membrane into a region of lower pressure, lower molecular weight components are permeated preferentially, as they diffuse more rapidly. When the pore size is much smaller than the mean free path of gas molecules, the gases diffuse independently by Knudsen diffusion. The diffusivity is proportional to the pore size of membrane and average molecular velocity of gas molecules, which varies inversely with the square root of the molecular weight. Kundsen diffusion of gas in cylindrical pores is (Gilron, 2002) given by;

$$D_K = \frac{d_p}{3}\sqrt{\frac{8RT}{\pi M}}$$

where, d_p is nominal pore diameter, R is universal gas constant, T is absolute temperature and is D_K is gas diffusivity. For standard gas separation applications, though membranes following Kundsen diffusion are not commercially attractive due to low selectivities, some specialty applications are known, e.g. membrane reactors (Koros, 1993).

The molecular sieving separation mechanism is based primarily on much higher diffusion rates of the smallest molecules. Diffusion coefficient for this mechanism can be expressed as (Gilron, 2002):

$$D_{MS} = D_{MS}^{0} \exp\left(\frac{-E_{a,MS}}{RT}\right)$$

where, D_{MS}^{0} is pre-exponential factor and $E_{a,MS}$ is an energy of activation for molecular sieving. The sorption level difference may be important for similarly sized penetrants like O_2 and N_2. The membranes are based on either ultramicroporous carbon or glass hollow fiber membranes. This mechanism received attention since higher productivities and

selectivities than solution-diffusion membranes are known (Koros, 1993). Some of these membranes are commercialized for producing enriched hydrogen streams at high pressure from mixed hydrocarbon (Acharya, 2000). Fragility and fouling by condensable gas has made this mode of separation unacceptable for commercialization.

The more common model used to explain and predict gas permeation through *non-porous* polymers is the solution-diffusion model. It is based on both solubility and diffusivity (mobility) of gases into the membrane matrix. The diffusivity selectivity favors the smallest molecule, while solubility selectivity favors the most condensable molecule. It states that permeability coefficient P is the product of diffusivity coefficient D (a kinetic term) and solubility coefficient S (a thermodynamic term).

$$P = DS$$

If the permeability of gas pairs; P_A and P_B is known then the selectivity of a polymer to gas A relative to another gas B can be expressed in terms of an ideal selectivity, α_{AB}, defined by the relation,

$$\alpha_{AB} = P_A / P_B = D_A / D_B \bullet S_A / S_B$$

The ratio D_A/D_B is termed as mobility selectivity, which is favored for smallest molecule; while the ratio S_A/S_B is solubility selectivity and is favored for molecules having high condensability. Selectivity in rubbery polymers is generally favored by solubility selectivity, while in case of glassy polymers; diffusivity selectivity dominates to determine overall selectivity. Both, rubbery and glassy polymer can be effectively utilized in gas separation applications. High solubility of acidic gases such as CO_2 and H_2S at low partial pressure as compared with CH_4 with low diffusivity and solubility entails use of rubbery polymers offering a good selectivity of former gases over CH_4 (Chatterjee, 1997). On the other hand, diffusive selectivity is favored by glassy polymers. For example, diffusive selectivity of N_2 over pentane of 100 000 is favored in poly(vinyl chloride) (Baker, 2000).

Gas solubility (S) mainly depends upon penetrant condensability, polymer-penetrant interactions and polymer morphology (i.e. crystallinity, orientation, fractional free volume, etc.). Gas diffusivity depends on the ability of a gas molecule to undergo diffusive jumps, which occur when thermally driven, random, cooperative polymer segmental dynamics form transient gaps, those are large enough to accommodate

penetrant, in the immediate vicinity of the gas molecule (Ghosal, 1994). Thus, diffusion coefficient D decreases with increases in size of the penetrant. In addition, it also depends on flexibility of the polymer backbone, available free volume, etc. Mobility selectivity for a given gas pair increases as the polymer matrix becomes more and more rigid. The mobility selectivity is dominant for most glassy polymers. Hence, the transport of smaller molecules is favored. On the other hand, solubility of gases generally increases with molecular size, because the intermolecular forces between the gas and the polymer increase. Most rubbers show low mobility selectivity due to their flexible polymer chains, but their ability to separate gases is dominated by their solubility selectivity (Nunes, 2001).

Usually, polymers with high permeability tend to have low selectivity and vice versa (trade-off relationship). To make membrane-based separations more competitive, membrane material design which would have both, high permeability and high permselectivity is envisaged. Variation in chemical structure of the polymer allows control over its permeation properties. In view of this, it becomes essential to address physical properties of polymers as well as of penetrants affecting the permeation behavior.

1.5.3 Physical parameters affecting gas permeation

i) Chain packing density

The *d*-spacing (average intersegmental distance) and fractional free volume (V_f or FFV) reveals the chain packing density in polymers. Larger *d*-spacing as well as FFV indicates more openness structure of the polymer matrix. Free volume (V_f) is simply the volume of the polymer mass not occupied by the molecules themselves. In other words, it is the fraction of the total polymer specific volume that is not occupied by polymer molecules. It can be calculated as follows

$$V_f = V - V_o$$

where, V is the polymer specific volume and V_o is the occupied volume by the polymer chains at 0° K. V_o can be calculated from the relation $V_o = 1.3\ V_w$, where V_w is Van der Waals volume and is calculated by group contribution method (Van Krevelen, 1997).

ii) Chain and subgroup mobility

Structural alterations which inhibit chain packing while simultaneously inhibiting rotational motion about flexible linkages on polymer backbone tend to increase permeability while maintaining or increasing selectivity (Coleman, 1990). Inhibition of the segmental and sub-segmental mobility can be judged by glass transition (T_g) or sub-T_g temperatures. Typical methods to characterize torsional mobility include dynamic mechanical relaxation spectroscopy, differential scanning calorimetry, dipole relaxation spectroscopy and nuclear magnetic resonance (Ghosal, 1994).

iii) Polarity

Since polarity leads to net forces of attraction between macromolecules, d_{sp} and V_f in polar polymers tend to be smaller. Gases such as CO_2, which has a quadrupole moment, are in general, more soluble in polar polymers (Hirayama, 1999). Presence of polar groups like bromo, chloro, nitro, sulfonic/carboxylic acid group and their salts, etc. generally lead to a decrease in permeability and increase in selectivity. This was observed for various types of polymers such as poly(phenylene oxide) (Bhole, 2005), polysulfone (Ghosal, 1992), polyarylate (Murugandam, 1987; Houde, 1995, Bhole, 2007 etc.)

iv) Crystallinity

Crystalline regions in polymers typically preclude penetrant solubility (Ghosal, 1994) and thus are impermeable regions. They act to increase the tortuosity of the path followed by penetrant molecules through a polymer. They may also restrict segmental mobility in the non-crystalline regions of the polymer. Both effects tend to reduce gas diffusivity. Thus, crystallinity in gas permeation membrane materials is generally undesirable.

v) Crosslinking

Diffusion coefficients typically decrease with increasing crosslink density, since crosslinking reduces polymer segmental mobility (Crank, 1956) as demonstrated in case of vulcanization of natural rubber (Barrer, 1948). On the other hand, crosslinking can be taken into benefit for reducing plasticization effects by gases like CO_2 (Wind, 2003).

vi) Molecular Weight

In low molecular weight polymers, a large contribution to segmental mobility comes from chain ends, which are less constrained by chain connectivity requirements and are therefore more mobile (Freeman, 1990). As polymer molecular weight increases, concentration of chain ends decreases and, in turn, the polymer free volume decreases. As a result, penetrant diffusivity decreases with increasing molecular weight.

vii) Penetrant condensability

Gas permeability increases due to the increased condensability of the gas. Gas critical temperature (T_c), normal boiling point (T_b), or Lennard-Jones force constant (ε/κ) are all measures of condensability that correlate well with the solubility coefficients in a polymer. For example, in most polymers, CO_2 (T_c= 31°C) is more soluble than CH_4 (T_c= -82.1°C), O_2 (T_c= -118.4°C) or N_2 (T_c= -147°C) (Bird, 2002).

viii) Penetrant size and shape

In general, a diffusion coefficient decreases with increasing penetrant size and is also sensitive to penetrant shape. The diffusivity of linear penetrant molecules such as CO_2 is higher than the diffusivities of spherical molecules of equivalent molecular volume. The sorption coefficient also increases with molecular diameter, because large molecules are normally more condensable than smaller ones. Hence permeability increases for the penetrants with high diffusion and sorption coefficient.

ix) Penetrant – polymer interactions

Gas solubility is sensitive to specific interactions between gas and polymer molecules. Gases such as CO_2 has a quadrupole moment and more soluble in polar polymers. The interaction energy Γ, between a quadrupole and a dipole is given by (Ghosal, 1994),

$$\Gamma = \frac{\mu^2 Q^2}{r^8 \kappa T}$$

where, μ is the dipole moment, Q is the quadrupole moment, r is the distance between the dipolar and quadrupolar moieties, κ is Boltzmann's constant and T is the absolute temperature. The strength of interaction between a quadrupole and a dipole increases rapidly as the dipole or quadrupole moment increases or as the separation between the quadrupole and dipole decreases.

x) Temperature

The temperature dependence of the permeation coefficient can be expressed as,

$$P = P_o \exp(-E_P/RT)$$

where P_o is preexponential constant (equal to S_oD_o) and E_p is the activation energy of permeation, which is equal to the algebraic sum of E_d and ΔH_s. The diffusivity is generally a stronger function of temperature., than the solubility coefficient (i.e. $E_d > \Delta H_s$). As a result, gas permeability usually increases with temperature. Diffusivity selectivity is affected with temperature since molecules having highest kinetic diameter possess higher activation energy and therefore their diffusivity increases. Diffusion of small molecules, a thermally activated process can be expressed as.

$$D=D_o \exp(-E_D/RT)$$

where, E_D is the activation energy for diffusion and D_o is a constant.

Gas solubility increases with its condensability factor and is governed by van't Hoff relation as (Robeson, 1994)

$$S=S_o \exp(\Delta H_s / RT)$$

where S_o is preexponential and ΔH_s is the partial molar enthalpy of sorption.

xi) Pressure

The gas solubility, diffusivity and, in turn, permeability may vary appreciably with pressure of penetrant in contact with the polymer changes. The gas solubility decreases with increasing pressure, which is typically observed in the permeation of glassy polymers to penetrants such as CO_2. With increasing pressure, diffusivity is enhanced.

Polyimides can be easily modified by use of diamines of different chemical structures to modify the properties to suit targeted applications. Wide varieties of

modified PIs with different chemical structures are reported in the literature. Sulfonated PIs (SPIs) is one such modification, projected as possible candidate for application as membrane material for fuel cells (PEMFC). Presently, significant research work is being conducted to study the electrochemical and other properties of SPIs of different structures. Since, one of the objectives of present dissertation is to synthesize novel SPI containing sulfonic acid group in side chain and study general and electrochemical properties of this SPI to assess possible application as membrane material for polymer electrolyte for fuel cell, a general literature survey on sulfonated PIs is given below.

1.6 Sulfonated polyimides as polymer electrolyte membrane (PEM) materials

Ability of forming numerous sulfonated monomer chemical structures for aromatic polyimides widens their breadth in PEMFC application. High susceptibility of conventional five membered imide rings towards hydrolysis under severe acidic environment makes them brittle demoting their application in PEMFC (Faure, 1997; Genies, 2001a; Fang, 2002). On the other hand, SPIs with six membered imide rings, based on 1,4,5,8-naphthalene tetracarboxylic dianhydride (NTDA) have proved to be stable towards acid hydrolysis, promoting them to be used in PEMFC (Fang, 2002; Yin, 2004 and 2006a). Group of Mercier (Genies, 2001a and 2001b; Marestin, 2008), McGrath (Gunduz, 2001; Einsla, 2004; 2005a and 2005b), Okamoto (Fang, 2002; Yin, 2006a), Watanabe (Miyatake, 2003; Asano, 2006), Holdcraft (Rodgers, 2006; Savard, 2008) and Zhang (Li, 2007b; 2007c and 2008) have diligently worked towards the synthesis of six membered SPI in PEMFC application.

1.6.1 Synthesis of sulfonated polyimides (SPIs)

General method for the synthesis of SPIs is by sulfonating parent PI in suitable solvents using a sulfonating agents such as SO_3, oleum or chlorosulfonic acid. Sulfonated PIs precipitate out from solvents making it difficult to control the degree of sulfonation. Thus, SPIs with known degree of sulfonation are usually prepared by the polycondensation of a dianhydride with sulfonated diamine (SDA).

1.6.1.1 SPI based on sulfonated diamine (SDA) as monomers

SDA possess both basic ($–NH_2$) and acidic groups ($–SO_3H$), form zwitter ion and thus become insoluble in organic solvents. To make it soluble, protection of $–SO_3H$ group by an organic base such as triethyl amine (TEA) is usually done. In general, SPIs are prepared by polycondensation reaction between SDA and dianhydrides in *m*-cresol as the solvent (Genies 2001a; Fang, 2002). In the first step, SDA in its triethylammonium sulfonate form is prepared and after its complete dissolution in the solvent, equimolar quantity of dianhydride is added followed by the addition of benzoic acid. As explained earlier, the role of benzoic acid is to catalyze the polymerization reaction. CPIs are prepared with varying ratio of SDA to the non-sulfonated diamine. Li *et. al* (2008) synthesized random as well as block CPI from hexamethylene diamine with varying ratio of sulfonated and non-sulfonated dianhydrides.

Among the different types of CPIs, synthetic procedure for block CPI is quite different and is followed in two steps. In the first step, a block of SPI with desired molecular weight is prepared by condensing SDA with a dianhydride in the desired ratio. In the second step, this block was reacted with a non-sulfonated diamine and a dianhydride (Genies, 2001a; Li, 2008). While, for the statistical random CPI synthesis, all the reactants can be mixed at once in the beginning of polymerization (Li, 2008).

Most of the literature on SPIs constitute polycondensation of SDA with dianhydride; NTDA. Though, recent literature reveals synthesis of SPI involving large number of SDA, most of them have been synthesized in the laboratory and the least are commercially available including DABSA, DMBDSA, DSDSA and BDSA as shown in Figure 1.5. Genies *et al.* (2001a) synthesized sulfonated diamine; 4,4'-diamino-biphenyl 2,2'-disulphonic acid (BDSA). Its copolymers with various non-sulfonated diamines in different ratio with either ODPA or NTDA were prepared. They observed that phthalic-based SPI based on ODPA was highly prone to the hydrolysis leading to chain scission. On the other hand, naphthalic-based SPI prepared from NTDA demonstrated good performance as membrane material in fuel cell environment (Genies, 2001a and 2001b). Fang *et al.* (2002) synthesized ODADS and its SPI and compared PEM performance between these SPIs and BDSA-based SPIs (Genies, 2001a). The former revealed better hydrolytic stability than the latter. In BDSA-type SPI, steric hindrance due to two

sulfonic groups resists the rotation of two neighboring phenyl rings of BDSA resulting in induced strain with decreased hydrolytic stability (Fang, 2002; Yin, 2006a).

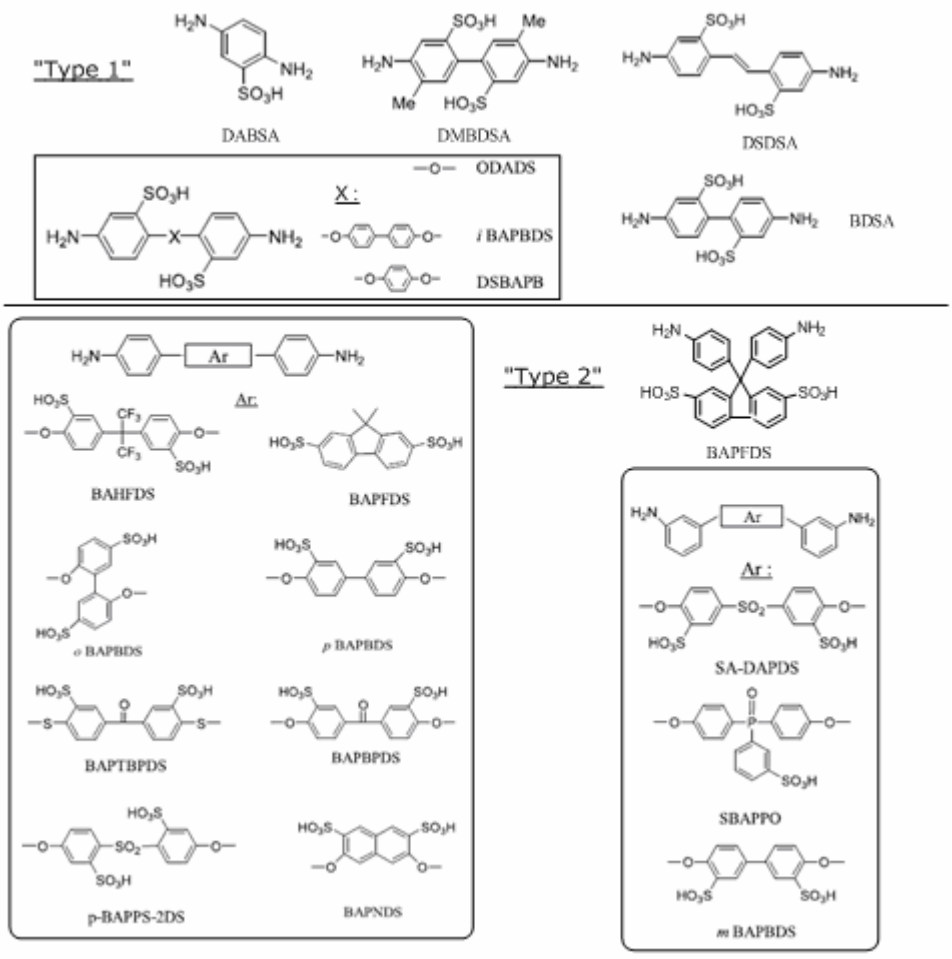

Figure 1.5 Main-chain-type sulfonated diamine

With advancement towards better PEM, Okamoto proved that SPI based on highly basic diamines possessed better hydrolytic stability. Due to this basicity, "main-chain-type" SPIs were further classified into "Type 1" and "Type 2". In "Type 1" the sulfonic group is directly attached to amino-phenyl ring, while "Type 2" consisted of bonding of sulfonic group to the phenyl ring other than amino-phenyl ring as shown in the Figure 1.3 (Yin, 2006a). Authors stated that "Type 1" SPIs have lower hydrolytic stability, since their basicity is decreased due to the electron withdrawing effect of sulfonic group resulting in more facile nature of carbon-nitrogen bond of imide group. In contrast, in case of "Type 2" SPIs, there is no such decrease in electron density on the

amino-phenyl ring. In addition, the electron density around the nitrogen atom of imide moiety is increased due to the electron donor effect of amino-phenyl ring, becoming imide linkage less vulnerable for the nucleophilic attack of water molecule. The net result is the improved hydrolytic stability for the "Type 2" SPIs.

With further design for SDA monomers, "side-chain-type" SPIs derived from these diamines have gathered major attention. The various structures of such SDA are shown in Figure 1.6. These types of SPIs can form micro-phase separation structures, similar as in case of Nafion. Such phase morphology not only facilitates the proton transport but also improves the mechanical strength needed for PEM after water swelling. In other words, positioning of $–SO_3H$ group away from the imide moiety restricts the migration of proton in hydrophilic ion-rich domains only. Thus "side-chain-type" SPIs constitute imide linkages in hydrophobic domain, while the sulfonic group in the hydrophilic domains. Since imide hydrolysis is an acid-catalytic reaction, restriction of proton mobility away from the polymer main chain can alleviate the hydrolysis of imide ring. Moreover, phase separation increases the proton conductivity in side-chain-type SPIs (Yin, 2004 and 2006a).

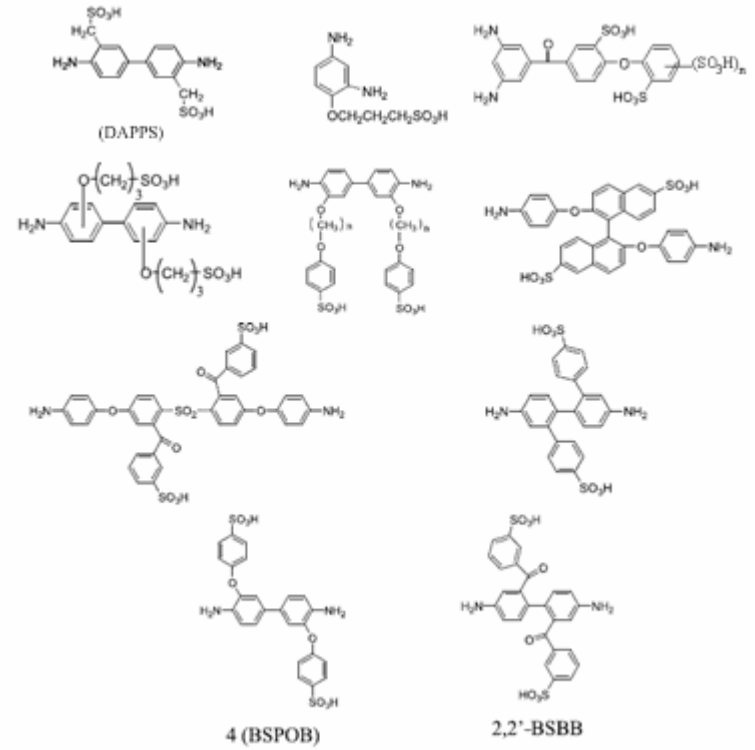

Figure 1.6 Side-chain-type sulfonated diamines

1.6.1.2 SPI based on naphthalic type dianhydrides (PNI)

The dense structures due to the planar and symmetric nature of NTDA make PNI more intractable than the five-membered ring (phthalic) polyimides. Thus, solubility of PNIs is limited only to strong acids (sulfuric, methylsulfuric, polyphosphoric) (Rusanov, 1994). It should be noted that the step wise approach for the synthesis of PNI becomes more difficult due to the low electrophilicity of the six membered anhydride as compared with the five membered anhydride moieties (Rusanov, 1994). Hence, efforts were diverted towards the synthesis of organic soluble PNI. The modification in NTDA structure such as introduction of "hinge" groups between two fragments of naphthalic anhydride (facilitating the bond rotation around the main chain axis) and embodiment of bulky group substituents can improve PNI solubility significantly (Rusanov, 1994). It was also said that structural modifications in NTDA to ease solvent solubility. The following types of bis(naphthalic anhydride) were used for making SPIs (Figure 1.7).

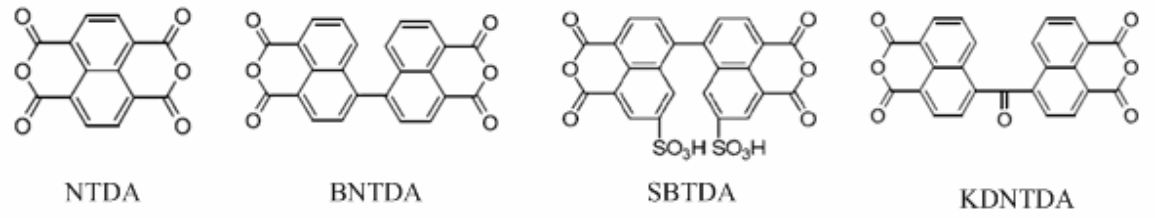

Figure 1.7 Various structures of naphthalenic dianhydride monomers

Li *et al.* (2008) proposed that use of BNTDA as compared with NTDA for making SPI should be more advantageous as it forms non-coplanar binaphthyl rings, separating their electronic conjugation. As a result, imide linkage possesses higher electron density and thus becomes less vulnerable for the nucleophilic attack of water molecule. Li *et al.* (2008) further sulfonated this BNTDA to SBTDA and observed the enhancement in water uptake and proton conductivity due to the increased free volume and kinked non-coplanar structure of SBTDA. Chen *et al.* (2006) synthesized SPIs based on more reactive dianhydride KDNTDA. These SPIs showed tough mechanical properties, high-reduced viscosity (0.8 to 4.5 $dL.g^{-1}$), good solubility in proton form and reasonable proton conductivity at their lower IECs.

Blends of SPIs with other polymers are demonstrated in the literature, as reviewed separately in Chapter 5.

1.6.2 Membrane preparation of SPIs

Membrane preparation of SPIs in pure sulfonic acid form is difficult since they are usually insoluble in common organic solvents. After synthesizing SPI, they are first isolated in the salt form (triethylammoium sulfonate form) by precipitating in a non-solvent like acetone. Subsequently, this SPI is purified by reprecipitation to remove traces of polymerizing solvent and catalyst. Generally, membranes of SPI in salt form are prepared and then they are acidified by immersing in acid to get the membrane in $–SO_3H$ form for the application as PEM for fuel cell.

1.7 Other polymers as polymer electrolyte membrane (PEM) materials

Polymers containing strong acid groups such as sulfonic acid are capable of conducting protons in presence of water. Basic polymers such as polybenzimidazole (PBI) on doping with acids such as phosphoric acid or sulfuric acid are also used (Wang, 1996). Sulfonated polymers can be further divided into fluorinated and non-fluorinated polymers. A brief literature survey on these polymers is given below.

1.7.1 Perfluorosulfonic acid (PFSA) membranes

PEMFC accomplished the major breakthrough in late 1960s, when Dupont developed the membrane based on perfluorinated ionomer; Nafion with superior chemical and mechanical stability. It is perfluorosulfonic acid ionomer consisting of Teflon like backbone with sulfonic acid located at the terminal of the side chain. The presence of C-F backbone offers several advantages. Its high C-F bond strength (441 kJ/ mol) improves its stability in severe redox environment as well as at higher potential (~1.0 V at cathode) than the low C-H bond strength (356 kJ/ mol). The peculiar arrangement of hydrophobic Teflon backbone in main chain and hydrophilic sulfonic acid ($–SO_3^-H^+$) in the side chain through flexible ether linkage organizes the phase morphology so as to separate the hydrophobic and hydrophilic regions. Because of such

ionic groups, large quantity of water can be imbibed in the polymer matrix making Nafion a dilute acid in solid state.

An important parameter of the Nafion is its equivalent weight (EW). Nafion is commercially available with trade name as Nafion 117, Nafion 115, Nafion 1110, Nafion 112, etc. The first two digits represents the EW as 1100, while the remaining digits show its thickness in mil. The chemical structure of Nafion is shown as in Figure 1.8.

Being perfluorinated polymer backbone, the characteristic properties of these membranes such as chemical, thermal and mechanical are elevated. However, high production cost, low proton conductivity at reduced humidity and/ or high temperature, high permeability for H_2, O_2 and MeOH, CO poisoning of platinum catalyst due to low operational temperature of these membranes have limited their widespread commercial application in PEMFC (Rikukawa, 2000; Rusanov, 2005). Therefore, efforts have been taken for the development of alternative membranes with fulfillment of the desired properties for PEMFC, as shown in Figure 1.8. Flemion, Aciplex and Dow membranes have been commercialized by Asahi Glass, Asahi Kasei Chemical Co. and Dow chemicals, respectively (Figure 1.8).

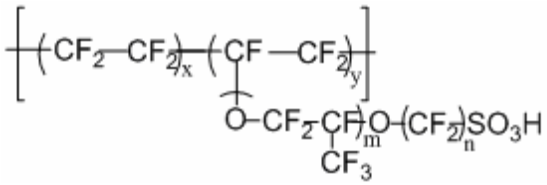

Nafion : m≥1, n=2, x=5-13.5, y=1000
Flemion : m=0 or 1, n=1-5, y=1000
Aciplex : m=0 or 3,n=2-5, x=1.5-14, y=1000
Dow : m=0, n=2, x=3.6-10, y=1000

Figure 1.8 A general structure of commercially available PFSA membranes

In PEMFC, the oxidation reduction rate (ORR) occurring at cathode is sluggish, which being further suppressed by low operating temperature. Thus, synthesizing novel non-fluorinated solid electrolyte addressing various drawbacks as given above becomes necessary.

1.7.2 Polymers with sulfonic acid group

These polymers can be synthesized by either sulfonating the high molecular weight aromatic polymers (post-sulfonation) or preparing the polymers from monomers containing sulfonic acid groups, as elaborated below.

1.7.2.1 Post-sulfonation of polymers

Various polymers including poly(1,4-phenylenes), poly(1,4-oxyphenylenes), poly(ether ether ketone) (PEEK), poly(arylene ether sulfone) (PEES), poly(phenylqunixalines), poly(phthalazinones), poly(imides), poly(benzimidazole), etc. can be sulfonated by using sulfonating agents such as concentrated sulfuric acid, oleum, chlorosulfonic acid, SO_3, a mixture of methanesulfonic acid and conc. H_2SO_4 and acetyl sulfonate (Roziere, 2003; Gao, 2003a and 2003b; Hickner, 2004; Liu, 2007; Mader, 2008). The feasibility of easy scale up due to the simple procedure and availability of inexpensive commercial high molecular weight thermoplastic polymers make post sulfonation more attractive. For instance, several researchers have studied sulfonation of the commercial Victrex (PEEK) (Hickner, 2004; Liu, 2007, etc.). However, drawbacks such as degradation of polymers while using strong acidic sulfonating agents (chlorosulfonic acid or fuming sulfuric acid), uneven distribution of sulfonic acid groups and difficulties in optimization of degree of sulfonation (DS) can cause the rough surfaces, crosslinking and excessive swelling in the post-sulfonated PEEK (Liu, 2007; Shin, 2004; Wu, 2006). Moreover, DS also determines the solvent solubility of sulfonated polymers. DS depends on the sulfonation time, temperature and sulfonating agents. The irregular placements of sulfonic acid groups can induce the stress formation when hydrated, making membrane cracking more feasible. PEEK and PEES confer sulfonation only to a phenylene ring attached to an electron donating ether linkage while restricting to phenylene ring that of electron withdrawing carbonyl and sulfone moieties as shown in following Figure 1.9.

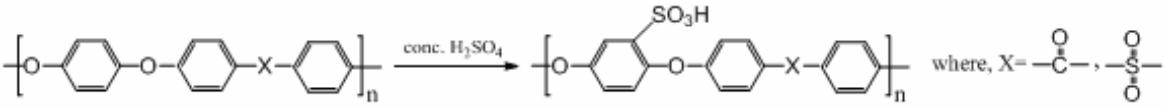

Figure 1.9 Sulfonation of PEEK and PEES (Pienemann, 2008)

These sulfonic groups are less acidic being situated *ortho* or *para* to electron-donating substituents and become more acidic when located *meta* to the electron withdrawing moiety (–CO– and $–SO_2–$). The latter sulfonated polymer becomes more stable towards thermal de-sulfonation (Shin, 2004; Hamrock, 2006; Wu, 2006; Li,

2007c). Desired or controllable DS in post-sulfonation can be achieved by sulfonating copolymers. Copolymers based on monomers with capability of different ease of sulfonation are synthesized first and then post sulfonated (Liu, 2007). Thus, the design of copolymers is done in such a fashion that some structures could not be sulfonated easily and letting degree of sulfonation to be dependant on feed ratio of such monomers as exemplified in the following Figure 1.10.

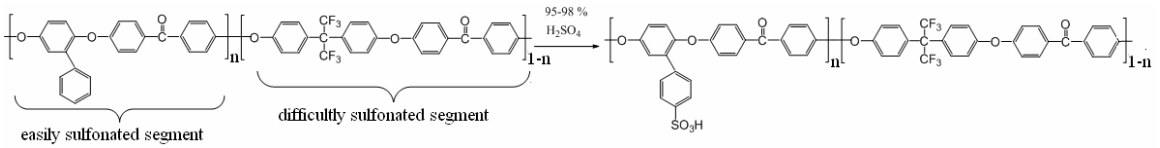

Figure 1.10 Sulfonation reaction of copolymers (Pienemann, 2008)

1.7.2.2 Sulfonated polymers and copolymers from sulfonated monomers

This method comprises the direct polymerization using sulfonated monomers. This technique enables copolymer synthesis with desired degree of sulfonation and hence IEC values. The synthesis of sulfonated monomer was reported by Robeson and Matzener (1983), whose primary interest was to check at its flame retarding additive property (Peinemann, 2008). Ueda *et al.* (1993) successfully demonstrated synthesis, characterization and purification of the sulfonated (*4,4'*-dichlorodiphenylsulfone) monomer and its polymer (sulfonated PES) by condensation polymerization route as shown in Figure 1.11.

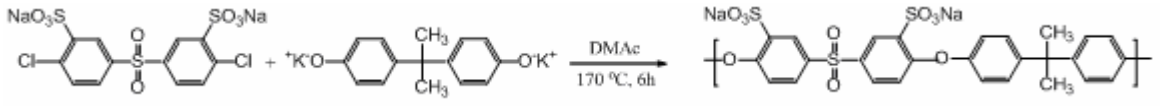

Figure 1.11 Sulfonated-PES from sulfonated (*4,4'*-dichlorodiphenylsulfone) monomer

Wang *et al.* (1998) added another analogous halogenated sulfonated monomer (5,5'-carbonylbis(2-fluorobenzenesulfonate)), which could offer various chemical structural alteration in the community of PAEKs. Difluorinated monomers though are expensive, they are highly reactive than the analogues dichlorinated monomers towards nucleophilic aromatic substitution reaction (Lau, 1989). With the progressive shift of

synthesizing sulfonated polymer, scientists soon started focusing on the sulfonation of important raw materials of the above mentioned HPP polymers such as dihalogenated monomers including aromatic diols (Gao, 2004 and 2005) as well. Synthesis of disulfonated dihalogenated monomers is documented (Shin, 2004; Einsala, 2005b)

The position of sulfonic acid group in phenyl ring becomes convincing when the enhanced acidic character is observed due to the location in the deactivated phenyl ring as compared with its location at *ortho* or *para* to electron donating groups (activated phenyl groups) (Shin, 2004; Hamrock, 2006; Li, 2007b and Li, 2007c). As a result, stability towards desulfonation is improved in the former case than in the later case. On the other hand, the access of sulfonation to such deactivated phenyl ring by post-sulfonation route become insupportable by mild sulfonating agents as observed in the case of poly(4-benzoyl)-1,4-phenylene [(PBP)] (Rikukawa, 2000).

The general method for making block copolymers includes the presynthesis of hydrophilic and hydrophobic oligomers containing reactive functional end groups and later pursuing their copolymerization (Hu, 2009). The existence of better phase separated morphology in block copolymers than random copolymers is due to the better agglomeration of hydrophilic sulfonic acid in the former due to the electrostatic interactions in ion pairs (Elabd, 2006). The hydrophilic domain transports protons while the hydrophobic domain provides morphological stability as well as prevents dissolution in water. Such system is highly resembled with the morphology of PFSA polymers. Properties of the PEM can be aligned with adjustment of either the length of hydrophilic or hydrophobic segments. For the copolymers with similar chemical structure, physical properties such as glass transition temperature, solvent solubility, IEC values, oxidative and hydrolytic stability, proton conductivity, etc. of the block copolymers behave significantly different as compared with random copolymers (Ding, 2001; Elabd, 2006; Hu, 2009).

From the above review, it is evident that efforts are mainly directed to develop sulfonated hydrocarbon polymer as alternative to expensive Nafion type polymers. Sulfonated PI is one of such alternatives. The objective of the present dissertation is to study electrochemical and other properties of new SPI containing sulfonic acid group in side chain for their application as PEMFC. Thus, it is essential to know about fuel cell. A

brief account of history and evolution of fuel cell, types of fuel cell, functioning of fuel cell, evaluation and other aspects of PEMFC, functioning of PEMFC and prerequisites for a polymer electrolyte membrane is given below.

1.8 Fuel Cells

The birth of fuel cell (FC) concept goes to Sir William Grove who in 1839 first achieved electrical energy from a chemical reaction of oxygen and hydrogen with platinum as catalyst (Grove, 1839; Bacon, 1969; Appleby, 1990). In 1893, Friedrich Wilhelm Ostwald paid attention on the theoretical understanding of fuel cell operation (Boudghene Stambouli, 2002). The technology revolution happened during World War II in 1930s, witnessing the birth of many technologies including alkaline fuel cell (AFC) invented by the British researcher F.T. Bacon for the reliable source of power for Royal Navy submarines. In 1959, Bratt and Whiteny licensed this idea of AFC in Appollo spacecrafts by using higher concentration (~85%) of alkali electrolytes (Perry, 2002). The long hibernation in fuel cell research for commercialization was strongly shaken in 1950s-60s when scientists in National Aeronautics and Space Agency (NASA), USA had been looking for power upcoming to manned space flights (Gemini program). Shortly, the collaborative work of General Electric and NASA's researchers lead to the development of new type fuel cell; proton exchange membrane fuel cell (PEMFC). The research in fuel cell areas had to be accelerated in late 20^{th} century due to the tremendous pressure built up to alleviate the greenhouse effect and global warming concerns.

Demand for energy has been growing with increase in population and living standards. The concurrent consciousness about environmental cost of energy has entailed various governments of nations, organizations and industries to find the new ways of accessing the expansion of energy sources. Efforts have been performed for generating plentiful energy sources, which have also been progressively shifting from solids (wood, coal) to liquids (petroleum) to gas (LNG, natural gas). This process is called "decarbonization", implying progressive shift to fuels with increasing hydrogen to carbon ratio (Devezas, 2008). Logically, the impending logical progression in this evolution is the use of only hydrogen as a fuel with complete elimination of carbon. Advent energy sources technologies would therefore largely dependant on hydrogen in the coming

decades (Tseng, 2005; Penner, 2006; Dincer, 2007). Fuel cells use hydrogen as the feed, are electrochemical devices which directly converts chemical energy into electrical energy. This one step process has higher efficiency than internal combustion engine (ICE) having multi step processes and lower efficiency (Wright, 2004). The conventional popular ICE follows the Carnot cycle adiabatically as well as isothermally with 40-50% theoretical efficiency. In contrast, fuel cells are operated isothermally with more than 80% (Barbir, 2005) efficiency provided by hydrogen as the fuel, as follows.

$H_2 + ½\ O_2 \rightarrow H_2O$ [$\Delta H° = -286.0\ kJ.mole^{-1}$ and $\Delta G° = -237.2\ kJ.mole^{-1}$]

Efficiency (%) = [$\Delta G° / \Delta H°$] = 83.0

The fuel cells produce only water, heat and electricity by electrochemical reaction isothermally. Moreover, absence of moving parts with resultant low noise operation in fuel cells eliminate complexity in FC systems making them more adaptable towards simpler designing as well as benignant to environment.

1.8.1 Types of Fuel cells (FC)

Classification of FC primarily depends on their operation at specified temperature as well as the types of ion conductive electrolyte used. Five major types of FC have been demonstrated. These include Proton Exchange Membrane Fuel Cell (PEMFC), Alkaline Fuel Cell (AFC), Phosphoric Acid Fuel Cell (PAFC), Molten Carbonate Fuel Cell (MCFC) and Solid Oxide Fuel Cell (SOFC) (Barbir, 2005), as shown in Table 1.1.

Table 1.1 General Aspects of fuel cells

Types of fuel cells	**Electrolyte**	**Electrodes**	**Catalyst**	**Operating Temp. range** (°C)	**Charge transport direction**	**Eff.** (%)	**Possible application**	**Water production at electrode**	**Redox reaction at electrodes**
AFC	Potassium hydroxide	Ni, Ag, PTFE powder, Cu web	Ni, Ag	60-120	OH^- from cathode to anode	45-60	Submarines and spacecraft (≈ 20 kW)	Anode	$H_2+2OH^-\rightarrow 2H_2O+2e^-$ $2H_2O+2e^-+½\ O_2\rightarrow 2OH^-$
MCFC	Immobilized liquid molten carbonate in ($LiAlO_2$)	Porous Ni, Ni-Cr, NiO (Li doped)	Non-precious metals	620-660	CO_3^{2-} from cathode to anode	45-60	Power stations (>1 MW)	Anode	$H_2+ CO_3^{2-}\rightarrow H_2O+CO_2+2e^-$ $CO_2+2e^-+½\ O_2 \rightarrow CO_3^{2-}$
PAFC	Imobilized liquid H_3PO_4	Porous carbon + Pt	Pt	160-200	H^+ from anode to cathode	35-40	Power stations (> 50 kW)	Cathode	$H_2\rightarrow 2H^++2e^-$ $½\ O_2+ 2H^++2e^-\rightarrow H_2O$
SOFC	Ceramic (Y_2O_3 stabilized ZrO_2; YSZ)	($La(Sr)MnO_3$) or LSM, (Ni-YSZ)	Non-precious metals	800-1000	O_2^- from cathode to anode	50-65	Power stations (> 200 kW)	Anode	$H_2+ O_2^-\rightarrow H_2O+2e^-$ $2e^-+½O_2\rightarrow O_2^-$
PEMFC	Ion Exchange Membrane	Porous carbon + Pt	Pt, Pt/Ru	60-140	H^+ from anode to cathode	40-60	Vehicles, Stationary (≈ 250 kW)	Cathode	$H_2\rightarrow 2H^++2e^-$ $½\ O_2+ 2H^++2e^-\rightarrow H_2O$

1.8.2 Evolution and major aspects of PEMFC

Thomas Grubb and Leonard Niedrach in General Electric (GE) company were working on fuel cell and ended up into a new type of fuel cells, referred as Grubb-Niedrach fuel cell (Grubb, 1959; Niedrach, 1964; Beuscher, 2005). At the same time, NASA had also been in search for building up a compact electricity generator for use on manned space missions. Recognizing the potential in Grubb-Niedrach fuel cell, a team of GE and NASA generated a new type of fuel cell; polymer electrolyte membrane fuel cell (PEMFC) (Perry, 2002). Utilization of this PEMFC in NASA's Gemini space program demonstrated the first successful implementation and commercialization of fuel cell technology. This PEMFC constituted polystyrene sulfonic acid as the membrane material for proton transportation and platinum as the electrocatalyst (Rikukawa, 2000). The high loading of platinum catalyst, poor oxidative stability of polystyrene sulfonic acid membrane after certain period leading to degradation and low attainable power density raised the question of its practicality. PEMFC accomplished the first major breakthrough in late 1960s, when Dupont developed the membrane based on perfluorinated ionomer, Nafion with superior chemical and mechanical stability (Rikukawa, 2000).

1.8.3 Advantages and functioning of PEMFC

PEMFC has progressively become more and more attractive due to its low operating temperature, quick start up and load following convenient way of electrolyte handling, low corrosion and system robustness due to solid electrolyte and its compactness. It also generates higher specific power (W/kg) and power density (W/cm^2) than other types of fuel cells. Hence wide application range of power as portable, stationary and automotive applications is possible. Furthermore, larger heat generated at cathode when greater number of stacks are used, can be effectively utilized. The basic design of single PEMFC stack is shown in Figure 1.12. Fabrication of PEMFC comprises polymer electrolyte membrane (PEM) sandwiched by catalyst coating from both the sides, constituting membrane electrode assembly (MEA). This is the 'heart' of the PEMFC. PEM not only transports the proton from anode to cathode but it also acts as barrier for unoxidized H_2 and unreduced O_2 from passing through.

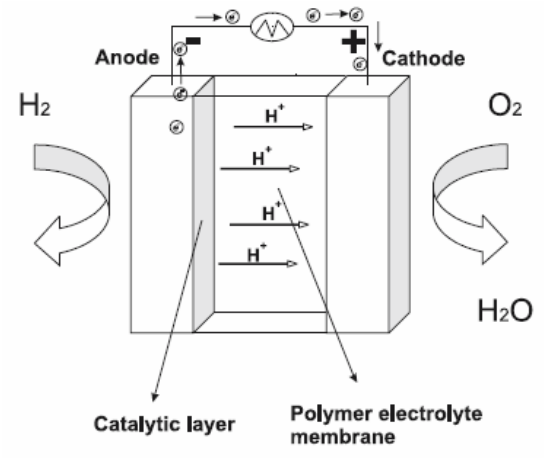

Figure 1.12 Schematic of PEMFC (Rusanov 2005)

Protons generated by oxidation of H_2 ($H_2 \rightarrow 2H^+ + 2e^-$) at the anode migrate towards cathode through the membrane. PEM also serves as barrier for evolved electrons.

The cathode is fed with O_2, which is reduced by the electrons reached through external circuit with the help of catalyst, resulting in production of water, heat and electricity.

At Cathode, $\frac{1}{2} O_2 + 2H^+ + 2e^- \rightarrow H_2O$ + heat + electricity ($E_{cathode} = 1.23$ V)
This electrochemical half-cell reaction at cathode is kinetically sluggish.

1.8.4 Criteria for PEM materials

PEM materials can be broadly categorized as polymer containing $–SO_3H$ functionality and others based on acid-base polyelectrolyte complexes. These two types have different properties and their own mechanism of proton transport. Their requisite properties can be described as given below.

For the $–SO_3H$ group containing polymers, high proton transport at low humidity, strong acidic functional groups with higher dissociation constant and lower pK_a constant, lower IEC values (< 2) coupled with better thermal, oxidative and hydrolytic stability in acidic medium are required. In addition, such PEM materials should exhibit low electro osmotic water drag, low swelling, better connectivity of proton conducting channels, almost zero electron conductivity, separation of hydrophilic and hydrophobic domains with lower interfacial tension are also importanat criteria. PEM should not contain any

pores and should have minimum H_2 and O_2 permeability. It should confer excellent mechanical strength in hydrated condition, at elevated temperature (≈150 °C), high flexibility particularly in dry state and high CO tolerance.

In order to be capable for membrane electrode assembly (MEA) fabrication, membrane must possess good adherence with porous gas diffusion electrodes. Hu *et al.* (2009) reported higher *through-plane* proton conductivity (conductivity in thickness direction of membrane) than *in-plane* conductivity (conductivity in plane direction) and lower *in-plane* swelling for better adhesion as well as mechanical stability of resulting MEA. It should also be environmental friendly with low production cost for effective commercialization.

PEM, containing $–SO_3H$ group conduct proton only in hydrated condition by vehicular mechanism, limiting the operation of PEMFC at < 100 °C. This entails permanent humidification system with auxiliary devices and making PEMFC expensive. Hence replacement of water with another species capable of proton transportation at higher temperature is being explored. In this context, azole group containing heterocyclic polymers like PBI while doping with phosphoric acid looks attractive due to its high CO tolerance, non-volatile nature of phosphoric acid, low metahanol-fuel crossover, operation performance up to 200 °C, almost zero osmotic drag coefficient and comparable proton conductivity (Li, 2003 and 2009; Mader, 2008; Potrekar, 2009a). Operating PEMFC at higher temperature confers fast electrode kinetics with less cathode flooding. Operating PEMFC above 100 °C becomes simplified due to the presence of water in single gas phase. Though PBI doped with amphoteric acid like phosphoric acid is emerging as PEMFC for high temperature application, it carries some drawbacks. These include poor solubility of pristine PBI in common organic solvents, leaching of phosphoric acid from the membrane, unestablished long term durability, effect of on-off cycle, etc. Large efforts are being made to overcome these drawbacks.

Future efforts towards increasing acid retention capability and acid content in PBI are being made. Incorporation of bulky groups improves solvent solubility of PBI as well as acid uptake due to the increased free volume with disruption of rigid structure in PBI. However, bulky group with additional basic sites in PBI can not only increase acid base interaction but also the acid retention capacity with higher proton conductivity (Kulkarni,

2008; Kim, 2009). PBI with high molecular weight is desirable since it improves the mechanical and chemical stability (Lobato, 2007). Functionalization, polymer blending and doping with different electrolytes have also been adopted towards improving performance of PBI as PEM material (Mader, 2008). Presence of basic benzimidazole group in PBI offers sites for interaction with polymers having acidic moieties and creating favorable environment for miscible blending. Blends of PBI are prepared in order to increase thermal stability, acid uptake and proton conductivity (Mader, 2008); which can be accomplished by blending with sulfonated polymer or addition of inorganic filler. Swelling and IEC of sulfonated polymer can be reduced by blending with PBI (Wysick, 2005; Mader, 2008). Hasiotis *et al.* (2001a and 2001b) reported higher conductivity of PBI/PSF blends than the acid doped PBI (Daletou, 2009). Blends of PBI with PSF copolymer containing pyridine units showed good oxidative stability (Daletou, 2005). High acid doping deteriorates mechanical strength of PBI film. In this context, addition of inorganic additives looks attractive, since with increasing proton conductivity, mechanical properties can also be greatly improved (Mader, 2008).

Polytriazole (PT) and polyoxadiazole (POD) also belong to azole group heterocyclic polymers and on doping with acids, they can conduct proton in absence of water. Potrekar *et al.* (2009b) synthesized PBI tethered with *N*-phenyl 1,2,4-triazole and reported maximum proton conductivity of 1.8 X 10^{-2} S/cm at 175 °C. Zaidi *et al.* (2000) demonstrated high proton conductivity of phosphoric acid doped POD, comparable with that of Nafion. Subbaraman *et al.* (2007) reported 4,5-dicyano-1*H*-[1,2,3]-triazole as a viable proton transport facilitator. Zhou *et al.* (2005) proved that poly(4-vinyl-1*H*-1,2,3-triazole) possessed higher conductivity with significant improvement in the electrochemical stability than poly-(4-vinylimidazole) suggesting the significance of triazole as proton conductor. Since 1*H*-1,2,3-triazole (pK_a1 =1.17 and pK_a2 = 9.26) possess higher acidic character than imidazole (pK_a1 = 7.18 and pK_a2 = 14.52) (Gagliano, 1989), solid electrolyte based on the former can offer significantly improved proton conductivity.

1.9 Aims and objectives

Aim of this thesis was to synthesize polyimides (PI) containing side chain substituent and assess their applicability in two promising areas, as a gas separation membrane material and as a polymer electrolyte membrane for fuel cell. The side chain incorporation in PI was anticipated to be better feasible with modification of amine moiety of PI than that of anhydride moiety.

Developing a viable synthesis methodology of systematically architected diamines, which would allow requisite architecture of diamine structure was the primary objective of the work. Polymerization of these structurally different side chain containing diamines with chosen dianhydrides, characterization of their physical properties, membrane preparation and their evaluation as gas separation membrane material or as polymer electrolyte membrane material was thought to be the path of this thesis work. These objectives can be further split as

a) Synthesis of a diamine, viz., 1-phenoxy-2,4-diaminobenzene (PDAB), which contains a phenoxy substituent on the *m*-phenylene diamine. This was thought to be achieved by condensation of 1-chloro-2,4-dinitrobenzene and phenol followed by reduction of nitro groups. Polymerization of PDAB with selected dianhydrides, physical property evaluation of formed polymers and their permeability determination would set a guideline towards further structural modification of the diamine.

b) Substitution of bulky alkyl groups on the aromatic ring of phenoxy linkage belonging to PDAB, their polymerization with select dianhydrides, physical property determination of formed polyimides, membrane preparation and evaluation of permeation properties using pure gases.

c) Sulfonation of PDAB, polymerization with selected dianhydrides, their blend preparation with PBI and proton conductivity evaluations.

1.10 Organization of the thesis

The present thesis provides synthesis, characterization and application of side-chain-type polyimides for gas permeability and polymer electrolyte for fuel cell. It has been presented in following chapters.

Chapter 1. Introduction and literature survey

This chapter presents a brief literature overview of synthesis and applications of polyimides. Properties of PIs as membrane material, particularly in gas permeation and PEMFC are illustrated. Scope and objective of the work is presented at the end of this chapter.

Chapter 2. Monomer synthesis and characterization

This chapter presents synthesis of various diamines used in the present investigation. These diamines were designed so that the formed polyimides exhibit side chain phenoxy groups. All diamines were synthesized from condensation of a single precursor, 1-chloro-2,4-dinitro benzene. It was condensed with various phenols possessing systematic structural variation. Characterizations of precursors and resulting diamines were performed by usual structural elucidation methods, viz., FT-IR, ^{1}H NMR, elemental analysis and melting point determination.

Chapter 3. Polyimide synthesis and their characterization

This chapter presents synthesis of polyimides by single step solution polycondensation method. All polyimides investigated possessed side chain oxy-phenyl ring possessing chosen substitutes either for gas permeation or for PEM material investigation. Physical characterizations of these PIs (requisite for gas permeation and PEM material) are presented. Blend membranes of sulfonated polyimides with polybenzimidazole (PBI) for PEM analysis are also described.

Chapter 4. Structure-gas permeability correlation in polyimides

This chapter presents investigation of gas permeability of PIs based on diamines possessing alkyl substitution on pendant phenoxy group. It presents physical properties, those are known to affect gas permeation properties and their correlation with permeability, of pure gases (He, H_2, Ar, N_2, O_2, CH_4 and CO_2). Gas permeation in SPIs as well as blend membranes (using dry as well as humidified gases) is also investigated.

Chapter 5. Investigation of polyimides towards their applicability as PEM materials

Evaluation of side-chain-type SPIs and blend of SPI with PBI as PEM material is discussed in this chapter. Physical properties influencing proton conductivity such as water uptake capacity, phosphoric acid uptake, ion exchange capacity (IEC), hydrolytic stability and oxidative stability were evaluated and proton conductivity analysis measured by electrochemical impedance spectroscopy (EIS) is discussed.

Chapter 6. Conclusions

This chapter presents conclusions with major results obtained.

Chapter 2

Monomer synthesis and characterization

2.1 Introduction

Tailor made structural variations in polymers to achieve desired properties is usually based on designing a suitable structure of their monomers. In case of polyimide structural architecture, polycondensation of a diamine with a dianhydride has played the major contribution. Between diamines and dianhydrides, synthesis of novel diamines have always surpassed over dianhydrides. This could be attributed to their relative ease of synthesis, comparatively lower number of synthetic steps, higher stability towards moisture, etc. In addition, precursors of diamines, viz., dinitro compounds are stable at ambient conditions and therefore can easily be stored. These can be reduced to diamines by a suitable reducing agent viz., Fe/HCl, Sn/HCl, $LiAlH_4$, $Co_2(CO)_8$ or H_2 in presence of Raney Ni, Pt or Pd/C at the time of utilization (Scriven, 1988; Kabalka, 1991; Huldlicky, 1996; Lee, 2004). Conversely, dianhydrides need to be stored in dry conditions, as they are highly susceptible to hydrolysis and need to be sublimed before polymerization.

Aromatic diamines offer more number of sites for substitution than the analogous aromatic dianhydrides. For instance, between, *p*-phenylene diamine (*p*-PDA) and pyrromellitic dianhydride (PMDA), the latter has only two sites for modification as compared to four sites in the former (Figure 2.1). Aromatic diamines also exhibit more number of structural isomers than that of analogous aromatic dianhydrides. For instance, in phenylene diamines, three isomers, viz., *p*-PDA, *m*-PDA and *o*-PDA are possible. On the other hand, in a dianhydride like PMDA, no structural isomer is possible.

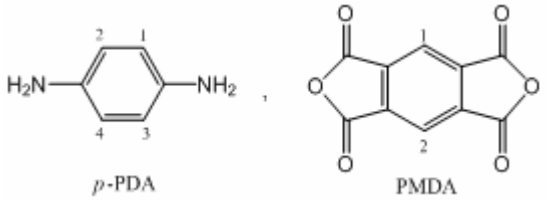

Figure 2.1 Number of available sites in common aromatic diamine and dianhydride

Though phenylene diamines are used in synthesis of polyimides possessing high tensile strength and heat resistance, these polymers are not easily processable. It is

necessary to synthesize PIs based on structurally modified diamines to fine-tune polymer properties. Such diamines can be prepared by introducing flexible and/or bulky pendant substituents on phenyl ring. This improves solubility/processability of resulting polymers while retaining thermal stability, in comparison to PI based on diamine monomers incorporating flexible groups in the main chain (Yang, 1993 and 1994). Substitutions on phenyl ring of a diamine moiety disrupt chain packing, renders amorphous nature and lead to improved solubility (St.Clair, 1976; Takekoshi, 1990). Bulky group substitution with aromatic nature would become more attractive since they not only reduce chain interactions, but also improve solubility without sacrificing thermal properties (de Abajo, 1999; Kim, 2002; Qiu, 2005). Among phenylene diamines, *m*–phenylene diamines induce kinks and disrupt the symmetry due to *meta*-linkage in resulting polymer (Takekoshi, 1990; Abajo, 1999; Kim, 2002). As a result, amorphous nature is rendered to such PIs leading to improved solubility.

Diamines are generally prepared either by ammonolysis route or by the reduction of dinitro compounds, dioximes or dinitriles. In first route, functional group like halogen (Muhlbauer, 1968), hydroxyl (MacKenzie, 1958), keto or aldehyde (Habermann, 1979) is replaced by amino group. Reports indicate that synthesis of amines by reduction route use reagents like (i) metal and acid (Fe, Zn or Sn along with HCl, H_2SO_4, CH_3COOH or HCOOH), (ii) metal and alkali (Zn or Fe in alkaline solutions), (iii) sulfides in alkaline solutions (sodium sulfide or disulfide, ammonium sulfide, polysulfides or hydrosulfides), (iv) sodium hydrosulfite in alkaline solution, (v) metal hydrides like $LiAlH_4$, LiH, or $NaBH_4$ and (vi) amalgams (March, 1992). The substrates used for reduction include nitro compounds, amides, oximes, isocyanates, isothiocyanates, azides, N-nitroso compounds, azo, azoxy or hydrazo compounds (Rylander, 1967; March, 1992). The reagents mentioned above produce large amounts of salts as by-products posing environmental issues. The alternative route, catalytic hydrogenation, is thought to be the most efficient route for synthesis of diamines and can be carried out using gaseous hydrogen (Rylander, 1967) or using hydrogen donors like NH_2-NH_2 with HCOOH (transfer hydrogenation) in presence of a catalyst (Sivanandaiah, 1985). The catalysts used for transfer hydrogenation include Raney nickel, platinum and palladium black. Hydrogenation using gaseous H_2 is more effective and requires shorter reaction times. Extensive studies have been carried

out on different types of catalysts, pressures, temperatures, solvents, reactant concentrations and mode of reactions. A number of patents are available on the synthesis of aliphatic (Williams, 1968), cycloaliphatic (Barkdoll, 1953; Arthur, 1967) and aromatic diamines (Reynolds, 1951; Gonzalez, 1970; Bhutani, 1976) by catalytic hydrogenation.

Present Chapter deals with synthesis of diamines possessing *meta* linkage and bulky substituent in the form of phenyl ether. This phenyl ether ring was also substituted with alkyl groups to elevate bulky characteristics, desirous in gas separation application.

2.2 Experimental

This section describes synthesis of dinitro precursors, respective diamines and their characterizations. Aromatic diamines possessing *meta*-linkage and flexible ether (Ar–O–Ar') side group were prepared in two steps. In the first step, 1-chloro-2,4-dinitrobenzene (CDNB) was condensed with various phenols to form dinitro precursors. These precursors were subsequently reduced to diamines by heterogeneous catalysis method using H_2 in presence of Pd/C in a high pressure Parr reactor as described in the following sections.

2.2.1 Materials

Phenol, *o*-cresol, *p*-cresol, *1*-chloro-*2*,*4*-dinitrobenzene (CDNB), triethylamine (TEA), potassium carbonate (K_2CO_3), anhydrous sodium sulfate (Na_2SO_4), benzoic acid, calcium chloride ($CaCl_2$), sodium hydroxide (NaOH), conc. HCl, conc. H_2SO_4 and various solvents of AR grade [chloroform, methanol, ethanol, acetone, pet ether, ethyl acetate and *N*,*N*-dimethylformamide (DMF)] were procured from S.D. Fine Chemicals, (India). 4-*t*-Butylphenol and 2,6-dimethyl phenol were procured from Aldrich Chemicals (USA). 4-*t*-Butylphenol was used as received, while other phenols were purified by vacuum distillation prior to use. Oleum (60%) was procured from Dharmasi Morarji Chemical Co. Ltd., Ambernath (India). Ultra-pure water was obtained using a Millipore Milli-Q water purification system.

2.2.2 Analytical methods

Elemental analysis of diamines and their precursors was performed on Elementar Vario-EL (Germany). FT-IR spectra were recorded on a Perkin Elmer 16 PC FT-IR

spectrophotometer (MA, USA) at ambient temperature. KBr pellet containing powdered sample (~10 mg in 90 mg KBr) was prepared and vacuum dried at 60 °C for 24 h prior to use. In case of compounds having melting point (*Mp*) lower than 60 °C, KBr pellets were dried in vacuum oven at room temperature for 24 h. ^{1}H NMR spectra were recorded on a Bruker AC-200 (Switzerland). Depending on the solubility, samples were either dissolved in $CDCl_3$ with tetramethylsilane (TMS) as an internal reference or in dimethyl sulfoxide (DMSO-d_6). Melting point was determined by using BUCHI Melting Point B-540 equipment (Switzerland)

Two sets of diamines were prepared. In the first set, the unsubstituted phenol was reacted with CDNB to obtain dinitro precursor (PDNB). This was subsequently reduced to obtain PDAB. This diamine was further sulfonated in view of applicability of resulting polyimides as proton exchange membrane materials. In the second set of diamines, alkyl substituted phenols were reacted with CDNB and reduced to obtain diamines.

2.2.3 Synthesis of PDNB, PDAB and SPDAB based on unsubstituted phenol

Scheme 2.1 given below describes the structure and synthetic route followed.

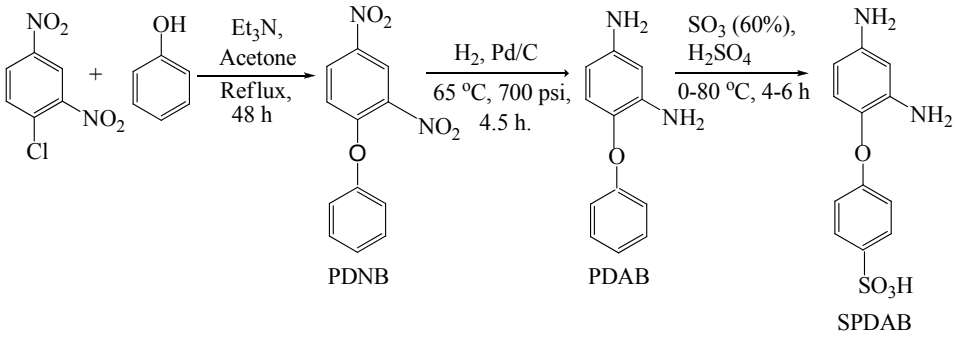

Scheme 2.1 Synthetic route to PDNB, PDAB and SPDAB

2.2.3.1 Synthesis of 1-phenoxy-2,4-dinitrobenzene (PDNB)

A 250 mL single neck round bottom flask, equipped with a condenser and a $CaCl_2$ guard tube was charged with 9.411 g (0.1 mol) of phenol, 10.1 g (0.1 mol) of TEA, 20.25 g (0.1 mol) of CDNB and 150 mL of acetone. The mixture was refluxed for 48 h. Solvent was distilled off and the residue was dissolved in $CHCl_3$. This solution was

washed with 5 % HCl, 2 % aq. NaOH, followed by water, till neutral to pH. The solution was dried over anhydrous Na_2SO_4, filtered and solvent was removed to obtain the crude product. It was recrystallized from methanol to obtain pale yellow crystals of PDNB.

Yield: 24.1 g (90%), *Mp:* 75 °C.

Elemental Analysis, ($C_{12}H_8N_2O_5$): Calculated: C, 55.4%; H, 3.1%; N, 10.8%. Found: C, 55.5%; H, 3.1%; N, 10.6%.

Figure 2.2 and 2.3 show FT-IR and ^{1}H NMR spectra of PDNB, respectively.

2.2.3.2 Synthesis of 1-phenoxy-2,4-diaminobenzene (PDAB)

A Parr reactor (250 mL) was charged with 10 g (0.03846 mol) of 1-phenoxy-2,4-dinitrobenzene (PDNB), 70 mL of methanol and 0.3 g of 5 % Pd/C. It was heated at 65 °C under 700 psi of H_2. When the absorption of H_2 was complete, the contents were cooled to room temperature and discharged after the pressure was released. The time required for this reduction process was ~4.5 h. The solution was then filtered to remove the catalyst. The filtrate was treated with activated charcoal and solvent was distilled off. Obtained crude product was recrystallized from methanol to offer faint brownish shiny crystals of PDAB. It was finally dried in vacuum oven for a day at room temperature and stored in the desiccators under N_2 atmosphere to prevent its oxidation.

Yield: 6.7 g (87 %), *Mp:* 60-61 °C.

Elemental Analysis, ($C_{12}H_{12}N_2O$): Calculated: C, 72.0%; H, 6.0%; N, 14.0%. Found: C, 2.0%; H, 6.4%; N, 14.0%.

Figure 2.2 and 2.4 show FT-IR and ^{1}H NMR spectra of PDAB, respectively.

2.2.3.3 Synthesis of 4′-sulfonic-1-phenoxy-2,4-diaminobenzene (SPDAB)

A three-necked 50 ml round-bottom flask equipped with a mechanical stirrer, a dropping funnel, $CaCl_2$ guard tube and gas inlet was purged with dry N_2 and charged with 3.0 mL of conc. H_2SO_4 (95 %). The flask was cooled to 0 °C in an ice bath followed by slow addition of finely crushed powder of 5.0 g (25 mmol) of diamine (PDAB) and 7.0 mL of 95 % conc. H_2SO_4 while stirring. After ensuring complete dissolution of PDAB in conc. H_2SO_4, 10.0 mL of fuming H_2SO_4 (60% SO_3) was slowly added at 0 °C for 30 min. The temperature of the reaction mixture was elevated at the ambient and kept stirring for

30 min. This was followed by heating at 80 °C for 1 h. The reaction mixture was subsequently cooled to the ambient and poured onto crushed ice. This acidic solution was then slowly neutralized with saturated solution of aq. NaOH at 0 °C, till precipitation of crude SPDAB. The crude product was filtered and added to 100 mL of deionised water at 0 °C. It was dissolved as its sodium salt by slow addition of 2% aq. NaOH solution. Obtained solution was filtered, followed by slow addition of 5% HCl at 0 °C till occurrence of brownish precipitate of pure SPDAB. The product was filtered, thoroughly washed with cold water till neutral to pH, followed by acetone wash and dried at 60 °C under reduced pressure for a day.

Yield: 3.8 g (65 %), *Mp:* 330 °C.

Elemental Analysis, ($C_{12}H_{12}N_2O_4S$): Calculated: C, 51.42%; H, 4.28%; N, 10.00%; S, 11.42%. Found: C, 51.08%; H, 4.29%; N, 9.75%; S, 11.13%.

FT-IR and ^{1}H NMR spectra of SPDAB are given in Figure 2.5 and 2.6, respectively.

2.2.4 Synthesis of dinitro precursors and diamines based on CDNB and substituted phenols

Scheme 2.2 given below describes the structure and synthetic route followed.

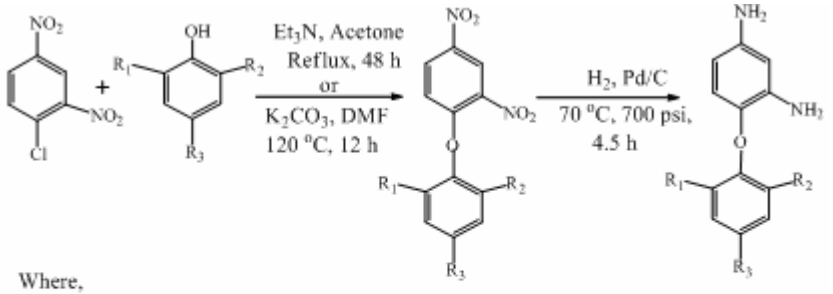

Where,

R_1 = -CH_3, R_2 = R_3 = H	2'MPDNB	2'MPDAB
R_1 = R_2 = H, R_3 = -CH_3	4'MPDNB	4'MPDAB
R_1 = R_2 = -CH_3, R_3 = H	2',6'DMPDNB	2',6'DMPDAB
R_1 = R_2 = H, R_3 = -$C(CH_3)_3$	4'*t*BPDNB	4'*t*BPDAB

Scheme 2.2 Synthesis of dinitro precursors and diamines based on alkyl substituted phenols

2.2.4.1 Synthesis of 2′-methyl-1-phenoxy-2,4-dinitro benzene (2′MPDNB)

A 500 mL single-necked round bottom flask, equipped with a condenser and a $CaCl_2$ guard tube was charged with 21.62 g (0.2 mol) of *o*-cresol, 16.58 g (0.24 mol) of

dry K_2CO_3 and 150 mL of DMF. The reaction mixture was stirred at ambient temperature for 30 minutes. To this solution, 40.51 g (0.2 mol) of CDNB dissolved in 150 mL of DMF was added and the mixture was heated for 12 h at 120 ºC. After cooling, the resulting solution was poured in stirred water (500 mL). Obtained slurry was filtered and solid was washed with water till neutral to pH. The crude product (2′MPDNB) was purified by recrystallization in methanol to yield orange crystals.

Yield: 41.0 g (75 %), *Mp:* 90 °C.

Elemental Analysis, ($C_{13}H_{10}N_2O_5$); Calculated: C, 56.94%; H, 3.68%; N, 10.22%. Found: C, 56.93%; H, 3.90%; N, 10.37%.

Figure 2.7 and 2.8 show FT-IR and ^{1}H NMR spectra of 2′MPDNB, respectively.

2.2.4.2 Synthesis of 2′methyl-1-phenoxy-2,4-diamino benzene (2′MPDAB)

2′MPDAB was obtained by reducing 10 g 2′MPDNB in the Parr reactor using similar procedure described in the Section 2.2.3.2. The crude product was purified by recrystallization in methanol, conferring faint brown crystals.

Yield: 5.8 g (74 %), *Mp:* 78 °C.

Elemental Analysis, ($C_{13}H_{10}N_2O$): Calculated: C, 72.87%; H, 6.59%; N, 13.07%. Found: C, 72.66%; H, 6.61%; N, 13.03%.

Figure 2.7 and 2.9 show FT-IR and ^{1}H NMR spectra of 2′MPDAB, respectively.

2.2.4.3 Synthesis of 4′-methyl-1-phenoxy-2,4-dinitro benzene (4′MPDNB)

A 500 mL single-necked round bottom flask, equipped with a reflux condenser and a $CaCl_2$ guard tube, was charged with 21.62 g (0.2 mol) of *p*-cresol, 27.8 ml (0.2 mol) of TEA and 150 mL of acetone and stirred at ambient temperature for 30 minutes. To this solution, 40.51 g (0.2 mol) of CDNB dissolved in 150 mL of acetone was added and the reaction mixture was refluxed for 48 h. Acetone was distilled off to obtain crude product, 4′MPDNB, with green-yellowish color. It was dissolved in 500 mL of $CHCl_3$ and washed with 5% HCl, 2% aq. NaOH and finally with water (till neutral to pH), sequentially. The $CHCl_3$ solution was dried over anhydrous Na_2SO_4, filtered and solvent distilled off to recover crude product. It was purified by recrystallization in methanol and dried in vacuum oven at 60 °C for a day.

Yield: 45.2 g (82 %), *Mp:* 91 °C.

Elemental Analysis, ($C_{13}H_{10}N_2O_5$): Calculated: C, 56.94%; H, 3.68%; N, 10.22%. Found: C, 56.53%; H, 3.51%; N, 10.6%.

Figure 2.10 and 2.11 show FT-IR and ^{1}H NMR spectra of 4′MPDNB, respectively.

2.2.4.4 Synthesis of 4′-methyl-1-phenoxy-2,4-diamino benzene (4′MPDAB)

4′MPDAB was obtained by reducing 10 g of 4′MPDNB in the Parr reactor using similar procedure described in the Section 2.2.3.2.

Yield: 6.2 g (80 %), *Mp:* 59 °C.

Elemental Analysis, ($C_{13}H_{10}ON_2$): Calculated: C, 72.87%; H, 6.59%; N, 13.07%. Found: C, 72.31%; H, 6.58%; N, 12.96%.

Figure 2.10 and 2.12 show FT-IR and ^{1}H NMR spectra of 4′MPDAB, respectively.

2.2.4.5 Synthesis of 2′,6′-dimethyl-1-phenoxy-2,4-dinitro benzene (2′,6′DMPDNB)

2′,6′DMPDNB was synthesized using 24.43 g (0.2 mol) of 2,6-dimethylphenol following the procedure described in Section 2.2.4.1. Obtained product could not be purified by recrystallization using common organic solvents or their mixtures. Therefore, purification was done by washing the obtained crude product with cold methanol. The purified product was vacuum dried at 60 °C for a day. Its analysis is given below.

Yield: 40.6 g (70 %), *Mp:* 121 °C.

Elemental Analysis, ($C_{14}H_{12}N_2O_5$): Calculated: C, 58.33%; H, 4.20%; N, 9.72%. Found: C, 58.35%; H, 4.55%; N, 9.74%.

Figure 2.13 and 2.14 show FT-IR and ^{1}H NMR spectra of 2′,6′DMPDNB, respectively.

2.2.4.6 Synthesis of 2′,6′-dimethyl-1-phenoxy-2,4-diamino benzene (2′,6′DMPDAB)

2′,6′DMPDAB was obtained by reducing 10 g of 2′,6′DMPDNB in a Parr reactor using similar procedure described in the Section 2.2.3.2. The crude product was

recrystallized in the mixture of pet ether: ethyl acetate (6:1). The analysis performed is as given below.

Yield: 5.4 g (68 %), *Mp:* 157 °C.

Elemental Analysis, ($C_{14}H_{16}N_2O$): Calculated: C, 73.66%; H, 7.06%; N, 12.27%. Found: C, 74.12%; H, 7.50%; N, 11.59%.

Figure 2.13 and 2.15 show FT-IR and ^{1}H NMR spectra of 2′,6′DMPDAB, respectively.

2.2.4.7 Synthesis of 4'-t-butyl-1-phenoxy-2,4-dinitro benzene (4′tBPDNB)

In a 1 L single neck round bottom flask, 27.64 g (0.2 mol) of 4-*t*-butylphenol and 40.50 g (0.2 mol) of CDNB was reacted by using 20.2 g (0.2 mol) of TEA in 500 mL of acetone, following the similar procedure as given in Section 2.2.4.3. The crude product was recrystallized in methanol to obtain needle shaped yellowish crystals. Its analysis was as given below.

Yield: 55.0 g (87 %), *Mp:* 108 °C.

Elemental Analysis, ($C_{16}H_{16}N_2O_5$): Calculated: C, 60.76%; H, 5.10%; N, 8.86%. Found: C, 60.90%; H, 5.27%; N, 8.88%.

Figure 2.16 and 2.17 show FT-IR and ^{1}H NMR spectra of 4′*t*BPDNB, respectively.

2.2.4.8 Synthesis of 4'-t-butyl-1-phenoxy-2,4-diamino benzene (4′tBPDAB)

This was synthesized using 5 g of 4′*t*BPDNB and 70 ml of methanol following the similar procedure as described in the Section 2.2.3.2. The crude product was purified by recrystallization in water: methanol mixture (1:1). The obtained crystals were floppy in nature and had silver shining.

Yield: 3.1 g (76 %), *Mp:* 97 °C.

Elemental Analysis, ($C_{16}H_{20}N_2O$): Calculated: C, 74.97%; H, 7.86%; N, 10.93%. Found: C, 74.57%; H, 7.77%; N, 10.92%.

Figure 2.16 and 2.18 show FT-IR and ^{1}H NMR spectra of 4′*t*BPDAB, respectively.

2.3 Results and Discussion

2.3.1 Reaction of CDNB with unsubstituted phenols

2.3.1.1 Synthesis and characterization of PDNB and PDAB

The reaction of CDNB with unsubstituted phenol proceeded smoothly as described in Section 2.2.3.1 to offer dinitro precursor, PDNB. The high yield was obtained using milder base, TEA. This indicated ease in chlorine replacement of CDNB by phenol. The presence of two nitro groups in CDNB would facilitate the chlorine replacement. PDNB was subsequently reduced in a Parr reactor with H_2 with 5% Pd/C as the catalyst to obtain PDAB in high yield (87%). Elemental analysis is in good agreement with calculated values. The structure of these compounds was further confirmed by IR and ^{1}H NMR spectra.

The IR spectrum of the precursor PDNB (Figure 2.2) showed absorption bands at 1532 and 1346 cm^{-1}. These are due to asymmetric and symmetric $–NO_2$ stretching vibrations, respectively (Yang, 2004a and 2004b). Bands at 1271 and 1070 cm^{-1} were attributable to Ar–O–Ar' asymmetric and symmetric stretching, respectively. A band at 875 cm^{-1} corresponds to aromatic C–N stretching vibration (Mathew, 2001).

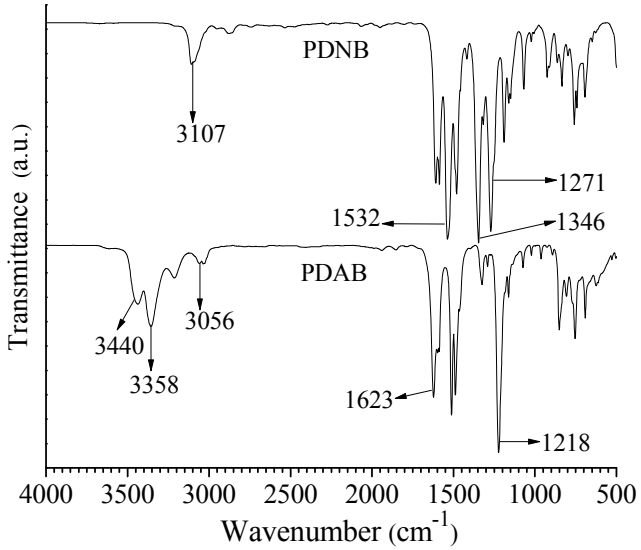

Figure 2.2 FT-IR spectra of PDNB and PDAB

In ^{1}H NMR spectrum of PDNB, aromatic protons in the region of 7.0-8.85 ppm showed expected multiplicity (Figure 2.3). The integration was in accordance with the

number of protons. The extreme downfield appearance of two aromatic protons, H_a and H_b belonging to the nitro-phenyl ring was due to the highly electron withdrawing nature of – NO_2 groups. Between these two protons, proton H_a resonated at the downfield region since it has been flanked by electron withdrawing two –NO_2 groups. The proton H_c appeared in the relative upfield region due to its *meta* position to –NO_2 groups. Moreover, to its ortho position, Ar–O–Ar' linkage would be in the conjugation effect. Aromatic protons corresponding to the phenyl ring of phenoxy group showed their expected multiplicity and integration in the region of 7.0-7.55 ppm as shown in Figure 2.3. The sharp melting point of PDNB at 74.3-75.1 °C indicated its good purity.

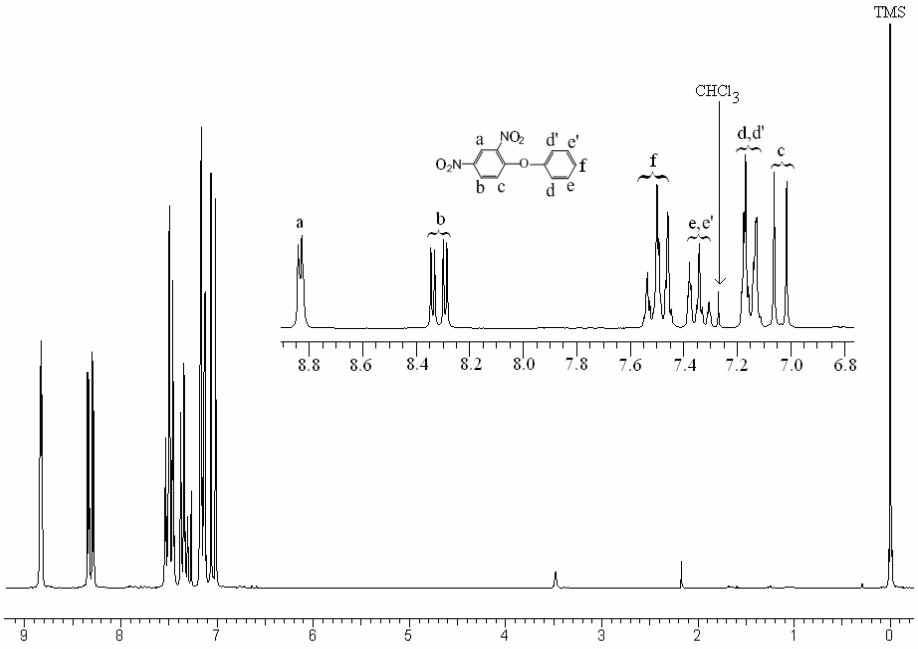

Figure 2.3 ^{1}H NMR spectrum of PDNB

The IR spectrum of PDAB (Figure 2.2) showed the characteristic bands of amino groups at 3358 and 3293 cm^{-1} (Yang, 2004a and 2004b). These were due to asymmetric and symmetric N-H stretching, respectively. Band at 1489 cm^{-1} corresponds to carbon-carbon stretching of aromatic ring. A band at 1218 cm^{-1} was due to the ether linkage, while the band at 1275 cm^{-1} was due to the C–N stretching (Mathew, 2001). The structure of diamine was further confirmed by the disappearance of the bands at 1532 and 1346

cm^{-1} due to asymmetric and symmetric stretching vibrations of $–NO_2$ group of the precursor PDNB.

The ^1H NMR spectrum of the PDAB (Figure 2.4) showed multiple peaks in the range of 6.0-7.3 ppm. This upfield shift of the aromatic protons in comparison to PDNB confirmed the reduction of PDNB. Protons of the amino-phenyl ring shifted to upfield as compared to protons of the phenoxy ring due to the activated amino-phenyl ring (electron donating nature of $–NH_2$ groups by mesomeric +R effect). Among the protons of amino-phenyl ring, proton H_c appeared at the downfield since it was located *meta* to both $–NH_2$ groups. It is interesting to note that, proton H_a resonated at the downfield region than proton H_b, despite being flanked by electron donating $–NH_2$ groups. Protons $H_{e,e'}$ corresponding to phenoxy group shifted to downfield region due to its *meta* location to the ether linkage. It also appeared as the triplet. The remaining protons $H_{d,d'}$ and H_f of the phenoxy group appeared in the region of 6.85 -7.05 ppm with expected multiplicity and integration. The signal appearing at the upfield region 3.5 ppm was corresponding to the primary aromatic amine protons. PDAB showed the sharp melting at 61 °C. Elemental analysis is also in good agreement with calculated values.

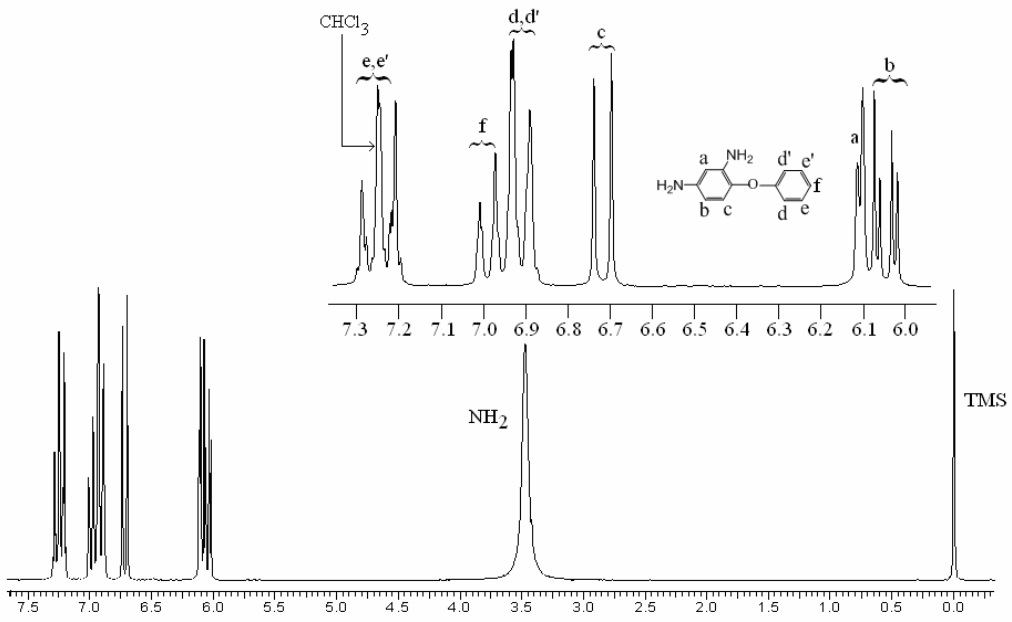

Figure 2.4 ^1H NMR spectrum of PDAB

2.3.1.2 Synthesis and characterization of SPDAB

A new diamine, 4′-sulphonic-1-phenoxy-2,4-diaminobenzene (SPDAB), was synthesized by sulfonating PDAB (Scheme 2.1) as described in Section 2.2.3.3. After dissolving in 95% H_2SO_4 solution, the amino-phenyl ring became deactivated due to the transformation of *meta*-linked electron donating $–NH_2$ groups to the electron withdrawing ammonium sulfonate groups ($–NH_3^+HSO_4^–$). Thus, electrophilic substitution by SO_3H group preferentially occurred at *para* position of pendant phenoxy ring in PDAB.

The IR spectrum of sulfonated diamine; SPDAB is shown in Figure 2.5. Characteristic bands at 3409 cm^{-1} and 3308 cm^{-1} corresponded to asymmetric and symmetric –N–H stretching, respectively. The bands at 1229 cm^{-1} and 1308 cm^{-1} were due to the Ar–O–Ar' linkage and C–N stretching, respectively. Various peaks corresponding to $–SO_2$ stretching were observed at 1168, 1089 and 1026 cm^{-1}.

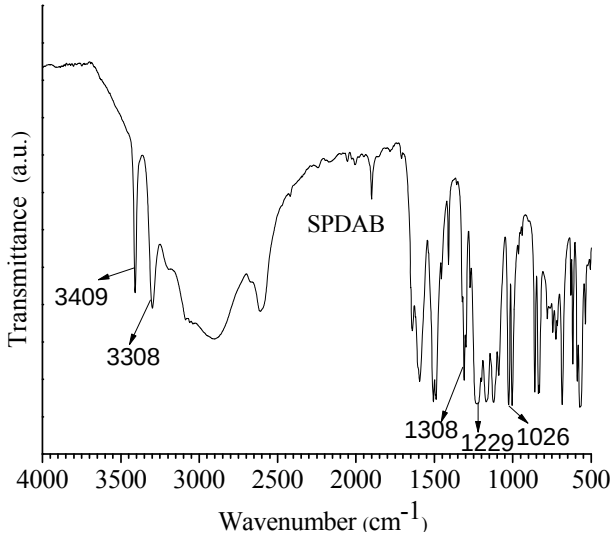

Figure 2.5 FT-IR spectrum of SPDAB

The ^1H NMR spectrum of SPDAB (Figure 2.6) showed aromatic proton signals in the range of 5.83-7.52 ppm. The aromatic protons corresponding to the amino-phenyl ring (H_a, H_b and H_c) appeared in the upfield region due to the activation of this phenyl ring by electron donating nature of$–NH_2$ groups. While, the remaining aromatic protons corresponding to the pendant mono sulfophenoxy moiety showed two doublets ($H_{d,d'}$ and $H_{e,e'}$) at 6.75 and 7.52 ppm, respectively. This confirmed the attachment of sulfonic acid

group, to *para* position of phenoxy moiety. The appearance of signals at two different chemical shifts (4.7 and 4.5 ppm) in the upfield region was peculiar of the *meta*-amino groups and suggested their different basicity. Its melting point was 329-331 °C.

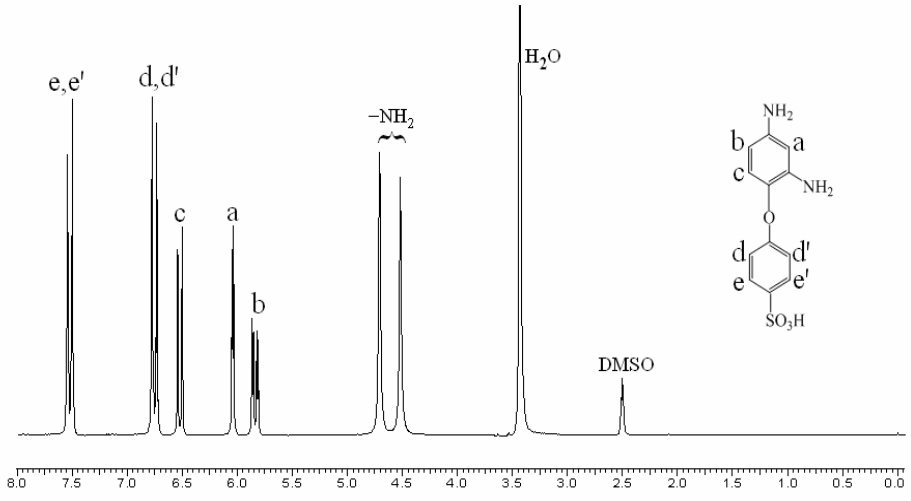

Figure 2.6 ^{1}H NMR spectrum of SPDAB

Observed values of elemental analysis for PDNB, PDAB and SPDAB matched well with the calculated values. This along with FT-IR and ^{1}H NMR analysis confirmed respective structure of these compounds.

2.3.2 Reaction of CDNB with substituted phenols

The rational for the design of attempted alkyl substituted diamine monomers was to investigate effects of systematic structural variations on gas permeability of polyimides based on these diamines. Four novel diamines viz., 2′-methyl-1-phenoxy-2,4-diaminobenzene (2′MPDAB), 4′-methyl-1-phenoxy-2,4-diaminobenzene (4′MPDAB), 2′6′-dimethyl-1-phenoxy-2,4-diaminobenzene (2′,6′DMPDAB) and 4′-*t*-butyl-1-phenoxy-2,4-diaminobenzene (4′*t*BPDAB) were synthesized in two steps as described in experimental Section 2.2.4.

2.3.2.1 Synthesis and characterization of 2′MPDNB and 2′MPDAB

Alkyl substituted phenol such as *o*-cresol could not be reacted with CDNB at low temperature in acetone. So, high boiling polar solvent, DMF, was used for the reaction.

Anhydrous K_2CO_3 was used as acid acceptor. The compound 2′MPDNB was obtained in high yield (75 %). 2′MPDNB was subsequently reduced in a Parr reactor with H_2 with 5% Pd/C as the catalyst to obtain 2′MPDAB in good yield (74%). Calculated and observed values of elemental analysis for 2′MPDNB and 2′MPDAB matched well. The purity of these compounds reflected in their sharp melting points (Section 2.2.4). Structures of these compounds were further confirmed by FT-IR and ^{1}H NMR analysis.

In the FT-IR spectrum of 2′MPDNB, absorption bands appearing at 3058 and 3109 cm^{-1} were due to aromatic C–H stretching (Figure 2.7). The sharp C–H stretching band corresponding to the methyl group was observed at 2858 and 2926 cm^{-1}. Occurrence of bands at 1609 and 1477 cm^{-1} was due to the presence of –C=C– aromatic stretching. The strong band at 1271 and a weak band at 1067 cm^{-1} were due to C–O–C stretching of asymmetric and symmetric type, respectively. The strong band at 748 cm^{-1} was due to *ortho*-substitution in the benzene ring (Silverstein, 2006). Bands appearing at 1539 and 1346 cm^{-1} were due to asymmetric and symmetric –NO_2 stretching, respectively.

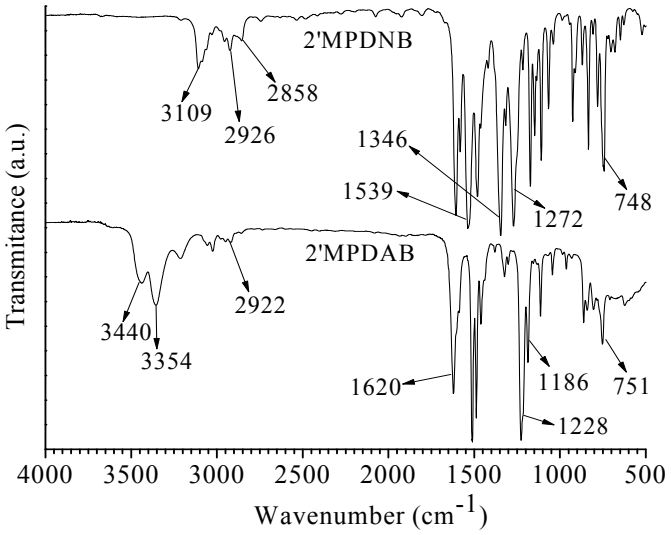

Figure 2.7 FT-IR spectra of 2′MPDNB and 2′MPDAB

The ^{1}H NMR spectrum of 2′MPDNB is shown in Figure 2.8. The aromatic protons appeared in the range of 6.84-8.8 ppm. Among them, protons in the vicinity of electron withdrawing –NO_2 groups, protons H_a and H_b were shifted to the downfield

region. On the other hand, proton H_c of the same phenyl ring containing nitro groups appeared in upfield. This could be attributed to its *meta* position to the $–NO_2$ moieties as well as *ortho* to the electron donating effect of Ar–O–Ar' linkage. The signals of remaining aromatic protons appeared between the positions of protons H_a *and* H_c in the range of 6.84-8.8 ppm with expected multiplicity and integration. The sharp singlet in the upfield region at 2.20 ppm belongs to the methyl protons.

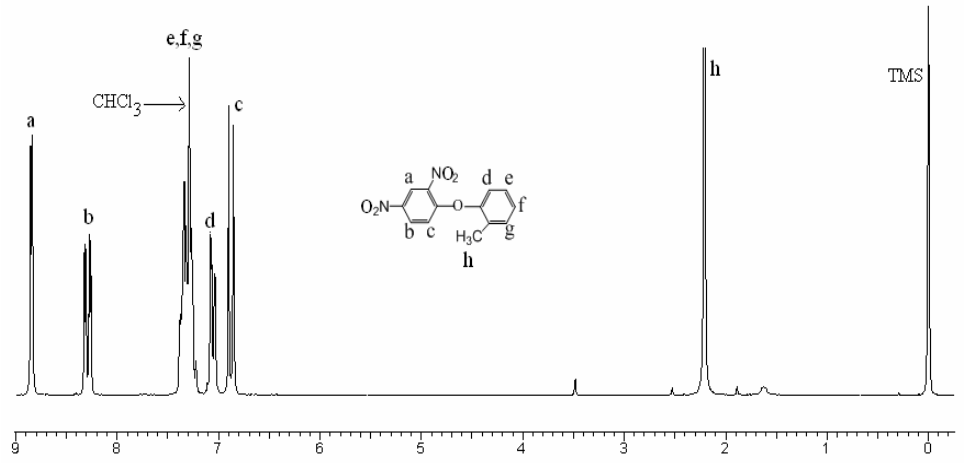

Figure 2.8 ^{1}H NMR spectrum of 2′MPDNB

In case of FT-IR spectrum of 2′MPDAB, absence of peak of $–NO_2$ stretching (Figure 2.7) indicated complete conversion of nitro to amine functionality. Characteristic absorption of N–H stretching appeared in the region 3300-3500 cm^{-1}. The asymmetric and symmetric stretching occurred at 3440 and 3354 cm^{-1}, respectively. The strong absorption peak near 1620 cm^{-1} could be assigned to the N–H bending. The Ar–O–Ar' stretching peak shifted to lower frequency at 1228 cm^{-1} as compared to higher frequency at 1271 cm^{-1} in case of 2′MPDNB. This could be due to electron donating effect of amino groups. The strong band due to C–N stretching was observed at 1186 cm^{-1}. The absorption bands appearing between 2923 and 2862 cm^{-1} correspond to the asymmetric and symmetric stretching of $–CH_3$ groups, respectively.

The ^{1}H NMR spectrum of 2′MPDAB is shown in the Figure 2.9. Aromatic protons appeared in the range of 6.06-7.2 ppm. Among them, protons of *meta*-amino-phenyl ring appeared in the upfield region due to activation of the phenyl ring by electron

donating $–NH_2$ groups. The signal of proton H_b appeared in the form of doublet of a doublet, since it was *ortho* to the proton H_c and *meta* to the proton H_a. The proton H_a showed a doublet at 6.17 ppm due its *meta* coupling with proton H_c. Among the aromatic protons of methyl substituted phenoxy ring, proton H_e and proton H_f appeared as a triplet at 7.07 and 6.92 ppm, respectively. While proton H_d and proton H_g appeared as doublet at 6.7 and 7.2 ppm, respectively. Protons of the $–NH_2$ appeared in the upfield region at 3.4 ppm as a broad peak, while the signal of methyl protons appeared at 2.35 ppm.

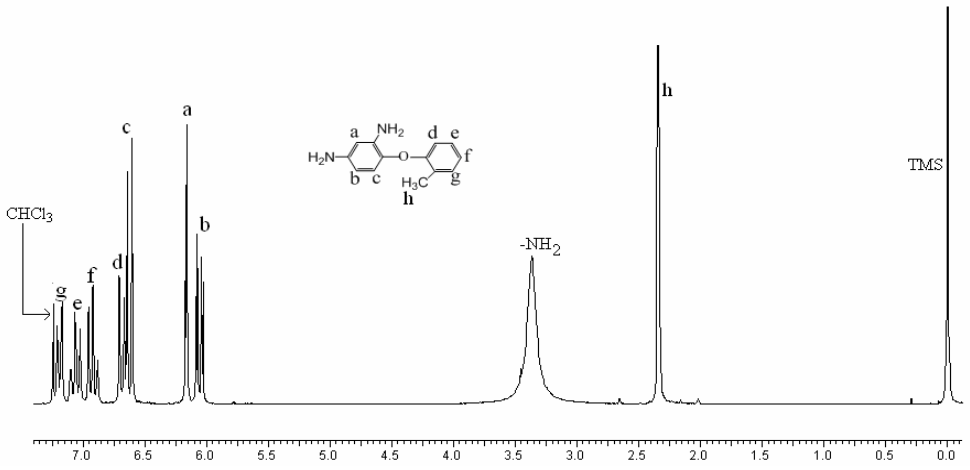

Figure 2.9 ^{1}H NMR spectrum of 2′MPDAB

2.3.2.2 Synthesis and characterization of 4′MPDNB and 4′MPDAB

Both compounds, 4′MPDNB and 4′MPDAB were synthesized in good yields by the procedure described in experimental part (Section 2.2.4). Besides, well matched calculated and observed values of elemental analysis, the structure of these compounds was confirmed by, FT-IR and ^{1}H NMR analysis.

The FT-IR spectra of the 4′MPDNB and 4′MPDAB are shown in Figure 2.10. In the case of 4′MPDNB, the aromatic C–H stretching band appeared at 3107 cm^{-1}, while the asymmetric and symmetric methyl C–H stretching vibrations were observed at 2923 and 2855 cm^{-1}, respectively. The aromatic –C=C– stretching bands were observed at 1600 and 1533 cm^{-1}. The strong band at C–O–C stretching was observed at 1270 cm^{-1}. The *para* substitution in 4′MPDNB could be further confirmed by the appearance of

strong band at 831 cm^{-1} (Silverstein, 2006). The asymmetric and symmetric $-NO_2$ stretching frequencies appeared at 1534 and 1348 cm^{-1} in 4′MPDNB, respectively.

The ^1H NMR spectrum of 4′MPDNB is shown in the Figure 2.11. The aromatic protons appeared in the range of 7.02-8.82 ppm. The order as well as positions of aromatic protons H_a and H_b of the *meta*-nitro-phenyl ring was similar as in the case of 2′MPDNB (Figure 2.8). While, the proton H_c at 7.02 ppm was merged with that of the protons $H_{d,d'}$ of the *para*-methyl substituted phenoxy ring. Protons $H_{e,e'}$ were located at 7.28 ppm. The sharp singlet at 2.20 ppm was corresponding to the methyl protons.

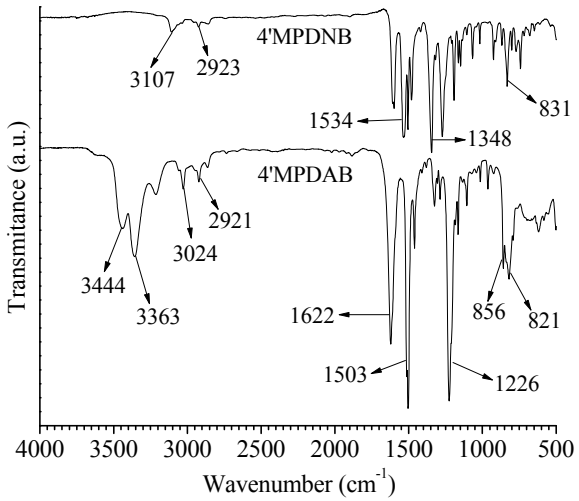

Figure 2.10 FT-IR spectra of 4′MPDNB and 4′MPDAB

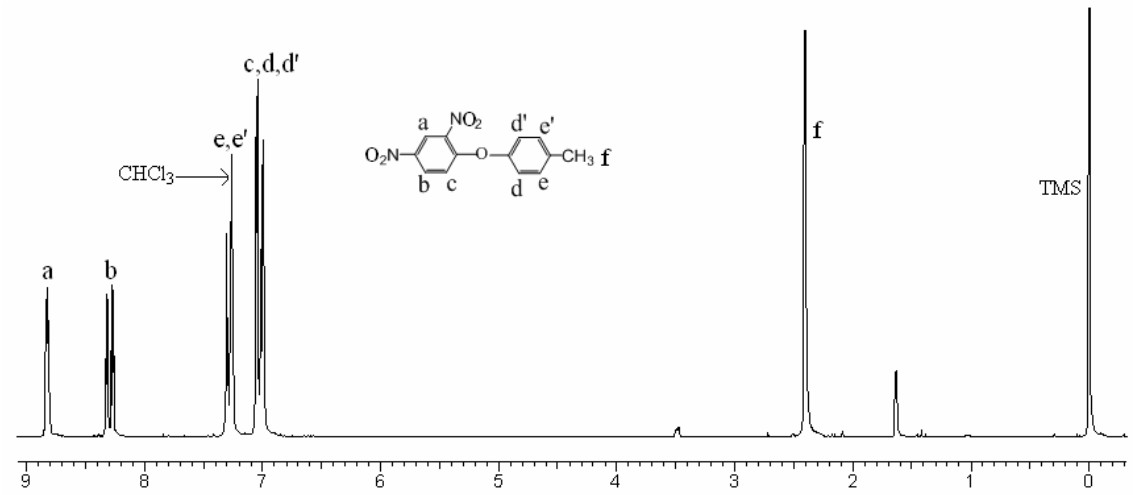

Figure 2.11 ^1H NMR spectrum of 4'MPDNB

In 4′MPDAB, $-NO_2$ stretching peaks of 4′MPDNB at 1534 and 1348 cm^{-1} disappeared (Figure 2.10) and the new peaks at 3444 and 3363 cm^{-1} corresponding to the respective asymmetric and symmetric –N–H stretching appeared, authenticating the reduction of $–NO_2$ to $–NH_2$ (Yang, 2004a and 2004b). The bending vibrations of –N–H appear at 1622 cm^{-1}. The sharp band appearing at 1226 cm^{-1} was due to the C–O–C stretching, which shifted to lower wave number (Mathew, 2001; Yang, 2002). The appearance of bands at ~1505 cm^{-1} corresponding to the aromatic –C=C–stretching proved that aromatic ring had not been affected by hydrogenation. The –C–H stretching bands of methyl group were observed at 2861 and 2921 cm^{-1}, while that of aromatic region appeared at 3024 and 3213 cm^{-1}. The strong peaks appeared at 821 and 856 cm^{-1} validated the *para*-substitution in 4′MPDAB (Silverstein, 2006). The intense characteristic peak in the region of 821-856 cm^{-1} in 4′MPDNB and 4′MPDAB confirmed the *para*-substitution of $–NH_2$ and $–CH_3$ groups to the Ar–O–Ar' ether linkage.

The ^1H NMR spectrum of 4′MPDAB is shown in the Figure 2.12. Aromatic protons appeared in the upfield region of 6.07 - 7.05 ppm as compared to same protons appearing at in the range of 7.02-8.82 ppm for its dinitro precursor, 4′MPDNB. Moreover, the signal obtained at 3.25 ppm corresponding to $–NH_2$ group could confirm the reduction of nitro to amine. The protons H_a, H_b and H_c corresponding to the *meta*-amino-phenyl ring appeared at 6.16, 6.07 and 6.72 ppm, respectively. The remaining protons viz., $H_{d,d'}$ and $H_{e,e'}$ of the *para*-methyl substituted phenoxy ring appeared at 6.82 and 7.05 ppm, respectively. The methyl protons appeared at 2.3 ppm.

The calculated values of elemental analysis were in good agreement with the observed values, as given in Section 2.2.4.1.

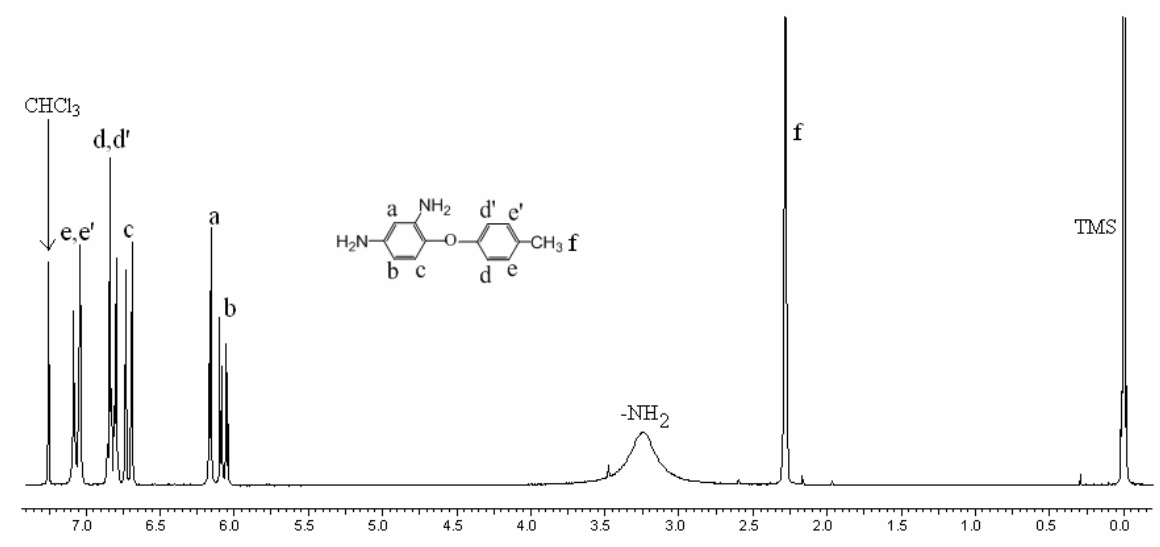

Figure 2.12 ^{1}H NMR spectrum of 4'MPDAB

2.3.2.3 Synthesis and characterization of 2′6′DMPDNB and 2′6′DMPDAB

The compound 2′6′DMPDNB could be obtained in good yields by synthetic procedure described in experimental section 2.2.4.5. However, this compound could not be crystallized from common solvents. So, the compound was purified by washing of crude compound with cold methanol. The purity of the compound was ascertained by sharp melting point and well matched observed and calculated elemental analysis values, while the structure was further confirmed by FT-IR and ^{1}H NMR spectral analysis.

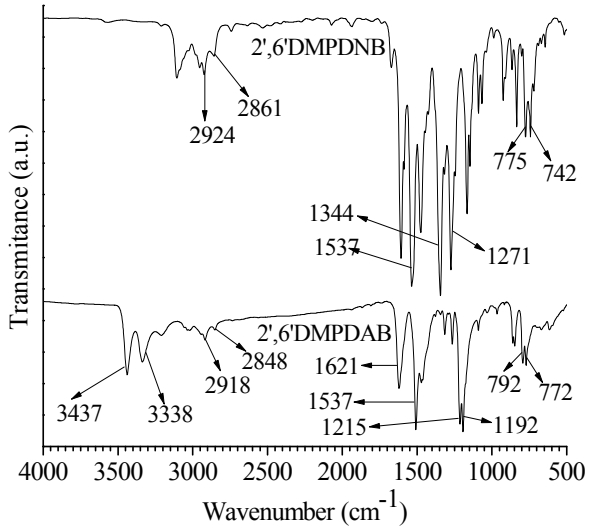

Figure 2.13 FT-IR spectra of 2′,6′DMPDNB and 2′,6′DMPDAB

The FT-IR spectra of the 2′6′DMPDNB and 2′6′DMPDAB are shown in Figure 2.13. The band observed at 3108 cm^{-1} in 2′6′DMPDNB was due to the aromatic –C–H stretching. Bands at 2861 and 2924 cm^{-1} were due to the symmetric and asymmetric stretching of two $–CH_3$ groups. The band displayed at 1607 and 1477 cm^{-1} were due to the –C=C– aromatic stretching. The strong band at 1271 cm^{-1} was due to C–O–C stretching. Two sharp shoulder peaks at 775 and 742 cm^{-1} could be ascribed to the presence of ortho substitution in benzene ring. Bands appearing at 1537 and 1344 cm^{-1} were corresponding to the asymmetric and symmetric $–NO_2$ stretching, which subsequently disappeared in the respective diamine (2′6′DMPDAB) after hydrogenation, confirming complete reduction. In addition, the asymmetric and symmetric stretching of primary aromatic amine occurred at 3437 and 3338 cm^{-1}. In 2′6′DMPDAB, N–H bending was observed at 1621 cm^{-1}. The sharp bands appearing at 1215 and 1192 cm^{-1} were due to the C–N and C–O–C stretching, respectively. The bands at 2918 and 2848 cm^{-1} informed the presence of methyl groups. Two sharp shoulder peaks at 792 and 772 cm^{-1} could be ascribed to the presence of *ortho* substitution in benzene ring.

The ^1H NMR spectra of 2′6′DMPDNB and 2′6′DMPDAB are shown in the Figure 2.14 and Figure 2.15, respectively. In 2′,6′DMPDNB, aromatic protons were observed in the range of 6.70-8.86 ppm, while for 2′,6′DMPDAB, they were located in the range of 5.88-7.05 ppm with expected multiplicity and integration. It was noticed that, among all the dinitro precursors as well as diamines, proton H_c in 2′,6′DMPDNB and 2′,6′DMPDAB had acquired the most upfield region. The donating effect of dimethyl substituted phenoxy moiety was responsible for this effect. Elemental analysis indicated good match between experimental and theoretically calculated values.

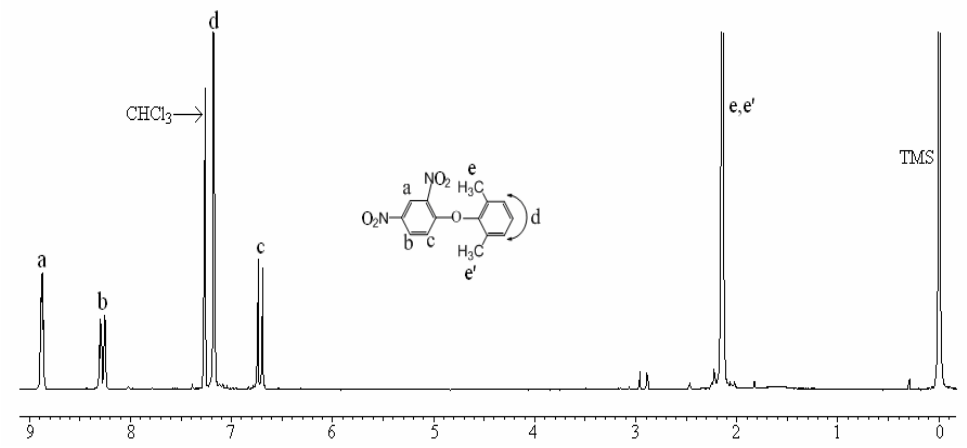

Figure 2.14 ^{1}H NMR spectrum of 2′,6′DMPDNB

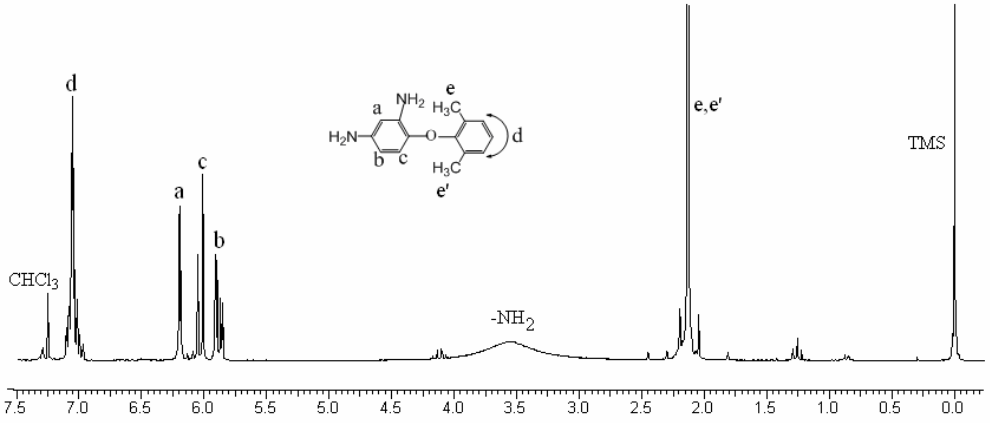

Figure 2.15 ^{1}H NMR spectrum of 2′,6′DMPDAB

2.3.2.4 Synthesis and characterization of 4′tBPDNB and 4′tBPDAB

Both 4′*t*BPDNB and 4′*t*BPDAB were obtained in good yield (Section 2.2.4). Due to low solubility of *t*-butyl phenol and 4′*t*BPDNB, the quantity of solvent required for the reaction was higher. 4′*t*BPDNB was obtained as needle shaped yellowish crystals on crystallization from methanol, while 4′*t*BPDAB was crystallized from water: methanol (1:1) mixture as silver shining crystals. Elemental analysis of both the compounds matched well with calculated values.

The FT-IR spectra of the 4′*t*BPDNB and 4′*t*BPDAB are shown in Figure 2.16. In 4'*t*BPDNB, the aromatic C–H stretching was observed at 3110 cm^{-1}. Sharp bands at 2965 and 2872 cm^{-1} were due to the asymmetric and symmetric C–H stretching of *t*-butyl

group, respectively. The aromatic –C=C– stretching band was observed at 1610 cm^{-1}. The strong band of C–O–C stretching was observed at 1272 cm^{-1}. The asymmetric and symmetric $–NO_2$ stretching was observed at 1540 and 1345 cm^{-1}, respectively. The sharp and strong band at 835 cm^{-1} indicated the presence of *para* substitution in 4′*t*BPDNB.

In 4′*t*BPDAB, appearance of bands at 3367 and 3417 cm^{-1} was due to asymmetric and symmetric –N–H stretching, respectively (Figure 2.16). The appearance of –N–H bending at 1619 cm^{-1} and disappearance of $–NO_2$ stretching peaks (1540 and 1345 cm^{-1}) revealed the complete hydrogenation of dinitro precursor to diamine. The sharp bands appearing in the spectra of 4′*t*BPDAB at 1235 and 1212 cm^{-1} were due to the C–N and C–O–C stretching, respectively. The intense asymmetric and symmetric C–H stretching corresponding to *t*-butyl group were detected at 2960 and 2867 cm^{-1}. The band at 3039 cm^{-1} was due to the aromatic C–H stretching. The strong peak at 838 cm^{-1} was attributable to the presence of *para*-substitution in 4′*t*BPDAB.

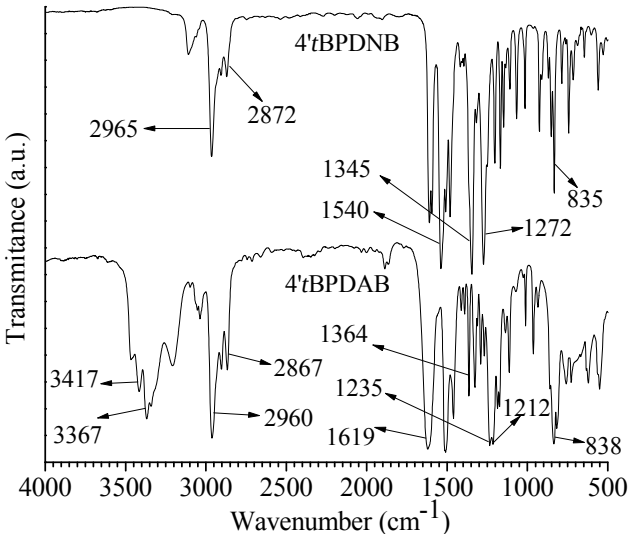

Figure 2.16 FT-IR spectra of 4′*t*BPDNB and 4′*t*BPDAB

The ^{1}H NMR spectra of 4′*t*BPDNB and 4′*t*BPDAB are shown in the Figure 2.17 and 2.18, respectively. The placement of aromatic protons was observed to be similar with that of 4′MPDNB and 4′MPDAB. In 4′*t*BPDNB, aromatic protons were observed in the range of 7.05-8.82 ppm while that of 4′*t*BPDAB was in the range of 6.05-7.27 ppm with expected multiplicity and integration. Protons of *t*-butyl group were shifted to

upfield region at ~ 1.3-1.35 ppm than that of methyl at ~ 2.3-2.35 ppm in 2′MPDAB and 4′MPDAB. This was obvious as methyl group was attached to the more electron withdrawing sp^2 hybridized carbon of benzene ring in 4′MPDNB and 4′MPDAB, while they were attached to the sp^3 hybridized carbon of *t*-butyl group in 4′*t*BPDNB. The broad shaped peak at 3.65 ppm was due to the $–NH_2$ group.

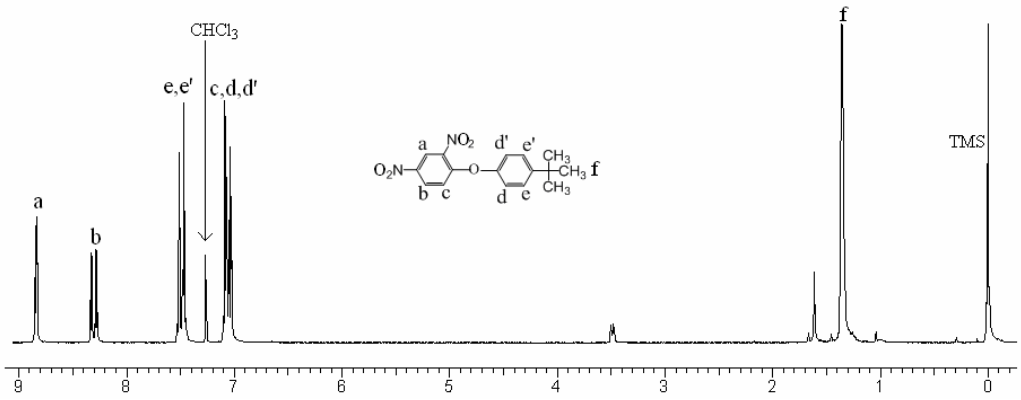

Figure 2.17 ^{1}H NMR spectrum of 4′*t*BPDNB

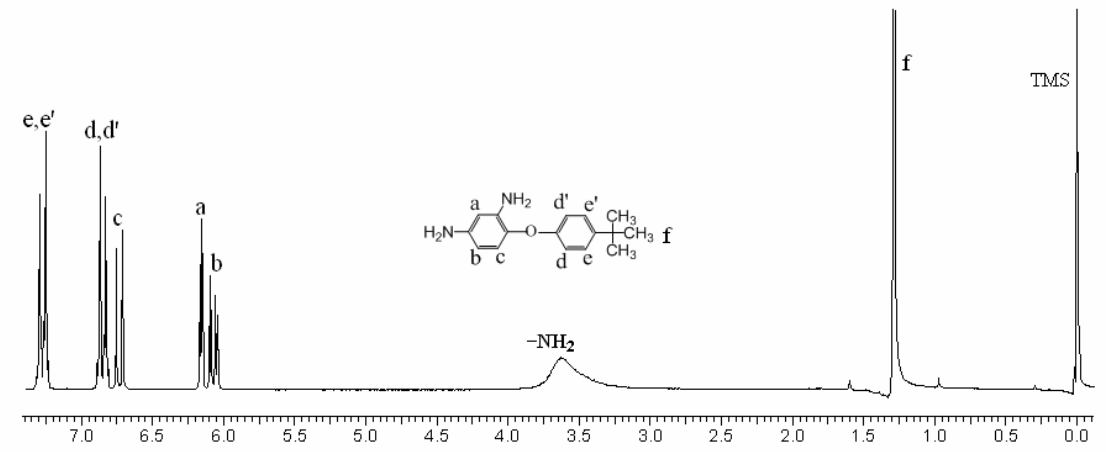

Figure 2.18 ^{1}H NMR spectrum of 4′*t*BPDAB

Thus, the elemental analysis, FT-IR and ^{1}H NMR spectral analysis confirmed the expected structures of all diamines as well as their intermediate dinitro compounds.

2.4 Conclusions

1. Various diamines, namely, 1-phenoxy-2,4-diaminobenzene (PDAB), 4'-sulphonic-1-phenoxy-2,4-diaminobenzene (SPDAB), 4'-methyl-1-phenoxy-2,4-diaminobenzene (4'MPDAB), 2'-methyl-1-phenoxy-2,4-diaminobenzene (2'MPDAB), 2',6'-dimethyl-1-phenoxy-2,4-diaminobenzene (2',6'DMPDAB) and 4'-*t*-butyl-1-phenoxy-2,4-diaminobenzene (4'*t*BPDAB) were synthesized by simple condensation reaction. These were designed with specifically aiming application of PIs based on them; either as PEM or gas separation membrane materials.
2. The reaction pathway for the synthesis of these diamines was same, wherein first step was etherification followed by reduction of $-NO_2$ group to $-NH_2$ using H_2 Pd/C.
3. Simple, cheap and easily available phenols were successfully utilized for the synthesis of these novel diamines.
4. Condensation of *para*-substituted phenols with CDNB could be carried out at low temperature using acetone as the solvent and TEA as an acid acceptor. The *ortho*-substituted phenols required high temperature and these reactions were conducted in DMF using K_2CO_3 as the base.
5. The duration of etherification reactions was longer in the case of organic base (TEA), as compared to the inorganic base (K_2CO_3).
6. Synthesis of all the monomers were architectured in such a fashion that the resultant diamine would be placed at *meta*-position to each other and simultaneously possess phenoxy ring at 4-position.
7. All the monomers, except SPDAB could be easily crystallized.
8. Melting point of the dinitro precursors was in the order PDNB < 2'MPDNB ≈ 4'MPDNB < 4'*t*BPDNB. In case of the diamines, the following order of increasing *Mp* was observed: SPDAB > 2',6'DMPDAB > 4'*t*BPDAB > 2'MPDAB > 4'MPDAB ≈ PDAB.
9. The monomers as well as their dinitro precursors were characterized by FT-IR and ^{1}H NMR, elemental analysis and melting point determination. The FT-IR and ^{1}H NMR confirmed their structures, while elemental analysis and melting point conveyed their good purity.

Chapter 3

Polyimide synthesis and their characterization

3.1 Introduction

Aromatic polyimides (PI) represent a major class of high performance polymers with excellent thermal, chemical, mechanical, dielectric properties and good permeation. Some of their important application areas include alignment layers for liquid crystal display devices, interlayer dielectrics for semiconductor devices, membrane material for gas separation, proton exchange membrane for fuel cell (PEMFC) applications, etc. However, difficulty in their processing due to the strong interchain attractions is an issue. Therefore, industrious efforts are devoted to synthesize processable PIs.

Attempts to understand the structure-property relationship in polyimides by systematically changing the diamine and dianhydride moiety have been numerous. As a result of these studies, several criteria have been proposed to obtain polyimides with improved solubility. These include (1) introduction of aliphatic or other kinds of flexible linkages that reduce chain stiffness, (2) introduction of bulky side chain substituents, which help in the separation of the polymer chains and hinder molecular packing and crystallization, (3) use of enlarged monomers containing angular bonds, which suppress coplanar structures, (4) use of 1,3-substituted instead of 1,4-substituted monomers, which lower regularity and molecular ordering and (5) copolymerization of two or more diamines or dianhydrides (de Abajo, 1999).

The incorporation of ether groups or other flexible linkages into the main chain generally leads to an improvement in solubility (de Abajo, 1999; Liaw, 2001), whereas the glass transition temperatures (T_g) and thermal stability are lowered significantly (Tamai, 1996). On the other hand, introduction of bulky groups into the polymer main chain or the attachment of bulky pendant groups like phenyl along the backbone helps in retaining the thermal properties, while providing a good solubility due to decrease in packing density and crystallinity (Jeong, 1994; Liou, 1998). Pendant ether and thio groups are also known to improve the solubility (Kakimoto, 1988). Incorporation of *meta*-linkages with pendant aromatic ring can significantly improve the solubility of

polyimides (Tsuda, 2000). It was expected that suitable combination of these structural modifications would minimize the trade off between the processability and thermal properties of aromatic polyimides and provide PI with desired properties for specific application.

The objective of this thesis was to synthesize polyimides based on phenyl ether substituted *meta*-phenylene diamines and assessment of their performance, both as gas permeation and proton exchange membrane (PEM) materials. With this as an aim, present chapter describes synthesis of various PIs based on systematically designed monomers as described in Chapter 2. It also describes blending of sulfonated polyimide (SPI) with polybenzimidazoles (PBI) with specific aim of using acid-base blend membranes as PEM materials.

3.2 Materials

Monomers with defined structural variations, viz.; 1-phenoxy-2,4-diaminobenzene (PDAB), 4′-sulphonic-1-phenoxy-2,4-diaminobenzene (SPDAB), 4′-methyl-1-phenoxy-2,4-diaminobenzene (4′MPDAB), 2′-methyl-1-phenoxy-2,4-diaminobenzene (2′MPDAB), 2′,6′-dimethyl-1-phenoxy-2,4-diaminobenzene (2′,6′DMPDAB) and 4′-*t*-butyl-1-phenoxy-2,4-diaminobenzene (4′*t*BPDAB) were synthesized as described in the experimental section of Chapter 2. Select dianhydrides, monomers and reagents viz.; 4,4′-Oxydiphthalic dianhydride (ODPA), 3,3′,4,4′-biphenyltetracorboxylic dianhydride (BPDA), 3,3′,4,4′-benzophenone tetracarboxylic dianhydride (BTDA), 4,4′-(hexafluoroisopropylidene)diphthalic anhydride (6FDA), pyrromellitic dianhydride (PMDA), 1,4,5,8-naphthalene tetracarboxylic dianhydride (NTDA), 4,4′-oxydianiline (ODA), 3,3′-diaminobenzedine (DAB), isophthalic acid (IPA), 5-*tert*-butyl isophthalic acid (BuI) and imidazole were purchased from Aldrich chemicals, USA. All dianhydrides and a diamine, ODA were purified by sublimation prior to use. *m*-Cresol was procured form S.D. Fine Chemicals, (India) and vacuum distilled prior to use. Other solvents viz., chloroform ($CHCl_3$), *sym*-tetrachloroethane (TCE), methanol, acetone, *N,N*-dimethylacetamide (DMAc), *N,N*-dimethylformamide (DMF), dimethyl sulfoxide (DMSO), nitrobenzene (Nitro-Bz), triethylamine (TEA), benzoic acid, *N*-methyl-*2*-pyrrolidone (NMP), conc. sulfuric acid (H_2SO_4), conc.

hydrochloric acid (HCl), polyphosphoric acid (PPA), *ortho*-phophoric acid (H_3PO_4) and tetrahydrofuran (THF) (all AR grade) were procured from S.D. Fine Chemicals, (India) and used as received. Ultra-pure water was obtained from a Millipore Milli-Q water purification system.

3.3 Polymer Synthesis

Syntheses of polymers are categorized into three sections, depending on the diamine used.

(I) Polyimides (PIs) and copolyimides (CPIs) based on 1-phenoxy-2,4-diaminobenzene (PDAB) with various dianhydrides,

(II) Sulfonated polyimides (SPIs) based on SPDAB with two select dianhydrides, NTDA and ODPA; their blend membranes with PBIs,

(III) Polyimides based on alkyl substituted phenoxy diamines (2'MPDAB, 4'MPDAB, 4'*t*BPDAB and 2',6'DMPDAB).

3.3.1 Polyimides (PIs) and copolyimides (CPIs) based on PDAB

3.3.1.1 Synthesis of PIs

Polyimides based on PDAB with various dianhydrides were synthesized by one step polymerization process as shown in Scheme 3.1.

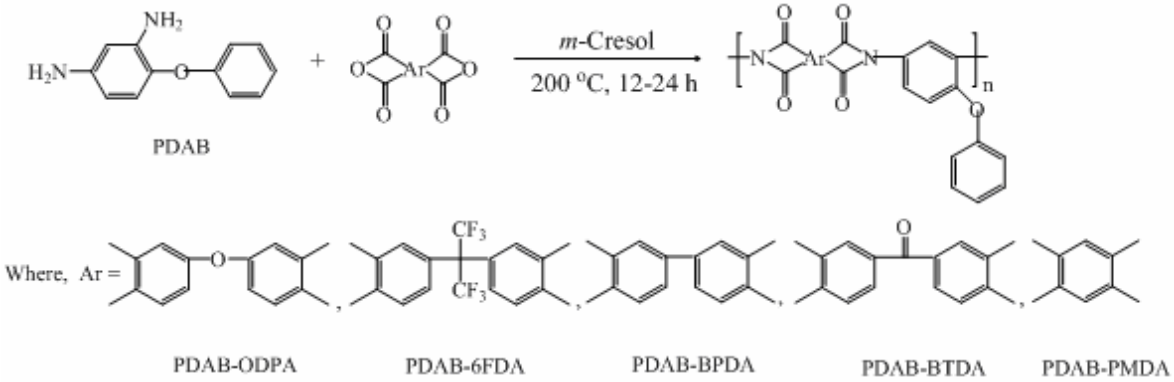

Scheme 3.1 Synthetic route to PDAB based PIs

A 50 mL three necked round bottom flask, equipped with a mechanical stirrer, N_2 gas inlet and a guard tube was charged with 2.002 gm (0.01 mol) of PDAB and 10 mL of *m*-cresol. This mixture was stirred for 15 minutes under a stream of N_2 at room

temperature to dissolve the diamine. To the formed solution, 0.01 mol of dianhydride and 15 mL of *m*-cresol were added. The temperature was raised to 200 °C and maintained for 12-24 h, depending on the dianhydride used. Water formed during the imidization was removed continuously with a stream of N_2. The resultant viscous solution was cooled and poured into 300 mL of stirred methanol to precipitate the polymer. It was filtered, washed several times with methanol and dried at 100 °C for 24 h. The polymer was further purified by dissolution in either TCE or DMAc, followed by precipitation in methanol. After filtration, it was dried at 60 °C under vacuum for a week. Abbreviation for polymer synthesized (Scheme 3.1) is based on the monomer abbreviation as used in Chapter 2. The polymer synthesized from oxydianiline (ODA) and 4,4′-oxydiphthalic dianhydride (ODPA) is abbreviated as ODA-ODPA.

Copolyimides based on the mixture of diamines, PDAB and ODA in a ratio of 5:95, 25:75 and 50:50 with ODPA were prepared using similar procedure described above. The polymer designation is given in Scheme 3.2 below.

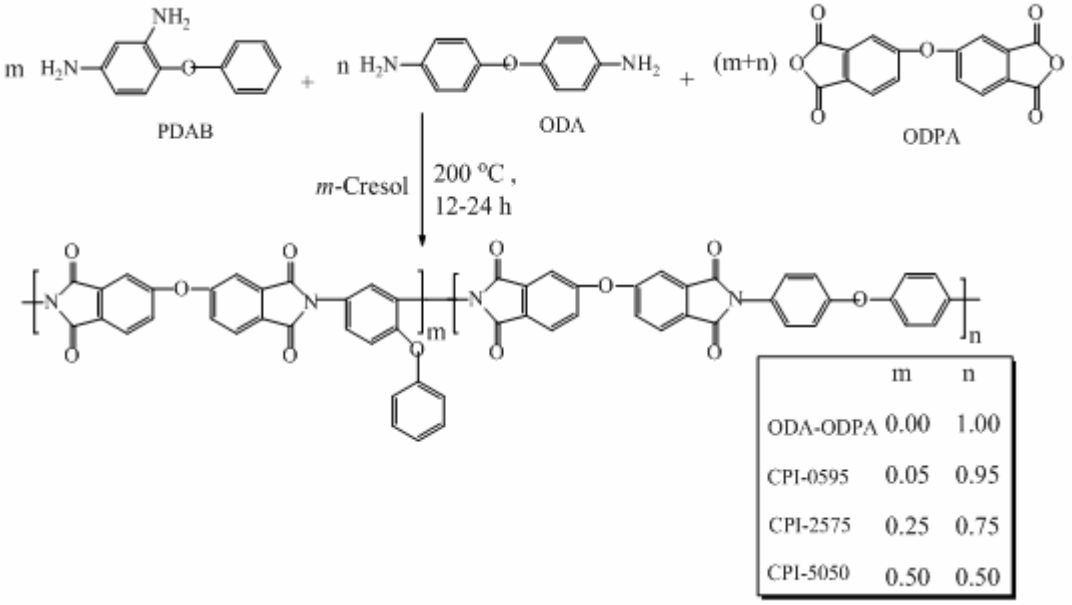

	m	n
ODA-ODPA	0.00	1.00
CPI-0595	0.05	0.95
CPI-2575	0.25	0.75
CPI-5050	0.50	0.50

Scheme 3.2 Synthetic route to copolyimides

3.3.1.2 Preparation of dense membrane

The dense membranes of PDAB-ODPA were prepared by casting its 3 wt % tetrachloroethane (TCE) solution at 60 °C on a flat glass surface under dry atmosphere. Though, it is soluble in chloroform, TCE was used as the solvent for membrane casting

since those prepared with chloroform as the solvent exhibited wavy surface. The TCE casted membrane was transparent and tough in nature. In the case of PDAB-6FDA based membrane preparation, the solvent used was chloroform and casting was done at 40 °C. For all the remaining polyimides and copolyimides (PDAB-BPDA, PDAB-BTDA, CPI-0595, CPI-2575, CPI-5050) dense membranes were prepared using their DMAc solution and casting was done at 80 °C. After initial evaporation of the solvent, formed film was peeled off and dried in a vacuum oven at 60 °C for 1 week in order to remove residual solvent. In case of membranes casted from DMAc, vacuum oven temperature was 80 °C. The complete removal of solvent was confirmed by DSC.

3.3.2 Sulfonated polyimides (SPIs) based on SPDAB

3.3.2.1 Synthesis of SPI

SPIs based on SPDAB with two different dianhydrides, NTDA and ODPA, were prepared as follows (Scheme 3.3).

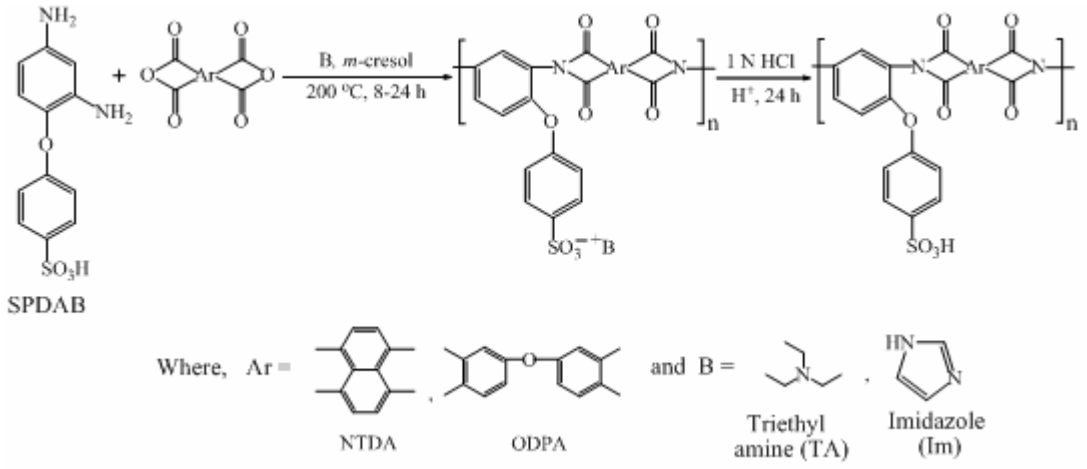

Scheme 3.3 Schematic presentation for the synthesis of sulfonated polyimides (SPIs)

To a 50 mL three-necked round bottom flask equipped with a mechanical stirrer, N_2 gas inlet and a guard tube, were added 1.4 g (5.0 mmol) of 4'-sulphonic-1-phenoxy-2,4-diaminobenzene (SPDAB), 10.0 mL of *m*-cresol and 0.6 g (6.0 mmol) of TEA or 0.408 gm (6.0 mmol) of imidazole while stirring. After SPDAB was completely dissolved, 1.34 g (5.0 mmol) of NTDA and 0.866 g (7.1 mmol) of benzoic acid were

added, followed by addition of 15 mL of *m*-cresol at ambient under N_2 atmosphere. The mixture was heated gradually to 200 °C and stirred further at this temperature for 8 h, in case of imidazole as the base, or 24 h in case of TEA as the base. Water formed during the imidization was continuously removed with a stream of N_2. The resultant viscous solution was cooled to ambient and poured onto stirred acetone. In case of use of imidazole as the base, the solution became highly viscous within 8 h at 200 °C. Hence, additional 18 mL of *m*-cresol was added and then precipitated. Obtained fibrous polymer was stirred in an excess of acetone to remove *m*-cresol, followed by drying at 80 °C in the vacuum oven for a day. After drying, polymer was further purified by dissolving in DMAc and re-precipitating in acetone. The purified SPI was dried at 80 °C in vacuum oven for 3 days. The polymer obtained using triethyl amine as the base is designated as SPDAB•TA-N; while polymer synthesized with imidazole as the base is designated as SPDAB•Im-N.

Similar procedure was followed for the synthesis of SPI based on ODPA and SPDAB. In this case, only TEA was used as the base. Polymerization was carried out for 24 h. This polymer was abbreviated as SPDAB•TA-O.

3.3.2.2 Synthesis of polybenzimidazoles (PBIs)

Polybenzimidazoles used for blending with sulfonated PIs were synthesized as follows (Scheme 3.4).

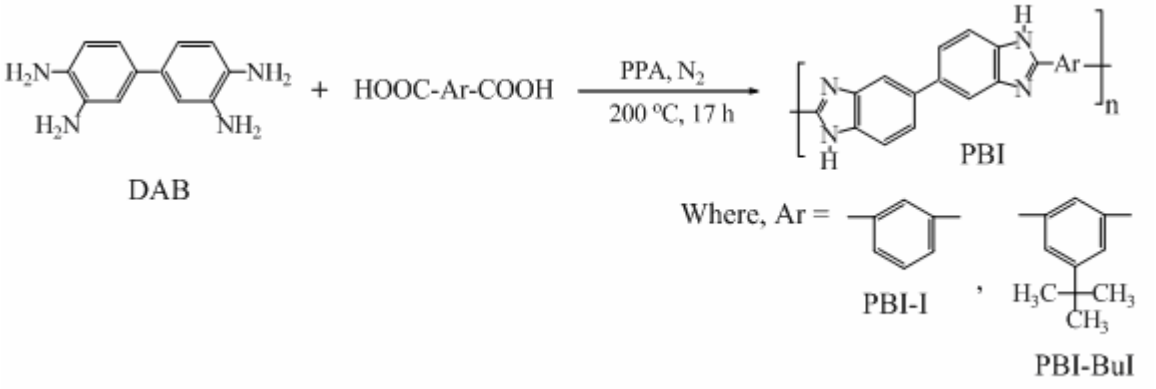

Scheme 3.4 Synthetic scheme to Polybenzimidazoles

Polybenzimidazoles were synthesized by solution polycondensation method using PPA, which acts as a solvent as well as condensation agent (Iwakura, 1964; Saegusa, 1997). Typically, a 250 mL three-necked flask equipped with a mechanical stirrer, N_2 inlet and $CaCl_2$ drying tube was charged with 60 g of PPA and 2 g (0.0093 mol) of DAB and temperature was raised to 140 ºC. After complete dissolution, 0.0093 mol of dicarboxylic acid (isophthalic acid or 5-*tert*-butyl isophthalic acid) was added and the temperature was slowly raised to 170 ºC and maintained for 5 h under constant flow of nitrogen. The temperature was further raised to 200 ºC and maintained for 12 h. After completion of the reaction, temperature was lowered and the reaction mixture was poured into the stirred water. The precipitated polymer was crushed and thoroughly washed with water till it was neutral to *pH*. The polymer was then kept overnight in 10% aqueous Na_2CO_3 for 24 h, washed with water until neutral to *pH* and soaked in acetone for 16 h to extract water. The dried polymer (100 ºC, 3 days) was further purified by dissolving in DMAc, removing undissolved material, if any, by centrifugation at 3000 rpm for 3 h and reprecipitation from stirred water. The polymer was finally dried at 60 °C for 24 h and then in vacuum oven at 100 °C for 3 days. The polymer based on isophthalic acid is designated as PBI-I; while the one based on *t*-butyl isophthalic acid is designated as PBI-BuI.

3.3.2.3 Preparation of dense membrane based on sulfonated PIs and their proton exchange

Dense membranes of the SPIs in salt form (SPDAB•TA-N, SPDAB•Im-N and SPDAB•TA-O) were prepared by casting their DMAc solutions (~ 3 wt %) on a flat glass surface, under dry conditions at 80 °C for 24 h. The formed film was peeled off and soaked in deioinised water for a day at 60 °C and then vacuum dried at 60 °C for a week. In this way, dense membranes with average thickness of 40 μm and 120 μm were prepared for the gas permeation and proton conductivity measurements, respectively. To measure proton conductivity, proton exchange treatment was done by immersing these membranes into 1 N hydrochloric acid solution for a day, followed by thorough washing with deionised water. The proton exchanged membranes based on SPDAB•TA-N, SPDAB•Im-N and SPDAB•TA-O were abbreviated as $SPDAB_I$-N, $SPDAB_{II}$-N and

SPDAB-O, respectively. Thus, after HCl treatment, these membranes are in sulfonic acid form.

3.3.2.4 Preparation of dense membrane based on PBIs

Dense membranes were prepared by solution casting method under identical conditions using 3% (w/v) polymer solution in DMAc. The solution was prepared by stirring at 80 °C for 14–18 h under dry atmosphere. The solution after centrifugation at 3000 rpm (to remove undissolved particles, if any) was poured on to the flat glass surface and heated at 80 °C for ~18 h under inert atmosphere. Formed film was peeled off and soaked in water at 60 °C for 3 days in order to remove traces of DMAc. Such films were finally dried in vacuum oven at 100 °C for a week and used for subsequent analysis.

3.3.2.5 Preparation of blend membranes based on SPI and PBI

SPI-PBI blend membranes were prepared in their, 30:70, 40:60, 50:50 weight ratio. The blend membranes based on PBI-I were found to disintegrate and were not pursued further. PBI-BuI was dissolved in DMAc by stirring at 80 °C for 10 h while SPDAB•TA-N was dissolved in DMAc by stirring at ambient for 2 h. SPI solution was subsequently added to the DMAc solution of PBI-BuI at 60 °C and stirred for 1 h. The dense blend membranes were obtained by casting this mixed solution at 80 °C on a flat glass surface under dry atmosphere for 24 h in an oven. Formed film was peeled off and dried in a vacuum oven at 80 °C for 3 days in order to remove residual solvent. The average thickness of membranes for proton conductivity measurement was ≈120 μm and for the gas permeation analysis, it was 40 μm. The blend membrane constituting SPI in triethylammonium salt form was subsequently converted sulfonic acid form by immersing it in 1 N HCl for 48 h at ambient conditions. On the other hand, membranes based on PBI-BuI were quite stable and maintained their integrity. The membranes thus obtained in the sulfonic acid form were thoroughly washed with deionised water, followed by soaking in water for 24 h. These membranes were kept in a vacuum oven at 80 °C for three days. The membranes were again kept in the deionised water for 24 h prior to their proton conductivity measurements.

3.3.3 Polyimides based on alkyl substituted phenoxy diamines

3.3.3.1 Synthesis of polymers

The synthetic route to these PIs is as shown below in Scheme 3.5. The abbreviations for polymers are based on monomers used.

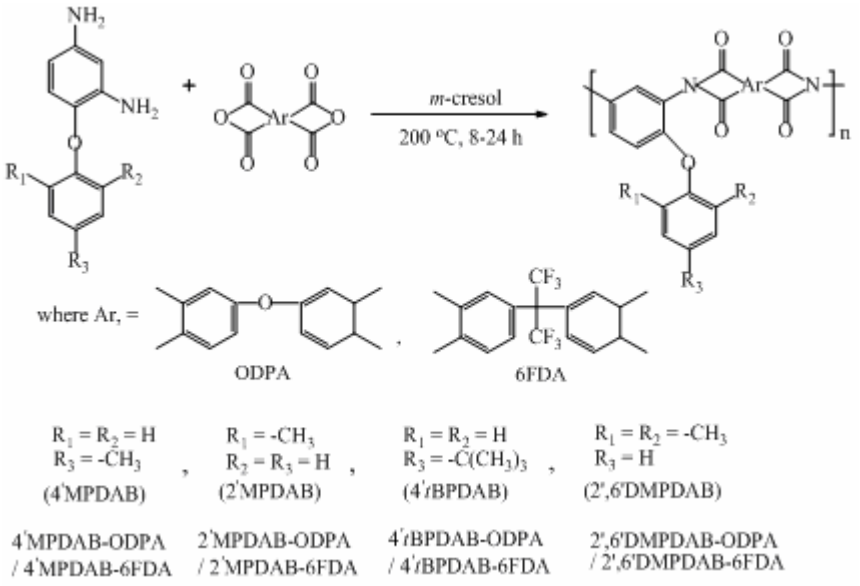

Scheme 3.5 Synthetic route to PIs based on alkyl substituted phenoxy diamines

Polyimides (PIs) based on alkyl substituted phenoxy diamines (2'MPDAB, 4'MPDAB, 4'*t*BPDAB and 2',6'DMPDAB) were prepared by the single step solution polycondensation in *m*-cresol. Typically, 0.01 mol of alkyl substituted diamine and 10 mL of *m*-cresol were added to a 50 mL three-necked round bottom flask equipped with a mechanical stirrer, N_2 gas inlet and a guard tube. This solution was stirred for 15-20 minutes under a stream of N_2 at ambient condition to dissolve the diamine. To this solution 0.01 mol of dianhydride (either ODPA or 6FDA) was added, followed by the addition of 10 mL *m*-cresol. The temperature was raised gradually to 200 °C and maintained for 8-24 h. For 2',6'DMPDAB-based polyimides, highly viscous solution was formed within 8 h. Hence, 20 mL of *m*-cresol was added before precipitating in methanol. While in case of other polyimides, it took 15-24 h to complete the polymerization. This was also dependant on the dianhydride used. Between ODPA and 6FDA reacted with the same diamine, the former took lesser time than the latter for the polymerization. Water

formed during the imidization was removed continuously with a stream of N_2. The resulting polymer solution was cooled and poured onto 500 ml of stirred methanol. The precipitated polymer was washed several times with methanol and dried at 80 °C for a day in vacuum oven. It was further purified by dissolving in chlorinated solvents (ODPA-based PI in TCE and 6FDA-based PI in chloroform), reprecipitating in methanol and finally drying in vacuum oven at 60 °C for a week in order to ensure complete removal of the solvent.

3.3.3.2 Preparation of dense membranes

The dense membranes of polyimides based on ODPA were prepared by solution casting from 3 wt % *sym*-tetrachloroethane (TCE) solution at 70 °C on a flat glass surface under dry atmosphere. In case of polyimides based on 6FDA, the solvent used was chloroform and the membrane preparation was done at 40 °C. After initial evaporation of the solvent, formed film was peeled off and dried in a vacuum oven at 70 °C for a week in order to remove residual solvent. Absence of solvent was confirmed by DSC.

3.4 Characterization of polymers

Elemental analysis of polymers was obtained using Elementar Vario-EL (Germany). The IR spectra were recorded on a Perkin Elmer 16 PC FT-IR spectrophotometer. Inherent viscosity of PDAB based PIs was determined at 0.5 $g.dL^{-1}$ concentration in DMF (ODA-ODPA in *m*-cresol and CPI-0595 in TCE) at 35 °C (± 0.2 °C) using an Ubbelohde viscometer. Intrinsic viscosity [η] of polyimides based on alkyl substituted phenoxy diamines was determined in TCE at 35 °C. The inherent as well as reduced viscosity of the SPIs was measured under isothermal condition at 35 °C in the thermostat in DMAc with varying concentrations. Inherent viscosity of PBI-I and PBI-BuI was determined using conc. H_2SO_4 solution (0.2 $g.dL^{-1}$). Efflux time of the dilute polymer solutions and the pure solvent was recorded by a digital timer (Q&Q, Japan CBM Corp., Japan) having a least count of 1 milisecond. Time measurements were continued till three consistent readings were obtained and then averaged. Solubility of PIs in various solvents was determined with 0.5 % (w/v) concentration. Thermogravimetric

analysis (TGA) was performed on Perkin Elmer TGA-7 (TA instruments, USA) in N_2 atmosphere at a heating rate of 10 °C. min^{-1}. The glass transition temperature (T_g) of all polymers was measured on DSC Q-10 (TA instruments, USA) in N_2 atmosphere at a heating rate of 10 °C. min^{-1}.

The density (ρ) of polyimides used for gas permeation was obtained in the film form by floatation method using aq. K_2CO_3 solution. Based on density measurement, solubility parameter [$\delta=(E_{coh}/ V_{sp})^{1/2}$] was estimated by the group contribution method (Van Kravelen, 1997), where V_{sp} is the specific free volume (ratio of the molecular weight of the repeat unit and measured density), V_o is the occupied volume calculated from the correlation $V_o = 1.3V_w$, (V_w is the Van der Waals volume calculated from Bondi's group contribution method). E_{coh} is the cohesive energy of the polymer and V_{sp} is the molar volume of the polymer. The wide-angle X-ray diffraction (WAXD) spectra of the dry membrane samples were obtained at ambient using Rigaku Dmax 2500 diffractometer (Tokyo, Japan). Samples were scanned in the 2θ range of 4-40° at the scan rate of 2°.min^{-1} with a Cu-Kα radiation source. The amorphous peak maxima on each X-ray scattering profile was ascribed to the average intersegmental distance of polymer chains, and the *d*-spacing was calculated by substitution of the scattering value (2θ) of the peak into the Bragg's equation, $n\lambda= 2d \sin(\theta)$, where, n=1 and λ=1.54 Å for Cu-Kα radiation.

3.5 Results and discussion

3.5.1 Synthesis and physical characterization of polyimides based on PDAB

3.5.1.1 Synthesis

New polyimides based on PDAB containing pendant phenoxy group with various aromatic dianhydrides, viz., ODPA, BTDA, BPDA, 6FDA and PMDA were prepared by one step high temperature solution polymerization in *m*-cresol, as described in the experimental Section 3.3.1.1. All the polymerization reactions proceeded homogeneously without gelation or precipitation, except for the PMDA based polyimide; which precipitated from the solution during polymerization. This could be probably due to the rigid and closed packed structure of PDAB-PMDA. It is known that PMDA based polyimides are rigid (de Abajo, 1999; Liu, 2005). The polymers were obtained by

pouring the resultant viscous polymer solution into methanol with vigorous stirring. The copolyimides of PDAB and ODA with ODPA containing 5, 25 and 50 mol % PDAB were synthesized with a similar procedure.

Dense membranes of these polymers, with varying thickness prepared by solution casting method and tough films were obtained. For FT-IR spectral analysis, dense membranes of relative lower thickness (~10 μm) were prepared. These polymers were characterized by elemental analysis, FT-IR spectroscopy, WAXD, viscosity measurement and thermal analysis as elaborated below.

3.5.1.2 Elemental analysis

The elemental analysis for polyimides based on PDAB is shown in the following Table 3.1. The observed values of elemental analysis were in good agreement with the calculated values, except for the PDAB-PMDA. Due to partial solubility of PDAB-PMDA at high concentration (> 2 wt%) even in DMF, it could not be purified. This could have resulted in larger difference in calculated and observed values of elemental analysis.

Table 3.1 Elemental analysis of PDAB based polyimides

Polymer abbreviation	Formula and molecular weight of chain repeat unit (CRU)		Element analysis		
			% C	% H	% N
PDAB-ODPA	$(C_{28}H_{14}N_2O_6)_n$ (474)	Calculated	70.89	2.95	5.90
		Observed	*70.59*	*3.49*	*5.57*
PDAB-6FDA	$(C_{31}H_{14}N_2O_5F_6)_n$ (608)	Calculated	71.18	2.30	4.60
		Observed	*72.05*	*2.72*	*4.07*
PDAB-BPDA	$(C_{28}H_{14}N_2O_5)_n$ (458)	Calculated	73.36	3.05	6.11
		Observed	*71.68*	*3.00*	*5.85*
PDAB-BTDA	$(C_{29}H_{14}N_2O_6)_n$ (486)	Calculated	71.60	2.88	5.76
		Observed	*71.49*	*3.60*	*4.80*
PDAB-PMDA	$(C_{22}H_{10}N_2O_5)_n$ (382)	Calculated	69.10	2.61	7.32
		Observed	*67.50*	*3.22*	*5.64*

3.5.1.3 Solubility and solution viscosity

The solubility of the PDAB based polyimides and copolyimides was determined at a 0.5% concentration in common organic solvents at the ambient temperature, as

shown in Table 3.2. Polyimides based on 6FDA and ODPA were soluble in many solvents, including chlorinated solvents. The high solubility of the 6FDA-based polyimides was attributed to the presence of the $–C(CF_3)_2–$ linkage, which is known to increase the free volume and decrease the intermolecular interaction between the polymer chains (Stern, 1989). Similarly, polyimides prepared from the ODPA dianhydride showed good solubility in polar aprotic solvents such as NMP, DMF, DMAc, nitrobenzene, *m*-cresol and chlorinated solvents. Polyimides based on BTDA (PDAB-BTDA) and BPDA (PDAB-BPDA) were soluble at the ambient temperature only in *m*-cresol and on heating in polar aprotic solvents such as DMF, DMAc and nitrobenzene, possibly because of their rigid structure. The polyimide based on PMDA (PDAB-PMDA) was soluble in DMF and *m*-cresol only on heating. The polyimide based on ODA and ODPA (ODA-ODPA) was insoluble in all solvents except *m*-cresol, and that too on heating. Thus, the solubility of ODA- and ODPA-based polyimides could be enhanced by the incorporation of PDAB as evidenced by the good solubility of the copolyimides in many solvents. All these copolyimides were soluble in TCE at the ambient temperature. The presence of the pendant phenoxy group on asymmetrically (meta) linked PDAB could also be responsible for the better solubility observed for these polyimides. The pendant phenoxy group with a flexible ether linkage could disrupt the chain packing in the polymer backbone to ease solvent solubility.

The inherent viscosity of polyimides and copolyimides is given in Table 3.3. The inherent viscosities of PDAB-ODPA, PDAB-6FDA, PDAB-BTDA, PDAB-BPDA, CPI-2575, and CPI-5050 were measured in DMF, whereas the viscosities of ODA-ODPA and CPI-0595 were determined in *m*-cresol and TCE, respectively, as they were not soluble in DMF. The viscosities of the polyimides based on PDAB ranged from 0.33 to 0.48 $dL.g^{-1}$ for homopolyimides and from 0.38 to 1.16 $dL.g^{-1}$ for copolyimides (Table 3.3). The ODA (structural isomer of PDAB) based polyimide showed higher viscosity than the PDAB-based polyimide obtained from the same dianhydride (ODPA).

The lower viscosity exhibited by PDAB based PIs could be attributed to the relative lower basic character due to the *meta*-substituted amino groups and the steric hindrance created by the bulky substitution of phenoxy moiety, *ortho* to one of the amine groups. This phenomenon is supported by the fact that among *m*-, *o*- and *p*-PDA, *m*-PDA

has the highest oxidation potential. Thus, it has least tendency to loose an electron pair, resulting in lower basic character (Li, 2002). In PDAB, the electron donating ether group should enhance the basicity of amino groups and being located *ortho* and *para*- to amino groups, it's donating ability would be even more effective (Clayden, 2001). Such effect of enhanced basicity of aromatic diamine by electron donating ether linkage is well known (Yin, 2004). However, in PDAB, the increased basicity of amine group by electron donating ether linkage (Ar-O-Ar') should counteract by the steric hindrance of bulky phenoxy ring. At higher temperature, the feasibility of rotation of flexible phenoxy group would be more, creating steric hindrance towards its reactivity with dianhydride molecule. Thus, PDAB could be considered as the sterically hindered diamine, which is known to react slowly (Grubb, 1999). In contrast to PDAB, ODA has two amino-phenyl ring bridged by electron donating ether linkage (Ar-O-Ar'), which enhances basicity of amino groups. In addition, in ODA, there is no substitution to the *ortho* position of $-NH_2$ groups making it sterically free. It has also been reported in the literature that ODA has higher pK_a (5.20) than that of *m*PDA (4.80) (Zubkov, 1981). Thus, this may be one of the reasons for PI based on ODA exhibiting higher viscosity than PDAB, due to high basicity of ODA compared to PDAB.

Table 3.2 Solubility of PDAB based polyimides and copolyimides

Polymer	$CHCl_3$	DMF	DMSO	NMP	Nitro-Bz	*m*- Cresol	DMAc	THF	TCE
PDAB-ODPA	++	++	–	++	++	++	++	–	++
PDAB-6FDA	++	++	–	++	++	++	++	–	++
PDAB-BTDA	–	+	–	±	+	++	+	–	–
PDAB-BPDA	–	+	–	+	+	++	+	–	–
PDAB-PMDA	–	+	–	–	–	+	–	–	–
ODA-ODPA	–	–	–	–	–	+	–	–	–
CPI-0595	–	–	–	–	–	+	–	–	++
CPI-2575	+	+	–	±	–	+	+	–	++
CPI-5050	+	+	–	+	+	+	+	–	++

++: soluble at room temperature; +: soluble on heating at 80 °C; ±: partially soluble; –: insoluble.

3.5.1.4 FT-IR analysis

FT-IR spectra of polyimides are shown in Figure 3.1. The characteristic absorption bands of the 5 membered imide ring appeared at 1785 cm^{-1} and 1720 cm^{-1}. They correspond to asymmetric and symmetric C=O stretching, respectively. A band at 1350 cm^{-1} was due to C−N stretching. The imide ring deformations appeared at 1100 cm^{-1} and 720 cm^{-1}. A band at 1240 cm^{-1} was due to ether group of diamine. The complete imidization of polymers was confirmed by the absence of peaks at 1650, 1534, 1712 cm^{-1} (acid C=O) and 3250 cm^{-1} (N−H and O−H groups) of amic acid (Mathew, 2001).

Thus, elemental and FT-IR analysis confirm the formation of polyimides containing pendant phenoxy groups.

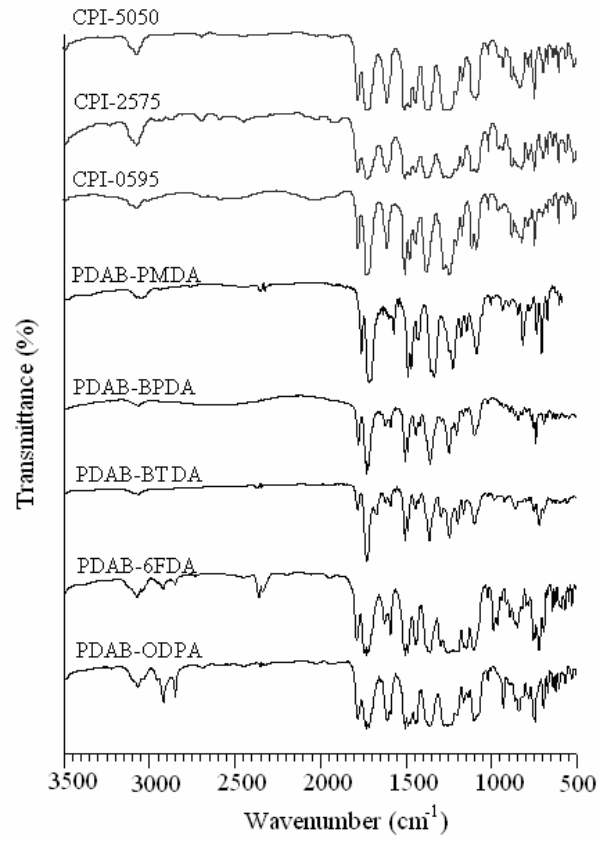

Figure 3.1 IR spectra of PDAB based PIs and CPIs

3.5.1.5 Thermal Properties of Polymers

High thermal stability is one of the important physical properties of PI. The thermal behavior of present PIs and copolyimides was studied by TGA and DSC. Results

are summarized in Table 3.3. The DSC curves of these polyimides are shown in Figure 3.2. All polyimides and copolyimides had a high T_g (> 248 °C). The increase in T_g generally corresponded to an increase in the rigidity of the dianhydride monomer like 6FDA.

Table 3.3 Physical properties of PDAB based polyimides and copolyimides

Polymer	Diamine	Dianhydride	η_{inh} ($dL.g^{-1}$)	T_g (°C)	IDT (°C)	T_{10} (°C)	Char yield (%)
PDAB-ODPA	PDAB	ODPA	0.47[a]	256	580	608	59.02
PDAB-6FDA	PDAB	6-FDA	0.43[a]	281	537	551	52.15
PDAB-BTDA	PDAB	BTDA	0.34[a]	264	553	584	59.76
PDAB-BPDA	PDAB	BPDA	0.32[a]	248	555	594	58.65
PDAB-PMDA	PDAB	PMDA	----	250	543	564	56.46
ODA-ODPA	ODA	ODPA	1.91[b]	269	576	618	55.00
CPI-0595	5% PDAB + 95%ODA	ODPA	0.38[c]	259	571	627	53.41
CPI-2575	25% PDAB + 75% ODA	ODPA	1.16[a]	272	606	622	56.14
CPI-5050	50% PDAB + 50% ODA	ODPA	0.57[a]	273	590	633	57.60

[a]: 0.5g/dL in DMAc at 35 °C, [b]: 0.5g/dL in *m*-Cresol at 35 °C, [c]: 0.5g/dL in TCE at 35 °C

It is evident that, bridging group (–O–, –C=O) between the two phenyl rings present in the dianhydrides like ODPA and BTDA, facilitating the bond rotation would decrease the T_g. Among these, all PDAB based polyimides with different dianhydrides, in particular the one based on 6FDA showed the highest T_g because of the polarizable hexafluoroisopropylidene group, which inhibited the molecular motions. It has also been reported that bulky $–C(CF_3)_2–$ linkage restricts the segmental mobility of the polymer

main chain (Stern, 1989). The T_g of copolyimides synthesized by addition of ODA to PDAB were marginally higher than T_g of the PDAB based homopolymer.

The TGA thermograms of the polyimides and copolyimides are shown in Figure 3.3. All synthesized polyimides showed an initial decomposition temperature (IDT) above 500 °C and T_{10} values in the range of 551-633 °C, thus exhibiting high thermal stability. However, among all the polyimides, the IDT of PDAB-6FDA was the lowest, despite the high C–F bond strength (441 kJ/mol) (Van Krevelen, 1997). It is known that the voluminous size of the CF_3 retards the free rotation around its own axis resulting in high torsional strain as well as gain in high conformational energy (Hougham, 1999; Yang, 2004c). It leads to the low thermal stability of CF_3 group, (Lee, 2006) which is lost in the form of a CF_3 radical (Yang, 2004c). Because of the strong electron affinity of F atom, the C-C bond energy in CF_3-C-CF_3 becomes lower (Ren, 2004). Hence, polymer with –$C(CF_3)_2$– linkage demonstrated low thermal stability, which was exhibited by the lowest weight residue of 6FDA-based polyimide in the series. All polyimides showed a char yield greater than 50 %.

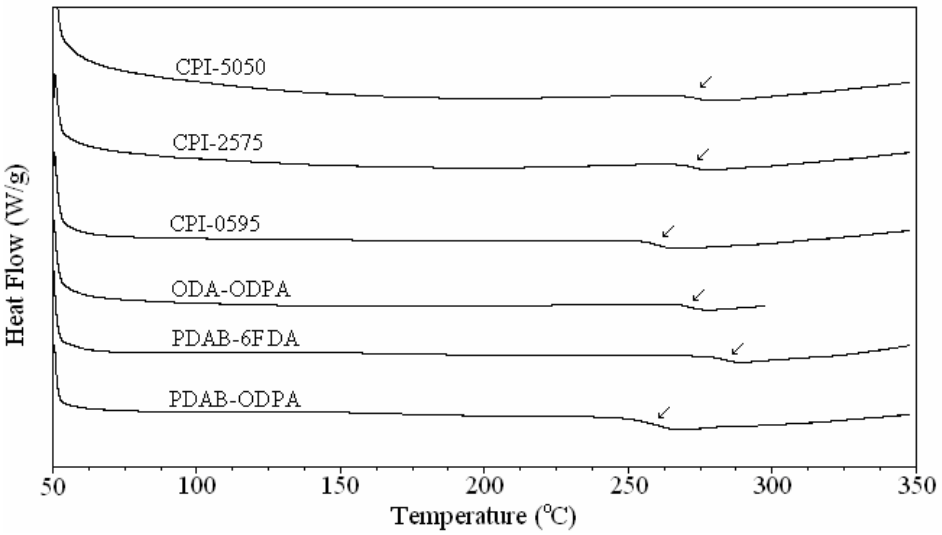

Figure 3.2 DSC of PDAB based polyimides and copolyimides

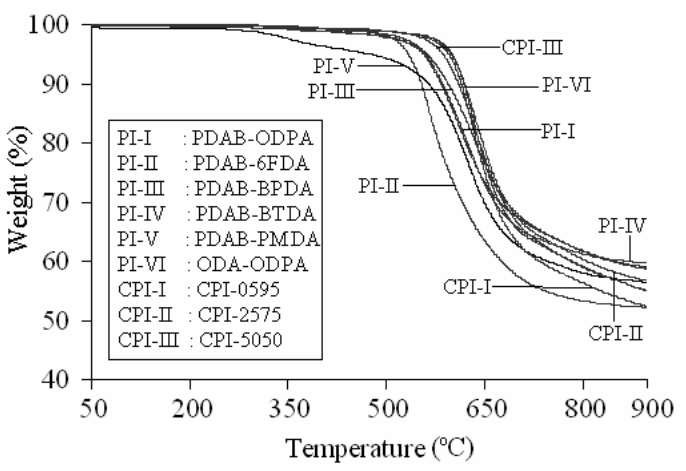

Figure 3.3 TGA of PDAB based PIs and CPIs

3.5.1.6 Wide-angle X-ray diffraction (WAXD)

Crystallinity in a polymer has significant effect on solubility, thermal behaviors and other properties of the polymers. WAXD patterns of present PIs revealed their complete amorphous nature (Figure 3.4). This observation was reasonable because the presence of the non-coplanar conformation of the 1-phenoxy-2,4-diamino benzene might have reduced the intermolecular forces between polymer chains. Amorphous nature of these polymers is also reflected in good solubility of these polymers in solvents. The high *d*-spacing value of PDAB-6FDA (5.82 Å) than that of PDAB-ODPA (4.23 Å) was due to the bulky nature of $–C(CF_3)_2–$ linkage, which could reduce the interchain interaction.

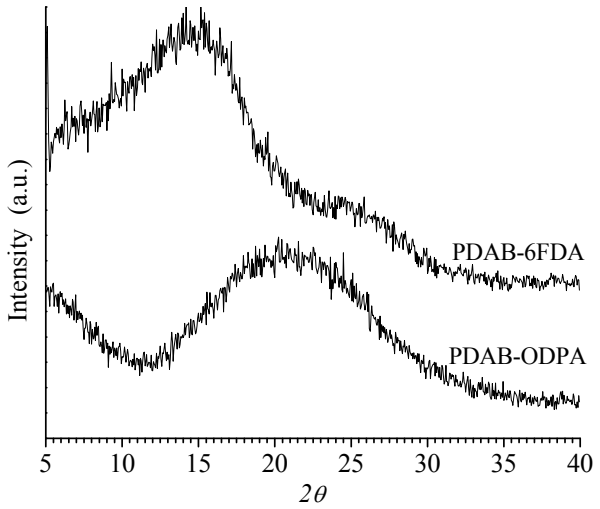

Figure 3.4 WAXD spectra of PDAB-ODPA and PDAB-6FDA

Thus, having confirmed the good solubility, film forming property and thermal stability of polyimides containing pendant phenoxy group based on PDAB, the study was further extended to look for possible application of these polymers as PEMFC by introducing $–SO_3H$ group in pendant phenoxy moiety. Most of the sulfonated polyimides (SPIs), studied as PEMFC bears $–SO_3H$ group in the main chain. Much work has not been reported on effect of $–SO_3H$ groups in flexible side chain of PI on performance of these polymers as polymer electrolytes in fuel cell. So, in the present work, we synthesized novel polyimides containing $–SO_3H$ groups in flexible pendant phenoxy in side chain, based on SPDAB.

Much work has also not been reported on effect of pendant phenoxy group in PI on gas permeability. Therefore study of PDAB based PIs was also extended for application of PIs in gas permeability field. In view of this, we decided to synthesize novel diamines in such a fashion that their resultant PIs would contain alkyl substituted phenoxy group as a side chain. So the present dissertation also comprises synthesis of novel PIs based on alkyl substituted pendant phenoxy group in view of investigations of these PIs towards gas permeability.

3.5.2 Synthesis and physical characterization of sulfonated polyimides (SPIs)

3.5.2.1 Synthesis

New SPIs containing pendant sulfophenoxy group were prepared by one step high temperature solution polycondensation of SPDAB and NTDA in *m*-cresol with benzoic acid as the catalyst. Protection of sulfonic acid group in SPDAB was done with two different organic bases; TEA and imidazole, separately, as described in the experimental Section 3.3.2.1. In presence of TEA as the base, all reactions proceeded homogeneously without gelation. Whereas, polymerization of SPDAB with NTDA by using imidazole as the base resulted in viscous solution within 8 h. This phenomenon could be attributed to the catalytic role of unreacted excess imidazole (1.2 moles of SPDAB), which is amphoteric in nature having pK_a 7.1 (Clayden, 2001; Lv, 2008).

Six-membered ring anhydride exhibits lower reactivity towards an amine group due to its strain free and hence more stable form than strained and more reactive five-membered ring analogues (Sek, 1992; Sek, 1995). Hence, use of catalyst becomes an

essential step for such dianhydrides in order to enhance their electrophilicity. It has also been reported that the addition of organic acids such as benzoic acid and organic heterocyclic base such as isoquinoline, quinoline or imidazole during polymerization increases viscosity of the PI (Sek, 1992). In the present condensation polymerization based on NTDA, benzoic acid was added along with both of the organic bases, TEA or imidazole. A short polymerization period of 8 h required for the polymerization with SPDAB in presence of imidazole, as compared to 24 h period in presence of TEA, infers catalytic activity of imidazole. The unreacted imidazole, remaining after salt formation with SPDAB (0.2 mole) can form the imidazole-amic acid derivative of NTDA. In this case, excess of imidazole first activates NTDA turning it to more electrophilic followed by nucleophilic attack of imidazolium salt of SPDAB forming amic-acid derivative. In other words, imidazole hydrolyzes six-membered anhydride moiety to imidazole-amic acid derivative, which reacts faster with SPDAB forming poly(amic-acid) in the first step. In this step imidazole is removed owing to its good leaving group capacity and thus, molecular weight could be built up by propagating poly(amic-acid) with regeneration of imidazole. Such condensation reactions of amide and imide formation from carboxylic acids and dianhydride with amine, promoted and catalyzed by imidazole, its derivative and carbonyl diimidazole (CDI) have been reported (Kingston, 1969; Jung, 1995; Baldwin, 1996; Eastmond, 2002). Jung *et al.* (1995, 1996) has reported the synthesis of polyimides with imidazole blocked isocyantes. Imidazole and its derivatives have been used as the catalyst for various condensation reactions like acetylation of carbohydrates (Tiwari, 2005), ester synthesis (Morton, 1988; Hirao, 2003; Hirose, 2003), peptide synthesis (Nakashima, 1987) and curing of an epoxide group (Klaren, 1973). Lin *et al.* (2006) prepared polybenzoxazines by using imidazole as the catalyst.

It should also be noted that, imidazole not only accelerates the poly(amic-acid) formation, but it can also further catalyze imide formation. The similar catalytic activity by benzimidazole has also been reported in the imidization of polyamic acids to polyimides (Nelson, 1988). It is reported that imide formation could be substantially enhanced with imidazole blocked isocynates (Wenzel, 1987; Helmer-Metzmann, 1989). Thus, rapid polymerization with increasing viscosity of SPDAB•Im-N in the polymerizing solvent (*m*-cresol) can be attributed to the catalytic role of imidazole.

Whereas, another base; TEA only neutralizes sulfonic acid group to enhance solubility of SPDAB in *m*-cresol, without any catalytic activity.

The polymer in fiber form was obtained by adding polymer solution in acetone. It could not be precipitated in methanol (conventional non-solvent for PI) properly from *m*-cresol solution (Mathew, 2001). It was observed that polymer solution of SPDAB•Im-N became too viscous to be precipitated in acetone at room temperature, even after pouring additional *m*-cresol, indicating formation of high molecular weight polymer.

Dense membranes of SPIs in salt form (triethylammonium sulfonate and imidazolium sulfonate) were prepared by casting their 3 wt% solution onto clean glass substrate at 80 °C for 24 h. These formed reddish (SPDAB•TA-N), dark greenish (SPDAB•Im-N) and faint greenish (SPDAB•TA-O) colored tough films on casting from their DMAc solution. Dense membrane of imidazolium sulfonate salt form (SPDAB•Im-N), possessed wavy nature. Membranes in their triethylammonium sulfonate (SPDAB•TA-N) as well as imidazolium sulfonate (SPDAB•Im-N) salt forms were converted to the corresponding $–SO_3H$ form ($SPDAB_I$-N and $SPDAB_{II}$-N, respectively) by immersing in 1N HCl for 24 h at ambient followed by soaking in deionised water for 24 h at ambient and then dried. In case of proton conductivity measurements, these membranes were equilibrated with water for at least 24 h at ambient, prior to measurements.

3.5.2.2 FT-IR analysis

The formation of SPI was confirmed by FT-IR spectroscopy (Figure 3.5). The presence of sulfonic acid moiety was confirmed by broad band around 1200-1250 cm^{-1}. Asymmetric and symmetric S=O stretching occurred at 1123 cm^{-1} and 1032 cm^{-1}, respectively; which showed maximum intensity due to more polar $–SO_3^-$ group in SPDAB•Im-N and SPDAB•TA-N than their respective sulfonic acid form ($SPDAB_I$-N and $SPDAB_{II}$-N) (Yin, 2004; Hu, 2006). The bands corresponding to carbonyl asymmetric and symmetric stretching of naphthalic based imides were observed at 1714 cm^{-1} and 1682 cm^{-1} (Li, 2008), while that of phthalic based imides at 1780 cm^{-1} and 1722 cm^{-1} (Genies, 2001b), respectively. The stretching and out of phase bending bands of

C−N−C of naphthalic based imides were observed at 1344 cm^{-1} and 768 cm^{-1}, while corresponding bands for phthalic based imides were observed at 1368 cm^{-1} and 746 cm^{-1}.

In SPDAB•Im-N, characteristic peaks in the range 2600-3200 cm^{-1} could be assigned to the presence of imidazolium ring and its strong aromatic C−H stretching vibrations occurred at 3154 and 2988 cm^{-1} (Dong, 2006; Iimori, 2007) and out of plane bending band at 901 cm^{-1} (Cordes de N.D.; 1968). While, -N-H out of plane bending vibration occurred at 631 cm^{-1}. In addition, the intensity of the peak at 1450 cm^{-1} was maximum due to the, corresponding added C=N conjugation with C=C bond present in imidazolium ring. Bands appeared at 1066 cm^{-1} and 1054 cm^{-1} corresponded to the -N-C-H frequency in the salt membrane SPDAB•TA-N and SPDAB•Im-N, respectively, and subsequently disappeared after treatment of acid (1M HCl) in $SPDAB_I$-N and $SPDAB_{II}$-N, hence confirming the complete exchange of proton.

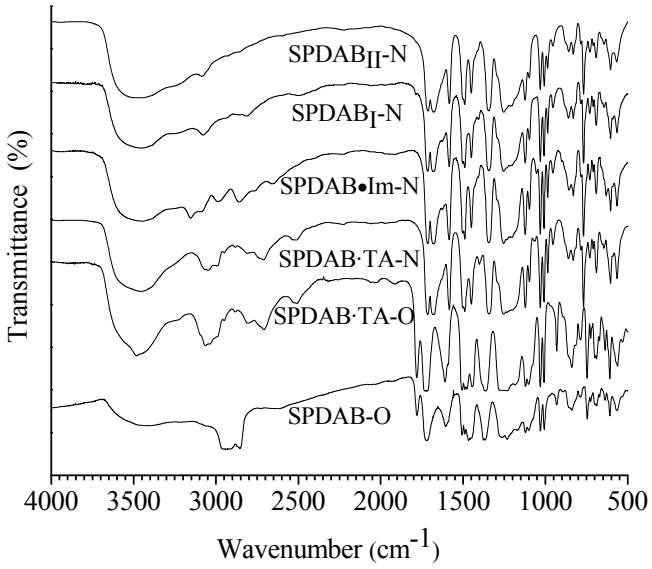

Figure 3.5 FT-IR spectra of SPIs

3.5.2.3 Solubility and solution viscosity

The solubility of SPIs was determined for 0.5 % concentration on stirring for a day at ambient and then at 80 °C for 24 h. These SPIs revealed excellent solubility in organic solvents such as DMAc, DMF, DMSO, NMP and *m*-cresol. They were also soluble in conc. H_2SO_4 (Table 3.4). SPDAB•TA-O and SPDAB•TA-N could readily be dissolved in these solvents. SPDAB•Im-N also exhibited good solubility in these

solvents, however, the relative time for dissolution of SPDAB•Im-N was higher (4-24 h). In addition, it was dissolved in DMAc and NMP only on heating at 80 °C. This could be attributed to the higher anticipated molecular weight.

In general, NTDA based SPIs in their sulfonic acid form are known to exhibit poor organic solvent solubility (Yin, 2006a). However, in the present case, NTDA based SPI in sulfonic acid form also exhibited good solvent solubility at ambient, except for the partial solubility in NMP and insolubility in *m*-cresol. The improved solubility may be due to asymmetric side-chain substitution of bulkier pendant sulfophenoxy group as well as formation of kink structure by the presence of *meta*-imido moiety.

It is interesting to note that SPDAB•Im-N got precipitated from DMAc solution of 0.5% concentration on increasing the temperature above 95 °C and redissolved on lowering the temperature below 95 °C. This procedure was repeated 3 times and same phenomenon of dissolution below and precipitation above 95 °C temperature was noticed. Thus, 0.5% concentration solution of SPDAB•Im-N in DMAc exhibited the critical solution temperature (CST) phenomenon. Investigation of this phenomenon for different concentration revealed that the phenomenon was observed at and above 0.5% concentration till 3% concentration. At 0.25% concentration, this CST phenomenon was not observed. In case of SPDAB•TA-N solution in DMAc, such phenomenon at various concentration was not observed. A peculiar flat structure and aromatic nature of imidazolium cation in SPDAB•Im-N can play the major role for such CST phenomenon. Such phenomenon is observed in ionic liquids (IL) (Anthony, 2001; Crosthwaite, 2005; Domanska, 2006) based on alkyl substituted imidazolium cation. It is therefore possible to have accommodated such planar structure of imidazolium cation in the available free volume between the polymer chains in SPDAB•Im-N, resulting in close packing, hence requiring more time for dissolution in the above mentioned solvents. It should be noted that, gel formation was observed for SPDAB•Im-N at the end of polymerization in *m*-cresol, probably due to build up of high molecular weight resulting in decrease in solubility. Gelation of SPDAB•Im-N in *m*-cresol and precipitation in DMAc could be attributed to the difference of interaction induced by aromatic imidazolium cation with aromatic solvent *m*-cresol and non-aromatic solvent DMAc. The electrostatic or π-π interaction of aromatic imidazole with π-cloud of *m*-cresol could have been increased

with either increasing concentration or molecular weight (Domanska, 2007). As a result, gelation was observed instead of precipitation. While in DMAc, there were no such interactions, besides on increasing temperature as well as concentration, there might have been close contact ion-pairs of imidazolium rings resulting in precipitation. Such phenomenon has been observed in case of IL, which become more soluble in aromatic solvents than non-aromatic solvents of equivalent molecular weight and polarity (Blanchard, 2001).

Table 3.4 Solubility of SPIs in various solvents

Polymer	DMAc	DMF	DMSO	NMP	*m*-cresol	$CHCl_3$	Conc. H_2SO_4	THF
SPDAB•TA-N	++	++	++	++	++	–	++	–
SPDAB •Im-N	+	++	++	+	++	–	++	–
SPDAB $_{I}$-N	+	++	++	±	–	–	++	–
SPDAB $_{II}$-N	+	++	++	±	–	–	++	–
SPDAB•TA-O	++	++	++	++	++	–	++	–
SPDAB-O	++	++	++	++	++	–	++	–

++: soluble at room temperature, +: soluble on heating at 80 °C, ±: partially soluble on heating at 80 °C, – : insoluble.

The reduced viscosity of the SPI was determined in DMAc at different concentration with Ubbelohde viscometer at 35 °C. From the Figure 3.5, it is observed that reduced viscosity increases non-linearly with lowering concentration, indicating the typical polymer ionomer characteristics for these SPIs (Contois, 1955; Lundberg, 1982; Hara, 1989; Campos, 1997). This anomalous viscosity behavior can be attributed to coalescing of polymer ionomer molecules at high concentration due to increased intra or intermolecular ionic association. While on dilution, these aggregated molecules go away from each other due to greater electrostatic repulsion among them, which leads to expansion of the polymer chain and hence displaying increased viscosity (Hara, 1989; Campos, 1997). The higher viscosity of the SPDAB•Im-N than SPDAB•TA-N could either be ascribed to the probable formed high molecular weight due to rapid polymerization or discrepancy in solute-solvent interaction owing to different nature of

pendant imidazolium and triethylammonium salt form. The viscosity of $SPDAB_I$-N and $SPDAB_{II}$-N were measured after acidifying SPDAB•TA-N and SPDAB•Im-N membrane, respectively. A slight higher viscosities of $SPDAB_{II}$-N with concentration as compared to $SPDAB_I$-N may be assigned to higher viscosity of parent SPDAB•Im-N (Figure 3.6). It should be noted that, the molecular weight of the $SPDAB_{II}$-N could have been further increased by increasing period of polymerization to 24 h for SPDAB•Im-N, i.e. similar to period for SPDAB•TA-N, by using more solvent (*m*-cresol). Thus, it may be concluded that polymerization of SPI with imidazole as base, can increase viscosity of SPI compared to that of TEA.

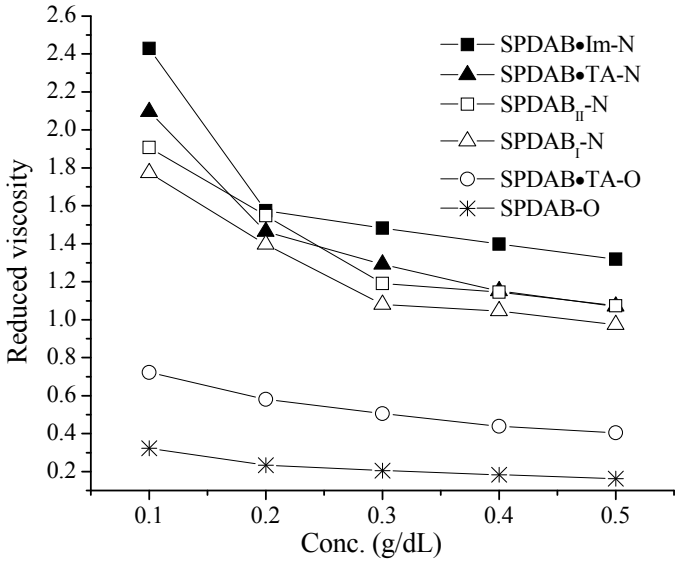

Figure 3.6 Variation in reduced viscosity of SPIs with concentration

3.5.2.4 Thermal Properties of Polymers

Thermal stability of SPIs was investigated by TGA in N_2 atmosphere at a heating rate of 10 °C. min^{-1} and the results are summarized in Table 3.5. Samples were taken in film form, except for SPDAB-O, which was in powder form. These samples exhibited water loss at 50-100 °C. It could be seen that SPIs exhibited typical two-step degradation (Figure 3.7). The initial decomposition temperature (IDT) was ~260 °C, attributable to desulfonation in the side chain. The SPI in sulfonic acid form viz., $SPDAB_I$-N and $SPDAB_{II}$-N showed the similar two step degradation pattern with residue 44.5 % and 44.9 %, respectively. Moreover, these two curves were almost superimposable with each

other. It could thus be deduced that, after acid hydrolysis of the corresponding membranes in salt form, resulting membranes in sulfonic acid form $SPDAB_I$-N and $SPDAB_{II}$-N yielded the same type of polymers. Among all the SPIs, the IDT for SPDAB•Im-N occurred at the highest temperature (348 °C) and ~68 °C higher than its analogous SPDAB•TA-N, indicating stronger interaction between the pendant sulfonic and imidazolium moiety. In addition, aromatic nature of imidazolium ring could also elevate the thermal stability. On the other hand, SPDAB•TA-N membrane (in triethylammonium salt form) exhibited lower IDT as well as char yield (23.82 %) than the acidified membrane $SPDAB_I$-N and $SPDAB_{II}$-N. Same pattern of lower IDT and char yield of SPIs in triethylammonium salt form than that of their respective sulfonic acid form has also been observed earlier (Einsla, 2004). Same was the pattern for SPIs based on ODPA. Thermal stability for six membered imides decreases in the order SPDAB•Im-N > $SPDAB_I$-N ≈ $SPDAB_{II}$-N > SPDAB•TA-N. In conclusion, between the polymerization of SPI with a base (TEA or imidazole), the latter not only improved the IDT, but also increased the char yield as compared with the former demonstrating its fire retardant tendency. The second stage weight loss occurring above 500 °C in SPIs represented the decomposition in their main chain. SPI containing five membered imide ring based on ODPA (SPDAB•TA-O) decompose at lower temperature compared to SPI with six membered imide ring.

Attempts were made to determine the glass transition temperature (T_g) of these SPIs by DSC at a heating rate of 10 °C min^{-1} in N_2 atmosphere. However, when the samples were scanned in a temperature range of 50−350 °C, within which, no obvious glass transition could be detected. This indicated the stronger interaction among the chains of SPI induced by the pedant sulfonated moiety. In NTDA based SPI, presence of rigid planar naphthalo–imide ring in main chain would further assist in increasing the glass transition temperature. It had also been observed that splitting-off sulfonic group (cleavage of C_{Ar}−SO_3H bond) occured around 260 °C as explained earlier in TGA. Furthermore, T_g of these SPIs could also be raised by their increased rigidity due to an alternate *ortho* substituted bulkier sulfophenoxy group, which had an ability to restrict the bond rotation between phenyl ring and nitrogen (Ar–N bond) in main chain. Considering all these aspects, the apparent T_g of polymer appears to be above the decomposition

temperature (~260 °C), which could not be located. It also implied that free volume made available by pendant bulkier short side chain sulfophenoxy group, was not sufficient to lower T_g below the temperature corresponding to splitting-off sulfonic acid group i.e IDT (260 °C). Some of the SPIs have also been reported, which do not show glass transition (Yasuda, 2005; Rodgers, 2006).

Table 3.5 Thermal properties of SPIs

Polymer	Degradation temperature (°C)		Residue (%)
	I	II	
SPDAB•TA-N	272	512	23.82
SPDAB•Im-N	340	555	40.87
$SPDAB_I$-N	295	526	44.91
$SPDAB_{II}$-N	302	518	44.55
SPDAB•TA-O	262	402	15.14
SPDAB-O	288	520	27.36

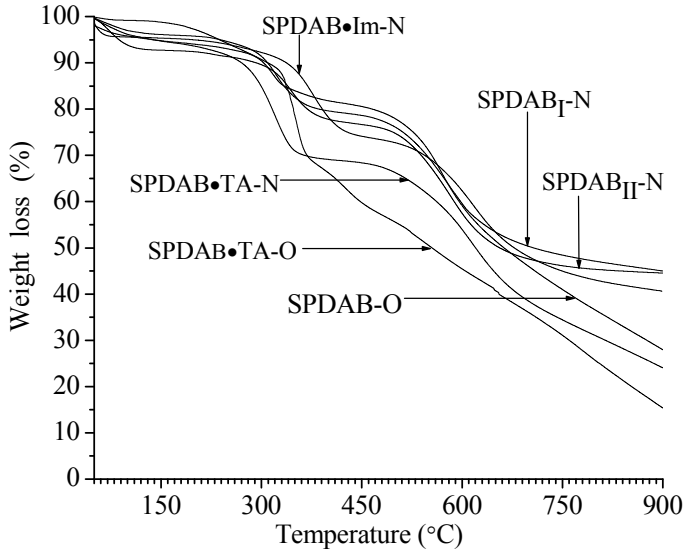

Figure 3.7 TGA of SPIs

3.5.2.5 WAXD Analysis

Dry form of the membrane samples were used for WAXD analysis except for SPDAB-O, which was analyzed in powder form. Initially salt form of the membrane

samples viz. SPDAB•TA-N and SPDAB•Im-N were scanned and the same samples, after converting to their analogous sulfonic acid form ($SPDAB_I$-N and $SPDAB_{II}$-N) by acid treatment were used for WAXD analysis. The obtained WAXD pattern for all SPIs showed their complete amorphous nature as shown in Figure 3.8. SPDAB•TA-N shows the amorphous peak at lower angle (24.32°) than the peak of SPDAB•Im-N at higher angle (25.88°), indicating more densely packed structure in the later. The possible π-π interaction among the pedant imidazolium rings and their flat nature in SPDAB•Im-N may assist in the close packing. Such types of π-π stacking interactions among imidazolium rings leading to dense packing in ILs are known (DuPont, 2004). It is significant to notice that, after acid hydrolysis, membranes in acidified form i.e. $SPDAB_I$-N and $SPDAB_{II}$-N showed the same WAXD pattern. In other words their WAXD images could be superimposed with each other, indicating similar types of molecular packing of the polymer chains in both the polymers.

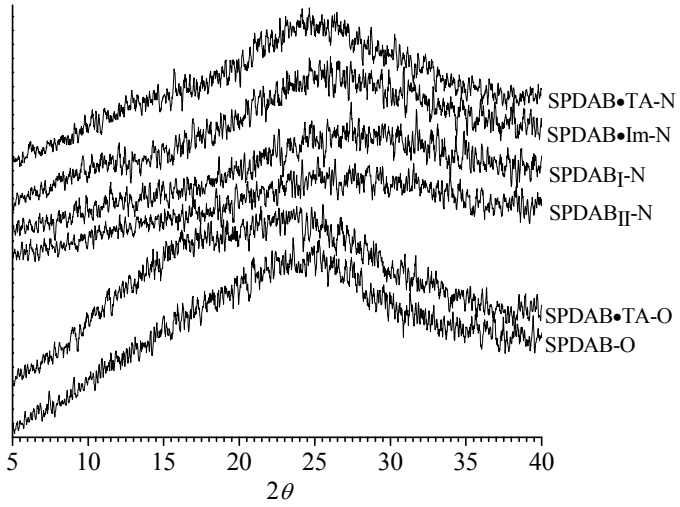

Figure 3.8 WAXD spectra of SPIs

3.5.3 Preparation and physical characterization of blend membranes based on SPIs and PBI-BuI

Acid-base blends of sulfonated polymers with basic polymers are known to conduct protons at higher temperature. Such polymer blends are being probed as polymer electrolytes for fuel cell (Kerres, 2000; Hasiotis, 2001a). In present study, blends of SPIs with PBI-I were prepared. However, looking at brittle nature of these blend membranes,

blends of SPI and PBI-BuI were prepared with objective to study proton conduction of these blend membranes.

3.5.3.1 Membrane preparation

Blend membranes were prepared from SPI and polybenzimidazole (PBI) in different weight ratio in order to evaluate their performance as material for PEMFC. SPI in triethylammonium sulfonate (TEA) form (SPDAB•TA-N) and PBI (inherent viscosity of 1.8) based on DAB and IPA were initially attempted to prepare blend membranes. However, membranes cast from them were brittle, though homogeneous solution of these polymers in different weight ratio could be made. Hence we replaced PBI-I by PBI-BuI. It was observed that, though flexible blend membranes based on SPDAB•TA-N and PBI-BuI could be made, the membranes containing more than 50 wt% of SPDAB•TA-N became brittle.

Thus, blend membranes based on SPI and PBI-BuI with a weight ratio 50:50, 40:60 and 30:70 were prepared and named as SPI(*TEA*)/PBI-BuI*(a/b)*, where *a* and *b* represents weight percentage of SPI and PBI-BuI, respectively, while '*TEA*' denotes SPI in triethylammonium sulfonate form. In order to evaluate the performance of these blend membranes as polymer electrolyte membrane (PEM) for fuel cell, they were transformed into sulfonic acid form after treating with 1N HCl for 24 h followed by washing with deionised water. These membranes were named as SPI(*H*)/PBI-BuI*(a/b)*. Here, '*H*' represents proton form of SPI. The blend membranes doped by 12 M H_3PO_4 were named as SPI(*PA*)/PBI-BuI*(a/b)*, where '*PA*' denotes the exchange of triethylamine by phosphoric acid protons.

3.5.3.2 FT-IR analysis of blend membranes

Figure 3.9 shows the FTIR spectra of $SPDAB_I$-N, PBI-BuI and their respective blends. In $SPDAB_I$-N, bands at 1715 cm^{-1} and 1680 cm^{-1} correspond to carbonyl asymmetric and symmetric stretching, respectively present in naphthalic imide group. The characteristic absorption bands at 1252, 1180 and 1030 cm^{-1} are associated with the stretching of the sulfonate groups. In, PBI-BuI the sharp bands in the region 3380-3430 cm^{-1} are assigned to the isolated -N-H stretching of the imidazole ring. However there is

no observable sharp band within 3100-3140 cm^{-1} corresponding to the associated -N-H stretching which is usually present in the conventional PBI based on IPA (Wang, 2007b; Kumbharkar, 2009). This implies that, bulky *t*-butyl group in PBI-BuI has lower interchain interactions (Kumbharkar, 2006). In PBI-BuI, two distinct bands at 2962 cm^{-1} and 2872 are due to the asymmetric and symmetric stretching of the –C–H bonds of *t*-butyl group, respectively. The peaks obtained in the range between 1650 and 1500 cm^{-1} are the characteristics of the benzimidazole rings (Musto, 1993).

It can be seen that the peak at 1626 cm^{-1} corresponding to -C=N stretching of the imidaozle ring in PBI-BuI was shifted to higher frequency at 1634-1636 cm^{-1} in the respective blend, implying the involvement benzimidazole ring interaction. The peak at the 804 cm^{-1} corresponding to the five-member heterocyclic ring in PBI-BuI shifts to higher wavenumber 807, 809 and 810 cm^{-1} with decrease in PBI-BuI content. This was obvious, since with increase in relative sulfonic content, quantitative interaction between five membered heterocyclic benzimidazole ring and SPI would be more. Such observation was also made in the blend prepared from sulfonated PEEK (SPEEK) and PBI, where a peak of −C=N stretching at 1625 cm^{-1} and five membered imidazole peak at 806 cm^{-1} shifts to 1645 and 814 cm^{-1}, respectively (Zhang, 2008), indicating the interaction between SPEEK and PBI. However, it should be noted that, shift of these peaks was relatively lower in the present blend system. The characteristic bands of benzimidazole are seen at 1625 cm^{-1} (C=N stretching) and aromatic C=C stretching at 1602 cm^{-1} of the benzene ring. The peak at 3634 cm^{-1} in PBI-BuI can be assigned to the O−H stretching of absorbed water. Brooks *et al.* (1993) and Li *et al.* (2004) have also mentioned the occurrence of the same peak at 3620 cm^{-1}, which disappeared on heating at 120 ºC. Among the blends made, the appearance of this peak at 3621 cm^{-1} can be observed only in case of SPI (*H*)/PBI-BuI *(30/70)* due to high content of PBI-BuI.

The peak corresponding to imidazole ring vibration at 1284 cm^{-1} (Musto, 1993) is intensified with increase in PBI-BuI content in the blend. The peak at 1344 cm^{-1} corresponding to the O=S=O asymmetric stretching shifts to a lower wavenumber at 1340, 1339 and 1338 cm^{-1} with decrease in SPI content indicating its involvement in the interaction for blend formation. The characteristic intensity of the asymmetric and symmetric imide ring at 1715 and 1680 cm^{-1}, respectively has neither been intensified nor

shifted, suggesting that imide ring might not have participated for interactions with PBI-BuI. So the probable H-bonding may be involved between imidazole and sulfonic acid moiety. Similarly, with increase in PBI-BuI content the same heterocyclic ring vibration at 700 cm^{-1} is shifted to 692, 693 and 697 cm^{-1}. The peak at 1032 due to SO_3^- in SPI(*H*)/ PBI-BuI*(50/50)* has been intensified than parent SPI and remaining blend system also. This can be attributed to the more polarized nature of SO_3^- group due to the more dissociated form of sulfonic acid group into SO_3^- and H^+. This observation is reasonable as in SPI(*H*)/PBI-BuI*(40/60)* and SPI(*H*)/PBI-BuI*(30/70)* blend system, the number of sulfonic groups available for H-bonding becomes less as compared with SPI(*H*)/PBI-BuI*(50/50)*.

It is interesting to note that in the respective blend a change in shift of the corresponding frequency pertaining to particular moiety interactions was within the range 3-10 cm^{-1}, suggesting the either medium or weak interaction. This can be attributed to the presence of pendant sulfonic acid group in the side chain of NTDA based SPI as well as the presence of pendant bulky *t*-butyl group in the main chain of PBI, which would screen the imidazole moiety from interaction, leading to weak intermolecular H-bonding. This can be further justified by the absence of associated H-bonding occurring in the range of 3100-3140 cm^{-1} in PBI-BuI (Kumbharkar, 2009) and present in PBI-I (Musto, 1989). The shift in specific bands of both components of polymers in blends indicates the specific interaction between the groups, a characteristic of miscible blend formation.

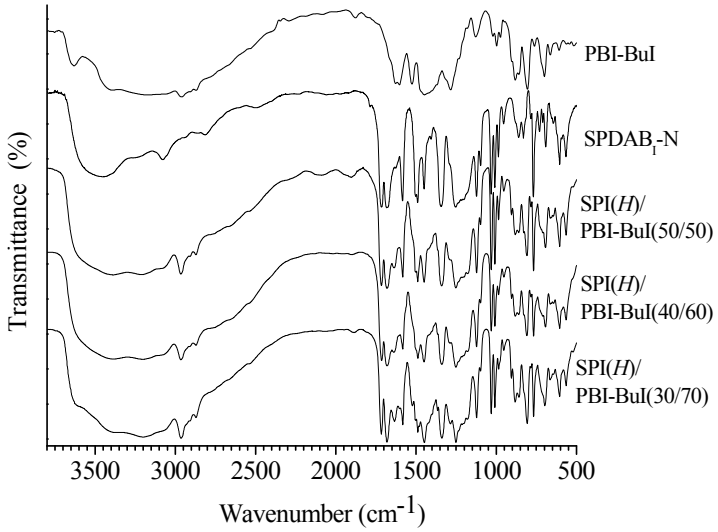

Figure 3.9 FT-IR spectra of blends in the sulfonic acid form

3.5.3.3 Thermal analysis of blend membranes

The thermal stability of the blend membrane was measured by TGA. The blend membranes exhibited 2 step degradation processes as shown in Figure 3.10. The initial little weight loss at ~100 °C is due to the loss of absorbed moisture. The first weight loss corresponds to the thermal splitting of sulfonic group either in salt form with TEA or free sulfonic acid group form. The second weight loss is due to the decomposition of main chain backbone of the polymer components viz; SPI and basic polymer, PBI-BuI, respectively.

It is interesting to note that, there is noticeably improved thermal stability of blend membranes in sulfonic acid form viz; SPI(*H*)/PBI-BuI*(a/b)*, than their counterpart in triethylammonium salt form viz; SPI(*TEA*)/PBI-BuI*(a/b)*. The splitting of $–SO_3H$ of SPI (*H*)/PBI-BuI*(a/b)* blend system occurs above 400 °C compared to 250 °C for SPI(*TEA*)/ PBI-BuI*(a/b)*, indicating the thermal splitting of $–SO_3H$ stability was better for blend membrane in sulfonic acid form. This result indicated that acidic $–SO_3H$ is involved in the interaction with the imidazole of PBI-BuI. While comparing the degradation behavior among the blend system, 10 % weight loss for SPI(*H*)/PBI-BuI*(a/b)* blend system occurs at a higher temperature in the range of 443-480 °C than SPI(*TEA*)/PBI-BuI*(a/b)* blend system (258-327 °C) as shown in the Table 3.6. Thus, result proves that free sulfonic acid group ($–SO_3H$) is more liable for ionic interaction than in triethylammonium sulfonate salt form with the imidazole ring of the basic polymer; PBI-BuI. In this way, improvement in the thermal $–SO_3H$ splitting of stability can be distinctly accomplished by the blending of SPI with the basic polymers such as PBI-BuI. The specific acid-base interactions in the blend as well as the extraordinary thermal stability of the PBI-BuI (Kumbharkar, 2006) assist in the improvement of thermal stability of the blend.

We endeavored for determining the glass transition temperature (T_g) of these blend membranes by DSC at a heating rate of 10 °C min^{-1} in N_2 atmosphere, however no apparent glass transition could be seen. This could be attributed to the probable stronger interaction between the sulfonic acid moieties of SPIs with the bezimidazole ring PBI-BuI. Because of this segmental mobility of the polymeric chains in the resultant blend membrane can be reduced. The T_g of these polymers is probably higher than the decomposition temperature of sulfonic acid groups, hence it could not be detected by

DSC. Moreover, the glass transition temperature for the parent polymers PBI-BuI as well as SPIs, could also not be detected.

Table 3.6 Thermal properties of blend membranes

Polymer	T_{10}	Residue (%)
SPDAB•TA-N	270.4	23.8
$SPDAB_I$-N	309.2	44.9
PBI-I	649.8	66.9
PBI-BuI	564.5	64.9
SPI(*TEA*)/PBI-BuI*(30/70)*	257.9	49.8
SPI(*H*)/PBI-BuI*(30/70)*	451.6	60.5
SPI(*TEA*)/PBI-BuI*(40/60)*	326.8	55.3
SPI(*H*)/PBI-BuI*(40/60)*	431.5	58.8
SPI(*TEA*)/PBI-BuI*(50/50)*	320.2	54.5
SPI(*H*)/PBI-BuI*(50/50)*	443.2	55.2

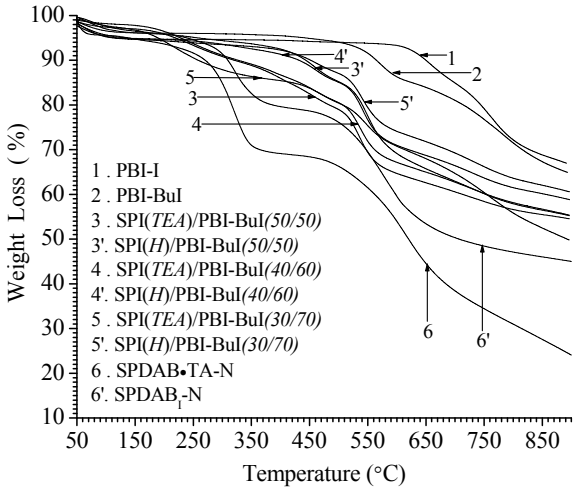

Figure 3.10 TGA of blends

Thus, SPI and PBI-BuI form miscible blends having high thermal stability in sulfonic acid form.

3.5.4 Synthesis and physical characterization of polyimides based on various alkyl substituted phenoxy diamines

The aromatic PIs with alkyl substituents in different position of pendant phenoxy ring were synthesized with the objective to study effects of alky substituents on the gas permeability. PIs were substituted with methyl groups at *ortho*, *para* and 2,6-positions; while bulky *t*-butyl group was situated at *para* position to the ether linkage. These PIs were synthesized by condensing corresponding diamine with ODPA and 6FDA. These two dianhydrides were chosen in order to compare the effect between the presence of flexible (C-O-C) link with bulk and rigid (–$C(CF_3)_2$–) groups in the main chain of the resultant PIs on their gas permeation properties. The purpose of utilizing these two commercially available dianhydrides, for the preparation of present PIs lies in excellent gas permeation performance of PIs based on these dianhydrides (Stern, 1989; Li, 1997). 6FDA based PIs have well been acknowledged in gas permeation field due to their intrinsic high permeability as well as selectivity. Moreover, 6FDA improves solvent solubility, even in chlorinated organic solvents such as TCE and chloroform (de Abajo, 1999; Tamai, 2001).

3.5.4.1 Synthesis

Aromatic polyimides were prepared by the classical one-step solution polycondensation technique at 200 °C in *m*-cresol. Their preparation involved the addition of solid dianhydride to the diamine solution in *m*-cresol at the ambient condition, followed by heating at 200 °C. Water formed during the process of imidization was removed continuously with the flush of N_2, to obtain high viscosity polymer. All reactions proceeded homogeneously without gelation or precipitation in *m*-cresol. Depending on the reactivity of diamine and dianhydride, the polymerization time varied between 8-24 h. The diamine 2',6'DMPDAB being more basic, gave polymer with high viscosity within 8 h. The comparative short time for the 2',6'DMPDAB based PI can be credited to its increased basicity as compared with the other diamines. It is well known that basicity of a diamine can be increased with the embodiment of electron donating substituents (Yin, 2004 and 2006a; Marestin, 2008) and hence such diamines become more reactive. Such phenomenon of increased basicity in the amine group by the *ortho*-

substituted propoxy linkage has been observed by Yin *et al.* (2004). In the present case, basicity of 2',6'DMPDAB is enhanced due to the strong electron donating effect of the *ortho*-dimethyl substituted phenoxy group. The presence of these two $–CH_3$ groups at *2,6*-position of phenoxy ring bestowed two advantages. First, being *ortho* substituted to the ether linkage, electron donating ability of the oxygen atom in the ether linkage was boosted due to their +I effect. Second, the rotation of phenoxy ring and *meta*-amino phenyl ring around the Ar-O-Ar' linkage could become more energetic due to the steric hindrance of the *ortho*-substitution of two $–CH_3$ groups in the former and amino functionality in the later. As a result, phenyl rings of 2',6'DMPDAB become coplanar to each other. Hence, *ortho* located $-NH_2$ group of *meta*-amino phenyl ring (present at the vicinity of methyl disubstituted phenoxy group) experiences less steric hindrance of the bulky dimethyl substituted phenoxy group resulting in its enhanced reactivity with dianhydride. This observation can be proved by the ^{1}H-NMR of 2',6'DMPDAB (Figure 2.15), wherein the proton H_c of *meta*-amino phenyl ring (*ortho* to dimethyl substituted phenoxy group) shifts towards upfield as compared with the other diamines. This indicates stronger electron donating ability of dimethyl substituted phenoxy group in 2',6'DMPDAB as compared with the other alkyl substituted phenoxy group of other diamines. In this way, more basic character of 2',6'DMPDAB results in its PI with increased viscosity in the lesser duration.

Between ODPA and 6FDA based PIs with the same diamine, the former took less time than the latter for the polymerization, despite having high electron affinity (*EA*) of 6FDA. However, the polymerization duration for 2',6'DMPDAB with either ODPA or 6FDA was the same. Polymers were isolated by precipitating their viscous solution into methanol with vigorous stirring. The yield of polymers thus obtained was high (> 93 %).

Dense membranes of these polymers (40-50 μm thick), were prepared by solution casting method. For ODPA based PIs, dense membranes were prepared from TCE, while for 6FDA based PI, chloroform was used. In case of FT-IR spectral analysis, dense membranes of relatively lower thickness (~10 μm) were prepared, while for density measurements, films of comparatively higher thickness (~100 μm) were prepared.

Obtained polymers were characterized by elemental analysis, FT-IR spectroscopy, solvent solubility, WAXD, viscosity measurements and thermal analysis. The physical properties investigated of these PIs are given in Table 3.7, Table 3.8 and Table 3.9.

3.5.4.2 Elemental analysis

The elemental analysis calculated for PIs based on alkyl substituted diamines are shown in Table 3.7. Observed elemental analysis values of these PIs showed good agreement with the calculated values.

Table 3.7 Elemental analysis of PIs based on alkyl susbtituted phenoxy diamines

Polymer	Formula and Molecular weight		Element analysis			
			% C	% H	% N	% F
2′MPDAB-ODPA	$(C_{29}H_{16}O_6N_2)_n$	Calculated	71.31	3.30	5.74	–
	$(488)_n$	*Observed*	*70.42*	*3.80*	*6.19*	–
2′MPDAB-6FDA	$(C_{32}H_{16}O_5N_2F_6)_n$	Calculated	61.75	2.59	4.50	18.31
	$(622)_n$	*Observed*	*61.38*	*2.45*	*4.71*	*17.19*
4′MPDAB-ODPA	$(C_{29}H_{16}O_6N_2)_n$	Calculated	71.31	3.30	5.74	–
	$(488)_n$	*Observed*	*70.75*	*3.71*	*6.12*	–
4′MPDAB-6FDA	$(C_{32}H_{16}O_5N_2F_6)_n$	Calculated	61.75	2.59	4.50	18.31
	$(622)_n$	*Observed*	*61.08*	*3.01*	*3.96*	*17.39*
2',6'DMPDAB-ODPA	$(C_{30}H_{18}O_6N_2)_n$	Calculated	71.71	3.61	5.58	–
	$(502.48)_n$	*Observed*	*71.25*	*3.89*	*5.86*	–
2',6'DMPDAB-6FDA	$(C_{30}H_{18}O_5N_2F_6)_n$	Calculated	62.27	2.85	4.40	17.91
	$(636.5)_n$	*Observed*	*62.24*	*2.69*	*4.72*	*16.18*
4′*t*BPDAB-ODPA	$(C_{32}H_{22}O_6N_2)_n$	Calculated	72.45	4.18	5.28	–
	$(530)_n$	*Observed*	*71.09*	*4.82*	*5.13*	–
4′*t*BPDAB-6FDA	$(C_{35}H_{22}O_5N_2F_6)_n$	Calculated	63.26	3.34	4.22	17.15
	$(664)_n$	*Observed*	*62.89*	*3.57*	*3.88*	*15.67*

3.5.4.3 FT-IR analysis

IR spectra of present alkyl substituted polyimides (Figure 3.11) showed characteristic absorption bands of the 5 membered imide ring at 1779-1784 cm^{-1} and 1722-1727 cm^{-1} (corresponding to asymmetric and symmetric –C=O stretching), respectively and 1360-1365 cm^{-1} (C–N stretching). Imide ring deformation peaks appeared at 1100-1106 and 720-745 cm^{-1} (Mathew, 2001). Absence of peaks at 1650 cm^{-1} (–C=O of amic acid) and 3250 cm^{-1} (N–H and O–H groups) confirmed complete imidization. In case of 6FDA based polyimides, C–F multiple stretching bands appeared at 1100-1300 cm^{-1} (Jeong, 2001) and the C–O–C stretching appeared at 1240-1250 cm^{-1} (Mathew, 2001).

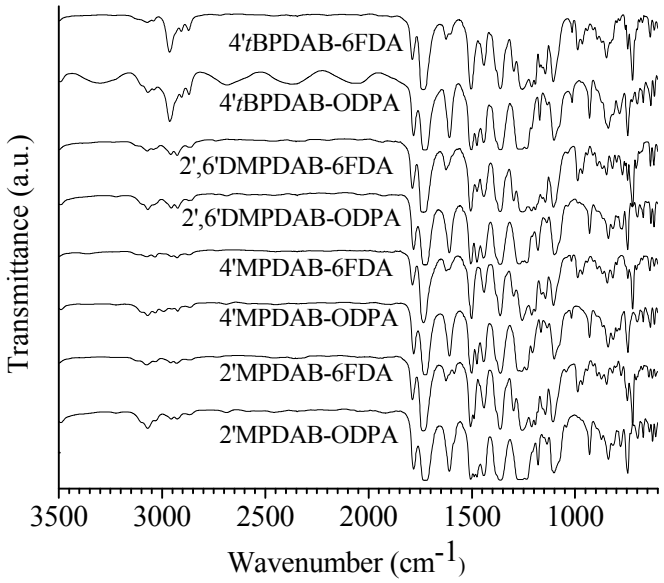

Figure 3.11 IR spectra of polyimides based on alkyl substituted phenoxy diamines

Thus, elemental analysis and FT-IR spectral analysis indicate formation of alkyl substituted PIs of desired structures.

3.5.4.4 Solubility and solution viscosity

The solvent solubility of polyimides was determined for 0.5 % concentration in common organic solvents (Table 3.8). All PIs showed appreciable solubility at ambient temperature, which could be advantageous in membrane formation. Excellent solubility could be attributed to the presence of pendant phenoxy group with alkyl substitution

situated at the *ortho* position to the nitrogen of an alternate imide group. Another factor contributing to the improved solubility could be *meta* connected imide linkages forming the 'kink' arrangement and thus disrupting the chain packing (de Abajo, 1999). PI based on 6FDA showed better solubility in THF and 1,4-dioxan than their ODPA based counterparts. The bulky $–C(CF_3)_2–$ linkage in PIs increases free volume, decreases intermolecular chain interaction and weakens charge transfer complex (CTC) effect thus improving solubility (Tanaka, 1992a; Matsumoto, 1993b; Hsiao, 2000; Jeong, 2001; Liaw, 2006). Solubility parameter (δ), calculated by Bondi's group contribution method, was found to be lower for 6FDA based PIs than analogous ODPA based PIs. In addition, it also decreased with the increase in alkyl content in the diamine. Thus, the interchain interaction could not only be reduced with bulky $–C(CF_3)_2–$ linkage but also with increase in alkyl content.

Table 3.8 Solvent solubility of polyimides based on alkyl substituted phenoxy diamines

Polymer	$CHCl_3$	TCE	THF	1,4-dioxan	NMP	DMAc	DMF	DMSO	*m*-cresol
2′MPDAB-ODPA	++	+	±	±	++	++	++	±	++
2′MPDAB-6FDA	++	++	++	++	++	++	++	++	++
4′MPDAB-ODPA	++	++	++	±	++	++	++	++	++
4′MPDAB-6FDA	++	++	++	++	++	++	++	++	++
2',6'DMPDAB-ODPA	++	++	±	++	++	++	++	++	++
2',6'DMPDAB-6FDA	++	++	++	++	++	++	++	++	++
4′*t*BPDAB-ODPA	±	++	±	±	++	++	++	±	++
4′*t*BPDAB-6FDA	++	++	++	++	++	++	++	++	++

++: soluble at ambient temperature, +: soluble on heating at 60 °C for 4 h, ±: partially soluble.

The intrinsic viscosities [η] of these polyimides were in the range of 0.33-0.55 $dL.g^{-1}$ in TCE, which was high enough to offer strong and tough films. The intrinsic viscosity increased in the order for diamines 2'MPDAB ≈ 4'MPDAB < 4′*t*BPDAB < 2',6'DMPDAB.

3.5.4.5 Thermal Properties of Polymers

Thermal properties of all polyimides were evaluated by DSC (Figure 3.12) and TGA (Figure 3.13) and results are summarized in Table 3.9. These polymers exhibit high T_g in the range of 265-315 °C. It is observed that ODPA based PI of a particular diamine shows lower T_g than the corresponding 6FDA based analogue, owing to the presence of flexible ether linkage in ODPA. The voluminous –$C(CF_3)_2$– linkage in 6FDA would impose limitations on free rotation around the CF_3─C─CF_3 bond leading to restricted torsional motion of neighboring phenyl rings. Such increase in T_g due to inhibited segmental motion is well known (Matsumoto, 1993b; Coleman, 1994). T_g values are dependant on structure of diamine also. In the present series of PIs based on either ODPA or 6FDA, T_g of PI increased in the order of 4'MPDAB ≈ 4'*t*BPDAB < 2'MPDAB < 2',6'DMPDAB. This indicated that methyl substitutions at *2* and *6* positions on the pendant phenoxy ring in 2',6'DMPDAB based PI would hinder the rotational motion around phenoxy group the most, followed by *ortho*-substituted 2'MPDAB based PI; while the least hindrance by the substitution at *4*-position, irrespective of its bulk (4'MPDAB and 4'*t*BPDAB based PIs). This also signifies that position of alkyl substituent is more crucial in depicting the rotational barrier than the bulk of substituent.

It is interesting to compare the trend of T_g between PI based on two dianhydrides for different diamines. In case of ODPA based PI with different diamines T_g decreases in the order PDAB (256 °C) < 4'MPDAB (267 °C) < 4′*t*BPDAB (270 °C) < 2'MPDAB (282 °C) < 2',6'DMPDAB (311 °C). While, for 6FDA based PIs with different diamines, T_g decreased in the order 4'MPDAB (278 °C) < PDAB (281 °C) ≈ 4′*t*BPDAB (282 °C) < 2'MPDAB (289 °C) < 2',6'DMPDAB (313 °C). This indicates that, in case of ODPA based PIs, chemical structure of diamine plays the dominant role in governing the T_g while for 6FDA based PIs, diamine-structural effect becomes prevailing only when they have *ortho*-substitution.

Thermal stability of the PIs was evaluated by the TGA (Figure 3.12) in N_2 atmosphere at a heating rate of 10 °C. min^{-1} and the results are summarized in Table 3.9. These PIs show IDT in the range 473-515 °C and 10% weight loss in the range 495-545 °C. It is interesting to look at the char yield data of these PIs. PI based on diamines such as 2',6'DMPDAB and 2'MPDAB exhibited lower thermal stability and hence lower weight residue than PI based on 4′*t*BPDAB and 4'MPDAB. This could be assigned to the increased rotational barrier of the pendant phenoxy group and hence inducing high torsional strain due to the *ortho*-substitution of methyl groups on the pendant phenoxy moiety. It should also be noted that, char yield of the 6FDA based PIs is lower than the ODPA based PIs. This could be assigned to the loss of CF_3 radical in the former case as explained earlier in the Section 3.5.1.5.

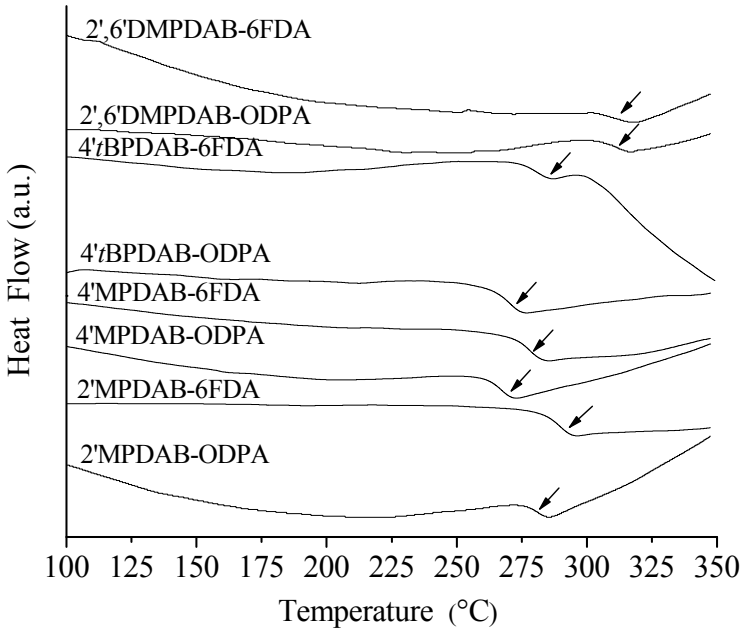

Figure 3.12 DSC curves of polyimides based on alkyl substituted phenoxy diamines

Table 3.9 Physical properties of polyimides based on alkyl substituted phenoxy diamines

Polymer	[η] ($dL.g^{-1}$)	d_{sp} (Å)	δ $(cal.cm^{-3})^{1/2}$	ρ ($g.cm^{-3}$)	T_g (°C)	IDT (°C)	$T_{10\%}$ (°C)	Char yield at 900 °C (%)
2′MPDAB-ODPA	0.34	4.23	12.22	1.402	282	478	496	50.8
2′MPDAB-6FDA	0.32	5.70, 3.38	10.97	1.404	289	493	500	45.0
4′MPDAB-ODPA	0.38	4.53	12.20	1.404	267	515	545	54.0
4′MPDAB-6FDA	0.30	6.08, 3.62	10.97	1.403	278	486	543	53.3
2',6'DMPDAB-ODPA	0.50	4.36	12.04	1.375	311	473	494	53.0
2',6'DMPDAB-6FDA	0.55	6.29, 3.46	10.87	1.387	313	477	494	45.4
4′*t*BPDAB-ODPA	0.47	4.18	11.69	1.333	270	504	530	55.4
4′*t*BPDAB-6FDA	0.45	5.32, 3.52	10.57	1.335	281	506	540	54.5

[η]: Intrinsic viscosity using TCE at 35 °C.

ρ: Density determined by floatation method at 40 °C using aq. K_2CO_3 solutions.

d_{sp}: Average interchain distance from WAXD spectra.

δ: Solubility parameter (Van Krevelen, 1997).

T_g: Glass transition temperature measured by DSC at a heating rate of 10 °C.min^{-1}.

$T_{5\%}$: Onset of 5% weight loss on TGA thermograms at a heating rate of 10 °C.min^{-1} under N_2 atmosphere.

Thus, T_g values and TGA analysis indicate high thermal stability of these polymers suitable for gas separation even at higher temperature.

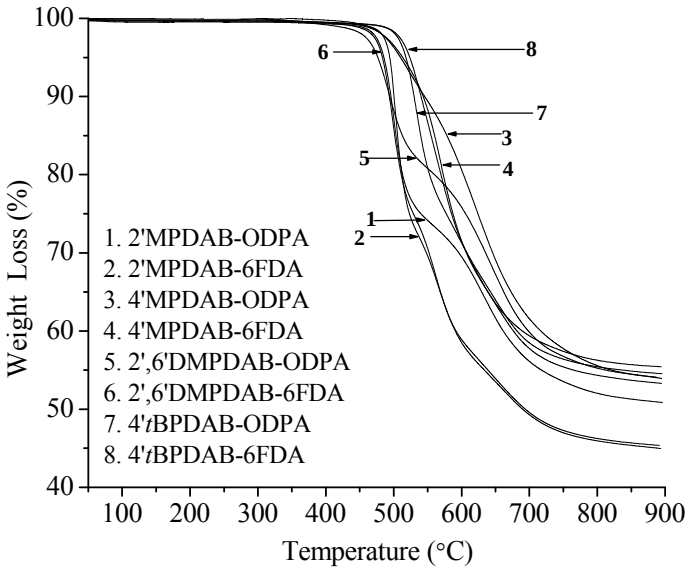

Figure 3.13 TGA curves of polyimides based on alkyl substituted phenoxy diamines

3.5.4.6 WAXD analysis

All these polyimides were amorphous in nature as could be seen from their WAXD spectra (Figure 3.14). 6FDA based PI shows two amorphous peaks suggesting that there could be two types of predominant chain packing. In ODPA based polyimides, the average intersegmental spacing (d_{sp}) varies marginally with the variation of alkyl content in their diamine moiety. 6FDA based alkyl substituted PIs show higher *d*-spacing at lower angle corresponding to *d*-spacing 5.32-6.29 Å, which is normally obtained for 6FDA based PI.

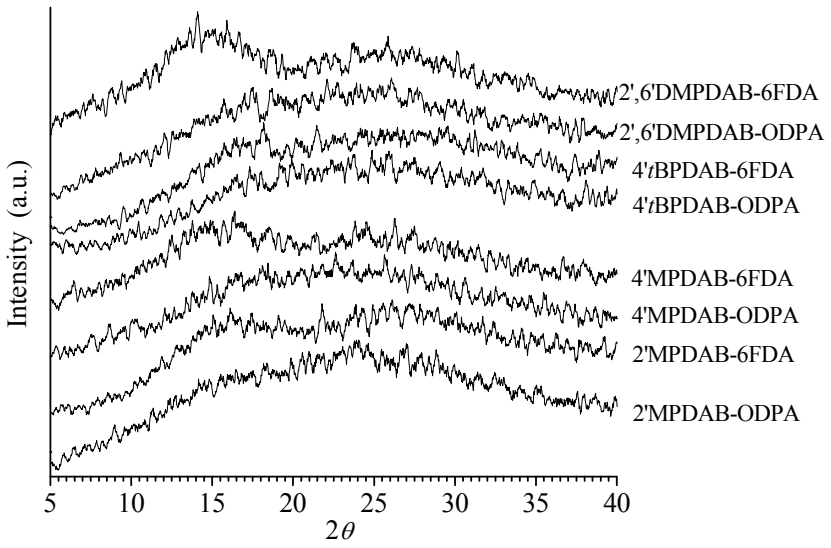

Figure 3.14 WAXD spectra of polyimides based on alkyl substituted phenoxy diamines

3.6 Conclusions

1. A diamine containing pendant phenoxy group, 1-phenoxy-2,4-diaminobenzene (PDAB) and polyimides based on this diamine with PMDA, ODPA, 6FDA, BTDA and BPDA were synthesized and characterized. These PI showed good solvent solubility in common organic solvents. The low viscosity of the homopolyimides can be attributed to the bulky phenoxy group substitution at *ortho* position of the diamine, which reduced the reactivity of one amino group due to steric hindrance. Thermal properties of all the PIs are high as evidenced by their high T_g (> 248 °C) and high IDT (> 500 °C). PDAB-6FDA showed high *d*-spacing, high density, high T_g but low IDT.
2. Novel side chain type sulfonated polyimides (SPIs) based on a new diamine, 4'-sulfonic,1-phenoxy-2,4-diaminobenzene (SPDAB) with dianhydrides viz., NTDA and ODPA were synthesized and characterized. Imidazole as a base catalyses polymerization of NTDA with PDAB with high viscosity in short period compared with TEA as a base. SPIs, both in their salt form (SPDAB•TA-N and SPDAB•Im-N) and sulfonic acid form ($SPDAB_I$-N and $SPDAB_{II}$-N), exhibited good solvent solubility in polar aprotic solvents like DMF, DMAc, NMP and DMSO. The critical solution temperature (CST) phenomenon is observed for SPDAB•Im-N in DMAc. The low decomposition temperature in the range 270-350 °C of these polyimides shows their fair thermal stability. Among these SPIs, thermal stability for six membered imide moieties decreased in the order SPDAB•Im-N > $SPDAB_I$-N ≈ $SPDAB_{II}$-N > SPDAB•TA-N. These polymers did not reveal any glass transition. Being ionomer, SPIs shows increase in their reduced viscosity with lowering in concentration. WAXS pattern of SPIs reveals their complete amorphous nature. Blend membranes of SPI and PBI-I are brittle in nature. Whereas, SPI and PBI-BuI form flexible blends below 50 wt% of SPI in blend composition. Miscibility of these blends was confirmed by FT-IR analysis. Blend membranes in sulfonic acid form [SPI(*H*)/PBI-BuI*(a/b)*] exhibit higher thermal stability (443-480 °C) than that of in salt form [SPI(*TEA*)/PBI-BuI, 258-327 °C]. Blend membrane did not exhibit any glass transition.

3. Side chain type PIs with alkyl substituted pendant phenoxy moiety with two dianhydrides, ODPA and 6FDA, were successfully prepared and characterized. 2',6'DMPDAB based PI shows higher polymerization rate. FT-IR spectra of these PIs show their complete imidization. These PIs reveal good solvent solubility in common organic solvents. Solubility parameter (δ) decreases with increase in alkyl content. Alkyl substitution at *ortho* position of pendant phenoxy group increases T_g than at *para*-position. 6FDA based PIs shows higher T_g as compared with ODPA based PIs. These PIs exhibit high thermal stability with IDT > 473 °C. PIs based on 2',6'DMPDAB exhibits the highest intrinsic viscosity. All these PIs are amorphous in nature and have good film forming property.

Chapter 4

Structure-gas permeability correlation in polyimides

4.1 Introduction

Polyimides have been well recognized as gas separation membrane material and couple of reviews are available on their structure – permeation property relationship (Tsujita, 2003; Ding, 2007; Xiao, 2009). Effects of variation in diamine moiety (Langsam, 1993; Stern, 1993; Tanaka, 1995; Hirayama, 1996a; Li, 1997; Liu, 1999; Xu, 2003; Qiu, 2005 and 2006) as well as dianhydride moiety of polyimide on gas permeation and related physical properties are reported (Stern, 1989; Tanaka, 1992a, 1992b and 1995; Coleman, 1994; Qiu, 2006 and 2007). The incorporation of hexafluoroisopropylidene moiety in diamine (Stern, 1989; Tanaka, 1992a; Coleman, 1994) or dianhydride (Langsam, 1993; Stern, 1993; Hirayama, 1996a and 1996b; Xu, 2003) is known to improve permeation properties of resulting polyimide. It is known that better benefits of incorporation of this moiety in dianhydride can be drawn than its incorporation in diamine (Matsumoto, 1993b). This can be attributed to an enhanced electron affinity in dianhydride because of more electron withdrawing nature of $-C(CF_3)_2-$ linkage. This results in greater reduction in CTC complex with an increase in free volume and gas permeability in the PIs on dianhydrides having $-C(CF_3)_2-$ linkage. (Matsumoto, 1993b). A study on effect of various pendant groups on permeation properties and other physical properties of resulting polyimide would be very useful towards structural design of membrane material for gas separation.

The focus of present thesis is on polyimides obtained from diamines containing oxyphenyl linkage as pendant group and their application as membrane material for PEM and gas separation. Following section briefly discusses literature reports on gas permeation properties of polyimides containing pendant groups. Some of the polymers from present work which were evaluated as PEM materials were also investigated for their CO_2 and related gas permeability under dry and humidified gas conditions. Thus, literature reports investigating CO_2 gas permeation properties under humid atmosphere are also reviewed at the end.

4.1.1 Literature on PIs containing pendant groups: A brief review

One of the ways to develop processible polyimides (PIs) for targeted application comprises substitution of bulky pedant groups on its backbone. Such substituent reduces interchain interactions with increase in free volume necessitated for the penetration of solvent molecules, leading to better solubility and thus, processability. Substitution of phenyl group on PI backbone is well reported (Korshak, 1969; Imai, 1984; Akutsu, 1994; Spiliopoulous, 1997 and 1998; Mikroyannidis, 1999a and 1999b; Xu, 2003; Morikawa, 2005 and 2006; Qiu, 2005 and 2007; Ghaemy, 2009). Increasing the T_g along with attainment of solubility in PIs, can be achieved if such embodied group is able to decrease the segmental mobility (Takekoshi, 1990; Liu, 1999; Morikawa, 2005 and 2006; Qiu, 2006). This phenomenon was attributed to the decrease in rotational flexibility around the diphenyl ether unit due to the embodied phenyl substituents (Morikawa 2005 and 2006). Introduction of bulky groups at *ortho* position of the imide nitrogen can restrict the rotation around C-N bonds of the two neighboring phenyl rings in PIs and thus is known to decrease the intra-segmental mobility, which leads to increase in chain rigidity and T_g (Takekoshi, 1990; Liu, 1999; Hsiao, 1998b). This phenomenon can be beneficial in improving gas permeability of polyimides while retaining permselectivity (Qiu, 2006).

Efforts encompassing bulky group substitutions in PIs to increase chain rigidity with better processability are known to be beneficial towards improving gas permeation properties of polyimides. If the bulky substituent is phenyl or aromatic ring, it also offers sites for electrophilic substitution. Tanaka *et al.* (1992b) substituted a number of methyl groups at various *ortho* positions in *m*PDA and *p*PDA and observed an increase in FFV with number of methyl groups. Gas permeability increased due to decreased activation energy for diffusion with increasing FFV. Li *et al.* (1997) also observed increase in FFV and gas permeability for ODPA based PIs with number of methyl groups being located at *ortho* positions in *m*PDA. The T_g of these PIs was increased due to the restricted local mobility of chain segments arisen from *ortho* substitution of methyl groups to an imide linkage.

Liu *et al.* (1999) substituted three $-CH_3$ groups on the phenyl ring of *m*-PDA (3MPDA) and four $-CH_3$ groups on the phenyl ring of *p*-PDA (4MPDA). The gas permeability of resulting PIs based on BTDA and 6FDA was investigated. PIs based on 4MPDA revealed higher FFV and gas permeability than that of 3MPDA analogs. 6FDA based PIs could be placed above the upper bound relationships for O_2/N_2. Qiu *et al.* (2006) reported PIs with isomeric substitution of bulkier $-CF_3$ group at *ortho* and *meta* to the amine moieties of *1,4*-bis(*4*-aminophenoxy)benzene and observed almost same permselectivity with improved permeability as well as higher T_g for *ortho* isomers. This indicated the effectiveness of *ortho* substitution at imide nitrogen in PIs for improvement of permeability while retaining gas permselectivity.

Incorporation of bulky groups at *ortho* position to an imide linkage restricts the free rotation around C-N bond, leading to stiffening of polymer backbone and increase in T_g. This strategy can be helpful, since with increase in permeability, the stiffened polymer backbone can resist the decrease in selectivity to some extent. Similar approach has been proved in 6FDA based PIs, wherein the presence of bulky $-C(CF_3)_2-$ in main chain increases permeability with appreciable selectivity (Coleman, 1990; Matsumoto, 1993b; Chung, 2001).

4.1.2 Gas permeation in aromatic polymers with methyl and *t*-butyl group as substituent

In the present work, selection of alkyl group (methyl and *t*-butyl) as a substituent on the aromatic ring of oxyphenyl linkage of diamine monomer is based on promises of these groups in elevating gas permeation properties in various family of polymers as briefly discussed below.

Attractive gas permeation properties by methyl group substitution are demonstrated in polysulfone (McHattie, 1991a and 1992), polycarbonates (Murugandam, 1987; Zolandz, 1992; Koros, 1993), polyarylates (Chen, 1993), polyimides (Yamamoto, 1990; Li, 1997), etc. In polyarylate, polysulfone and polycarbonate, the methyl group substitution on one of their monomer, i.e. bisphenol-A resulted in general increase in permeability with marginal or no reduction in selectivity of different gas pairs. The methyl group substitution on acid moiety of polyarylate (Pixton, 1995) also led to

increase in permeability with marginal reduction in selectivity. In case of polyimide, as stated above, methyl group substitution on *m*-PDA resulted in increase in permeability and decrease in selectivity than polyimide based on unsubstituted *m*-PDA, obtained from same dianhydride (Yamamoto, 1990; Li, 1997). The substitution by *t*-butyl group on the monomer level generally increase permeability of the resulting polymer, coupled with lower selectivity, in comparison to the polymer based on unsubstituted monomer. This was exemplified by *t*-butyl group substitution in acid moiety of polyarylate, which led to 3-6.5 times increase in permeability and 6-25% decrease in selectivity (Pixton, 1995). Bhole *et al.* (2007) reported that gas permeation properties of polyarylate containing *t*-butyl group appear near the Robeson upper bond curve. Substitution of *t*-butyl group on acid moiety of polybenzimidazole led to 10-40 times increase in gas permeability, compared to PBI based on unsubstituted isophthalic acid (Kumbharkar, 2006).

4.1.3 Effect of moisture on CO_2 permeation properties

Various hydrophilic polymers, especially ion-exchange membrane have proved to be selective towards CO_2 (Pellegrino, 1988 and 1995; Quinn 1997a and 1997b). These membranes are known to be plasticized by H_2O and show increase in permeation. The permselectivity is increased due to the selective transport of polar gases like CO_2, H_2S over non-polar gases like H_2, N_2 and CH_4. Current CO_2-selective membrane transports CO_2 either by solution-diffusion mechanism or by facilitated transport mechanism. The latter mechanism is known to reveal high permeability with high permselectivity (Zhang, 2002, Zou, 2006).

Reports on enhanced permeability of CO_2 with increase in the water content are known (Quinn 1997a and 1997b; Zou, 2006). Matsuyama *et al.* (1996) reported the facilitated transport based separation of CO_2 in a cation exchange membrane, containing protonated amine as a carrier for CO_2. Increase in water content decreased the crystallinity and energy of diffusion of the gases. Increased diffusivity of the gases due to the enhanced flexibility or plasticization of the membrane is observed by Kim *et al.* (2004). Okamoto *et al.* (1996) reported the increase in polarity of the membrane with humidification and observed the enhanced solubility selectivity of the polar CO_2 over non-polar N_2. Increase in water content in the membrane or having functional group

results in the increased volume fraction of the ionic network, which significantly increases gas permeability (Pellegrino, 1988).

Present chapter deals with investigation of gas permeation properties in selected polyimides based on *m*-phenylene diamine possessing oxyphenyl pendant group. Initially, gas permeability in PIs based on PDAB (1-phenoxy-2,4-diamono benzene) and select dianhydrides (ODPA and 6FDA) were investigated. Encouraged by promising results of these polymers, the phenyl ring belonging to oxyphenyl moiety of PDAB was substituted by selected alkyl groups that are bulky in nature and polymerized with two dianhydrides (ODPA and 6FDA). Effects of bulk and position of substitution of alkyl group in oxyphenyl ring of diamine and dianhydride used for the polymer preparation on physical and gas permeation properties of resulting PIs is discussed. Some of the polymers possessing polar pendant groups (sulfonated PIs) in their backbone and blends of PI with PBI were also investigated for their gas permeability.

4.2 Experimental section

4.2.1 PI Synthesis and membrane preparation

Synthesis of diamines with desired structural variations aiming at application of resulting PIs for gas permeation is already described in Chapter 3. Diamines synthesized for this purpose were PDAB, 2′MPDAB, 4′MPDAB, 2′,6′DMPDAB and 4′*t*BPDAB. Polymerization of these diamines with ODPA and 6FDA was performed (Section 3.3.1.1 and 3.3.3.1). Sulfonated polyimides based on SPDAB with dianhydrides ODPA and NTDA were also investigated for gas permeation under dry as well as humidified gas conditions. Blends based on SPI and PBI-BuI were also investigated for permeation of H_2, O_2 and CO_2, in view of their importance as polymer electrolyte membrane for fuel cell (PEMFC). Synthesis, purification, characterization of physical properties and membrane preparation in dense film form based on these polymers is already discussed in Chapter 3.

Details of various polyimides used for gas permeation analysis and their abbreviation are given below in the Table 4.1.

Table 4.1 Polymers investigated for gas permeation

Sr. No.	Polyimide		Abbreviation used
	Diamine	Dianhydride	
1	PDAB	ODPA	PDAB-ODPA
2	PDAB	6FDA	PDAB-6FDA
3	2′MPDAB	ODPA	2′MPDAB-ODPA
4	2′MPDAB	6FDA	2′MPDAB-6FDA
5	4′MPDAB	ODPA	4′MPDAB-ODPA
6	4′MPDAB	6FDA	4′MPDAB-6FDA
7	2′,6′DMPDAB	ODPA	2′,6′DMPDAB-ODPA
8	2′,6′DMPDAB	6FDA	2′,6′DMPDAB-6FDA
9	4′*t*BPDAB	ODPA	4′*t*BPDAB-ODPA
10	4′*t*BPDAB	6FDA	4′*t*BPDAB-6FDA
11	SPDAB (as triethylammonium sulfonate)	NTDA	SPDAB•TA-N
12	SPDAB (as imidazolium sulfonate)	NTDA	SPDAB•Im-N
13	SPDAB in $–SO_3H$ form	NTDA	$SPDAB_I$-N
14	SPDAB (as triethylammonium sulfonate)	ODPA	SPDAB•TA-O
Other polymers investigated			
15	Polybenzimidazole based on 5-*tert*-butyl isophthalic acid (BuI)		PBI-BuI
16	Blends of SPI ($–SO_3H$ form) and PBI in ‘a’ and ‘b’ weight percent, respectively		SPI(*H*)/PBI-BuI(*a/b*)

4.2.2 Measurement of gas permeability

Gas permeability of dense membranes was measured using pure gases at upstream gas pressure of 10 atm and at 35 °C using variable volume method (Stern, 1963); while maintaining permeate side at the ambient pressure. A schematic representation of permeation equipment is shown in Figure 4.1. Design of the permeation cell, component specifications, material of construction, etc. are discussed elsewhere (Houde, 1991). One end of the feed side of the cell was connected through valve V_1 to feed gas cylinder outlet and a pressure gauge (0-550 psi range). The valve V_2 was used to control the feed pressure. On the permeate side of the permeation cell, a calibrated borosilicate glass capillary containing a small mercury slug (~ 4-6 mm in length) was connected. The membrane cell assembly was kept in a water bath maintained at 35 $\pm$ 0.1 °C. Pure gases, viz., He, H_2, Ar, N_2, O_2 with 99.9% purity were obtained from Inox Air Products Ltd., India, while CH_4 and CO_2, with purity of 99.995 % were obtained from Air liquid, USA. Displacement of the mercury slug was monitored against time using cathetometer. The permeability (P) of a gas was calculated using the following equation

$$P = \frac{14.7 \times d \times F.C. \times \ell}{76 \times A \times t \times \Delta p}$$

where,

d = distance traveled by the mercury slug (cm),

F.C. = flow meter constant (volume of the gas per unit length (cm^3/cm)),

ℓ = thickness of the membrane (cm),

A = effective membrane area (cm^2),

t = time (sec) and

Δp = pressure difference across the membrane (psi).

The permeation measurements were repeated with at least 3 different membrane samples prepared under identical conditions and the data averaged. Variation in the permeability measurement was upto ± 15% for different gases studied. The variation was dependant on type of the gas. It was lesser for lighter gas like He and was higher for

heavier gas like N_2 and CH_4. The unit of permeability (P) for different gases is expressed in Barrer, where, 1 Barrer = 10^{-10} cm^3 (STP) cm/ cm^2 s cm Hg. The ideal selectivity ($\alpha = P_1/P_2$) of various gas pairs was calculated by taking a ratio of pure gas permeability.

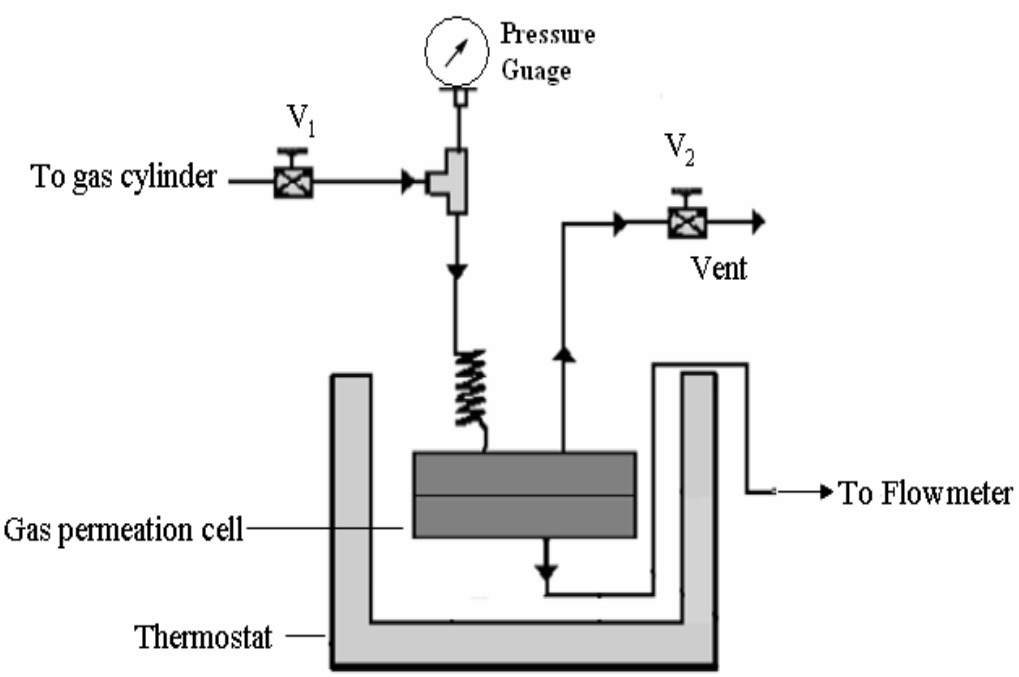

Figure 4.1 Gas permeation Equipment

Gas permeability in some of the polymers of interest (sulfonated polymers) was also studied under humidified conditions. In these cases, the feed gas was passed through a chamber filled with water, prior to its entry in the permeation cell. The membranes used for such study were initially humidified by immersing in deionised water for a day, before mounting in the permeation cell.

4.3 Results and discussion

Gas permeation properties of PDAB based polyimides are discussed initially as the base (unsubstituted O-Ph) case. This is followed by the gas permeability investigations of PIs containing O-Ph, substituted with alkyl groups. At the end, gas permeation properties of sulfonated polyimides and their blends with PBI-BuI are

discussed. Physical properties of these polyimides though are given in Chapter 3, some of these (those are known to affect gas permeation) are reproduced in this chapter for convenience.

4.3.1 Assessing capability of O-Ph group incorporation: Gas permeability of PIs based on 1-phenoxy-2,4-diamino benzene (PDAB)

To investigate the effect of side chain phenoxy group substituted at the 4-position in PDAB, gas permeation properties of two polyimides of PDAB with ODPA and 6FDA were investigated at 35°C and 10 atm upstream pressure. Dense membranes of these polymers of thickness ~ 40 μm prepared by solution casting method were used. Though, both the polymers, viz., PDAB-ODPA and PDAB-6FDA were soluble in chloroform, TCE was used as the solvent for casting PDAB-ODPA membrane; since this membrane prepared with chloroform as the solvent exhibited wavy surface. The TCE casted membrane was transparent and tough in nature and was able to withstand applied gas pressure in the permeation cell. Dense membrane of PDAB-6FDA was casted using chloroform as the solvent. The physical properties of these polymers are reproduced in Table 4.2, while gas permeability and selectivity of various gas pairs in these polyimide membranes is given in Table 4.3.

Table 4.2 Physical properties of PIs based on PDAB

Property	**PDAB-ODPA**	**PDAB-6FDA**
$\rho(g/cm^3)$	1.354	1.416
d_{sp} (Å)	4.23	5.82
FFV	0.1425	0.1728

Table 4.3 Gas permeability (P) and selectivity of PIs based on PDAB

Property	**PDAB-ODPA**	**PDAB-6FDA**
P(He)	6.9	58
$P(H_2)$	6.1	53
$P(O_2)$	0.3	5.8
P(Ar)	0.12	1.96
$P(N_2)$	0.045	1.44
$P(CH_4)$	0.017	0.44
$P(CO_2)$	1.26	16.8
$\alpha(He/N_2)$	164	41
$\alpha(He/CH_4)$	406	131
$\alpha(O_2/N_2)$	7	4.1
$\alpha(CO_2/N_2)$	30	12
$\alpha(CO_2/CH_4)$	74	37

It was observed that the permeability coefficient (P) of 6FDA based polyimide for gases studied were considerably higher than that of ODPA based polyimide. The fractional free volume as well as *d*-spacing as given in Table 4.2 of 6FDA based polyimide was higher than that of ODPA based polyimide; which led to higher permeability of all gases in PDAB-6FDA. Such increase in permeability as a result of lowering in packing density is known in case of polyimides containing $-C(CF_3)_2-$ group (Stern, 1989). Incorporation of this group restricts intra-segmental mobility of polymer chain resulting in increase chain stiffness as evidenced by the higher T_g of 6FDA based polyimide, PDAB-6FDA, as compared to that of ODPA based polyimide, PDAB-ODPA.

If permeability difference for individual gases in PDAB-ODPA and PDAB-6FDA is considered, the permeability in PDAB-6FDA was higher for bigger molecules like N_2 and CH_4, than that of smaller molecules like He and H_2. This phenomenon can be attributed to the availability of the free volume for diffusion and the kinetic diameter of the penetrants (Stern, 1989; Koros, 1993). In other words, effect of incorporation of hexafluoroisopropylidene group in increasing permeability coefficient was less significant for smaller gases like He and H_2, than for larger gases like N_2 and CH_4; in view of the fact that smaller gases can diffuse easily through the interstitial spaces (Xu, 2003). PDAB-ODPA exhibited excellent selectivity for various gas pairs. The potential for incorporation of pendant phenoxy linkage in polyimide was depicted by the O_2/N_2 selectivity of 7, high He based selectivity combined with high He or H_2 permeability and CO_2/CH_4 selectivity of 74. Observed high permeability of He and H_2 in PDAB-6FDA (58 and 53 barrer, respectively), coupled with appreciable selectivity of He/CH_4 (131) and CO_2/CH_4 (37) in PDAB-6FDA depicted usefulness of the phenoxy group substitution in improving permeation properties.

It could be worth comparing permeation properties of present polyimides with that of reported in the literature, exhibiting structural similarities. The gas permeability of present polyimides was higher than that of respective polyimides based on an unsubstituted *m*-phenylenediamine (*m*-PDA) with either ODPA (Li, 1997) or 6FDA (Yamamoto, 1990). This is attributable to the introduction of pendant phenoxy group in diamine moiety of present polyimides. This increase in permeability however was found to be lower than that obtained by the introduction of methyl group at the same position (Li, 1997). This could be ascribed to the flat nature of phenyl ring, which is known to reduce permeability and increase selectivity in other families of polymers like polyarylate (Houde, 1995), as compared to their methyl substituted analogs. It is interesting to note that the presence of flexible -O- linkage of phenoxy group in the PDAB did not adversely affect the selectivity performance in comparison to polyimides based on methyl substituted *m*-PDA and respective dianhydride. Owing to such promises, it was thought to substitute phenoxy linkage by alkyl groups like methyl and *t*-butyl at appropriate

positions and to investigate gas permeability of resulting polyimides, as elaborated in the following section.

4.3.2 Substitution of alkyl group on O-Ph of diamine moiety

It was thought to employ the capability of O-Ph group of PDAB towards accommodation of alkyl groups (methyl and *t*-butyl) by substitution at *ortho* and / or *para* positions to phenoxy linkage for altering gas permeation properties of resulting polyimides. Thus, four novel diamines, viz., 2′MPDAB, 4′MPDAB, 2′,6′DMPDAB and 4′*t*BPDAB were synthesized and polymerized with two selected dianhydrides, ODPA and 6FDA. These two dianhydrides were kept same as used for the polymerization with PDAB, so that the effect of substitution of alkyl group on gas permeation properties can be investigated.

4.3.2.1 Chain packing density and rigidity

The preparation of polyimides using alkyl substituted phenoxy diamines and two dianhydrides, ODPA and 6FDA is already described in Chapter 3. These polymers were also evaluated for physical properties those are known to affect gas permeation. These are reproduced in following Table 4.4 for ease. It could be seen that d_{sp} and FFV, which are representative of openness of polymer matrix are higher for 6FDA based PI than ODPA based PI based on the same diamine. Similar property variations were observed for density and T_g. Increase in T_g in 6FDA based PIs can be attributed to the bulky nature of -C(CF_3)$_2$- linkage, restricting the segmental mobility of the polymer main chain (Stern, 1989). It has been reported that density of halogenated polymer becomes higher than that of non-halogenated polymers such as polycarbonate (Hellums, 1989), polyarylate (Kharul, 1994), polysulfone (McHattie, 1992), etc. 6FDA based PIs shows lower values of solubility parameter (δ) than that of ODPA based PIs for the same analogous diamine, indicating the reduced molecular interaction and more free volume in the former than that of latter. Moreover, the bulky nature of -C(CF_3)$_2$- linkage and the steric effect induced by the -CF_3 group would disturb the efficient packing of the polymer chains leading to increase in FFV. In this way, for the polyimides based on same diamine, 6FDA based PIs shows higher d_{sp}, FFV and T_g with lower values of δ as shown in Table 4.4.

Table 4.4 Physical properties of polyimides based on diamines possessing substituted *o*-phenoxy side chain

Polymer	d_{sp} (Å)	FFV	δ $(cal.cm^{-3})^{1/2}$	T_g (°C)
PDAB-ODPA	4.23	0.1425	12.06	256
PDAB-6FDA	5.82	0.1728	11.03	281
2'MPDAB-ODPA	4.23	0.0998	12.22	282
2'MPDAB-6FDA	5.70, 3.38	0.168	10.97	289
4'MPDAB-ODPA	4.53	0.0985	12.20	267
4'MPDAB-6FDA	6.08, 3.62	0.167	10.97	278
2',6'DMPDAB-ODPA	4.36	0.102	12.04	311
2',6'DMPDAB-6FDA	6.29, 3.46	0.155	10.87	313
4'*t*BPDAB-ODPA	4.18	0.112	11.69	270
4'*t*BPDAB-6FDA	5.32, 3.52	0.178	10.57	281

The comparison of packing density parameters in a series of ODPA based polymers and different diamines indicates that methyl substitution lowered the packing density in comparison to unsubstituted PDAB-ODPA, irrespective of its position of substitution, either *ortho*- or *para*- to the phenoxy linkage. Though 4'MPDAB-ODPA exhibited slightly higher d_{sp} than that of 2'MPDAB-ODPA, both of them exhibited similar FFV. It is known that for similar kinds of substitution, *d*-spacing obtained by WAXD analysis may not necessarily show the same variation as that of fractional free volume. For example, Wilks *et al.* (2006) reported the increasing *d*-spacing in a series of polynorbornene (PNBs) with increasing alkyl side chain lengths such as methyl, butyl and hexyl groups. However FFV was found to be decreased with increasing alkyl side

chain lengths of PNBs. This anomalous trend in FFV was attributed to the filling up of the increased spaces with increasing side chain length. Pinnau *et al.* (2004) also observed decrease in FFV for poly(4-methyl-1-pentyne) with increasing the side chain length by either one or two methyl groups. Substitution of two methyl groups at 2 and 6 position of phenoxy linkage in 2',6'DMPDAB-ODPA did not loosen chain packing further as that of methyl substitution cases. This could be attributed to accommodation of second methyl group in the available free space, as also observed previously (Matsumoto, 1993b). Such accommodation of bulk of a small methyl group in available free space is also known in case of dimethylbisphenol-A based polysulfone (McHattie, 1991), polycarbonate (Schmidhauser, 1990) and polyarylate (Pixton, 1995; Bhole, 2003).

In case of 6FDA based polymers obtained from different alkyl substituted diamines, the effect of substitution on chain packing density can be better viewed in terms of FFV values of these polyimides, rather than their *d*-spacing. Their WAXD spectra though showed amorphous nature, they exhibited multiple peaks indicating at least two types of chain packing arrangement (Figure 3.14 in Chapter 3). Such multiple peaks were observed previously for polymers containing halogen, (Pixton, 1995; Langsam, 1993) or polymers possessing pendant phenyl ring, as observed in cases polystyrene (Mitchell, 1984) and poly(2,6-diphenyl-1,4-phenylene oxide) (Wrasidlo, 1971). In these polymers, the higher d_{sp} value corresponds to the average chain spacing while the lower d_{sp} value corresponds to the loose "stacks" of pendant phenyl rings on adjacent polymer chains (Pixton, 1995). In case of 6FDA based polyimide, occurrence of two *d*-spacing values was assigned to the probable helix structure (Matsumoto *et al.*, 1993c).

A close look at FFV of present polyimides based on 6FDA showed a general decrease in FFV after the methyl substitution in case of 2'MPDAB-6FDA, 4'MPDAB-6FDA and 2'6'MPDAB-6FDA in comparison to the parent case of PDAB-6FDA. This is indicative of the fact that in case of methyl substitution, the bulk of the added methyl group is accommodated in the available space created by inherent nature of 6FDA; leading to a reduction in available FFV. Such decrease in FFV of polymer with addition of small alkyl group like methyl has already been discussed. On the other hand, the FFV of 4'*t*BPDAB-6FDA is slightly higher than the parent case of PDAB-6FDA. Thus, bulk

of the added *t*-butyl group could further enhance the FFV, though to a small extent. FFV enhancement by *t*-butyl group in ODPA based PI (in comparison to base case of PDAB-ODPA) was much higher than in case of FDA based PI. This is indicative of the fact that 6FDA is responsible in a major way for governing the chain packing density than the diamine counterpart; while in case of ODPA based polyimides, diamine part was predominantly responsible for governing chain packing density.

The chain rigidity as evident from the glass transition temperature indicated that in case of ODPA based polyimides, alkyl substituent led to considerable increase in the T_g in comparison to the base case of PDAB-ODPA. This increase was by 11-55 °C by methyl and *t*-butyl substituents at various positions. On the other hand, comparison in case of 6FDA based PIs indicated that T_g was marginally changed by alkyl substituent irrespective of its nature or position. This could be because 6FDA by itself made polymer chains enough rigid, (as evident from increase in T_g of PDAB-ODPA from 256 °C to 281 °C for PDAB-6FDA); so that the addition of alkyl group had little effect in enhancing chain rigidity further.

4.3.2.2 Permeability and selectivity

The gas permeability and selectivity results of polyimides having alkyl substitution at the pendant phenoxy moiety are summarized in Table 4.5 and Table 4.6, respectively. In case of a particular diamine, PI based 6FDA shows higher permeability than its ODPA based counterpart. Though, the variation in permeability seems to be dependant upon the structure of dianhydride and diamine, position, bulk and number of alkyl substituent on the pendant phenoxy group also play a role, as explained in the following sections.

Table 4.5 Gas permeability (P) of polyimides based on alkyl substituted phenoxy group in *meta*-PDA

Gas Permeability	2'MPDAB -ODPA	4'MPDAB -ODPA	2',6'DMPDAB -ODPA	4'*t*BPDAB -ODPA	2'MPDAB -6FDA	4'MPDAB -6FDA	2',6'DMPDAB -6FDA	4'*t*BPDAB -6FDA
P(He)	5.4	8.8	11.8	15.8	40.1	46.1	77.0	78.0
$P(H_2)$	5.3	7.5	10.0	16.7	35.7	43.8	81.5	78.0
P(Ar)	0.11	0.17	0.34	0.53	1.04	1.52	3.8	3.7
$P(N_2)$	0.077	0.12	0.21	0.32	0.77	1.15	2.8	2.5
$P(O_2)$	0.32	0.53	0.85	1.32	3.47	4.25	10.9	10.8
$P(CH_4)$	0.028	0.047	0.13	0.17	0.26	0.53	1.01	1.3
$P(CO_2)$	1.06	2.3	3.6	5.0	12.8	14.6	38.0	36.7

Table 4.6 Gas permselectivity (α) of polyimides based on alkyl substituted phenoxy group in *meta*-PDA

Gas Permeability	2'MPDAB - ODPA	4'MPDAB -ODPA	2',6'DMPDAB -ODPA	4'*t*BPDAB -ODPA	2'MPDAB -6FDA	4'MPDAB -6FDA	2',6'DMPDAB -6FDA	4'*t*BPDAB -6FDA
$\alpha(He/H_2)$	1.02	1.18	1.18	0.95	1.12	1.05	0.95	1.0
$\alpha(He/N_2)$	69.5	74.0	56.0	49.4	52.0	40.0	28.0	31.4
$\alpha(He/CH_4)$	190.0	185.0	89.0	93.0	152.0	86.0	76.0	61.0
$\alpha(H_2/CH_4)$	187.0	158.0	75.0	98.0	135.0	82.0	80.0	61.0
$\alpha(Ar/N_2)$	1.43	1.42	1.62	1.66	1.35	1.32	1.36	1.48
$\alpha(O_2/N_2)$	4.1	4.5	4.0	4.1	4.5	3.7	4.0	4.35
$\alpha(CO_2/N_2)$	13.7	19.6	17.0	15.8	16.5	12.7	13.7	14.8
$\alpha(CO_2/CH_4)$	37.5	49.0	27.0	30.0	48.3	27.3	37.5	28.7
$\alpha(N_2/CH_4)$	2.7	2.5	1.6	1.9	2.9	2.2	2.7	2.0

4.3.2.3 Effect of dianhydride

PI based on 6FDA showed higher permeability (4.6 to 13.3 times) and lower selectivity (0.04 to 0.53 times) than its ODPA based counterpart for the same analogous diamines (Table 4.5 and Table 4.6). It has been well reported that 6FDA based PIs show higher permeability and lower selectivity than that of other dianhydrides such as ODPA, BTDA, PMDA, BPDA etc. with similar diamine structure (Koros, 1988; Tanaka, 1992; Stern, 1993; Matsumoto, 1993b; Hirayama, 1996a; Li, 1996; Wang 2005; Ding 2007). The major focus of this work is on the alkyl substitution on dianhydride moiety of PI. Effects of dianhydride could also be elaborated along with effect of alkyl substituent, as given below.

4.3.2.4 Effect of alkyl substituent

In case of ODPA based polyimides with alkyl substituent, the permeability increases in an order: 2'MPDAB-ODPA < 4'MPDAB-ODPA < 2',6'DMPDAB-ODPA < 4'*t*BPDAB-ODPA (Table 4.5). It is observed that substitution of alkyl group on the pendant phenoxy moiety of PI based on ODPA led to increase in permeability, except in case of 2'MPDAB-ODPA. In this case; permeability of O_2, N_2 and CH_4 increased while that of He, H_2, Ar and CO_2 was decreased compared to base case of PDAB-ODPA. 4'MPDAB-ODPA showed increase in permeability compared to PDAB-ODPA and 2'MPDAB-ODPA. This shows that $–CH_3$ group substitution on pendant phenoxy group at *para* position is more effective in increasing the permeability than that of substitution of this group at *ortho* position. There is an increase in permeability for 4'MPDAB-ODPA by 1.42 to 2.17 times and 1.23 to 2.78 times with respect to 2'MPDAB-ODPA and PDAB-ODPA, respectively. In spite of the increase in permeability, selectivity of various gas pairs for both the methyl group substituted PIs are almost similar (except a small lowering in $\alpha(H_2/CH_4)$ and a increase in CO_2 based selectivities for *para* substituted PI). With substitutions of two $–CH_3$ groups at *ortho* positions of pendant phenoxy group in 2',6'DMPDAB-ODPA, the permeability further increased by 1.89 to 4.60 times and 1.33 to 2.77 times than that of 2'MPDAB-ODPA and 4'MPDAB-ODPA, respectively. This led to a large decrease in He and H_2 based selectivities. Comparatively, CO_2 based selectivities were lowered to a smaller extent.

Among the alkyl substituted PIs, incorporation of bulky *t*-butyl group on the pendant phenoxy group (4'*t*BPDAB-ODPA) showed increase in permeability by 1.31 to 6.01 times than that of the base case. Though 4'*t*BPDAB-ODPA exhibited lowest *d*-spacing (4.18 Å), it revealed the highest FFV (0.112) with lowest value of solubility parameter (11.69) (Table 4.4). The later parameter is an indicative of the reduced interchain interactions and decrease in packing density, accounting for its higher permeability. Considering the voluminous size of *t*-butyl group (73.6 $Å^3$) than that of methyl (22.7 $Å^3$) (Langsam, 1993), the decreased interchain packing in the resultant PIs by the embodiment of former group would be more than that by the later. Increased permeability by incorporation of bulky *t*-butyl group in PIs (Kim, 2002 and 2005) and polyarylates (Pixton, 1995; Bhole, 2007) are known.

An interesting result is seen between 4'*t*BPDAB-ODPA and 2',6'DMPDAB-ODPA (Table 4.5 and 4.6). Former exhibits better selectivity performance despite its increase in permeability by a factor of 1.31 to 1.67 than that of latter. 4'*t*BPDAB-ODPA also exhibits highest Ar/N_2 selectivity (1.66) and its O_2/N_2 selectivity (4.1) is close as compared to other ODPA based PIs having alkyl substituent.

In case of 6FDA based polyimides, the permeability increases in an order 2'MPDAB-6FDA < 4'MPDAB-6FDA < 2',6'DMPDAB-6FDA ≈ 4'*t*BPDAB-6FDA. Substitution of a single $–CH_3$ group at either *ortho* or *para* (2'MPDAB-6FDA and 4'MPDAB-6FDA) on pendant phenoxy group demonstrated decrease in permeability and increase in selectivity of different gas pairs than that of the unsubstituted analogue (PDAB-6FDA); except for the increase in CH_4 permeability in 4'MPDAB-6FDA. On the other hand, such $–CH_3$ group substitution at *para* position in case of ODPA based PIs (4'MPDAB-ODPA) led to increase in permeability significantly (Table 4.5). In other words, dianhydride was predominantly responsible for governing permeation. This can be attributed to the voluminous $–C(CF_3)_2–$ linkage existing in 6FDA based PIs, which by itself causes the looser intersegmental packing. An incorporation of a $–CH_3$ group on the phenoxy group in diamine can be accommodated in the large free volume created by $–C(CF_3)_2–$ linkage. In other words, a single $–CH_3$ group substitution in 6FDA based PIs pays no role to disruption of chain packing; while there is an effective disruption in chain packing by $–CH_3$ group substitution (particularly at *para* position) in ODPA based PIs. A

decrease in permeability by $–CH_3$ group in PIs substitution has been observed by Matsumoto *et al.* (1993b). Similar effect of decrease in permeability by $–CH_3$ group substitution in polyarylates (Pixton, 1995; Kharul 1998; Bhole, 2003), polysulfone (McHattie; 1991) and polycarbonate (Schmidhauser, 1990) was also noted.

2'MPDAB-6FDA exhibits better selectivity for all the gas pairs, except Ar/N_2 (Table 4.6). This is in good agreement with the general trend of polymers exhibiting lower permeability and higher selectivity. With an embodiment of second $–CH_3$ group at *ortho* position on pendant phenoxy group (2',6'DMPDAB-6FDA) permeability further increases. However, permeability by incorporating *t*-butyl group in 4'*t*BPDAB-6FDA is almost same as that of 2',6'DMPDAB-6FDA, despite their large difference in intrasegmental mobility (difference in T_g). 2',6'DMPDAB-6FDA can be considered as the most rigid PIs as evidenced by its lowest intrasegmental mobility (highest T_g: 313 °C) since the two *ortho* substituted $–CH_3$ groups on pendant phenoxy group should sterically hinder the rotation of pendant phenoxy group. It has been observed in PIs that modifications conferring increased stiffness and a decrease in packing density result in an increase in permeability without loss of selectivity (Hoehn, 1980; Kim, 1988; Kulkarni, 1994; Pixton, 1995). In 4'*t*BPDAB-6FDA, voluminous *t*-butyl group being substituted at *para* position not only increases the side chain length but also confers more rotational freedom to the pendant phenoxy group. Such architecture should reduce the interchain interactions significantly contributing to an increase in FFV and hence rendering higher permeability. No considerable difference in selectivity between 2',6'DMPDAB-6FDA and 4'*t*BPDAB-6FDA is observed (Table 4.6). It should be noticed that, 4'*t*BPDAB based PIs exhibits highest permeability despite its lowest *d*-spacing values indicating that apart from average intersegmental distance some sort of other scattering features has been reflected by their X-ray spectra. Such phenomenon with lower *d*-spacing values and higher permeability has also been observed in polyarylates having *t*-butyl group as reported by Pixton *et al.* (1995). However, the lowest density and highest FFV exhibited by 4'*t*BPDAB based PIs further support the higher distance between their chains accounting their higher permeability.

Substituting alkyl group at the *para*-position as compared with at *ortho*-position bestows some advantages for increasing the gas permeation. In both the cases, there is an

increase in the volume of the resultant bulky side group with the substitution as shown in the Figure 4.2 and Figure 4.3.

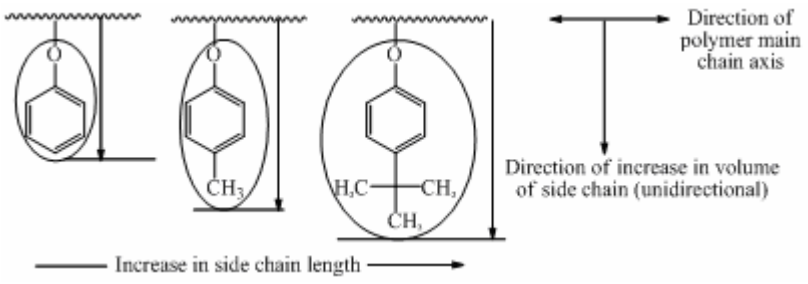

Figure 4.2 Lengthening of side chain due to substitution of alkyl groups at *para* position

The probability of reduction of interchain interaction due to the lengthening of the side chain with an increase in free volume in *para* substitution case may result in lower intermolecular hindrance to rotation of torsion mobility of main chain facilitating intrasegmental mobility. This phenomenon can be evidenced by the lower T_g of the ODPA based PIs with alkyl substituent at *para*-position than that of at *ortho*-position (Table 4.4). This phenomenon leads to increase in permeability of various gases (Table 4.5). This effect of increasing the side chain length is more pronounced in ODPA based PIs. In 6FDA based PIs, permeability increases in the order 4'MPDAB-6FDA < PDAB-6FDA < 4'*t*BPDAB-6FDA indicating that added bulk of substituent in 4'MPDAB-6FDA is accommodated in the free volume created by -$C(CF_3)_2$- linkage.

Form the Figure 4.3 below, it can be seen that the increase in volume of the side chain substituent due to alkyl substitution at *ortho* position does not increase the chain length (as in the case of *para* substituent) but increases the width of the side chain.

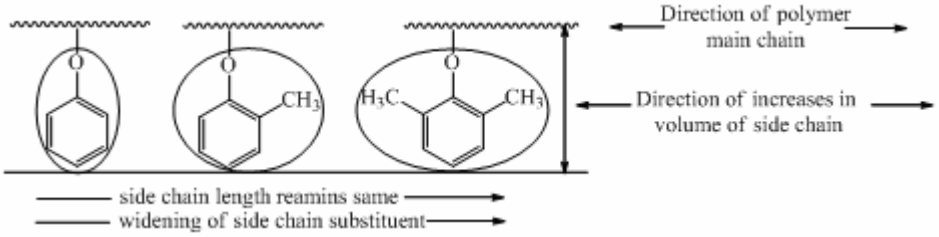

Figure 4.3 Widening of the side chain due to substitution of alkyl group at *ortho* position

Xu *et al.* (2003) reported that the relative rigid and longer side substituents impart a higher level of ring torsion leading to increase in permeability. In the present case, alkyl

substituent at *ortho*-position on pendant phenoxy moiety renders rigidity to the PI chain (as evidenced by higher T_g) while that of at *para*-position increase lengthening of the substituent. Both these effects lead to increase in permeability in present cases.

4.3.3 Gas permeability of sulfonated polyimides (SPI)

Dense membranes of SPIs were prepared by casting solutions of SPDAB•TA-O, SPDAB•TA-N and SPDAB•Im-N in DMAc at 80 °C under the dry atmosphere. These membranes possess triethyl amine/imidazole salt form of sulfonated group. These two types of membranes were then immersed in distilled water at 60 °C for a day in order to remove traces of DMAc, followed by drying in vacuum oven at 80 °C for 3 days. The membranes were converted to sulfonic acid form by immersing in 1N HCl for a day, followed by immersing in deionised water for a day and then drying in vacuum oven at 60 °C for 3 days.

4.3.3.1 Gas permeability in dry state

Membrane based on ODPA (SPDAB•TA-O) had poor hydrolytic stability and was disintegrated in water after 4 h. Gas permeation properties of dry membranes (average thickness of 40 μm) were investigated using three pure gases, viz., H_2, O_2 and CO_2 at 10 atm upstream pressure and at 35 °C. The results are given in Table 4.7 below.

Table 4.7 Gas permeability (P) and selectivity (α) of SPIs under dry conditions

Permeation property	SPDAB•TA-O	SPDAB•TA-N	SPDAB•Im-N	$SPDAB_I$-N
P (H_2)	2.16	1.89	0.96	2.23
P (O_2)	0.25	0.17	NM[a]	0.32
P (CO_2)	2.37	3.03	0.78	5.62
α(H_2/O_2)	8.64	11.1	-	6.9
α(CO_2/H_2)	1.1	1.6	0.81	2.5
α(CO_2/O_2)	9.5	17.8	-	17.5

Permeability of H_2 and O_2 in 4,4′-Oxydiphthalic dianhydride (ODPA) based polymer, SPDAB•TA-O was higher than that of naphthalene dicarboxylic dianhydride based polymers (SPDAB•TA-N, SPDAB•Im-N). SPDAB•TA-O has higher structural flexibility due to ether linkage in its dianhydride moiety, while naphthalene dianhydride based polymer SPDAB•TA-N is anticipated to be rigid. This difference in rigidity could be responsible for the observed difference in gas permeability. Between SPDAB•TA-N and SPDAB•Im-N, the former showed higher permeation than that of the later. This can be attributed to the peculiar planar structure of the imidazolium cation, rendering close chain packing.

In SPDAB•TA-N, the salt form has tetrahedral geometry for three ethyl groups of Et_3N^+–, vis-à-vis the flat nature of imidazolium cation (Im^+) in SPDAB•Im-N. Flat or planar structures are known to be accommodated in the available free volume of the polymer as compared with tetrahedral structure like Et_3N^+–, resulting in decrease in permeability. Such a phenomenon is explained earlier in Section 4.3.1. In the WAXD spectra of SPDAB•TA-N and SPDAB•Im-N (Figure 3.8 of Chapter 3), the latter shows amorphous peak maxima at higher angle (25.88°) than that of lower angle (24.32°) in the former (Section 3.5.2.5 of Chapter 3). Though this difference is small, it is indicative of the close-packed structure in SPDAB•Im-N. Flat structure and increase in aromatic character due to the imidazolium cation in SPDAB•Im-N may also lead to the π-π interaction between the imidazolium cation and other aromatic phenyl rings, resulting in close packing. Such types of π-π interactions between imidazolium rings and other aromatic structures are known (DuPont, 2004; Jiang, 2009).

CO_2 permeability through these polymers varied in the order as SPDAB•Im-N < SPDAB•TA-O < SPDAB•TA-N < $SPDAB_I$-N. It is interesting to note that all these polymers (except SPDAB•Im-N) exhibit higher CO_2 permeability than that of H_2. $SPDAB_I$-N exhibited the highest CO_2/H_2 selectivity among the series. Conversely, in most of the glassy polymers, smaller gas, H_2 usually shows higher permeability than that of CO_2. This dominance of penetrant size diffusivity in glassy state leads to CO_2/H_2 selectivity of < 1 (or H_2/ CO_2 selectivity of > 1). The observed behavior of higher permeation for CO_2 in present polymers reflects that this functionality (-SO_3H or its salt) leads to higher CO_2 solubility, enhancing its permeation than that of smaller gas H_2.

Imidazolium or triethyl ammonium based salt formation may be responsible for this behavior. It is well known that imidazolium based salts of organic molecules (typically called as ionic liquids; ILs) exhibit high CO_2 sorption properties (Bara, 2009)

4.3.3.2 Permeability with humidified gas

Owing to the observed behavior of high CO_2 pereambility, membrane samples (SPDAB•TA-N, SPDAB•Im-N and $SPDAB_I$-N) which were already analyzed for gas permeability were immersed in deionized water for a day. These wet membranes were then directly used for the analysis of permeability coefficient of humidified gases (H_2 and CO_2). The results are summarized in the following Table 4.8.

Table 4.8 Permeability (P) and selectivity (α) of SPIs under humidified gas conditions

Permeation property	SPDAB•TA-N		SPDAB•Im-N		$SPDAB_I$-N	
	Dry	Humidified	Dry	Humidified	Dry	Humidified
P (H_2)	1.89	4.41	0.96	5.51	2.23	6.30
P (CO_2)	3.03	12.9	0.78	22.1	5.62	27.9
α(CO_2/H_2)	1.6	2.92	0.81	4.02	2.5	4.43

From the above Table 4.8, it is seen that the permeability of both humidified gases increased in the order: $SPDAB_I$-N > SPDAB•Im-N > SPDAB•TA-N. The permeability of H_2 increased by 2.33, 5.73 and 2.82 fold, while that of CO_2 increased by 4.25, 28.33 and 4.97 fold in comparison to the dry gas permeability in SPDAB•TA-N, SPDAB•Im-N and $SPDAB_I$-N, respectively. SPDAB•Im-N demonstrated highest difference in permeability of dry and humidified gases (H_2 and CO_2). These membranes are of ion exchange membranes type, which are known for preferential CO_2 permeation (LeBlanc, 1980; Pellegrino, 1988; Quinn, 1997a; Yamaguchi, 1995; Zhang, 2002). Permeability of polar gases (CO_2 and H_2S) in such membranes depends on their ionic site density, IEC and water content (Matsuyama, 1994; Quinn, 1997a). Enhanced solubility of CO_2 with

increase in IEC and water uptake of cation-exchange membrane is known (Pellegrino, 1988; Quinn, 1995 and 1997a; Matsuyama, 1994 and 1999). The IEC in present membranes increases in the order SPDAB•TA-N (0.39) < SPDAB•Im-N (1.49) < $SPDAB_I$-N (1.92), while the water content increases in the order SPDAB•Im-N (30%) < SPDAB•TA-N (39%) < $SPDAB_I$-N (49%), (Table 5.2 in Chapter 5). Since $SPDAB_I$-N shows both, higher IEC (1.92 mequv/g) and water content (48.9%), both these parameters would lead to enhanced interaction with CO_2; leading to its enhanced permeability. Highly swollen state would also have its effect on increased permeability, as the polymer chains are more apart than from dry state and are more dynamic due to surrounded water (plasticization effect), facilitating diffusion process.

The transport of humidified CO_2 can be considered as the facilitated types of transport. The observed difference in the selectivity, α (CO_2/H_2) in dry and humidified state conveys the significance of humidified gas conditions. The largest jump in permeability was shown by SPDAB•Im-N; which could be the effect of imidazolium cation. Imidazolium based ionic liquids are well appreciated for high CO_2 sorption (Tang, 2005; Bara, 2009). These membranes even in dry state were selective for CO_2 over H_2. This indicates that these types of polyimides can be further tuned to manipulate diffusivity to draw an ultimate advantage of enhanced CO_2 interactions. Quantification of gas sorption and diffusion analysis would have led to better understanding towards effects of these modifications on the crucial permeation properties, which could not be attempted in present investigation.

4.3.4 Gas permeability of blend membranes

Dense membranes of blends of sulfonated PI and polybenzimidazole (PBI-BuI) were prepared as discussed earlier in Section 3.3.2.5 of Chapter 3. Membranes had an average thickness of 40 μm. These membranes were soaked in distilled water at 60 °C for a day in order to remove traces of DMAc and then acidified in 1N HCl in order to convert them from triethylammonium sulfonate to sulfonic acid form. This was followed by rinsing with deionized water and drying in vacuum oven at 80 °C for 3 days. These membranes were abbreviated as SPI(*H*)/PBI-BuI(a/b), where 'H' stands for sulfonic acid form of sulfonated PI, while 'a' and 'b' denotes the weight percentage of SPI and PBI-

BuI, respectively. Gas permeation properties of blend membranes, viz., SPI(*H*)/PBI-BuI(30/70), SPI(*H*)/PBI-BuI(40/60) and SPI(*H*)/PBI-BuI(50/50) were investigated using three pure gases, viz., H_2, O_2 and CO_2 at 10 atm and 35 °C. The results are summarized in following Table 4.9.

Table 4.9 Gas Permeability and selectivity of the blend membranes

Permeation property	PBI-BuI[a]	$SPDAB_I$-N	SPI(*H*)/PBI-BuI(30/70)	SPI(*H*)/PBI-BuI(40/60)	SPI(*H*)/PBI-BuI(50/50)
P (H_2)	10.7	2.23	4.11	3.95	5.48
P (O_2)	0.42	0.32	0.19	0.23	0.33
P (CO_2)	1.91	5.62	1.35	1.63	2.67
$\alpha(H_2/O_2)$	25.5	6.9	21.7	17.4	16.6
$\alpha(CO_2/H_2)$	0.18	2.5	0.33	0.41	0.49
$\alpha(CO_2/O_2)$	4.5	17.5	7.1	7.2	8.1

[a]: (Kumbharkar, 2006)

It is observed that, among the blends with different weight ratio, permeability coefficient increased with decreasing content of PBI-BuI, with an exception of H_2 permeation in SPI(*H*)/PBI-BuI(40/60) [3.95], which is slightly lower than that of SPI(*H*)/PBI-BuI(30/70) [4.11]. Among the blend membranes and parent polymers, PBI-BuI shows the highest permeability for H_2 and O_2, while $SPDAB_I$-N demonstrates the highest CO_2 permeation. The enhanced CO_2 permeation in blend can be attributed to the presence of polar sulfophenoxy moiety belonging to SPI, which acts as sites for interaction with polar CO_2 molecule. In addition, the increase in IEC of blend membrane with increasing content of SPIs also supports higher permeation of polar gases like CO_2. (IEC of blend membrane is explained in the impending Chapter 5 in Section 5.3.4). The higher CO_2 permeation in $SPDAB_I$-N can be attributed to the larger interaction between polar CO_2 as well as polar $–SO_3H$ moiety of SPI, which was explained in the Section 4.3.3.1. Among blend membranes, SPI(*H*)/PBI-BuI(50/50) shows the highest

permeability which can be attributed to the increased concentration of bulky pendant polar sulfophenoxy group due to the increased content of SPI. Such bulky pendant group should increase the available free volume for the diffusion of gases.

One of the interesting features in the permselectivity of the blend membranes is that permselectivity for H_2/O_2 decreases while that of CO_2 over H_2 and O_2 increases with increasing content of SPI. Thus, our attempt to make blends of polybenzimidazole (PBI-BuI) with sulfonated PI has improved the selectivity performance of polar gases such as over CO_2 over H_2 and O_2 than that of pristine PBI-BuI.

3.5 Conclusions

1) For the analogous diamine, 6FDA based PI shows higher d_{sp}, T_g and permeability coefficient than that of ODPA based PIs. Though the increase in permeability was by 4.6 to 13.3 times, the decrease in selectivity was just by a factor of 0.04 to 0.53.
2) In case of ODPA based PIs permeability increases in the order PDAB-ODPA ≈ 2'MPDAB-ODPA < 4'MPDAB-ODPA < 2',6'DMPDAB-ODPA < 4'*t*BPDAB-ODPA. In 6FDA based PIs permeability increases in the order 2'MPDAB-6FDA < 4'MPDAB-6FDA < PDAB-6FDA < 2',6'DMPDAB-6FDA ≈ 4'*t*BPDAB-6FDA. In ODPA based PIs, better selectivity performance is shown by PDAB-ODPA while in 6FDA based PIs 2'MPDAB-6FDA demonstrates the best selectivity.
3) Though *d*-spacing value for substitution of voluminous *t*-butyl group on pendant phenoxy group in PIs (4'*t*BPDAB-ODPA and 4'*t*BPDAB-6FDA) is low; these polymers demonstrated the highest permeability, which is in tune of variation in FFV. This indicated that the packing density is better expressed in terms of FFV for these polymers.
4) Between the PIs based on isomeric diamines 2'MPDAB and 4'MPDAB (with either ODPA or 6FDA), the later exhibited lower T_g, higher permeability and lower selectivity.
5) In case of ODPA based PIs, chain packing and gas permeability is largely affected by the structural variation in diamine moiety. Conversely, in case of PIs based on 6FDA, the dependence of structural variation in diamine moiety on gas permeability was

largely suppressed by the effects of hexafluoroisopropylidene (–$C(CF_3)_2$–) linkage of dianhydride moiety.

6) 4'*t*BPDAB-ODPA shows higher permeability without any appreciable loss of selectivity as compared with 2',6'DMPDAB-ODPA. In addition, selectivity performance of the former is higher for some of the gas pairs than of latter. 4'*t*BPDAB-6FDA and 2',6'DMPDAB-6FDA exhibits almost same permeability and no significant difference of selectivity is observed between them also.
7) In case of SPIs, though humidification of both gases and membranes of SPIs lead to an increase in permeability selectivity also increases. This effect is more pronounced in CO_2, indicating the importance of SPIs in CO_2 separation.
8) In blend membranes, permeability of CO_2 increases with increasing content of SPIs. In addition, permselectivity for H_2/O_2 decreases while that of CO_2 over H_2 and O_2 increases with increasing content of SPI.

Chapter 5

Investigation of polyimides towards their applicability as PEM materials

5.1 Introduction

Since inception of fuel cell almost half century ago, perfluorinated sulfonic acid copolymer, Nafion, is symbolized as the current state-of-the-art PEMs due to its high proton conductivity, excellent hydrolytic and redox stability (Roziere, 2003; Souzy, 2005; Hamrock, 2006). However, inherent drawbacks of Nafion, particularly their high cost (explained in Section 1.7.1 of Chapter 1) encouraged researchers to look for alternate polymers containing sulfonic acid groups. This resulted in synthesis and evaluation of various novel hydrocarbon polymers containing sulfonic acid group and acid-base polymer electrolytes as PEM material for fuel cells.

Among these, sulfonated polyimides (SPIs) prepared particularly from various sulfonated diamines (SDAs), have become the cynosure of all attention due to their proven ability as PEM (Guo, 2002; Fang, 2002; Asano, 2006). Besides, the ease of chemical structural modifications in SPI conferring low manufacturing cost, enhanced thermal and mechanical properties make them more attractive (Yin, 2006a; Marestin, 2008). However, under severe acidic environment of PEMFC, conventional five membered-imide linkage is susceptible towards hydrolysis (Genies, 2001a; Fang, 2002; Alvarez-Gallego, 2007). Attention towards SPIs with organic soluble six membered-imide linkages has therefore been favored; as they possess better thermal, hydrolytic and chemical stability (Fang, 2002; Marestin, 2008). Side-chain-type SPIs are being paid more attention since they hold better option for the above mentioned disadvantages (Fang, 2006; Hu, 2007; Yin, 2006a; Savard, 2008). Infact, SPIs can be categorized into two main types, as main-chain-type and side-chain-type, which is already described in Section 1.6.1 of Chapter 1.

Being a zwitter ion, sulfonated diamine (SDA) is insoluble in organic solvents. Therefore, protection of $–SO_3H$ group of SDA by an organic base; triethyl amine (TEA) is frequently followed in order to dissolve it in organic solvent (*m*-cresol). Subsequently,

SDA in its triethylammonium sulfonate form is then condensed with six-membered dianhydride to synthesize resultant SPI (Genies, 2001a; Fang, 2002; Lee, 2004; Li, 2007c; Savard, 2008; Chhabra, 2009). In water media, this resultant SPI in the salt form comprises Bronsted conjugate acid-base pair of mobilized triethylammonium cation with immobilized sulfonate anion tethered to either main chain or side chain. Subsequent acidification of SPI in the salt form confers SPI with free sulfonic acid group, behaving as proton exchange membrane (PEM) in fuel cell. However, utilization of myriad organic bases in place of TEA can constitute different skeleton of Bronsted conjugate acid-base pair in SPI and in-situ polymer-in-salt electrolyte can thus be generated. The present chapter focuses on such type of PEM.

Polymer blending is one of the adaptable techniques to develop new PEMs for tailor made application for PEMFC, which combine the excellent properties of more than one existing polymer (Kerres, 2000 and 2002; Deimede, 2002). However, the development of new useful blends is limited by the immiscibility of many polymer pairs of interest. Polymers can only be miscible when there is a negative free energy of mixing.

$$\Delta G_{mix} = \Delta H_{mix} - T.\ \Delta S_{mix}$$

However, considering the high molecular weight of the polymers, ΔS_{mix} becomes negligible. Thus only the deciding factor for the negative free energy of mixing of blend remains ΔH_{mix}. In other words the mixing must be exothermic, entitling the blend component with specific interaction, which range from strongly ionic to weak and non-bonding interaction such as hydrogen bonding, ion-dipole, dipole-dipole and donor-acceptor interaction. As a result, presence of ionic moieties, which in particular capable of specific interaction in either or both the polymer blend components, can tune blending towards miscible blend formation. We, therefore, determined to make the blends from functional group containing polymers like sulfonated polyimides with PBI. In the former, presence of acidic sulfonic acid group should interact favorably with the basic benzimidazole group of the latter. Though, several reports were available on blends of polyimides and PBI (Guerra, 1988; Jaffe, 1994; Ahn, 1997; Lee, 1999), no reports, till dates were available on blends of side-chain-type SPI and PBI to the best of our knowledge.

Aromatic polybenzimidazole (PBI) is a basic heterocyclic polymer having excellent thermal stability with outstanding high glass transition temperature, high chemical resistance, low gas permeability and excellent mechanical strength (Buckley, 1988; Kulkarni, 2008; Kumbharkar, 2009). Such basic polymer when doped with amphoteric acid, which both donates and accepts the proton, leads to proton migration by Grotthus mechanism (Bouchet, 2001; Ma, 2004). Additionally, proton migration becomes more feasible at higher temperature as the energy of activation (E_a) necessitated for the proton transportation becomes less. Another approach is to make acid-base polymer blend through the formation of hydrogen bridging and base protonation, reducing the swelling behavior as well as improving the proton conductivity, thermal stability and mechanical flexibility. Blends of PBI with different sulfonated polymers have already been used in PEMFC (Kerres, 1999; 2000 and 2004; Hasiotis, 2001b; Kosmala, 2002; Wysick, 2005). However, blending of PBI with SPI is advantageous as apart from interaction between sulfonic acid group and basic imidazole group, imide group also interacts with benzimidazole groups assisting formation of miscible blends (Guerra, 1988; Ahn, 1997; Pu, 2005).

Thus in the present Chapter, our study is focused on investigation of membranes prepared from SPI containing flexible sulfophenoxy group in the side chain, described earlier in Section 3.3.2 of Chapter 3. In addition, blends of this polymer with PBI based on 5-*tert*-butyl isophthalic acid (BuI) were also prepared for the application as PEM material.

5.2 Experimental

5.2.1 Syntheses of polymer electrolytes

5.2.1.1 Synthesis of Sulfonated Polyimide (SPI)

SPIs were synthesized from the novel sulfonated diamine viz., 4'-sulphonic-1-phenoxy-2,4-diaminobenzene (SPDAB) and dianhydrides such as ODPA and NTDA. NTDA based SPI was synthesized using two different organic bases viz., TEA and imidazole while for ODPA based SPI, only TEA was used as the organic base as given in the Section 3.3.2.1 of Chapter 3.

5.2.1.2 Synthesis of polybenzimidazole (PBI)

PBI based on 3,3'-diaminobenzedine (DAB) with aromatic dicarboxylic acids, viz., isophathalic acid (IPA) and *5-tert*-butyl isophthalic acid (BuI) were synthesized as explained earlier in the Section 3.3.2.2 of Chapter 3.

5.2.2 Membrane preparation

Dense membranes of SPIs, PBIs and blend of these polymers were prepared as described previously in Section 3.3.2.3, Section 3.3.2.4 and Section 3.3.2.5, respectively of Chapter 3.

Details of various PEM and their abbreviation are given below in the following Table 5.1.

Table 5.1 PEM and their abbreviation

Sr. No.	PEM used	Abbreviation used
1	Polybenzimidazole based on isophthalic acid (IPA)	PBI-I
2	Polybenzimidazole based on *5-tert*-butyl isophthalic acid (BuI)	PBI-BuI
3	SPI based on SPDAB and NTDA in triethylammonium sulfonate form	SPDAB•TA-N
4	SPI based on SPDAB and NTDA in $–SO_3H$ form after acidification of SPDAB•TA-N in 1N HCl, followed by washing with deionised water	$SPDAB_I$-N
5	SPI based on SPDAB and NTDA in imidazolium sulfonate form	SPDAB•Im-N
6	SPI based on SPDAB and NTDA in $–SO_3H$ form after acidification of SPDAB•Im-N in 1N HCl, followed by washing with deionised water	$SPDAB_{II}$-N
7	SPI based on SPDAB and ODPA in triethylammonium sulfonate form	SPDAB•TA-O
8	Blends prepared from SPI (SPDAB•TA-N) and PBI (PBI-BuI), where '*a*' and '*b*' denotes weight percentage of SPDAB•TA-N and PBI-BuI, respectively, while '*TEA*' shows SPI in triethylammonium sulfonate form	SPI(TEA)/PBI-BuI(a/b)
9	Corresponding blend, after acidification of SPI(TEA)/PBI-BuI(a/b) in 1N HCl followed by washing in deionised water, where 'H' denotes SPI in $–SO_3H$ form	SPI(H)/PBI-BuI(a/b)
10	Corresponding blend, after doping of SPI(TEA)/PBI-BuI(a/b) with either 1M or 12M H_3PO_4	SPI(PA)/PBI-BuI(a/b)
11	Corresponding blend, after doping of SPI(TEA)/PBI-BuI(a/b) with 1M H_2SO_4	SPI(SA)/PBI-BuI(a/b)

5.2.3 Determination of water uptake (WU) capacity of membranes

Initially, membranes of 5 X 5 cm^2 size and thickness of ~ 50 μm were kept in a vacuum oven at 80 °C for 48 h to ensure the constant weight of the dry membrane (W_d). It was then immersed in deionised water for 48 h at ambient condition. The membranes were then taken out and wiped instantly by a tissue paper to remove only the adhered water present on the membrane surface. Afterwards, the wet membranes were weighed (W_w) and thus, water imbibed inside the membrane could be determined. The precise WU capacity was subsequently calculated with the following equation,

$$WU = (W_w - W_d / W_d) \; X\,100 \; (\%)$$

A balance with 0.1 mg accuracy was used and at least three measurements were conducted under identical conditions and the values reported are the average of these measurements.

5.2.4 Determination of phosphoric acid uptake of membranes

Membranes of 4 X 3 cm^2 size based on parent polymers and blends were first dried in a vacuum oven at 80 °C for 3 days and then weighed (W_i). These membranes were then doped by immersing in 12 M H_3PO_4 for 3 days. Doped membranes were then wiped out with tissue paper to remove acid adhered on the membrane surface followed by drying in vacuum oven at 80 °C for 4 days. After taking out the sample form vacuum oven, it was immediately weighed (W_f). The acid uptake by the membrane was subsequently calculated with the following equation.

$$\text{Acid uptake} = [(W_f - W_i)/ W_i] \; X\,100 \; (\%)$$

5.2.5 Determination of Ion exchange capacity (IEC) of membranes

The ion exchange capacity (IEC) of PEM was determined by using classical acid-base titration method. The membranes were dried in a vacuum oven at 80 °C for 48 h, then immediately weighed (W_{dry}) followed by soaking in 2 M NaCl solution to exchange the available H^+ with Na^+. The exchange was performed in the shaking water bath for a day at ambient temperature. The H^+ released in the solution was titrated with standardized 0.01 N NaOH (against oxalic acid) solution with phenolphthalein as an indicator. At least five membrane samples of size 5 X 3 cm^2 having comparatively lower

thickness of ~20-25 μm were used. Afterward, separate titrations for these membranes were performed and the results of ion exchange capacities of three samples averaged. The following equation was used to determine the IEC.

$$IEC = \frac{(V \times N_{NaOH})}{W_{dry}}$$

where, V is the volume of standardized NaOH in mL and N_{NaOH} is the standardized normality of 0.01N NaOH.

In case of blend PEM, the theoretical IEC was calculated with the following equation (Zhao, 2007).

$$IEC_{Blend} = \frac{(IEC_{SPI} \times W_{SPI}) + (IEC_{PBI\text{-}BuI} \times W_{PBI\text{-}BuI})}{W_{Blend}}$$

where, IEC_{Blend} is the theoretical IEC of the PEM blend

W_{Blend} = Actual weight of the PEM blend in dry state

IEC_{SPI} = IEC of the SPI

i.e. theoretical value of IEC of $SPDAB_I$-N (1.95 mequv/g)

W_{SPI} = Actual weight of the SPI in W_{Blend} = [W_{Blend} * (% SPI)] / 100

$IEC_{PBI\text{-}BuI}$ = IEC of the PBI-BuI considered same as of PBI-I i.e. 0.02 mequv/g (Kerres, 2000)

$W_{PBI\text{-}BuI}$ = Actual weight of the PBI-BuI in W_{Blend} = [W_{Blend} * (% PBI-BuI)] / 100

5.2.6 Determination of hydrolytic and oxidative stability of membranes

Hydrolytic stability of the PEM samples having rectangular size 4 X 1 cm^2 and thickness ~40-50 μm was evaluated by immersing them in deionised water at 80 °C. The water bath was adjusted at a lower speed of 30 rpm for continuous shaking. Hydrolytic stability was then determined by recording the immersion period required for breaking the film when bent slightly, due to the loss of flexibility. If the blend films retained their shape even after folding, it was then said to be stable. The observed duration of these experiments were in the range of few hours to a week, depending on the stability of the resultant PEM.

Oxidative stability was tested by immersing membrane strips of the same size as mentioned above, into Fenton's reagent (3% H_2O_2 containing 3 ppm $FeSO_4$) at 80 °C. The stability towards oxidation was evaluated by recording the elapsed immersion time when the membrane had started breaking (τ_1) and dissolved completely (τ_2).

5.2.7 Determination of proton conductivity

Proton conductivity was measured with AC impedance spectroscopy (Autolab PGSTAT 30 with FRA software) over a frequency range of 1-10^6 Hz. The proton conductivity measurements were performed for the samples of SPIs, Nafion-117 and the blends prepared from SPI and PBI-BuI at various ratios in the humidified conditions (100% RH) at various temperatures. These membranes were fully hydrated in deionised water for 24 h prior to conductivity measurements. In case of 1M H_2SO_4 and 1M H_3PO_4 doped membranes, samples were directly used after taking out from the solution of acid at this concentration (1M) and the proton conductivity measurement were performed at 100% RH and at various temperature. For the membranes doped with 12 M H_3PO_4, measurements were performed in the temperature range of room temperature to 175 °C in anhydrous condition. Proton conductivity of PBI-I doped with 12M H_3PO_4 was also evaluated for comparison.

A round-shaped membrane sample with diameter of 2.0 cm and thickness 120 μm was placed between the two stainless steel electrodes, which were inserted in a cylindrical closed glass chamber, wrapped around with a resistance heater and equipped with a feed back temperature controller. A 200 mL of deionised water was placed at the bottom of the cylinder in order to maintain the humidifying atmosphere. The AC impedance measurement was performed in 100 % relative humidity (RH) at the desired temperature. The proton conductivity (σ) of membranes was measured using the following equation.

$$\sigma = L/(R_\Omega * A)$$

where, L is the thickness of the membrane in cm, R_Ω is the membrane resistance obtained from the high frequency intercept of imaginary component (Z", Y-axis) on the real component (Z', X-axis) and A is the area of circular stainless steel electrodes in cm^2.

5.3 Results and Discussion

5.3.1 Membrane preparation

Dense membranes based on the parent SPI, PBI and their blends were cast from their respective DMAc solution. The solution concentration was 3% (w/v). PBI solutions were centrifuged in order to remove the undissolved particles. While in case of SPI, their solutions were filtered through filter paper prior to casting in order to remove undissolved particles, if any. In order to maintain moisture free environment in the casting oven, the oven temperature was adjusted at 80 °C and fused $CaCl_2$ was kept inside it, 2 h before the casting procedure. All prepared dense membranes had a uniform surface except for the membranes belonging to SPDAB•Im-N, which had a wavy surface. These membranes, after peeling off from the glass surface were then immersed in water for a day at 60 °C in order to remove the traces of DMAc, followed by vacuum drying at 80 °C for 3 days. It was observed that membrane of SPDAB•TA-O was broken within a span of 4 h after keeping in water at 60 °C. This could be assigned to the lower hydrolytic stability of the five membered imide groups due to the induced ring strain (Genies, 2001a). Hence only SPIs membrane based on NTDA having strain free six-membered imide groups were investigated for further polymer electrolyte membrane (PEM) characterizations. Membranes viz., SPDAB•TA-N and SPDAB•Im-N were converted to respective sulfonic acid form ($SPDAB_I$-N and $SPDAB_{II}$-N) by keeping the membranes in 1N HCl and then in deionised water for 24 h each at ambient conditions.

Blend membranes were prepared by mixing solutions of SPDAB•TA-N (SPI in triethylammonium sulfonate form) and PBI-BuI in DMAc in different ratio. The concentration of each solution was 3% (w/v), while percentage of weight ratio of SPDAB•TA-N to PBI-BuI was 50:50, 40:60 and 30:70. These blend membranes were abbreviated as SPI(TEA)/PBI-BuI(a/b), where ‘a’ and ‘b’ denotes weight percentage of SPDAB•TA-N and PBI-BuI, respectively, while ‘TEA’ shows SPI in triethylammonium sulfonate form. These membranes were also soaked in distilled water for a day at 60 °C to remove the traces of DMAc, followed by vacuum drying at 80 °C for 3 days. These blend membranes were subsequently used for doping with different acids for proton conductivity measurements. They were transformed into sulfonic acid form after treating with 1N HCl for 24 h followed by washing with deionised water and abbreviated as

SPI(H)/PBI-BuI(a/b), where 'H' denotes SPI in $–SO_3H$ form. SPI(TEA)/PBI-BuI(a/b), when doped with either 1M or 12M H_3PO_4 were abbreviated as SPI(PA)/PBI-BuI(a/b) and for 1M H_2SO_4 doping, they were named as SPI(SA)/PBI-BuI(a/b).

5.3.2 Phosphoric acid doping

Pure PBI is an insulator having an intrinsic conductivity of about 10^{-12} $S.cm^{-1}$ at 25 °C (Xing, 2000; Bouchet, 2001; Ma, 2004b). It is known that, doping of PBI with strong acids (H_3PO_4 and H_2SO_4) bestows the proton conductivity in the range of 10^{-2} -10^{-3} $S.cm^{-1}$ (Glipa, 1999; Bouchet, 2001). PBI is generally doped with 85-88% phosphoric acid (16.2 M H_3PO_4). In our case, doping of membranes of SPI and blends with 88% phosphoric (16.2 M H_3PO_4) acids were either disintegrated or dissolved hence they were doped in 12 M H_3PO_4. Doping level was defined as the weight percentage of phosphoric acid present in per gram of the polymer membrane. Duration of doping was kept for 3 days, followed by drying in a vacuum oven at 80 °C for the same period, after wiping out adhered acid with tissue paper. In order to remove the water completely from the acid doped membrane, these doped membranes were kept at 100 °C for 3 days in vacuum oven. However, on following this procedure, doped blend membranes based on PBI-BuI and doped SPI membranes were broken. In order to compare the proton conductivity of blend membrane in anhydrous condition, both PBI-I and PBI-BuI were also doped with 12 M H_3PO_4.

The acid uptake for SPDAB•TA-N and SPDAB•Im-N is nearly same, being 67.7 wt% and 65.3 wt%, respectively as shown in Table 5.2. This is probably due to exchange of organic cations (triethylammoium and imidazolium cation) of both polymer membranes with H^+ released from phosphoric acid. In this way, the resultant polymer could absorb same quantity of acid using 12 M H_3PO_4 conferring same chemical structure with $–SO_3H$ group. The acid uptake of SPI can be attributed to the presence of N-heterocycle in the imide linkage as well as –O– in the side chain belonging to Ar-O-Ar' linkage, which can establish H-bonding with H_3PO_4. In addition, oxygen belonging to -SO_3H has also capability for H-bonding with H_3PO_4.

Table 5.2 Physical properties of membranes based on SPIs, PBIs and their blends

Polymer	IEC (mequiv/g)	WU[c] (%)	12 M H_3PO_4 uptake (%)	Hydrolytic Stability[f] (h)	Oxidative stability (h)	
					τ_1	τ_2
$SPDAB_I$-N	1.92	48.90	---	11	3.5	5
$SPDAB_{II}$-N	1.86	46.40	---	11.5	3.5	5
SPDAB•TA-N	0.39	39.30	67.7	> 168	10	21
SPDAB•Im-N	1.49	30.40	65.3	> 168	16	62
SPI(H)/PBI-BuI(50/50)	0.89	27.70	94.7[e]	153	82	> 168
SPI(H)/PBI-BuI(40/60)	0.66	26.77	100.3[e]	> 168	114	> 168
SPI(H)/PBI-BuI(30/70)	0.48	22.32	109.4[e]	> 168	> 168	> 168
PBI-BuI	0.02[a]	12.30[d]	165.2	Stable	NM	NM
PBI-I	0.02[b]	20.40[d]	150.5	Stable	30 min[g]	---

IEC: Ion exchange capacity measured by titration method in mequiv/g
[a]: Determined in the same way as that of PBI-I
[b]: Kerres, 2000
[c]: Water uptake capacity in wt %
[d]: Kumbharkar, 2009
[e]: 12M H_3PO_4 uptake of blend membranes having been abbreviated as SPI(PA)/PBI-BuI(a/b) (Table 5.1)
[f]: Elapsed time when membrane was broken while bending
[g]: Li, 2007b
τ_1: Elapsed time when membrane was broken
τ_2: Elapsed time when membrane had been completely dissolved
NM: Not measured

The membranes of PBI-I and PBI-BuI were also doped with 12 M H_3PO_4 for 3 days. PBI-BuI exhibited higher acid uptake of ~165.2 wt % compared to 150.5 wt % of PBI-I (Table 5.2). This can be attributed to comparatively higher initial free volume in PBI-BuI, wherein more number of H_3PO_4 along with water molecules can be imbibed. In addition, larger swelling of PBI-BuI on doping with H_3PO_4 also supports its higher acid uptake. Bulky *t*-butyl group in PBI-BuI, restricts efficient packing polymer chains as that

of PBI-I. This results in the reduction of inter-molecular H-bonding leading to reduced interchain interactions as well as increase in initial fractional free volume (0.3393 cm^3/cm^3) in PBI-BuI as compared with PBI-I (0.3096 cm^3/cm^3) (Kumbharkar, 2006). This observation can also be supported from the lower N-H group density in PBI-BuI (8.24%) than PBI-I (9.74%). In case of blend membranes, the acid uptake is in the range of 94-110 wt% and increases with PBI-BuI content. Thus, acid uptake decreases in the order PBI-BuI > PBI-I > SPI(PA)/PBI-BuI(30/70) > SPI(PA)/PBI-BuI(40/60) > SPI(PA)/PBI-BuI(50/50) > SPDAB•TA-N ≈ SPDAB•Im-N. This is attributed to the decreased content of PBI in the membrane.

5.3.3 Water uptake (WU) capacity

Since proton conductivity as well as the mechanical strength of PEM comprising sulfonated polymers, is highly dependant on water content, determination of their WU becomes an indispensable criterion. High water content in the membrane though increases the proton conductivity, it deteriorates the mechanical strength of PEM (Roziere, 2003). Hence sufficient amount of WU commensurate with proton conductivity of magnitude 0.1 S/cm is desirable for better performance in PEM. From Table 5.2, it is observed that WU of SPIs decreases in the order $SPDAB_I$-N ≈ $SPDAB_{II}$-N > SPDAB•TA-N > SPDAB•Im-N. Water uptake of $SPDAB_I$-N and $SPDAB_{II}$-N is 48.9 % and 46.4 %, respectively. The reported WU for different SPIs is in the range of 21-250 % (Fang, 2002; Fang, 2006; Yin, 2006a; Savard, 2008). The WU of present SPIs is thus at the lower level when compared to WU of reported SPIs. This can be mainly attributed to the lower IEC (<2) and presence of a single sulfonated moiety per chain repeating unit (CRU) of the present SPIs. It should be noted that most of the reported SPIs used as PEM are in the copolymer form since homopolymers are either soluble in water or show high swelling with poor mechanical resistance (Guo, 2002; Fang, 2006).

It is interesting to compare the water uptake between SPDAB•TA-N (39.3%) and SPDAB•Im-N (30.4%). The latter shows lower water uptake than the former despite its higher IEC. In general, WU increases with higher IEC conferring either high swelling or even dissolution in water of the membranes (Guo, 2002; Fang, 2006; Yin, 2006a). This anomalous behavior of SPDAB.Im-N can be assigned to the peculiar structural

arrangement of pendant imidazolium ring in SPDAB•Im-N. The planar and aromatic structure of the imidazolium ring is thought to be well accommodated in the available free volume of the polymer chains. On the other hand, the relative reduction between interchain interaction due to tetrahedrally attached three alkyl (ethyl) groups at the side chain end in SPDAB•TA-N may result in increased free volume as compared with that of planar structure of imidazolium ring in SPDAB•Im-N. As a result more number of water molecules can be harbored in the available free volume of former than that of latter. This observation can be supported from the permeability of H_2 and CO_2 explained earlier in Section 4.3.3 in Chapter 4, wherein the permeability of these gases are lower in SPDAB•Im-N than SPDAB•TA-N in dry state.

Water uptake of SPI is also governed by the chemical structure of SDA. SDA having angled or non-linear monomer leads to the greater chain entanglements in the resulting polymer structure, thereby offering more resistance to swelling and increasing proton concentration (Rodgers, 2006). The present SPDAB is a non-linear SDA, with asymmetric substitution of sulfophenoxy moiety on *meta*-amino phenyl ring, which acts as a 'kink' in the resulting structure of SPI. Hence present SPIs would be expected to exhibit larger number of entanglements. In addition, absence of any flexible linkage (C-O-C) in main chain of polyimide as well as the planar and rigid structure of the naphthalo-diimide structure (Gianolio, 2000) would further offer strong resistance towards the reorganization of individual polymer chains in the wet condition. Consequently, these SPIs offer strong resistance towards water swelling resulting in decrease in WU with better mechanical strength in wet conditions. Hence these SPIs, being homopolymer are stable in water. IEC and water uptake in membrane form of SPDAB•TA-O and its acidified form polymer (SPDAB-O) could not be measured due to lower stability of these polymer membranes in water, arisen from strained five-membered imide ring as also observed previously (Genies, 2001a).

WU capacity of the blend membrane in sulfonic acid form is shown in Table 5.2. Initially, the blend membranes SPI(TEA)/ PBI-BuI(a/b) was placed in 1N HCl for 48 h in order to regenerate $–SO_3H$ of SPI, followed by washing with deionised water at ambient [abbreviated as SPI(H)/PBI-BuI(a/b)]. The blend membranes SPI(H)/PBI-BuI(a/b) exhibits water uptake capacity in the range of 22.3% -27.70%, which is lower than parent

SPIs [$SPDAB_I$-N (48.9%) and $SPDAB_{II}$-N (46.4%)] and higher than parent PBI-BuI (12.20%) (Kumbharkar, 2009). In conclusion, water uptake is lowered with increase in PBI-BuI, in blend membranes. WU decreases in the order as SPI(H)/ PBI-BuI(50/50) > SPI(H)/PBI-BuI(40/60) > SPI(H)/PBI-BuI(30/70). Since the number of more hydrophilic $–SO_3H$ group are lower than that of benzimidazole groups even for the same weight percentage of blends constituting SPI and PBI-BuI (Table 5.3), the water uptake should be more dependant on the benzimidazole moieties of PBI-BuI having lower WU. Though the acid-base interaction in these blend membranes seems to be week as evidenced by the FT-IR spectra analysis (Chapter 3, Section 3.5.3.2), polymer chains can remain intact due to the rigid nature of both polymer chains, which can strongly resist the reorganization of the individual polymer chains in wet conditions leading to lower WU. Hydrophobic *t*-butyl group in PBI-BuI should also assist in lowering WU of these blends.

Table 5.3 Determination of benzimidazole and sulfonic acid group ratio in blends.

Polymer	Wt. (gm)	Mol. Wt. of CRU[a]	No. of moles of polymer	Moles Bz^b or SA^c groups	Ratio of (Bz/SA) groups	IEC (mequiv/gm)	
						The[d].	Exp[e].
PBI-BuI	0.5W	$(364.45)_n$	$1.37W \times 10^{-3}$	$(2.74W \times 10^{-3})^b$	3.36	0.98	0.89
SPDAB•TA-N	0.5W	$(612.64)_n$	$8.16W \times 10^{-4}$	$(8.16W \times 10^{-4})^c$			
PBI-BuI	0.6W	$(364.45)_n$	$1.64W \times 10^{-3}$	$(3.28W \times 10^{-3})^b$	5.02	0.79	0.66
SPDAB•TA-N	0.4W	$(612.64)_n$	$6.53W \times 10^{-4}$	$(6.53W \times 10^{-4})^c$			
PBI-BuI	0.7W	$(364.45)_n$	$1.92W \times 10^{-3}$	$(3.84W \times 10^{-3})^b$	7.85	0.60	0.44
SPDAB•TA-N	0.3W	$(612.64)_n$	$4.89W \times 10^{-4}$	$(4.89W \times 10^{-4})^c$			

W: total weight of polymer component present in the blend in gm
[a]: Molecular weight of chain repeat unit (CRU) of the polymer
[b]: Moles of Benzimidazole groups
[c]: Moles of sulfonic acid groups
[d]: IEC of PEM blend calculated theoretically
[e]: IEC of PEM blend determined experimentally

5.3.4 Ion exchange capacity (IEC)

The ion exchange capacity (IEC) values of the membranes were measured by classical acid-base titration method and results are summarized in Table 5.2. Membrane dipped in large excess of NaCl aqueous solution exchanges H^+ with Na^+ forming HCl in

the aqueous solution. This formed acid is then titrated with standardized 0.01 N NaOH using phenolphthalein as an indicator. The IEC values obtained from titration of the acidified membranes of SPIs viz; $SPDAB_I$-N (1.92) and $SPDAB_{II}$-N (1.86) are in good agreement with the theoretical value (1.95). This implied that almost all the protons from sulfonic acid groups are exchangeable. Thus, there are no concealed sulfonic acidic sites present in these polymers and all the protons from sulfonic acid groups should take part in the proton conduction through the well connected hydrophilic segments.

While comparing the IEC between the SPDAB•TA-N and SPDAB•Im-N, the later shows almost more than 3 times IEC value (1.49) than the former (0.39). These values are lower than their corresponding sulfonic acid form [$SPDAB_I$-N (1.92) and $SPDAB_{II}$-N (1.86)]. This discrepancy in IEC values can be better explained on the basis of their cationic structural formation and dissociation in aqueous medium. In SPDAB•Im-N, an imidazolium cation contains three hydrogen atoms belonging to carbon attached through covalent bonds (C_2, C_4 and C_5 as shown in the following Figure 5.1) while the remaining two hydrogen of the nitrogen are in more detachable form. Among hydrogen atoms of carbons, C_2 is the most acidic (Dupont, 2004) and hence can be considered to be exchangeable. Thus due to the presence of more number of exchangeable hydrogens in imidazolium cation as compared with only one in triethylammonium salt form, the former exhibited higher IEC value than the latter.

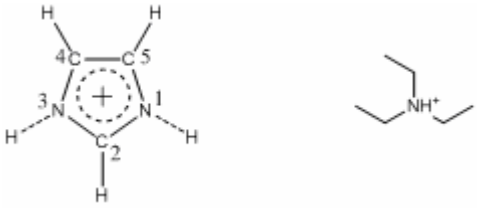

Imidazolium cation (ImH^+) Triethyl ammonium cation ($TEAH^+$)

Figure 5.1 Structures of cations in salt form

Different IEC of these salt type membranes can also be better illustrated by the comparison of their acidic nature of cation, dissociation and solvation of ion pairs in aqueous media. Since IEC was measured by using 0.01N NaOH, the acidic nature of cations should be one of the major contributors. Consequently, in aqueous medium,

SPDAB•Im-N could be more dissociated due to better solvation of an imidazolium cation (ImH^+) due to its higher acidic nature than that of triethylammonium hydronium ion ($TEAH^+$). Higher acidic nature of ImH^+ may be attributed to the better stabilization of its conjugate base imidazole due to its aromaticity as well as better solubility in aqueous media after loosing its proton. While in case of $TEAH^+$, capacity of proton donation is less since the conjugate base TEA is less soluble in water. It is known that, TEA has only 5.5% solubility in water whereas; imidazole is completely soluble in water. It should be noted that, TEA (pK_a=10.75) (Kailani, 1988b) is more basic than imidazole (pK_a= 7.1) (Clayden, 2001; Lv, 2008) hence the conjugate Bronsted acid; imidazolium cation (ImH^+) should be more acidic than triethylammonium cation ($TEAH^+$). Infact, SPDAB•Im-N and SPDAB•TA-N can be considered as protic neutral salt type membranes due to acidic nature of ImH^+ and $TEAH^+$ cations. Reports of acidic nature of ImH^+ and $TEAH^+$ cations are known (MacFarlane, 2006). Protic ionic liquids based on these cations have well been reported (Belieres, 2007; Greaves, 2008). Acid catalyzed reactions based on such type of acidic cations have also been reported. Moreover, ionic liquids containing Bronsted acidic nature of dialkyimidazolium cations forming a salt with a side chain containing $–SO_3H$ group have been demonstrated as acid catalysis in many conventional reactions such as Friedal-Crafts reaction (Qiao, 2004; Du, 2005), esterification (Fraga-Dubreuil; 2002, Du, 2005) and etherification (Cole, 2002; Du, 2005). Poor solvation of $TEAH^+$ in water can also be attributed to its hydrophobic three ethyl groups. Though SPDAB•TA-N reveals higher water uptake than SPDAB•Im-N, $TEAH^+$ is expected to be poor solvated than ImH^+ due to the hydrophobic three ethyl groups. This phenomenon may confer larger dissociation of SPDAB•Im-N than that of SPDAB•TA-N in aqueous media. In other words, dissociation constant for imidazolium sulfonate is more as compared with triethylammonium sulfonate as shown in the Figure 5.2. This can also be supported from the delocalization of positive charge on the imidazolium cation due to its aromatic character, which is effective for the improvement in the degree of salt dissociation in SPDAB•Im-N. While in case of $SPDAB_I$-N and $SPDAB_{II}$-N, $-SO_3H$ group is completely dissociated with complete exchange of H^+. In this way, IEC values increase in the order $SPDAB_I\text{-N} \approx SPDAB_{II}\text{-N} >$ SPDAB•Im-N > SPDAB•TA-N.

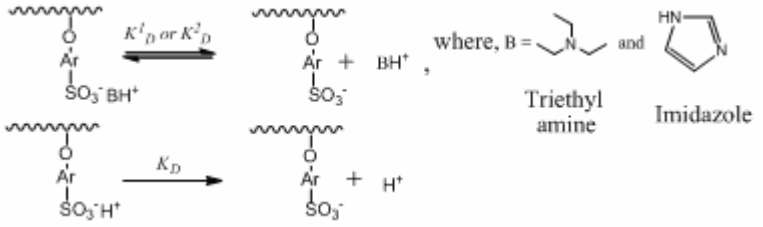

Figure 5.2 Dissociation of SPIs in aqueous medium

where,

K^1_D is the dissociation constant of SPI in triethylammonium sulfonate form

K^2_D is the dissociation constant of SPI in imidazolium sulfonate form

K_D is the dissociation constant of SPI in $-SO_3H$ form and ($K^1_D < K^2_D < K_D$)

In case of blend membranes, the membranes prepared in TEA form were first converted to sulfonic acid form and then IEC measured. IEC values decreases in the order SPI(H)/PBI-BuI(50/50) > SPI(H)/PBI-BuI(40/60) > SPI(H)/PBI-BuI(30/70) as shown in the Table 5.2. This suggests that IEC values increase with SPI content. Since the present blend system were prepared on the percentage of weight basis and not on the mole basis hence we thought that it was necessary to dig out the actual number of sulfonic acid groups available for proton exchange. If this exact number of sulfonic acid groups can be calculated, it would shed more light on the IEC values of blends. To calculate exact number of moles of sulfonic acid, moles of SPI in TEA form was considered instead of sulfonic acid form as SPI was taken in the TEA salt form while preparing blends. From the Table 5.3, it can be seen that number of sulfonic acid groups present in the blend is less as compared with the number of benzimidazole moieties even for the same weight percentage of the polymer. This discrepancy is attributed to the larger difference in molecular weight of chain repeat unit of respective polymers. Moreover, there is only a single sulfonic acid group in the CRU of SPI as compared with the two imidazole groups in the PBI-BuI. This also implies that blend prepared with equimolar quantities of SPI and PBI would also contain two fold of imidazole moieties than that of sulfonic acid moieties. Increase in benzimidazole to sulfonic acid ratio should raise acid-base interactions since more number of benzimidazole moieties available per

sulfonic acid group. In other words with increasing PBI-BuI content in the blend number of $–SO_3H$ group governing IEC should be decreased. This statement can be supported from the fact that percentage difference between theoretical IEC and experimentally determined IEC decreases with decreasing PBI-BuI content i.e. SPI(H)/PBI-BuI(30/70) (26.67%) < SPI(H)/PBI-BuI(40/60) (16.5%) < SPI(H)/PBI-BuI(50/50) (9.7%).

It is evident that the PEM exhibiting high IEC implies the existence of more number of free sulfonic acid groups. From the Table 5.3, it is observed that IEC of blend membranes determined experimentally is less than that of their theoretical values. This implies that some of the $–SO_3H$ groups have not participated in the H^+ exchange process indicating their involvement in other interactions which can probably be none other than acid-base interactions. However, the difference in IECs is not too high suggesting that most of the sulfonic acid groups have labile H^+. In case of the IEC's of blend system constituting acid-base interactions, protons can not become exchangeable to the solution to be titrated if acidic sulfonic group forms the strong interactions with the basic groups resulting in larger difference between theoretical and experimental IEC values (Kosmala, 2002). In the present blend component, this difference is not too high, indicating moderate or weak acid-base interactions. This observation is reasonable, as the presence of *t*-butyl group can shield the imidazole group in the main chain of PBI-BuI and thus can resist such interactions. Another factor contributing to such weak functional interactions is the rigidity of the main chain of these polymers. Though SPI has flexible sulfophenoxy group, it lacks such flexibility in its main chain, which can further resist the aligning of polymer main chains favorable for strong interactions with benzimidazole groups of PBI. PBI and polyimide comprise extreme rigid structures in their main chain. Polymer blends constituting extreme rigid structure in their main chain sterically hinder the interactions of functional groups (Wang, 2008). In other words, functional groups accessibility for enthalpic interactions required for the miscibility of polymers becomes less. Since the entanglement required for functional group association become less in such rigid structures, the probability of forming the interactions necessary for miscibility also becomes little (Cote, 1994). Radmard *et al.* (2001) also reported the reduction in intermolecular hydrogen bonding in the blend with increase in chain rigidity of polyether.

IEC of present blend system can therefore be attributed to the weakened acid-base interactions arising from the chain rigidity of PBI-BuI and SPI.

5.3.5 Hydrolytic stability

Table 5.2 lists the hydrolytic stability of PEM membrane. It was measured by immersing the membranes in water at 80 °C and determining the period required for breaking the film. SPIs viz., $SPDAB_I$-N and $SPDAB_{II}$-N could maintain their hydrolytic stability up to 11 h and 11.5 h, respectively. After this duration, membranes became brittle and remained un-dissolved in water. Some of the reported SPIs (homopolymers based on SDA with NTDA) displayed lower hydrolytic stability in the range of few seconds to 5h and became water soluble (Fang, 2002; Yin, 2006a). Comparatively the present SPIs displayed an improved hydrolytic stability. This can be attributed to the lower IEC (< 2 mequv/g) due to the presence of flexible sulfophenoxy group having single sulfonic group per CRU and comparatively low water uptake (46-49%). In SPIs, sulfonic acid group is at the *para* position of the pendant –OPh ring, thus located away from the functional imide groups. Consequently, the increased distance between the imide ring and sulfonic acid group (as compared in main-chain-type SPIs) has an ability to alleviate the acid-hydrolysis of imide linkage. This can be better represented by schematic representation as shown in the following Figure 5.3.

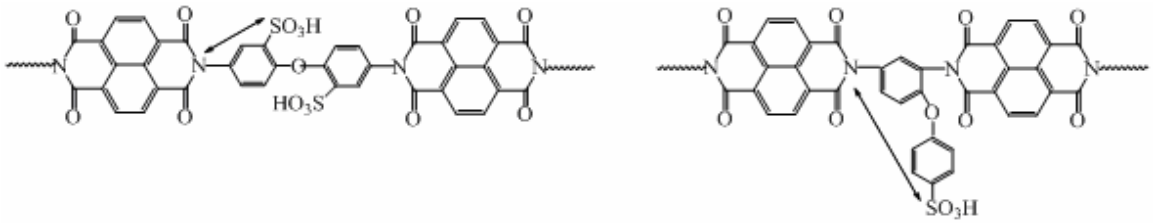

(a) Main-chain-type SPI (b) Side-chain-type SPI

Figure 5.3 Schematic representation of the SPIs showing relative distance of sulfonic acid group form the imide linkage

(a) $–SO_3H$ and imide moieties become nearer in main-chain type-SPI (Fang, 2002)

(b) $–SO_3H$ and imide moieties go away from each other (**e.g.** $SPDAB_I$-N and $SPDAB_{II}$-N)

Moreover, in hydrated state, region with large content of water is present to the proximity of sulfonic group only i.e. hydrophilic ion-rich domains which are away from the imide group in the main chain. Consequently, hydrolytic stability of $SPDAB_I$-N and $SPDAB_{II}$-N should increase. Thus, side-chain-type SPI membranes seems to be less vulnerable for hydrolysis, consequently exhibiting better hydrolytic stability than main-chain-type ones (Yin, 2004 and 2006a; Fang, 2006; Savard, 2008). It has been mentioned that hydrolytic stability is subjective towards chemical structure, basicity of the SDA, IEC, water uptake and flexible linkages (C-O-C) in the main chain (Yin, 2004; Marestin, 2008).

However, the brittleness induced after 11 h in $SPDAB_I$-N and $SPDAB_{II}$-N can be ascribed to the extreme rigid structure of the main chain. As explained earlier in section 5.3.3, these SPIs therefore offer strong resistance towards swelling since SPDAB is an angled or non-linear type monomer. Though these SPIs have flexible ether linkage in the side chain, they lack flexible linkages in main chain, which is prerequisite for the relaxation and orientation of polymer molecules in water medium (Yin, 2006b). This would further impart brittleness in these membranes. In addition, *ortho* substitution of pendant sulfophenoxy group present to alternative imide linkages restrict the rotation of neighboring phenyl rings attached to C-N bond resulting in reduced segmental mobility and hence enhancement in rigidity of SPI. Consequently, hydrolytic stability of these SPIs is decreased (Rodgers, 2006; Savard, 2008).

SPIs in salt form viz; SPDAB•TA-N and SPDAB•Im-N reveal better results and can maintain their hydrolytic stability even after dipping these membranes in deionised water for a week at 80 °C. This can be attributed to their lower IEC and water uptake values than SPI in sulfonic acid form ($SPDAB_I$-N ≈ $SPDAB_{II}$-N). However, enhanced basicity of the SPDAB in salt form could also corroborate for their increased hydrolytic stability (Yin, 2004). In fact, sulfonic acid group is electron withdrawing, however in the salt form (triethylammoium sulfonate and imidazolium sulfonate), its electron withdrawing capacity is appeased, as a result the oxygen in the C-O-C linkage becomes relatively electron donating towards amino phenyl ring resulting in increased basicity of the $–NH_2$ groups. Such phenomenon has also been proved for the sulfopropoxy linkage (Yin, 2004). Consequently, electron density is enhanced in the carbonyl carbon of

naphthalo-imido ring and became less vulnerable by the oxygen atom of water molecule. In this way, hydrolysis of naphthalo-imido ring can be alleviated in salt form as compared with sulfonic acid form. Though, we didn't continue our investigation after a period of a week (168 h), between SPDAB•TA-N and SPDAB•Im-N, the later might have shown increased hydrolytic stability than former. Since hydrolysis of imide linkage is nothing but the reverse reaction of polymerization (Yin, 2006b), the increased polymerization rate in SPDAB•Im-N would probably further lessen its imide hydrolysis. As explained earlier, strained five membered ODPA based SPI revealed lower hydrolytic stability than strain free six-membered NTDA based SPI counterpart (Genies, 2001a).

The evaluation of hydrolytic stability for the blend membranes reveals improved hydrolytic stability than that of SPIs. This can be due to their lower water uptake capacity. Besides, hydrolytic stability improves with increasing content of base component (PBI-BuI). It was observed that, blend membrane SPI(H)/PBI-BuI(50/50) was broken after 6 days (153 h) while the remaining blend membranes SPI(H)/PBI-BuI(40/60) and SPI(H)/PBI-BuI(30/70) could maintain their hydrolytic stability even after 7 days. This can be attributed to low percentage of SPI which is more prone to hydrolysis as compared with high content of better hydrolytically stable PBI-BuI.

5.3.6 Oxidative stability

Membrane stability of SPIs to oxidation was studied by determining the elapsed time for the membrane to disintegrate and/or its complete dissolution into Fenton's reagent (3% H_2O_2 and 3 ppm $FeSO_4$) at 80 °C. Oxidative stability decreases in the order SPDAB•Im-N > SPDAB•TA-N > $SPDAB_I$-N ≈ $SPDAB_{II}$-N (Table 5.2). In other words, oxidative stability increases with decreasing WU of SPIs. This observation is reasonable as the highly oxidizing generated radical species (•OH and •OOH) attack favorably in the hydrophilic region. It should be noted that the present SPI exhibits oxidative stability for longer duration as compared with reported sulfonated homopolyimides in same composition of Fenton's reagent (Miyatake, 2004; Zhou, 2005). Thus, our attempt to put hydrophilic sulfonated moiety away from main chain has resulted in improved oxidative stability. Among these SPIs, the effect of side chain sulfophenoxy group on prolonging the dissolving time in Fenton's reagent is more pronounced in SPDAB•Im-N (Table 5.2)

due to its peculiar structure. The planar and aromatic nature of this cation can effectively be accommodated in the available free volume of polymer chains which could restrict water molecules from being imbibed (explained earlier in Chapter 4). In addition, imidazolium cation, being aromatic becomes more stable to the radical attack as compared with the cation $TEAH^+$ in SPDAB•TA-N. However, it should be noted that the presence of flexible electron donating ether linkage (Ar-O-Ar') reduces the oxidative stability of SPIs as it is known to be susceptible to breaking by electrophilic hydroxyl radicals ($^{\bullet}OH$ and $^{\bullet}OOH$) (Hubner, 1999; Lee, 2007).

In the blend membrane same trend of increasing oxidative stability with decrease of water uptake is observed i.e. oxidative stability increases in the order SPI(H)/PBI-BuI(30/70) > SPI(H)/PBI-BuI(40/60) > SPI(H)/PBI-BuI(50/50) (Table 5.2). Thus, increase in SPI content decreases the oxidative stability or vice versa since hydrophilic content increases with SPI content. The probable acid-base interactions in blend, though week should also increase the oxidative stability as it prevents membrane from excessive water swelling.

5.3.7 Proton conductivity measurements

Proton conductivity (σ) of the PEM was measured by a two-probe impedance technique consisting of two stainless steel plates of diameter 2.0 cm. A circular membrane sample of diameter 2.0 cm having thickness in the range of 100-150 micron was placed in between the two SS electrodes. Proper ohmic contact was ensured by spring action. The impedance measurements were taken in the range of 1 to 10^6 Hz with a 10 mV rms amplitude at 10 points per decade. Proton conductivity of SPIs and blends of the type SPI(H)/PBI-BuI(a/b) was measured in 100% RH at various temperatures. Proton conductivity of PBI-BuI and blends after doping separately with 1M H_2SO_4 and 1M H_3PO_4 were also measured in 100% RH at various temperatures. Proton conductivity of PBI-I, PBI-BuI, blends and SPIs viz., SPDAB•Im-N and SPDAB•TA-N after doping with 12M H_3PO_4 was performed at dry condition and at various temperatures ranging from 30 to 175 °C. The schematic representation of the apparatus used for proton conductivity measurement is shown in the Figure 5.4.

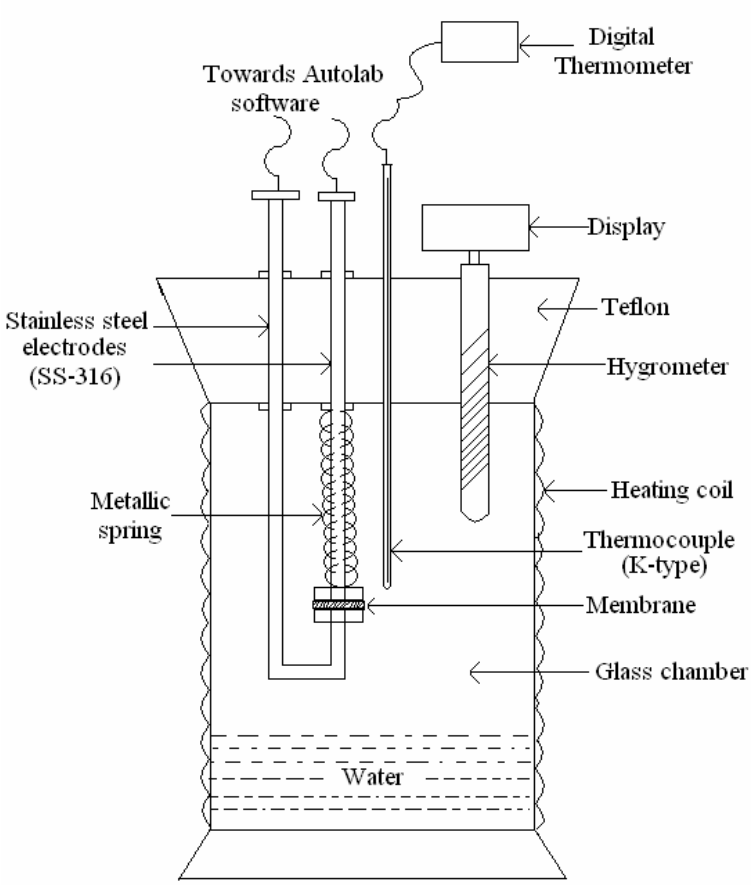

Figure 5.4 Schematic representation of the apparatus used for proton conductivity measurement

Proton conductivity of the polymer electrolyte membrane (PEM) was calculated from the plots obtained from electrochemical impedance measurements. The following Figure 5.5 elucidates the general pattern of impedance spectra of (PEM) sandwiched between two stainless electrodes at various temperatures and at ambient pressure. The results are presented in Nyquist plot comprising a plot of imaginary impedance (Z'') at Y-axis against the real impedance (Z') on X-axis (Figure 5.5 A). It can be seen that semicircle arc can be generated from high-frequency region to the low frequency region. The intercept of imaginary component on X-axis in the high frequency domain represents the ohmic resistance (R_Ω) of the PEM while the behavior of Z'' and Z' in the low frequency domain represents the mass transport related to the diffusion of H^+ (R_f) through the PEM. We used the basic Randles equivalent circuit as shown in (Figure 5.5

B) for comparing our results as it describes the different process related to membrane conductivity in a simple manner.

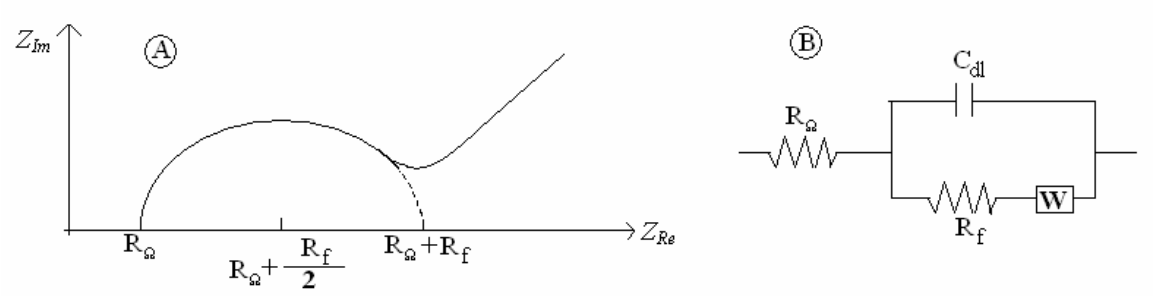

Figure 5.5 A) Nyquist plot for the impedance measurements

B) Randles equivalent circuit used for fitting this data.

where, R_Ω denotes the ohmic resistance between the electrode and membrane, R_f denotes the charge transfer resistance for diffusion of H^+ through PEM and C_{dl} is the capacitance. Proton conductivity was calculated by inserting the value of R_Ω in the following equation.

$$\sigma = L/(R_\Omega * A)$$

where, L is the thickness of the membrane in cm, R_Ω is the membrane resistance obtained from the impedance measurements and A is the area of the circular membrane in cm^2.

5.3.7.1 Proton conductivity of sulfonated polyimides (SPIs)

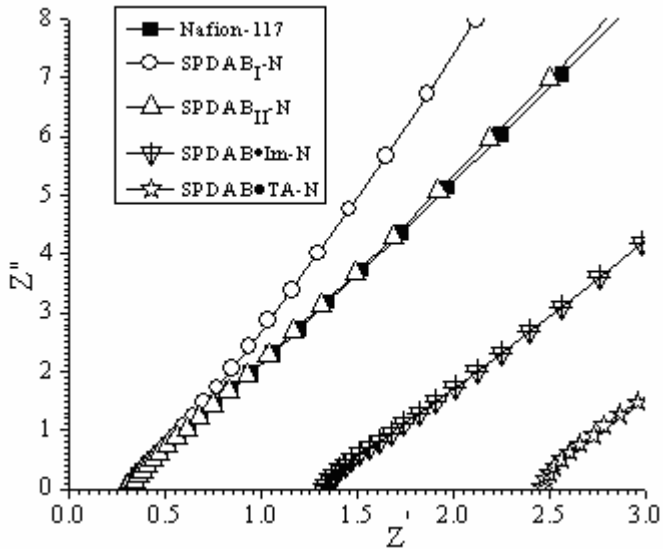

Figure 5.6 Impedance spectra of SPIs and Nafion-117 at 50 °C

Figure 5.6 represents the Nyquist plots measured for SPIs and Nafion-117 at 50 °C in 100 % RH. Figure 5.7 represents the temperature dependant proton conductivity (σ) of sulfonated polyimides and Nafion-117 at 100% RH.

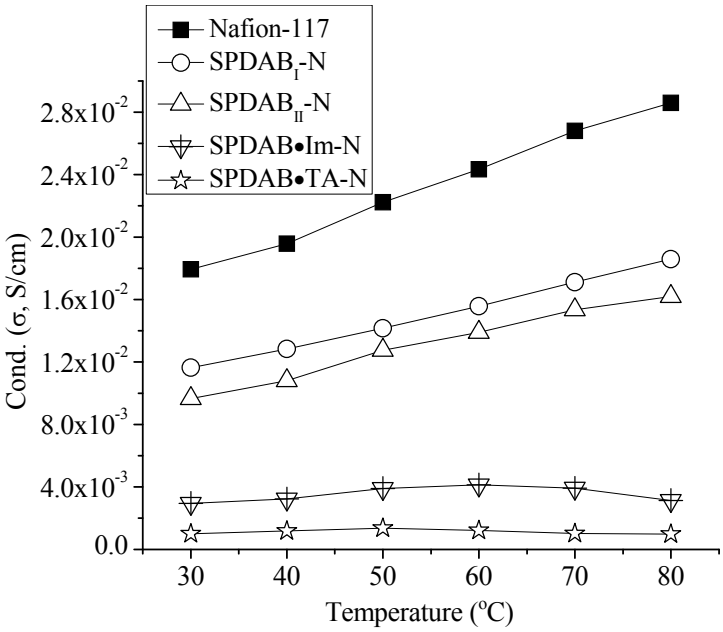

Figure 5.7 Proton conductivity of SPIs with temperature at 100% RH

In case of membranes of SPDAB$_I$-N, SPDAB$_{II}$-N and Nafion-117, proton conductivity linearly increases from RT to 80 °C and then further decreases sharply above 80 °C. While for N-SPDAB•TA and SPDAB•Im-N it increases from RT to 50 and 60 °C, respectively and then further decreases with increase in temperature. At a particular temperature, proton conductivity increases in the order SPDAB•TA-N < SPDAB•Im-N < SPDAB$_{II}$-N < SPDAB$_I$-N < Nafion-117. For example, conductivity at 50 °C for SPDAB•TA-N, SPDAB•Im-N, SPDAB$_{II}$-N, SPDAB$_I$-N and Nafion-117 is 1.35 X 10^{-3}, 3.91 X 10^{-3}, 1.27 X 10^{-2}, 1.41 X 10^{-2} and 2.22 X 10^{-2} S/cm, respectively. In SPIs, the trend of proton conductivity can be well matched with IEC which increases as SPDAB•TA-N < SPDAB•Im-N < SPDAB$_{II}$-N < SPDAB$_I$-N. The high conductivity of Nafion-117 is attributable to the higher acidity (pK_a,-6) (Chikvaidze, 2007; Sartori, 2009) of the –CF_2–SO_3H group as compared with –Ar–SO_3H group (pK_a, *2.70)* (Mauritz, 2004). Besides, in the swollen state, the phase separated morphology in Nafion-117

retains a bulk amount of water inside the hydrophilic domain due to the agglomeration of side chain hydrophilic $–SO_3H$ groups. As a result inter-sulfonate group separation becomes less with fine connectivity of hydrated domains, lower hydrophobic-hydrophilic interface and better proton transport performance (Kreuer, 2004). Hydrocarbon based sulfonated polymers seldom form such separated morphology. The present SPIs contain rigid main chain backbone with flexible pendant sulfophenoxy group as a short side chain. Hence reorganization of individual polymer main chains becomes difficult in wet conditions with less probable agglomeration of $-SO_3H$. This concept has earlier been well explained in Section 5.3.3. Hence, $SPDAB_I$-N and $SPDAB_{II}$-N exhibits lower proton conductivity than Nafion-117. However, proton conductivity of the order of 10^{-2}-10^{-3} $S.cm^{-1}$ of $SPDAB_I$-N and $SPDAB_{II}$-N, in spite of their comparatively lower IEC (<2) and optimum water uptake (46-49%) is worth noting. The lower proton conductivity of $SPDAB_{II}$-N as compared with $SPDAB_I$-N can be attributed to its wavy nature due to which better surface contact of electrodes with PEM ($SPDAB_{II}$-N) could not have been achieved.

It should be noted that proton conductivity is significantly dependant on IEC than on water uptake. In general, proton conductivity increases with water uptake (Rodgers, 2006). However, for better proton conduction in sulfonic acid based polymers, not only the higher water uptake but larger IEC i.e. actual number of exchangeable protons is also an indispensable factor (Xing, 2006). It is interesting to look at the proton conductivity between salt membranes viz; SPDAB•Im-N and SPDAB•TA-N which can be considered as PEM having protic neutral salts, i.e., imidazolium sulfonate and triethylammonium sulfonate, respectively. Former reveals higher IEC and lower water uptake than that of latter and has been thoroughly described in Section 5.3.3 and 5.3.4. Transport of protons through such types of protic neutral salts has been reported (Noda, 2003; Nakamoto, 2007). Despite lower water uptake of SPDAB•Im-N than SPDAB•TA-N, former shows higher proton conductivity than that of latter. One of the possible reasons for this phenomenon can be attributed to its higher IEC (1.49) than SPDAB•TA-N (0.39). In addition, more acidic nature, better cationic stability and solvation of imidazolium cation (ImH^+) in water should also enhance the proton conductivity of SPDAB•Im-N. However, conduction in these salt membranes is due to the ionic transport or by proton transport

remains ambiguous. It is reported that conductivity of SPI in proton form is 300 times larger as compared with triethylammonium form (Nakayama, 2003; Ueda, 2007). Cornet *et al.* (2000) studied the transport of different sizes of ammonium ion for SPIs in neutral form and observed the decrease in ionic conductivity with increase in ionic size. Few others have observed that SPI in -SO_3H form exhibited higher conductivity than that of SPIs in neutral form due to the lower mobility of cations in the latter as compared with higher mobility of H^+ in the former (Cornet, 2000; Marestin, 2008). Takahashi *et al.* (1976) reported amine based-protonic acid system wherein complexes of triethylenediamine and hexamethylenetriamine with H_2SO_4 demonstrated proton conductivity.

Higher conductivity of SPDAB•Im-N may also be attributed to the higher ability of ImH^+ to form H-bonding with water molecules due to more number of hydrogen atoms in it. Higher dissociation of SPDAB•Im-N ($K^2_D > K^1_D$, Figure 5.2) leads to the better solvation of ImH^+ in aqueous media facilitating H-bonding with water molecules. While in $TEAH^+$, possibility of H-bonding becomes less due to the three hydrophobic ethyl groups and lower dissociation of SPDAB•TA-N, which has previously been explained in Section 5.3.4. Furthermore, TEA (pK_a=10.75) (Kailani, 1988b) is more basic than imidazole (pK_a= 7.1) (Clayden, 2001; Lv, 2008), and therefore the conjugate Bronsted acid-imidazolium cation (ImH^+) formed in the aqueous media should be more acidic than triethylammonium cation ($TEAH^+$) resulting in increased conductivity for SPDAB•Im-N. However, if the surface of the membrane of SPDAB•Im-N could be smooth instead of wavy like that of SPDAB•TA-N, conductivity of the former could have also been increased.

We have also calculated the energy of activation (E_a) for the proton conductivity of SPIs in -SO_3H form and compared this with that of Nafion-117 from RT to 80 °C. Within this temperature range, the conductivity follows the following Arrhenius equation.

$$\sigma = \sigma_o \exp\left(\frac{-E_a}{RT}\right)$$

where, σ is the proton conductivity, T is the absolute temperature in Kelvin, R is the gas constant (8.314 $JK^{-1}mol^{-1}$) and E_a is the activation energy. E_a values were calculated form the slopes of log (σ) against 1/T plots as shown in the following Figure 5.8.

It is found that E_a for Nafion is 8.36 kJ/mole, while that of $SPDAB_I$-N, $SPDAB_{II}$-N is 8.55 and 9.50 kJ/mole, respectively. These values are well in accordance with the reported values of Nafion-117 (6-13 kJ/mole) and SPIs (9-15 kJ/mole) (Yin, 2004).

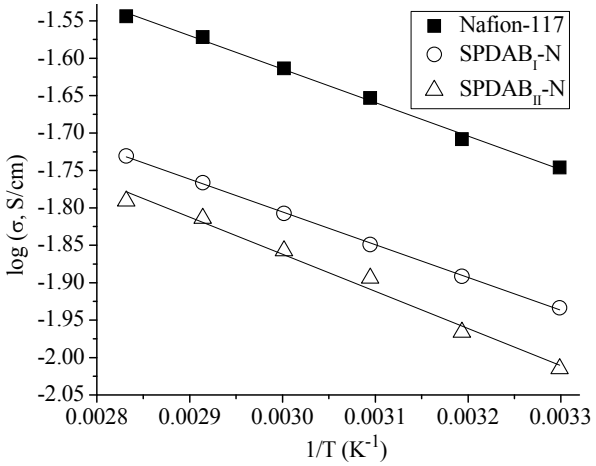

Figure 5.8 Arrhenius plot of proton conductivity of SPI with temperature at 100% RH

5.3.7.2 Proton conductivity of blends constituting SPI and PBI-BuI

(A) Proton conductivity of blend membranes [SPI(H)/PBI-BuI(a/b)]

Blend membranes of the type SPI(TEA)/PBI-BuI(a/b) in triethylammonium sulfonate form were transformed into sulfonic acid form i.e. SPI(H)/PBI-BuI(a/b) after treating with 1N HCl for 24 h followed by washing with deionised water. Proton conductivity of these blend membranes were measured in 100% RH at various temperatures and the results are summarized in the Table 5.4.

Table 5.4 Proton conductivity of blend membranes in humidified conditions

Temp. (°C)	Proton conductivity (σ) at 100 % RH ($S.cm^{-1}$)		
	SPI(H)/PBI-BuI(50/50)	SPI(H)/PBI-BuI(40/60)	SPI(H)/PBI-BuI(30/70)
30	2.25×10^{-5}	1.34×10^{-5}	2.93×10^{-5}
40	3.31×10^{-5}	1.44×10^{-5}	2.99×10^{-5}
50	3.54×10^{-5}	1.53×10^{-5}	3.22×10^{-5}
60	3.82×10^{-5}	1.74×10^{-5}	3.19×10^{-5}
70	2.03×10^{-5}	1.42×10^{-5}	2.58×10^{-5}
80	1.77×10^{-5}	1.31×10^{-5}	2.03×10^{-5}
90	1.48×10^{-5}	1.26×10^{-5}	1.91×10^{-5}
100	1.14×10^{-5}	1.01×10^{-5}	1.87×10^{-5}

The proton conductivity obtained is in the range of 10^{-5} $S.cm^{-1}$, which is lower than that of SPIs. It is observed that conductivity initially increases with increase in temperature till temperature reaches up to 50 or 60 °C and decreases with further increase in temperature. These blend membranes exhibit lower proton conductivity in the order of 10^{-5} $S.cm^{-1}$ in 100% RH. This may be attributed to the low content of SPI in blends. However, from Table 5.3, it can be observed that number of $–SO_3H$ groups are almost more than 3 times lower than that of the benzimidazole groups for the blend constituting same weight percentage of SPI and PBI-BuI and number of $–SO_3H$ groups further decrease with increase in PBI-BuI percentage. Thus, for a single $–SO_3H$ group more than three benzimidazole moieties are present and it reaches to almost 7.85 in the case of SPI(H)/PBI-BuI(30/70). Since $–SO_3H$ group are the major contributors for H^+ in the humidified atmosphere, its decreasing concentration should lower the proton conductivity. It has been reported that, for the blends of sulfonated PEEK and PBI, that the conductivity decreases with increase in PBI content also (Zhang, 2008). Proton conductivity of the order of 10^{-2} $S.cm^{-1}$, for the blends with maximum 20 wt% of PBI has been reported. In the present case PBI content is more than 50 wt%. We have already explained (Section 5.3.4 and Section 3.5.3.2 of Chapter 3) that these blends form weak interaction of $–SO_3H$ and benzimidazole functionality resulting in exchangeable H^+ from $–SO_3H$ group of SPI responsible for proton transport in aqueous medium. It is known

that, proton transports in sulfonated polymer is by vehicular mechanism, i.e. through the displacement of hydronium ion (H_3O^+) (Mauritz, 2004) and for better transportation of H^+ excellent connectivity of hydrophilic channels i.e. $–SO_3H$ group is a vital. Hydrophilic channels formation requires sufficiently high content of sulfonic acid groups and water. However in the present blends, understudy, low content of sulfonic acid groups and low water uptake due to the presence of hydrophobic *t*-butyl group in PBI-BuI, adversely affect formation of hydrophilic channels, which explains observed proton conductivity in the blends.

Considering these facts, we therefore expected that, rather than proton transportation as hydronium ion (H_3O^+), these blend membranes may show better performance by acid-base interactions or hopping mechanism. Hence we decided to dope these membranes with acids. Proton conductivity of these blend membranes doped with 12M H_3PO_4 in anhydrous condition and 1M H_3PO_4 in the humidified conditions (100% RH), at various temperatures was measured.

(B) Proton conductivity of polymer electrolyte membranes doped with 12 M H_3PO_4

Proton conductivity (σ) of membranes doped with 12 M H_3PO_4 was measured at various temperatures in anhydrous condition. Membranes viz., SPIs (SPDAB•TA-N and SPDAB•Im-N), polybenzimidazoles (PBI-I and PBI-BuI) and blends [SPI(PA)/PBI-BuI(a/b)] were doped with 12 M H_3PO_4 and evaluated for proton conductivity measurements.

(I) Proton conductivity of SPIs (SPDAB•TA-N and SPDAB•Im-N) doped with 12 M H_3PO_4

Proton conductivity (σ) of SPDAB•TA-N and SPDAB•Im-N, doped with 12M H_3PO_4 was measured at various temperatures (Figure 5.9). It can be seen that proton conductivity increases with temperature till 100 °C and then it decreases. At room temperature proton conductivity of SPDAB•TA-N is 6.20 X 10^{-4} $S.cm^{-1}$, which increases to 2.66 X 10^{-3} $S.cm^{-1}$ at 100 °C and decreases further continuously with increase in temperature. The same pattern of proton conductivity is observed in SPDAB•Im-N.

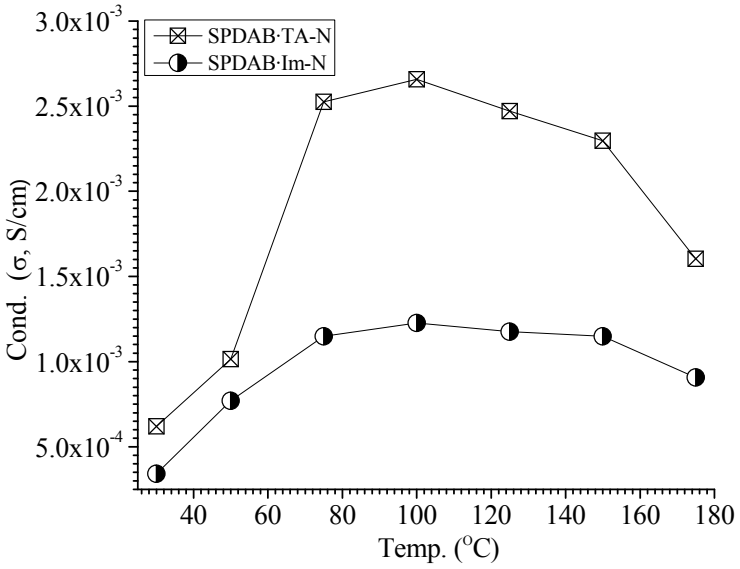

Figure 5.9 Proton conductivity of SPIs doped with 12M H_3PO_4 against temperature

In general, acid doped basic polymers, such as PBI, transports proton by a hopping or Grotthus mechanism. In H_3PO_4 doped PBI, the basic imidazole abstracts the proton from doped acid generating $H_2PO_4^-$ as a conjugate base, transporting proton through acid-base moieties. However, in SPI imide linkage possess N-heterocycle, which is a much weaker base than imidazole group due to the strong electron withdrawing effect of its neighboring two carbonyl groups. As a result, in H_3PO_4 doped SPI, extent of dissociation of H_3PO_4 generating $H_2PO_4^-$ becomes less therefore transport of proton by Grotthus mechanism is doubtful. Pu *et al.* (2005) reported the H_3PO_4 doped polyimide as anhydrous PEM and mentioned proton transport through H-bonding. The present SPI doped with H_3PO_4 can also transport through such H-bonding as the carbonyl group, the oxygen attached through pendant sulfophenoxy group and oxygen belonging to $–SO_3H$ group can form H-bonding with the acid H_3PO_4. Besides, $–SO_3H$ group present in SPI can also contribute to the proton conductivity. However, at higher temperature although proton conductivity decreases, it is still higher than that of lower temperatures viz., RT and 50 °C. This can be attributed to the increased dissociation of H_3PO_4 as well as $–SO_3H$

group at higher temperature than that of at lower temperature which can enhance the proton conductivity. In addition, these membranes were doped with lower concentration of H_3PO_4 (12M) and dried in a vacuum oven at 80 °C hence complete removal of water can also be not ascertained. As a result, role of water in proton conduction can also be not neglected. In summary, doped H_3PO_4, $–SO_3H$ group and presence of small concentration of conjugate base $H_2PO_4^-$ and water can assist in proton transportation.

It should be noted that, SPDAB•Im-N shows lower proton conductivity than that of SPDAB•TA-N despite having same phosphoric acid uptake (≈65-68%). This difference of proton conductivity can be attributed to the wavy nature of membrane of SPDAB•TA-N, because of which proper electrode and electrolyte contact could not have been achieved. The same decrease in proton conductivity in case of $SPDAB_{II}$-N than that of $SPDAB_I$-N due to the wavy nature of the former was observed and explained previously in Section 5.3.7.1.

(II) Proton conductivity of PBIs (PBI-I and PBI-BuI) and blend membranes [SPI(PA)/PBI-BuI(a/b)] doped with 12M H_3PO_4

Proton conductivity of blend membranes of the type SPI(PA)/PBI-BuI(a/b) and PBIs; PBI-BuI and PBI-I doped with 12M H_3PO_4 were measured in anhydrous conditions at various temperatures. Membrane resistance (R_Ω) is shown in Table 5.5 while proton conductivity trend with temperature is seen Figure 5.10. It can be seen that, proton conductivity is in the range of 2.07 X 10^{-4} to 1.12 X 10^{-2} S/cm, which varies with both acid uptake and temperature. For all the membranes, it increases from room temperature to 150 °C and further decreases at 175 °C. For example SPI(PA)/PBI-BuI(30/70) shows proton conductivity of 5.78 X 10^{-4} S/cm at room temperature which increases to 9.86 X 10^{-3} S/cm at 150 °C and further decreases to 4.97 X 10^{-3} S/cm at 175 °C (Figure 5.10). The decrease in proton conductivity at 175 °C can be attributed to the self-dehydration of phosphoric acid at this temperature to the less conductive pyrophosphoric acid (Lobato, 2007). In general, for the H_3PO_4 acid doped membranes such as PBI, proton conductivity increases with the uptake of phosphoric-acid due to the increase in proton carriers (Ma, 2004b).

Table 5.5 Change in R_Ω for the blends and PBIs with temperature

Temp. (°C)	R_Ω in ohms				
	SPI(PA)/PBI-BuI(50/50)	SPI(PA)/PBI-BuI(40/60)	SPI(PA)/PBI-BuI(30/70)	PBI-BuI	PBI-I
RT	27.51	13.1	10.75	5.89	13
50	8.25	5.53	3.97	2.24	3.8
75	2.8	1.80	1.67	0.89	1.84
100	1.35	1.11	1.06	0.68	1.65
125	0.89	0.86	0.76	0.57	1.54
150	0.76	0.76	0.63	0.52	1.45
175	1.28	1.03	1.25	1.11	1.65

From the Table 5.5, it can be seen that membrane resistance (R_Ω) decreases from RT to 150 °C and further increases at 175 °C. It is also noticed that, among all membranes, PBI-BuI shows the least values for R_Ω at all temperatures indicating its higher proton conductivity. For example, as shown in Figure 5.10, proton conductivity of PBI-BuI at RT is 9.86 X 10^{-4} S/cm which increases till 150 °C to 1.12 X 10^{-2} S/cm and further decreases to 5.23 X 10^{-3} S/cm at 175 °C. On the other hand, PBI-I demonstrates the highest R_Ω, particularly above the temperature 75 °C. In other words, blend membrane also show higher proton conductivity than PBI-I despite having their lower uptake of H_3PO_4. From the Table 5.2, it is seen that acid uptake of PBI-I is 150.4 wt% and that of PBI-BuI is 165.2 wt%. While that of blend membranes is in the range of 94.7 to 109.4 wt% only. Considering H_3PO_4 uptake, the maximum number of moles of acid taken per chain repeating unit (CRU) for PBI-I and PBI-BuI is 4.7 and 6.2, respectively. Though the membranes were heated at 80 °C under reduced pressure, the complete removal of water can not be ascertained. As a result, moles of acid uptake for these PBIs should definitely be lower than these values (4.7 and 6.2).

Both acid uptake and RH were found to have significantly effect on proton conductivity of PBI doped with H_3PO_4 (Wainright, 1995; Li, 2001; He, 2003; Ma, 2004b). Proton conductivity increases with increase in acid uptake and RH (Fontella, 1998). Ma *et al.* (2004a) obtained proton conductivity value of 4.7 X 10^{-3} S/cm at 5% RH

and 5.9 X 10^{-2} S/cm at 30% RH at 150 °C temperature. Li *et al.* (2004) also observed a higher proton conductivity value with an increase in RH at a H_3PO_4 doping level of 5.6 moles per CRU of PBI-I.

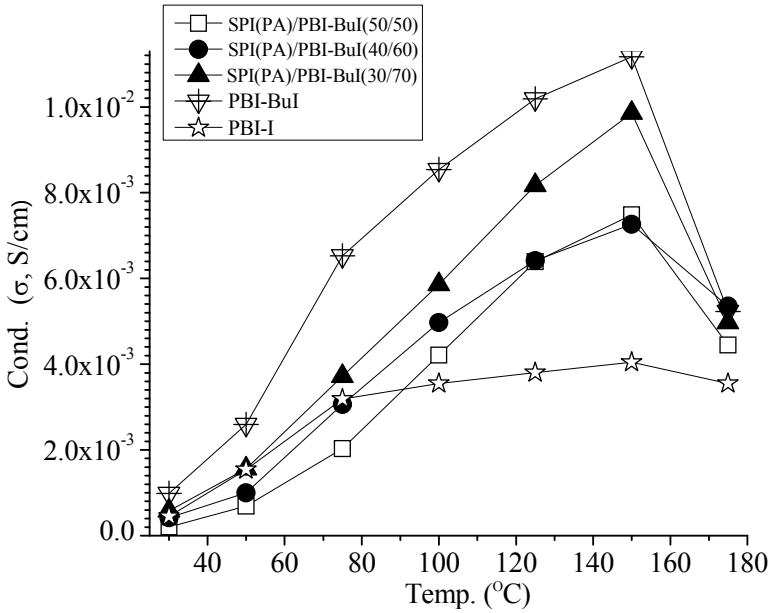

Figure 5.10 Variation of proton conductivity of blend membranes and PBI-BuI doped with 12 M H_3PO_4 at different temperature

From the Table 5.2, it can be clearly seen that, acid uptake decreases in the order PBI-BuI (165.2 wt%) > PBI-I (150.5 wt%) > SPI(PA)/PBI-BuI(30/70) (109.4 wt%) > SPI(PA)/PBI-BuI(40/60) (100.3 wt%) > SPI(PA)/PBI-BuI(50/50) (94.7 wt%). In the present study, it is also observed that, proton conductivity increases sharply from RT to 75 °C while increase in proton conductivity from 75 °C to 150 °C is smooth. This behavior is particularly observed in case of PBI-I (Figure 5.10). Since we doped the membranes with lower concentration of H_3PO_4 (12 M) and dried the membrane in vacuum oven below 100 °C i.e. at 80 °C, presence of water in the membrane can not be neglected. Hence, we attribute the proton transportation to be governed by water as well as H_3PO_4. In other words, in the temperature range from RT to 75 °C, transportation of proton could be by both vehicular and Grotthus mechanism. While above the 75 °C, role of water for proton transportation becomes insignificant while that of H_3PO_4 becomes prominent resulting in proton transportation by Grotthus mechanism. The pattern of

proton conductivity of the present blend membranes doped with H_3PO_4 can be better illustrated by electrochemical impedance spectroscopy (EIS) analysis as discussed below (Figure 5.11).

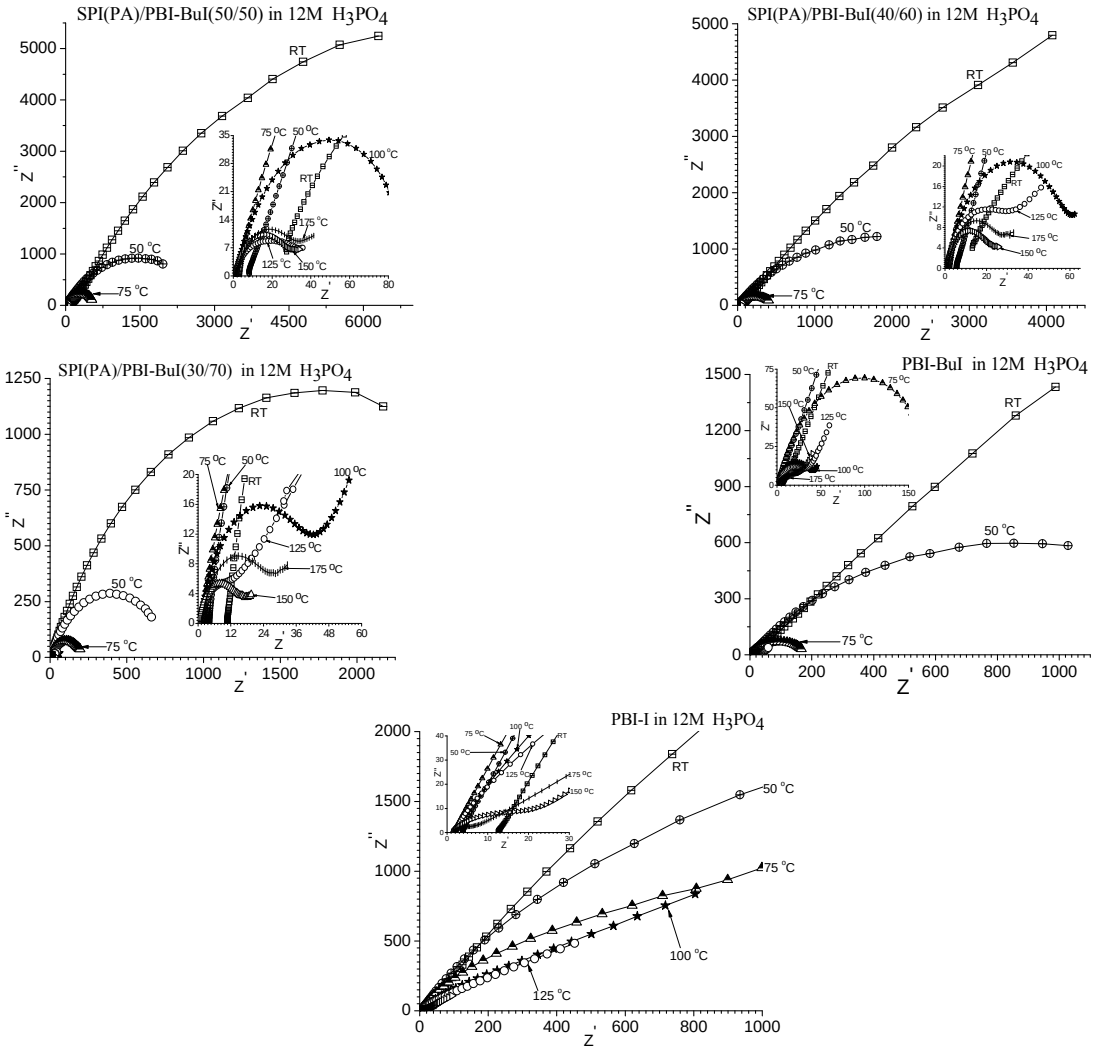

Figure 5.11 Impedance spectra of blend membranes doped with 12M H_3PO_4

Although 12 M H_3PO_4 uptake of blend membranes was lower than that of PBI-I, the former shows the least value for R_Ω, in particular above 75 °C (Table 5.5). This can be attributed to the probable participation of H^+ from $–SO_3H$ group belonging to SPI in the proton conductivity of the blend membrane. It is possible to have proton donation from the $–SO_3H$ group of SPI to the imidazole or conjugate base of ($H_2PO_4^-$) in the blend components resulting in decrease in R_Ω. In the present case, we have determined the

conductivity in anhydrous conditions, hence only the water present in 12 M H_3PO_4 should be considered. It is known that water promotes dissociation of H_3PO_4 (Ma, 2004a). In the PBIs (PBI-I and PBI-BuI), H_3PO_4 can only be dissociated by both, basic PBI and water. However, PBI is more basic, it contributes to the larger dissociation of H_3PO_4 than water as shown in following equation.

$$\text{PBI and } H_2O + H_3PO_4 \rightleftharpoons \text{PBI-}H^+ \text{ and } H_3O^+ + H_2PO_4^-$$

Proton transportation in PBI is due to the H_3PO_4, $H_2PO_4^-$ and water. On the other hand, in case of blend system, along with H_3PO_4, sulfonic group can also be dissociated due to PBI and water. In addition, the conjugate base formed $-SO_3^-$ can also take the H^+ from H_3PO_4 while that of another conjugate base $H_2PO_4^-$ can also take up H^+ from $-SO_3H$ of SPI in the blend. This can be better illustrated as follows (Scheme 5.1).

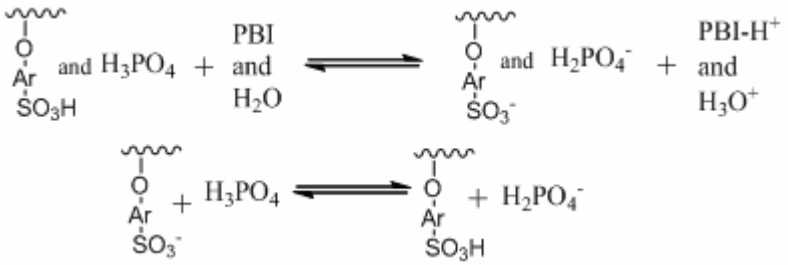

Scheme 5.1 Probable exchange of protons in 12M H_3PO_4 doped blend membranes.

Moreover, the difference in pK_a of $-SO_3H$ group of SPI and 12M H_3PO_4 should also govern the proton conductivity in blend membranes. Nevertheless, from the Table 5.3, the number of benzimidazole groups is almost more than 3 times higher than that of $-SO_3H$ group even for the same weight percentage of blend. Hence proton conductivity would be largely dependant on benzimidazole moieties, which is known to transport it by hopping mechanism. In this way, in blend membranes proton conductivity is contributed by H_3PO_4, $-SO_3H$ group, H_2O, H_3O^+, $H_2PO_4^-$, $-SO_3^-$, PBI and PBI-H^+ species. At higher temperature, i.e. above 75 °C role of H_2O and H_3O^+ diminishes due to loss of water.

Table 5.6 Change in R_f for the blends and PBIs with temperature

Temp. (°C)	SPI(PA)/PBI-BuI(50/50)	SPI(PA)/PBI-BuI(40/60)	SPI(PA)/PBI-BuI(30/70)	PBI-BuI	PBI-I
RT	--	---	3769.25	--	>10k Ω
50	2702.75	4061.47	830.03	1960.76	>10k Ω
75	597.2	506.2	195.33	189.11	>10k Ω
100	86.65	73.89	54.94	52.32	>10k Ω
125	50.11	52.14	23.24	44.43	>10k Ω
150	38.24	26.24	17.37	34.48	>10k Ω
175	45.72	38.97	29.75	39.89	>10k Ω

From the Table 5.6 and the above Figure 5.11, it can be seen that with increasing PBI-BuI content in the blend, R_f decreases in particular in the range of 75-175 °C. In case of PBI-I, R_f values are too large hence they are not discussed in detail. Since the acid uptake would be commensurate with the PBI-BuI content in the blend and at higher H_3PO_4 uptake the proton diffusion happens with the least resistant path resulting in more facile proton conduction. As a result, semicircle with least R_f can be obtained in 12M H_3PO_4 blend membrane, which is shown by SPI(PA)/PBI-BuI(30/70) blend. It is worth to mention that, though phosphoric acid uptake is lower for blend membrane than that of PBI-I, the blend membrane shows a semicircle with less diameter than that of PBI-I. This indicates the active participation of the $–SO_3H$ moiety in the proton transportation from one of the blend components; SPI. It is also noticed that with increasing temperature, R_f decreases till 150 °C i.e. proton conductivity increases. This is obvious as the diffusion of the proton would become faster at higher temperatures. However, at the highest temperature (175 °C) measured, the R_f increases indicating the conversion of phosphoric acid to more resistive pyro phosphoric acid that results in reduced conductivity and charge transport at this temperature. (Lobato, 2007).

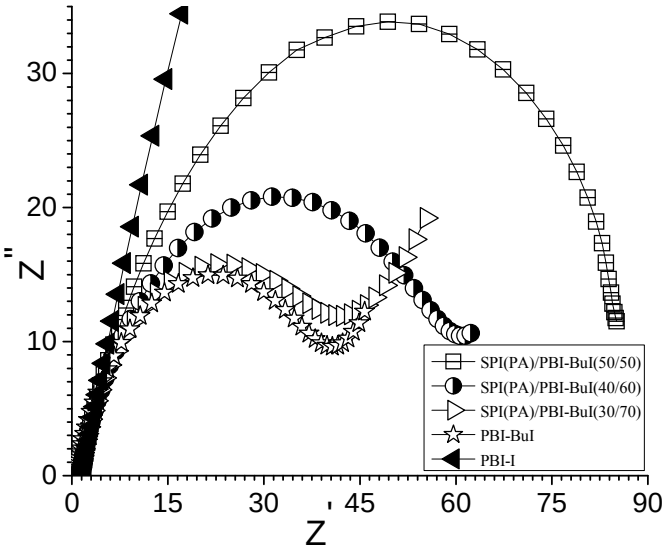

Figure 5.12 Comparative EIS spectra of blends and PBIs doped with 12M H_3PO_4 at 100 °C

From the above Figure 5.12, it can be seen that, at 100 °C, among the 12 M H_3PO_4 doped membranes, PBI-BuI shows the semicircle with least diameter indicating lower R_f value. With increasing SPI content however the diameter of the semicircle increases demonstrating higher hindrance for proton transport. This fact can be supported from the lower uptake of phosphoric acid with increasing SPI content coupled with dehydration of the membrane that effectively removes the -SO_3H moieties from the channel network (OR) contributing towards proton transport.

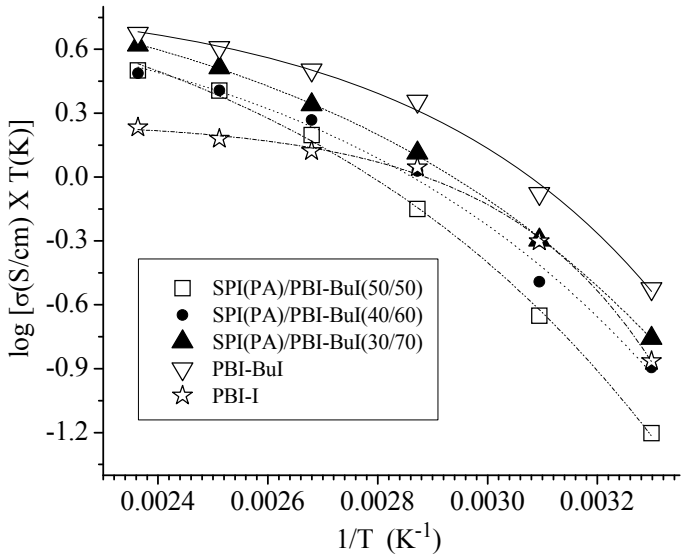

Figure 5.13 Arrhenius plot of proton conductivity of 12 M H_3PO_4 doped membranes against temperature

For 12M H_3PO_4 doped membranes, we used the following Arrhenius equitation in order to determine the temperature dependence of proton conductivity.

$$\sigma = \sigma^0 \exp\left(\frac{-E_a}{RT}\right) = \frac{A}{T}\exp\left(\frac{-E_a}{RT}\right)$$

Figure 5.13 shows log (σT) against *1/T* curves for 12M H_3PO_4 doped membrane for temperatures from 30 °C to 150 °C. It is observed that proton conductivity follows the non-Arrhenius behavior as inferred from the non-linear curves. This may be attributed to the enhanced segmental mobility of the polymer chains after doping with acid as well as with increase in temperature.

In all the blends, benzimidazole group content is more than sulfonic acid groups on molar basis (Table 5.3). In these blends benzimidazole groups are not neutralized by sulfonic acid groups and they may not contribute to proton conductivity without doping. On doping with high molar concentration (12M) of H_3PO_4, H_3PO_4 acts as vehicle for H^+ transport by Grotthus mechanism in an anhydrous condition. To understand, H^+ behavior with a low acid content of blends sufficient to neutralize free benzimidazole groups, study was conducted to determine the proton conductivity by doping with low concentration of two acids; 1M H_3PO_4 and 1M H_2SO_4. Proton conductivity of these blend membranes were measured particularly in 100% RH since low proton conductivity in anhydrous condition due to lower concentration of these acids was expected.

(C) Proton conductivity of blend membranes and PBI-BuI doped with 1M H_2SO_4 and 1M H_3PO_4

Blend membranes were separately dipped in 1M H_2SO_4 and 1M H_3PO_4 for three days and then directly used for the proton conductivity analysis with 100% RH at various temperatures.

*(i) Proton conductivity of blend membranes [*SPI(*SA*)/PBI-BuI*(a/b)] and PBI-BuI doped with 1M H_2SO_4*

The results of the membrane resistance (R_Ω) are summarized in Table 5.7. Plot of proton conductivity against temperature can be seen from the Figure 5.14.

Table 5.7 R_Ω values of blend membranes and PBI-BuI in 1M H_2SO_4

Temp. (°C)	Membrane resistance in (R_Ω)			
	SPI(SA)/PBI-BuI(50/50)	SPI(SA)/PBI-BuI(40/60)	SPI(SA)/PBI-BuI(30/70)	PBI-BuI
30	1.31	1.52	1.14	1.90
40	1.17	1.23	1.08	1.43
50	0.86	1.0	0.98	1.06
60	1.13	0.86	0.87	1.02
70	2.83	0.84	0.72	1.03
80	7.01	1.30	0.63	1.79
90	16.42	3.87	0.80	8.49
100	43.89	43.74	9.43	42.96
110	153	353	24.76	163

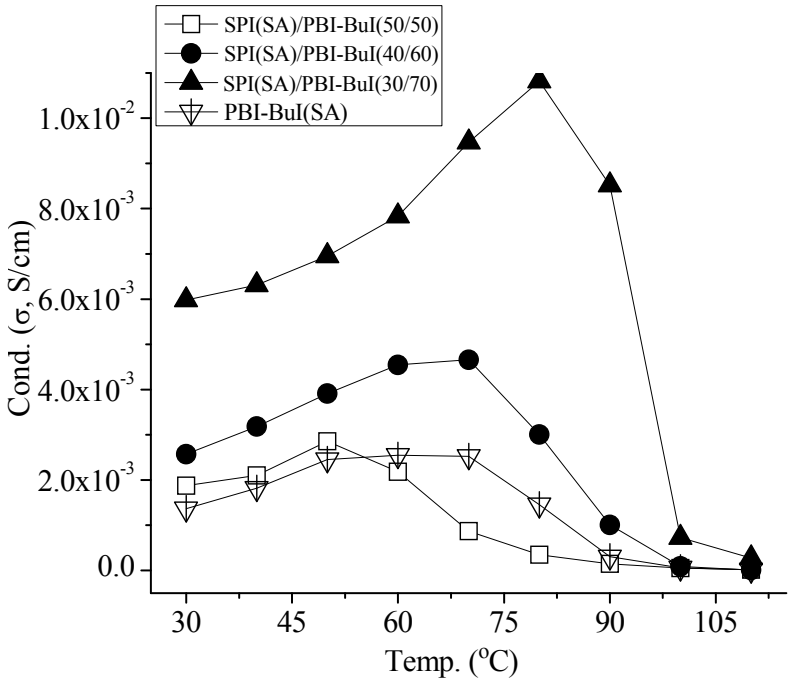

Figure 5.14 Variation of proton conductivity of blend membranes [SPI(SA)/PBI-BuI(a/b)] and PBI-BuI doped with 1M H_2SO_4 against temperature.

From the above Table 5.7, R_Ω decreases with increase in temperature up to a certain temperature and there after it increases. As the PBI-BuI content increases, R_Ω decreases becoming less with increasing temperature. Thus, maximum proton conductivity obtained at higher temperature for the blend membrane having higher content of PBI-BuI. From the above Figure 5.14, among the blend membranes conductivity becomes higher at elevated temperature with increasing content of PBI-BuI. For example, at 70, 80 and 90 °C conductivity decreases in the order SPI(SA)/PBI-BuI(30/70) > SPI(SA)/PBI-BuI(40/60) > SPI(SA)/PBI-BuI(50/50). Thus, at 90 °C conductivity values for SPI(SA)/PBI-BuI(30/70), SPI(SA)/PBI-BuI(40/60) and SPI(SA)/PBI-BuI(50/50) are 8.52 X 10^{-3}, 1.01 X 10^{-3} and 1.50 X 10^{-4} S/cm, respectively. This result shows that at higher temperature the presence of benzimidazole groups dominates proton conduction, which can possibly arise due to the exchange of proton from H_2SO_4 to the benzimidazole moieties. However, PBI-BuI shows lower proton conductivity than that of blend membranes, in particular for SPI(SA)/PBI-BuI(40/60) and SPI(SA)/PBI-BuI(30/70) from RT to 100 °C indicating the optimum quantity of SPI in the blend for better proton conductivity after being doped with 1M H_2SO_4. In other words our attempt to make the blends for enhancing proton conductivity, is revealed, these blends was doped with 1M H_2SO_4. However, at further higher temperatures (100 and 110 °C) proton conductivity suddenly decreases. This can possibly due to the loss of water indicating that water is an essential medium for transportation of protons. The results are better illustrated from the Nyquist EI plots that describe the trend.

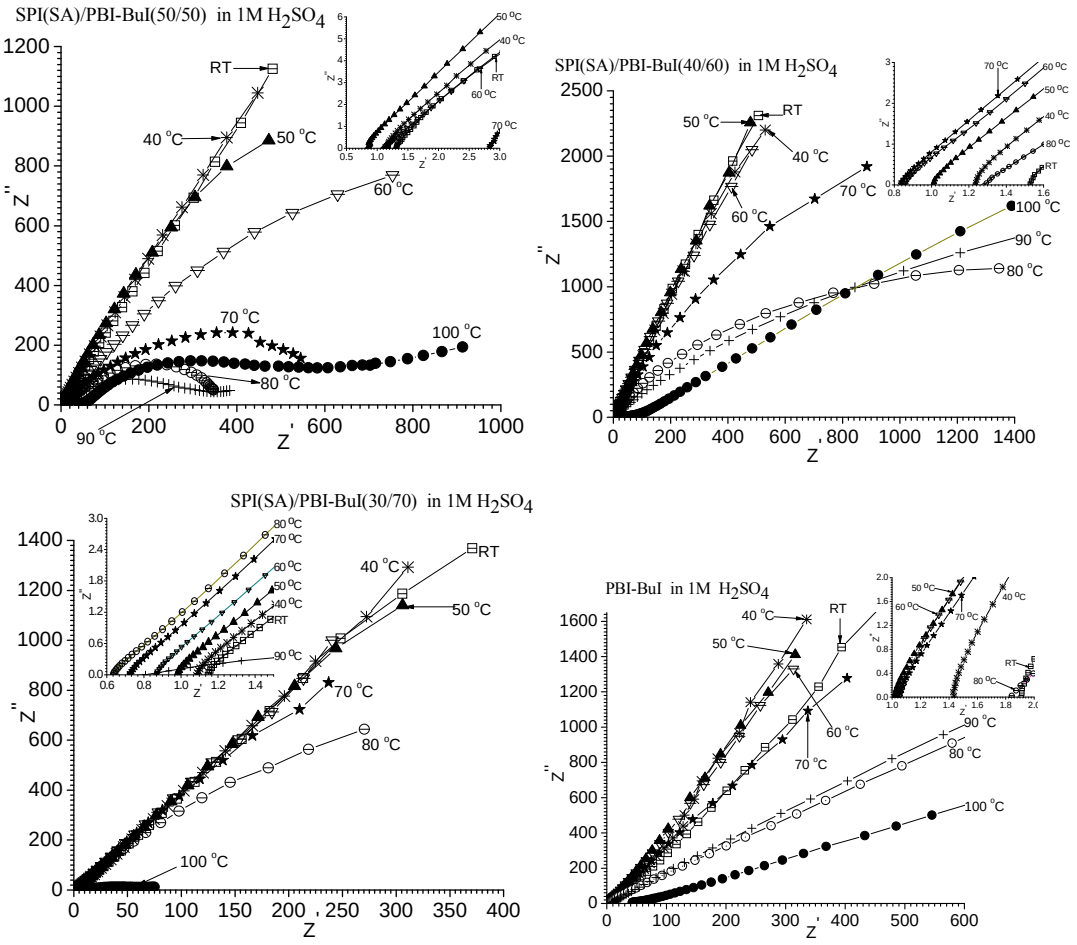

Figure 5.15 Impedance spectra of blend membranes and PBI-BuI doped with in 1 M H_2SO_4

From above Figure 5.15, it is seen that only SPI(SA)/PBI-BuI(50/50) blend membrane having higher SPI content gives the semicircle at high temperatures, which indicates the charge transport of controlled behavior (proton, R_f). Increasing PBI-BuI content in blends results in the disappearance of semicircle which indicates a less facile transport of proton. However, on the other hand, increasing the temperature also improves the proton transport that results in a semicircle at low frequency range. In case of SPI(SA)/PBI-BuI(50/50), the semicircle can only be observed at higher temperature (70, 80 and 90 °C) and diameter of which become less at 90 °C indicating the facile diffusion of proton at these temperatures. However, at this temperature (90 °C), R_Ω increases with rapid decrease in proton conductivity. At further higher temperature (100 °C), not only R_Ω increases but the diameter of the semicircle is also enhanced indicating

increase in membrane resistance as well as reduced proton transport, in other words, R_f also increases. Similarly, in SPI(SA)/PBI-BuI(40/60) and SPI(SA)/PBI-BuI(30/70), rapid increase in R_Ω is observed with sharp decrease in conductivity from 90 °C to 100 °C. This can be attributed to the evaporation of water which acts as a medium for proton transportation. This observation specifies that proton transport perhaps occurs through a vehicular mechanism in 1M H_2SO_4 doped blend membranes. The higher conductivity with increasing content of PBI-BuI at higher temperature also shows the possibility of Grotthuss mechanism in blends containing high PBI-BuI content.

Since maximum proton conductivity of blend membrane and PBI-BuI is observed at different temperatures and sufficient data for comparing their proton conductivity can not be obtained, hence Arrhenius plots of these membranes doped with 1M H_2SO_4 have not been drawn.

*(ii) Proton conductivity of blend membranes [*SPI(*PA*)/PBI-BuI*(a/b)] and PBI-BuI doped with 1M H_3PO_4*

In order to investigate the effect of different acids in the proton conductivity behavior of the blend membranes, we doped blend membranes and PBI-BuI with 1M H_3PO_4 and the results of membrane resistance (R_Ω) are summarized in the Table 5.8. Proton conductivity of these membranes can be seen from the Figure 5.16.

Table 5.8 R_Ω values of blend membranes and PBI-BuI in 1M H_3PO_4

Temp. (°C)	Membrane resistance in (R_Ω)			
	SPI(PA)/PBI-BuI(50/50)	SPI(PA)/PBI-BuI(40/60)	SPI(PA)/PBI-BuI(30/70)	PBI-BuI
30	11.31	8.60	12.82	7.65
40	9.70	8.00	10.61	5.4
50	8.38	6.50	8.08	3.91
60	7.19	6.00	6.24	2.95
70	6.00	5.35	4.76	2.50
80	5.07	4.76	4.53	2.30
90	4.85	4.67	4.41	3.42
100	6.90	5.26	9.56	45
110	48.67	16.19	59.46	62

From the Table 5.8, among the blend membranes, membrane resistance (R_Ω) decreases with increase in temperature till 90 °C in 100% RH. However, R_Ω increases with a sharp increase in resistance from 100 °C to 110 °C. While comparing the values of R_Ω of blend membrane with that of PBI-BuI, latter shows lesser R_Ω up to 90 °C. This behavior is exactly the reverse of results seen in membrane doped with 1M H_2SO_4, where PBI-BuI exhibits higher R_Ω than that of blend membrane. This shows that presence of $-SO_3H$ group in the blend improves the proton conductivity as compared with that of PBI-BuI on doping with 1M H_2SO_4. While, opposite behavior is observed when membranes are doped with 1M H_3PO_4. It should also be noted that, comparing R_Ω between membranes doped with 1M H_2SO_4 and 1M H_3PO_4, former shows much lower R_Ω than latter. This can be due to higher dissociation constant of the H_2SO_4 (pK_a: *-3*) than H_3PO_4 (pK_a: *2.15*). As a result, availability of $[H^+]$ is more in 1M H_2SO_4 than that of 1M H_3PO_4, resulting in more number of protonated benzimidazole moieties on doping with former than that of latter. Proton conductivity of these membranes doped with 1M H_3PO_4 is shown in the following Figure 5.16.

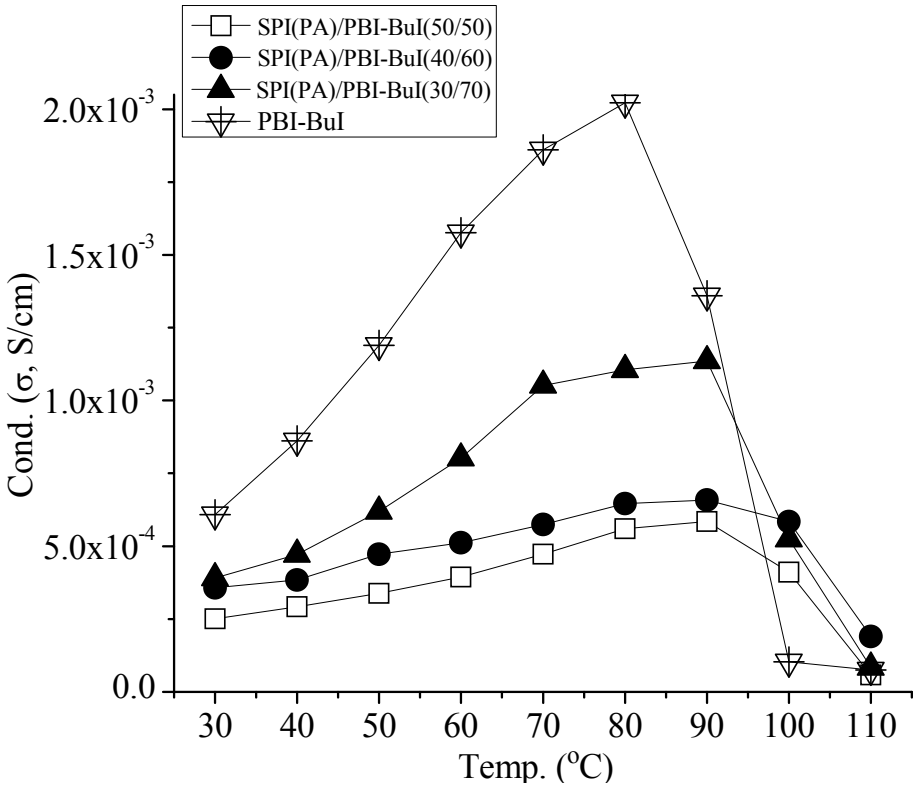

Figure 5.16 Variation of proton conductivity of blend membranes and PBI-BuI doped with 1M H_3PO_4 with temperature

From the Figure 5.16, it is seen that PBI-BuI shows higher proton conductivity than that of blend membranes, in particular from RT to 90 °C. For example proton conductivity at 60 °C for PBI-BuI, SPI(PA)/PBI-BuI(30/70), SPI(PA)/PBI-BuI(40/60) and SPI(PA)/PBI-BuI(50/50) is 1.58 X 10^{-3}, 8.02 X 10^{-4}, 5.12 X 10^{-4} and 3.95 X 10^{-4} S/cm, respectively. In this case, conductivity increases with increase in PBI-BuI content, being highest for PBI-BuI. This is because of the increase in protonated benzimidazole moieties. This also indicates that PBI-BuI is the main contributor for proton transportation while SPI plays the supporting role by efficiently interconnecting the channels with $–SO_3H$ groups after doping with 1M H_3PO_4. This further supports the fact that proton transport between basic benzimidazole and acidic H_3PO_4 is presumably by exchange which suggests a Grotthus type mechanism. However, conductivity decreases above 90 °C, demonstrating strong dependence on water also.

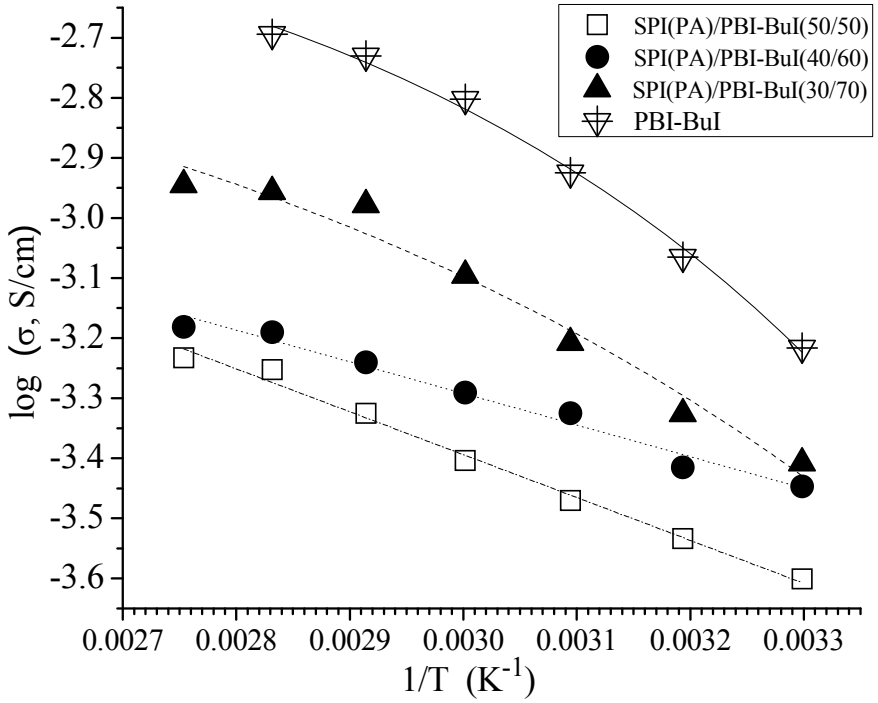

Figure 5.17 Arrhenius plot of proton conductivity of 1M H_3PO_4 doped membranes with temperature

We have attempted to investigate the proton conductivity behavior of blend membranes on doping with 1M H_3PO_4, by using following Arrhenius equation

$$\sigma = \sigma_o \exp\left(\frac{-E_a}{RT}\right)$$

From the above Figure 5.17, it is observed that PBI-BuI and SPI(PA)/PBI-BuI(30/70) shows a slight deviation from Arrhenius type of behavior for proton transport when doped with 1M H_3PO_4. While the blends SPI(PA)/PBI-BuI(40/60) and SPI(PA)/PBI-BuI(50/50) show Arrhenius type of behavior with E_a values of 10 and 14 kJ/mole, respectively. This indicates that with increase in SPI content, proton conductivity is also governed by sulfonic acid group content in the blend even when doped with 1M H_3PO_4. In other words, with increasing SPI content in the blend, it shows Arrhenius behavior.

Following Figures 5.18 represents EIS spectra of the blend membranes when doped with 1M H_3PO_4, which can shed more light on proton transportation.

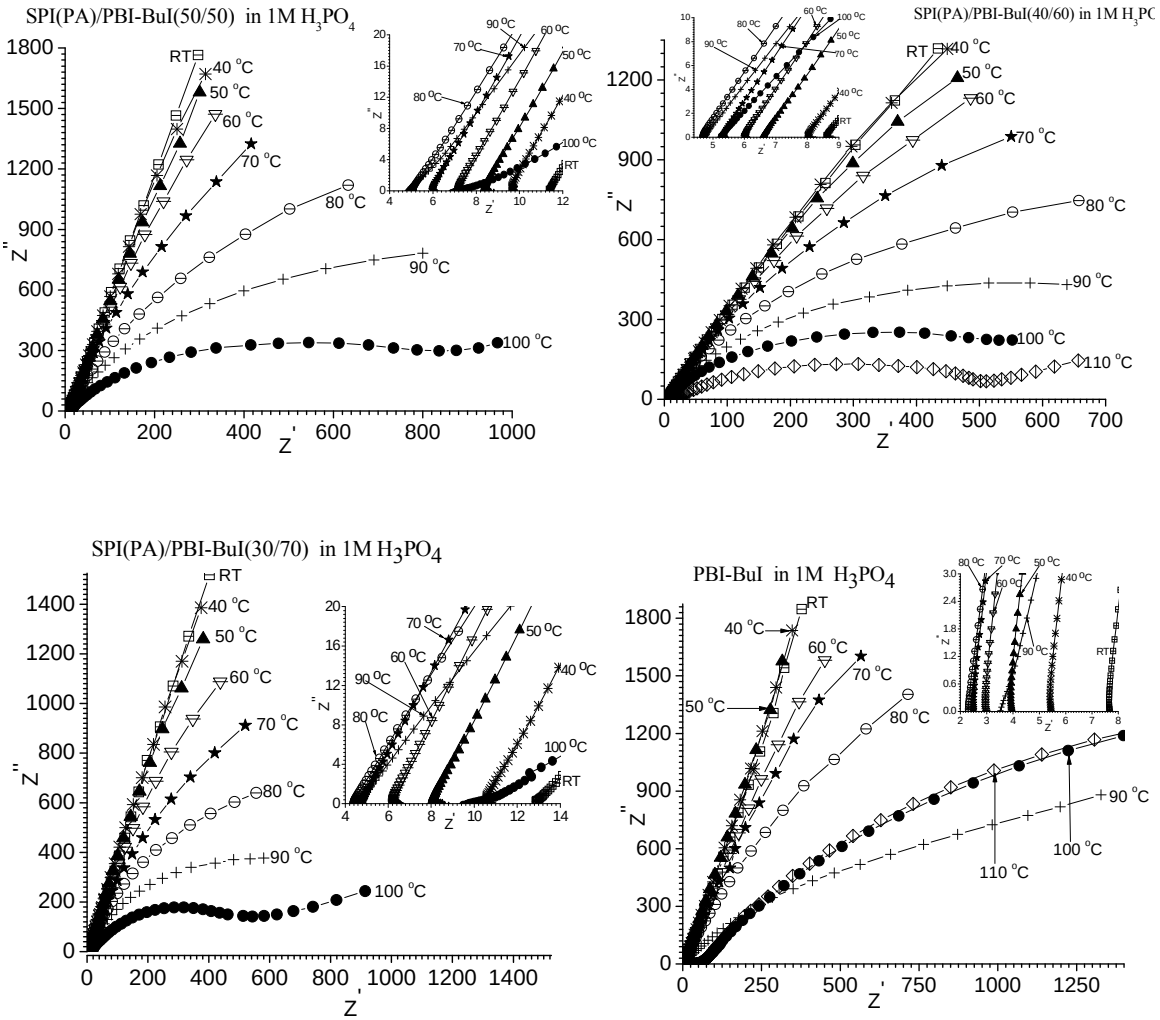

Figure 5.18 Impedance spectra of blend membranes and PBI-BuI doped with 1M H_3PO_4

Among membranes doped with 1M H_3PO_4 (Figure 5.18), PBI-BuI shows the least R_Ω at all temperatures as seen in the Table 5.8. Among 1M H_3PO_4 doped blend membranes the decrease in R_Ω shifts at higher temperature with increase in PBI-BuI content. This can be attributed to the higher benzimidazole content which can take up the proton from the phosphoric acid. In addition, in these blend membranes, with increase in temperature, the diameter of the semicircle keeps decreasing indicating more facile transport of proton at higher temperatures (Figure 5.18). In these blend membranes least value of R_Ω is obtained at 90 °C. From RT to 90 °C, R_Ω decreases gradually and increases suddenly at 100 °C. This indicates that water is an essential medium for proton transportation perhaps by vehicular mechanism.

From Tables 5.7 and 5.8 and Figure 5.15 and 5.18, it could be seen that, 1M H_2SO_4 doped blend membranes exhibit lower value of R_Ω as compared with that of 1M H_3PO_4 doped membranes. This indicates that the former has less membrane resistance than the latter. However, the semicircle region is clear, in particular at higher temperature in 1M H_3PO_4 doped blend membranes, indicating enhanced proton transport. On doping these membranes either with 1M H_2SO_4 or 1M H_3PO_4, both types of mechanism i.e. by vehicular and Grotthus for proton conductivity have been observed.

5.4 Conclusions

1. Water uptake (WU) of SPIs decreases in the order $SPDAB_I$-N ≈ $SPDAB_{II}$-N > SPDAB•TA-N > SPDAB•Im-N while incase of blend membranes WU decreases in the order as SPI(H)/PBI-BuI(50/50) > SPI(H)/PBI-BuI(40/60) > SPI(H)/PBI-BuI(30/70). In other words WU increase with SPI content and decreases with PBI-BuI content.
2. Ion exchange capacity (IEC) decreases in the order $SPDAB_I$-N > $SPDAB_{II}$-N > SPDAB•Im-N > SPDAB•TA-N. In case of blend membranes, it decreases in the order as SPI(H)/PBI-BuI(50/50) > SPI(H)/PBI-BuI(40/60) > SPI(H)/PBI-BuI(30/70).
3. For sulfonated polyimides, hydrolytic stability as well as oxidative stability is higher for SPIs in salt form (SPDAB•TA-N and SPDAB•Im-N) as compared with SPI in –SO_3H form ($SPDAB_I$-N and $SPDAB_{II}$-N). While incase of blend membranes hydrolytic and oxidative stability increases with increase in PBI-BuI content.

4. Proton conductivity (σ) of SPIs increases in the order SPDAB•TA-N < SPDAB•Im-N < $SPDAB_{II}$-N < $SPDAB_{I}$-N < Nafion-117. SPDAB•Im-N exhibits higher proton conductivity, IEC and lower water uptake than that of SPDAB•TA-N. Blend membranes with SPI in $–SO_3H$ form [SPI(H)/PBI-BuI(a/b)] exhibits much lower proton conductivity in the order of 10^{-5} S/cm.
5. PBI-BuI membrane, on doping with 1M H_2SO_4, show lower conductivity than blend membranes, while on doping with 1M H_3PO_4, it exhibits higher proton conductivity than blend membranes.
6. In case of 12 M H_3PO_4 doped membranes, highest conductivity was exhibited by PBI-BuI. Among the blend membranes, conductivity increases with increase in PBI-BuI content. Above 75 °C, blend membrane exhibits higher proton conductivity than that of PBI-I.
7. For the 12M H_3PO_4 doped membranes, H_3PO_4 uptake decreases in the order PBI-BuI > PBI-I > SPI(PA)/PBI-BuI(30/70) > SPI(PA)/PBI-BuI(40/60) > SPI(PA)/PBI-BuI(50/50) > SPDAB•TA-N ≈ SPDAB•Im-N.
8. In case of membranes doped with 12 M H_3PO_4, blend membrane, SPI(PA)/PBI-BuI(30/70) exhibits proton conductivity almost equivalent to that of PBI-BuI even though it is having lower phosphoric acid uptake. This is especially important as membranes with lower acid uptake are expected to be more robust than that with higher acid uptake.

Chapter 6

Conclusions

Successful methodology was developed for the synthesis of diamines containing pendant phenoxy group which would allow synthesis of PIs with systematic structure architecture. 1-phenoxy-2,4-diamino benzene (PDAB) was synthesized as a primary monomer of this family. Substitution of bulky group was done on aromatic ring of oxyphenyl (phenoxy) ring of PDAB. This methodology yielded four types of diamines having methyl and *t*-butyl substitution on phenoxy group. In this way, novel diamines viz., 2′methyl-1-phenoxy-2,4-diamino benzene (2′MPDAB), 4′-methyl-1-phenoxy-2,4-diamino benzene (4′MPDAB), 2′,6′-dimethyl-1-phenoxy-2,4-diamino benzene (2′,6′DMPDAB) and 4'-*t*-butyl-1-phenoxy-2,4-diamino benzene (4′*t*BPDAB) were succefully syntesized and characterized. Sulfonated diamine, viz., 4′-sulfonic-1-phenoxy-2,4-diaminobenzene (SPDAB) was synthesized by sulfonation of PDAB using a simple methodology to offer quantitative substitution of $–SO_3H$ moiety at *para*-position of aromatic ring at oxyphenyl (phenoxy) linkage.

Polycondensation of a diamine (PDAB) with selected dianhydrides by one step solution condensation technique yielded polyimides with flexible pendant phenoxy group, which were characterized for requisite physical properties. This methodology was subsequently followed for the polycondensation of other diamines with commercial dianhydrides (ODPA, 6FDA and NTDA). All these PIs exhibited good solvent solubility, high T_g (> 250 °C) and high thermal stability (IDT > 500 °C). PI based on 6FDA (PDAB-6FDA) showed high *d*-spacing, high density, high T_g but low IDT compared to PI based on ODPA. Copolyimides (CPIs) of PDAB and ODA in different ratios were prepared. These CPIs also showed good solubility and high thermal stability. Results indicate that incorporation of pendant phenoxy group in PIs enhance solvent solubility without sacrificing thermal stability.

Polyimides with alkyl substituted phenoxy groups as a side chain were successfully synthesized with two select dianhydrides (ODPA and 6FDA). Intrinsic viscosity of these polyimides was in the range of 0.30-0.55 dL/g and dense membranes

could be cast in chlorinated solvents. Solubility parameter of PIs decreases with increase in alkyl content. Polyimides based on 6FDA showed better solubility, higher T_g, lower decomposition temperature, lower solubility parameter and higher *d*-spacing than that of ODPA based polyimides. Structural isomers of PIs based on diamines, viz., 4'MPDAB and 2'MPDAB with either ODPA or 6FDA revealed different *d*-spacing. Polyimides with $–CH_3$ substitution at *ortho* position in pendant phenoxy group exhibited high T_g. WAXS pattern revealed their amorphous nature. While, 6FDA based PIs disclosed two humps in their corresponding WAXS spectra, indicating their two types of chain packing.

Gas permeability investigations of these PIs reveal that 6FDA based PIs exhibit higher permeability than that of ODPA based PIs obtained from same diamine. Increase in permeability was by 4.6 to 13.3 times, while decrease in selectivity was by a factor of 0.04 to 0.53, confirming the importance of $–C(CF_3)_2–$ linkage in gas permeability of PIs. In ODPA based PIs, better selectivity is shown by PDAB-ODPA, while in 6FDA based PIs 2'MPDAB-6FDA demonstrates the best selectivity for various gas pairs. In the case of ODPA based PIs, permeability for different gases increase in an order PDAB-ODPA ≈ 2'MPDAB-ODPA < 4'MPDAB-ODPA < 2',6'DMPDAB-ODPA < 4'*t*BPDAB-ODPA. In 6FDA based PIs, permeability increases in the order 2'MPDAB-6FDA < 4'MPDAB-6FDA < PDAB-6FDA < 2',6'DMPDAB-6FDA ≈ 4'*t*BPDAB-6FDA. Intrasegmental mobility (T_g) largely governs gas permeation in these PIs. Alkyl substituent on the pendant phenoxy group at *para* position is more effective than at *ortho* substitution for increasing permeability in PIs. As a result, PIs based on isomeric diamines 2'MPDAB and 4'MPDAB (with either ODPA or 6FDA), the later exhibited lower T_g, higher permeability, but lower selectivity. Though *d*-spacing for substitution of voluminous *t*-butyl group on pendant phenoxy group in PIs (4'*t*BPDAB-ODPA and 4'*t*BPDAB-6FDA) is low; these polymers demonstrated the highest permeability, which is in tune of variation in FFV. Between 4'*t*BPDAB-ODPA and 2',6'DMPDAB-ODPA, former reveals better selectivity for some of the gas pairs. On the other hand, 4'*t*BPDAB-6FDA and 2',6'DMPDAB-6FDA exhibits almost same permeability and no significant difference in selectivity. In ODPA based PIs, structural variation in diamine moiety greatly affects chain packing and thus gas permeability. On the other hand in 6FDA based PIs, dependence of structural variation in diamine moiety on gas permeability was largely

suppressed by the effects of–$C(CF_3)_2$– linkage of 6FDA. In case of SPIs, feed gas humidification lead to an increase in permeability as well as selectivity. This effect is more pronounced in CO_2 based permeation properties. In blend membranes, permeability of CO_2 increases with increasing content of SPIs.

Polyimides containing sulfonic acid group in pendant phenoxy were synthesized by polycondensation of SPDAB with NTDA. Polycondensation in presence of imidazole is faster than TEA. These SPIs in corresponding salt form as well as in $–SO_3H$ form revealed good solubility in polar aprotic solvents like DMF, DMAc and DMSO and their reduced viscosity increased with decreasing concentration in the solution of DMAc, thus showing a typical ionomer behavior. Tough and flexible films of these SPIs in their corresponding salt form could be cast from their DMAc solution and on converting these membranes into their respective $–SO_3H$ form. NTDA based SPIs could retain their mechanical strength while ODPA based SPI became brittle. Thermal stability of SPIs decreased in the order SPDAB•Im-N > $SPDAB_I$-N ≈ $SPDAB_{II}$-N > SPDAB•TA-N and they did not show any glass transition. SPDAB•Im-N showed some interesting features such as critical solution temperature (CST) phenomenon, high thermal stability, delayed time for dissolution in solvents and close packing from its WAXD spectrum. Blends prepared from PBI-I with SPDAB•TA-N are brittle while that of with PBI-BuI become flexible below 50 wt% of SPDAB•TA-N. These blends are miscible as supported by their FT-IR spectra.

Physicochemical characterizations and proton conductivity analysis of SPIs as well as blend membranes as PEM material was evaluated. It is observed that water uptake and IEC of SPIs in $–SO_3H$ form ($SPDAB_I$-N and $SPDAB_{II}$-N) is higher than that of their salt forms (SPDAB•Im-N and SPDAB•TA-N). While reverse is the trend for hydrolytic and oxidative stability. Proton conductivity (σ) of SPIs decreases in the order Nafion-117 > $SPDAB_I$-N > $SPDAB_{II}$-N > SPDAB•Im-N > SPDAB•TA-N. Proton conductivity of the order of 10^{-2}-10^{-3} $S.cm^{-1}$ of SPIs in $–SO_3H$ form in spite of their comparatively lower IEC (<2) and optimum water uptake (46-49%) indicates their importance as PEM material. Arrhenius type of behavior is observed for SPIs in $–SO_3H$ form with E_a in the range of 8-9.5 for kJ/mole. These values matched well with reported ones for other SPIs and sulfonated hydrocarbon polymers. The lower time for the polymerization of SPDAB•Im-

N and higher proton conductivity, higher hydrolytic as well as oxidative stability, higher IEC and lower water uptake than that of SPDAB•TA-N indicate the effectual of SPIs in an imidazolium sulfonate salt form.

In case of blend membranes [SPI(*H*)/PBI-BuI*(a/b)*] as PEM material, water uptake and IEC values increase with SPI content and decrease with PBI-BuI content. While hydrolytic stability and oxidative stability of such blend membranes show the reverse trend. 12M H_3PO_4 uptake of blend membranes increases with increasing PBI-BuI content, as anticipated. Their proton conductivity also increases with PBI-BuI content, which being highest for one of their components i.e. 12M H_3PO_4 doped PBI-BuI at all temperatures. Proton conductivity of 12M H_3PO_4 doped membranes was observed to follow non-Arrhenius behavior. This implies importance of blend membranes while doping with 12M H_3PO_4 despite of their low acid doping level. This is especially important as membranes with lower acid uptake are expected to be more robust than that with higher acid uptake. Though, proton conductivity of 1M H_3PO_4 doped membranes in 100% RH is found to be lower than that of membranes doped with 12M H_3PO_4 in anhydrous condition, however proton conductivity of the former in the range of 10^{-3}-10^{-4} $S.cm^{-1}$ at such lower concentration (1M) of acid is worth noting.

References

Acharya M. and Foley H. C., *AIChE Journal*, 46, 5, **2000**, 911.

Ahn T. K., Kim M., and Choe S., *Macromolecules, 30,* **1997**, 3369.

Akutsu F., Kataoka T., Shimizu H., Naruchi K. and Miura M., *Macromol. Rapid Commun.*, 15, **1994**, 411.

Al-Haq M. I., Lebrasseur E., Tsuchiya H. and Torri T., *Crystall. Rev*., 13, 1, **2007**, 29.

Alvarez-Gallego Y., Nunes S. P., Lozano A. E., de la Campa J. G. and de Abajo J., *Macro. Rap. Comm.*, 28, **2007,** 616.

Anthony J. L., Maginn E.J. and Brennecke J. F., *J. Phys. Chem. B,* 105, **2001,** 10942.

Appleby A. J., *J. Power Sources*, 29, **1990**, 3.

Arthur W. J., *U. S. Pat.*, 3347917, **1967**.

Asano N., Aoki M., Suzuki S., Miyatake K., Uchida H. and Watanabe M., *J. Am. Chem. Soc*., 128, **2006,** 1762.

Bacon F. T., *Electrochimica Acta.*, 14, **1969**, 569.

Baker R. W., *Membrane Technology and Application, 2nd Edition, John Wiley and Sons, Ltd.*, England, **2004**.

Baldwin B. W., Hirose T. and Wang Z. H., *Chem. Commun.*, **1996**, 2669.

Bara J. E., Carlisle T. K., Gabriel C. J., Camper D., Finotello A., Gin D. L. and Noble R. D., *Ind. Eng. Chem. Res.*, 48, **2009**, 2739.

Barbir F., *PEM Fuel Cells: Theory and Practice*, Elsevier Academic Press, Chapter 2, **2005**.

Barkdoll A. E., England D. C., Gray H. W., Kirk W. J. and Whiltman G. M., *J. Am. Chem. Soc.*, 75, **1953**, 1156.

Barrer R. M. and Skirrow G., *J. Polym. Sci.*, 3, **1948**, 549.

Beliers J.-P. and Angell C. A., *J. Physc. Chem. B*, 111, **2007**, 4926.

Bergemeister J. J., Rancourt J. D., Taylor L. T., *Chem. Mater.*, 2, **1990**, 640.

Beuscher U., Cleghorn S. J. C. and Johnson W. B., *Int. J. Energy Res*., 29, **2005**, 1103.

Bhole Y. S. and Kharul U.K., *Polym. Int.*, 52, **2003**, 1474.

Bhole Y. S., Karadkar P. B. and Kharul U. K., *J. Polym. Sci., Part B: Polym. Phys.*, 45, **2007**, 3156.

Bhole Y. S., Kharul U. K., Somani S. P. and Kumbharkar S.C., *Eur. Polym. J.*, 41, **2005**, 2461.

Bhutani S. K., *U. S. Pat.,* 3935264, **1976**.

Biswas M. and Mukherjee A., *Adv. Polym. Sci.*, 115, **1994**, 90.

Blanchard L. A. and Brennecke J. F., *Ind. Eng. Chem.*, 40 (1), **2001**, 287.

Bogert M. T. and Renshaw R. R., *J. Am. Chem. Soc*., 30, **1908,** 1135.

Bollinger W. A., MacLean D. L. and Narayan R. S., *Chem. Eng. Prog.*, 78, **1982**, 27.

Bouchet R., Miller S., Duclot M. and Souquet J. L., *Solid State Ionics*, 145, **2001,** 69.

Boudghene Stambouli A. and Traversa E., *Renew. Sust. Energy Rev.*, 6, **2002**, 433.

Bower G. M. and Frost L. W., *J. Polym. Sci., Part A: Polym. Chem.*, 1, **1963**, 3135.

Brooks N. W., Duckett R. A., Rose J., Ward I. M. and Clements J., *Polymer*, 34 (19), **1993**, 4038.

Bryant R. G., *Polyimides, Kirk-Othmer Encyclopedia of Chemical Technology*, Vol. 20, page no. 268, John Wiley and Sons, Inc. **2006**.

Buckley A., Stuetz D.E. and Serad G.A., *Encycl. Polym. Sci. Eng.*, 11**, 1987**, 572.

Campos A., Garcia R., Suner I. and Figueruelo J. E., *Polymer*, 38 (12), **1997**, 3011.

Cassidey P. E., Fawcett, N. C., *"Kirk-Othmer Encyclo. Chem. Technol."*, John Wiley and Sons, New York, 18, **1982**, 704.

Chatterjee G., Houde A. A. and Stern S. A., *J. Membr. Sci.*, 135, **1997**, 99.

Chen C., Huang X. and Qin W., J. *Macromol. Sci., Part B: Phys.*, 47, **2008**, 109.

Chen N., Tien C.-F., Patton S. M., Langsam M. and Burgoyne W.F., *Polym. Mater. Sci. Eng.*, 69, **1993**, 161.

Chen X., Yin Y., Tanaka K., Kita H. and Okamoto K.-I., *High Perform. Polym.*, 18, **2006,** 637.

Chhabra P. and Choudhary V. *Eur. Polym. J.*, 45, **2009**, 1467.

Chikvaidze G., Gabrusenoks J., Kleperis J. and Vaivars G., *Functional Materials and Nanotechnologies, J. Phys., Conference Series*, 93, **2007**, 012026, 1.

Chung T. S., Lin W.-H. and Vora R. H., *J. Appl. Polym. Sci.*, 81, **2001**, 3552.

Clayden J., Greeves N., Warren S. and Wothers P., *Organic Chemistry*, Oxford University Press, New York, **2001**.

Cole A. C., Jensen J. L., Ntai I., Tran K. L. T., Weaver K. J., Forbes D. C. and Davis J. H. Jr., *J. Am. Chem. Soc*., 124, **2002,** 5962.

Coleman M. R. and Koros W. J., *J. Membr. Sci.,* 50, **1990**, 285.

Coleman M. R. and Koros W. J., *J. Polym. Sci., Part B: Polym. Phy.*, 32, **1994**, 1915.

Contois L. L. and Trementozzi Q. A., *J. Polym. Sci.*, XVIII, **1955**, 479.

Cordes De N. D. M. and Walter J. L., *Spectrochimica Acta*, 24A, **1968**, 237.

Cornelius C. J., *Ph. D. Dissertation,* Virginia Polytechnic Institute and State University, **2000.**

Cornet N., Diat O., Gebel G., Jousse F., Marsacq D., Mercier R. and Pineri M, *J. New Mater. Electrochem. Syst.*, 3, **2000**, 33.

Cote P. and Brisson J., *Macromolecules*, 27, **1994**, 7329.

Crank J., "*The mathematics of diffusion*", *Clarendon Press*, **1956**.

Crosthwaite J. M, Aki S. N.V. K, Maginn E. J. and Brennecke J. F., *Fluid Phase Equilibria*, 228, **2005**, 303.

Daletou M. K., Gourdoupi N. and Kallitsis J. K., *J. Membr. Sci*., 252, **2005**, 115.

Daletou M. K., Kallitsis J. K., Voyiatzis G. and Neophytidesa S. G., *J. Membr. Sci*., 326, **2009**, 76.

de Abajo J. and de la Campa J. G., *Adv. Polym. Sci.*, 140, **1999**, 23.

Deimede V., Voyiatzis G. A. Kallitsis J. K., Qingfeng L. and Bjerrum N. J., *Macromolecules*, 33, **2002**, 7609.

Devezas T., LePoire D., Matias J. C.O. and Silva A.M.P., *Features*, 40, **2008**, 1.

Dickinson P. R. and Sung C. S. P., *Macromolecules*, 25, **1992**, 3758.

Dincer I., *Int. J. Energy Res.*, 31, **2007**, 29.

Dine-Hart R. A. and Wright W. W., *J. Appl. Polym. Sci*., 11, **1967**, 609.

Ding J., Chuy C. and Holdcroft S., *Chem. Mater.*, 13, 7, **2001**, 2231.

Ding M., *Prog. Polym. Sci*., 32, **2007**, 623.

Domanska U., *Thermochimica Acta.*, 448, **2006**, 19.

Domanska U., Zolek-Tryznowska Z. and Krolikowski M., *J. Chem. Eng. Data*, 52, **2007**, 1872.

Dong K., Zhang S., Wang D. and Yao X., *J. Phys. Chem. A*, 110 (31), **2006**, 9775.

Dotcheva D., Klapper M. and Mullen K ., *Macromol. Chem. Phys.*, 195, **1994**, 1905.

Du Z., Li Z., Guo S., Zhang J., Zhu L. and Deng Y., *J. Physc. Chem. B*, 109, **2005**, 19542.

Dupont J., *J. Braz. Chem. Soc.*, 15, 3, **2004**, 341.

Eastmond G. C., Gibas M., Pacynko W. F. and Paprotny J., *J. Membr. Sci.*, 207, **2002**, 29.

Edward, W. M. and Robinson, I. M., *U. S. Pat*., 2867609, **1959a**.

Edward, W. M. and Robinson, I. M., *U. S. Pat*., 2880230, **1959b**.

Einsla B. R., Hong Y.-T., Kim S. Y., Wang F., Gunduz N. and McGrath J. E., *J. Polym. Sci. Part A: Polym. Chem.*, 42, **2004**, 862.

Einsla B. R., Kim S. Y. Hickner M. A., Hong Y.-T., Hill M. L., Pivovar B. S. and McGrath J. E., *J. Membr. Sci.*, 255, **2005a**, 141.

Einsla B. R., *Ph. D. Dissertation*, Virginia Polytechnic Institute and State University, Blacksburg, Virginia, **2005b**.

Elabd Y. A., Napadensky E., Walker C. W. and Winey K. I., *Macromolecules*, 39, **2006**, 399.

Endrey A. L., *U. S. Pat.*, 3179631, **1965a**.

Endrey A. L., *U. S. Pat.*, 3179633, **1965b.**

Fang J., Guo X., Harada S., Watari T., Tanaka K., Kita H. and Okamoto K., *Macromolecules*, 35, **2002,** 9022.

Fang J., Guoa X., Xua H. and Okamoto K., *J. Power Sources*, 159, **2006,** 4.

Faure S., Cornet N., Gebel G., Mercier R., Pineri M. and Sillion B. *Proceedings of Second International Symposium on New Materials for Fuel Cell and Modern Battery Systems*, Montreal, Canada, July 6–10, **1997**, p. 818.

Fontanella J. J., Wintersgill M. C., Wainright J. S., Savinell R. F. and M. Litt, *Electrochim. Acta.*, 43 (10-11), **1998**, 1289.

Fraga-Dubreuil J., Bourahla K., Rahmouni M., Bazureau J. P. and Hamelin J., *Catal. Commun.*, 3, **2002**, 185.

Freeman B. D., Bokobza L., Sergot P., Monnerie L. and De Schryver F. C., *Macromolecules*, 23, **1990**, 2566.

Gagliano A. R., Knowlton R. C. and Byers L. D., *J. Org. Chem.*, 54, **1989**, 5247.

Gao Y., Robertson G. P., Guiver M. D. and Jian X., *J. Polym. Sci., Part A: Polym. Chem.*, 41, **2003a**, 497.

Gao Y., Robertson G. P., Guiver M. D., Jian X., Mikhailenko S. D., Wang K. and Kaliagaine S., *J. Polym. Sci., Part A: Polym. Chem.*, 41, **2003b**, 2731.

Gao Y., Robertson G. P., Guiver M. D., Mikhailenko S. D., Li X. and Kaliagaine S., *Macromolecules*, 37, **2004**, 6748.

Gao Y., Robertson G. P., Guiver M. D., Mikhailenko S. D., Li X. and Kaliagaine S., *Macromolecules*, 38, **2005**, 3237.

Genies C., Mercier R., Sillion B., Cornet N., Gebel G. and Pineri M., *Polymer*, 42, **2001a**, 359.

Genies C., Mercier R., Sillion B., Petiaud R., Cornet N., Gebel G. and Pineri M., *Polymer*, 42, **2001b**, 5097.

Ghaemy M. and Alizadeh R., *Eur. Polym. J.*, 45, **2009**, 1681.

Ghosal K. and Chern R. T., *J. Membr. Sci.*, 72, **1992**, 91.

Ghosal K. and Freeman B. D., *Polym. Adv. Tech.*, 5, **1994**, 673.

Ghosh M. K. and Mittal K. L., *Polyimides: Fundamentals and Applications*, Marcel Dekker, New York, **1996**.

Gianolio D. A., Segismundo J. M. and Mclaughlin L.W., *Nucleic Acids Research*, 10, **2000**, 2128.

Gilron J. and Soffer A., *J. Membr. Sci.*, 209, **2002**, 339.

Glipa X., Bonnet B., Mula B., Jones D. J. and Roziere R., *J. Mater. Chem.*, 9, **1999,** 3045.

Gonzalez R. A., *U. S. Pat.*, 3499034, **1970**.

Greaves T. L. and Drummond C. J., *Chem. Rev.*, 108, **2008**, 206.

Grove W. R., *Phil. Mag. Ser.*, 3, 14, **1839**, 127.

Grubb T. L., Ulery V. L., Smith T. J., Tullos G. L., Yagci H., Mathias L. J. and Langsam M., *Polymer*, 40, **1999**, 4279.

Grubb W. T., *U. S. Pat.*, 2913511, **1959**.

Guerra G., Choe S., Williams D. J., Karasz F. E. and MacKnight W. J., *Macromolecules*, 21, **1988,** 231.

Gunduz N., *Ph. D. Dissertation*, Virginia Polytechnic Institute and State University, Blacksburg, VA, **2001**.

Guo X., Fang J., Watari T., Tanaka K., Kita H. and Okamoto K., *Macromolecules, 35,* **2002,** 6707.

Habermann C. E., *U. S. Pat.*, 4153581, **1979**.

Hamrock S. J. and Yandrasits M. A., *J. Macrom. Sci., Part C: Polym. Rev.*, 46, **2006**, 219.

Hara M., Wu J. and Lee A. H, *Macromolecules*, 22, **1989**, 754.

Hasanain F. and Wang Z. Y., *Polymer*, 49, **2008**, 831.

Hasiotis C., Deimede V. and Kontoyannis C., *Electrochimica Acta.*, 46, **2001b**, 2401.

Hasiotis C., Qingfeng L., Deimede V., Kallitsis J. K., Kontoyannis C. G. and Bjerrum N. J., *J. Electrochem. Soc*., 148 (5), **2001a**, A513.

He R., Li Q., Xiao G. and Bjerrum N. J., *J. Membr. Sci.*, 226, **2003**, 169.

Hedrick J. L., Carter K. R., Labadie J. W., Miller R .D., Volksen W., Hawker C. J., Yoon D. Y., Russell T. P., McGrath J. E. and Briber R. M., *Adv. Polym. Sci.*, 141, **1999a**, 1.

Hedrick J. L., Labadie J. W., Volksen W. and Hilborn J. G., *Adv. Polym. Sci.*, 147, **1999b**, 61.

Hellums M. W., Koros W. J., Husk G. R. and Paul D. R., *J. Membr. Sci*., **1989**, 46, 93.

Helmer-Metzmann F., Ballauff M., Schulz R. C. and Wegner G., *Makromol. Chem.*, 190, **1989**, 985.

Hickner M. A., Ghassemi H., Kim Y. S., Einsla B. R. and McGrath J. E., *Chem. Rev.*, 104, **2004**, 4587.

Hirao T., Santhitikul S., Takeuchi H., Ogawa A. and Sakurai H., *Tetrahedron,* 59, **2003**, 10147.

Hirayama Y., Kase Y., Tanihara N., Sumiyama Y., Kusukia Y. and Haraya K., *J. Membr. Sci.*, 160, **1999**, 87.

Hirayama Y., Yoshinaga T., Kusuki Y., Ninomiya K., Sakakabira T. and Tamari T., *J. Membr. Sci.*, 111, **1996a**, 169.

Hirayama Y., Yoshinaga T., Kusuki Y., Ninomiya K., Sakakabira T. and Tamari T., *J. Membr. Sci.*, 111, **1996b**, 183.

Hirose T., Kopek B. G., Wang Z. H., Yusa R. and Baldwin B. W., *Tetrahedron Letters*, 44, **2003**, 1831.

Hoehn H. and Richter J. W., *U.S. Patent Reissue*, 30, **1980**, 351.

Houde A. Y., Kulkarni S. S., Kharul,U. K., Charati C. G. and Kulkarni M. G., *J. Membr. Sci.*, 103, **1995**, 167.

Hougham G., Cassidy P. E., Jones K. and Davidson T., *Fluoropolymers 2: Properties*, Eds., Plenum Press, New York, **1999**, p 233.

Hsiao S. H. and Huang P. C., *J. Polym. Sci., Part A: Polym. Chem.*, 36, **1998a,** 1649.

Hsiao S.-H, Yang C.-P and Lo T.-K., *J. Polym. Res.*, 5,3, **1998b**, 193.

Hsiao S.-H., Yang C.-P. and Chen S.-H., *J. Polym. Sci. Part A: Polym. Chem.*, 38, **2000**, 1551.

Hu Z., Yin Y., Chen S., Yamada O., Tanaka K., Kita H. and Okamoto K. I., *J. Polym. Sci. Part A: Polym. Chem.*, 44, **2006**, 2862.

Hu Z., Yin Y., Kita H., Okamoto K.-I., Suto Y., Wang H. and Kawasato H., *Polymer*, 48, **2007,** 1962.

Hu Z., Yin Y., Yaguchi K., Endo N., Higa M. and Okamoto K.-I., *Polymer*, 50, **2009**, 2933.

Hubner G. and Roduner E., *J. Mater. Chem.*, 9, **1999**, 409.

Hudlicky M., *Reductions in Org. Chem.*, 2nd Ed., ACS Monograph, **1996**.

Iimori T., Iwahashi T., Kanai K., Seki K., Sung J., Kim D., Hamaguchi H. and Ouchi Y. *J. Phys. Chem. B*, 111 (18), **2007**, 4860.

Imai Y., Maldar N. N. and Kakimoto M-A., *J. Polym. Sci., Polym. Chem. Ed.*, 22, **1984,** 2189.

Iwakura Y., Uno K. and Imai Y., *J. Polym. Sci. Part A: Polym. Chem.*, 2 (6), **1964**, 2605.

Jaffe M., Chen P., Choe E. W., Chung T. S. and Makhija S., *Adv. Poly. Sci*., 117, **1994,** 298.

Jeong H.-J., Kobayashi A., Kakimoto M. and Imai Y., *Polym. J.*, 26 (3), **1994**, 373.

Jeong K. U., Kim J.-J. and Yoon T.-H., *Polymer*, 42, **2001**, 6019.

Jiang P., *Acta Cryst.*, E65, **2009**, o2178.

Johnston N. J., *J. Polym. Sci., Part A-1*, 10, **1972**, 2727.

Jung J. C. and Park S. B., *J. Polym. Sci. Part A: Polym. Chem.*, 34, **1996**, 357.

Jung J. C. and Park S. B., *Polym. Bulletin*, 35, **1995**, 423.

Kaas R. L., *J. Polym. Sci., Part A: Polym. Chem. Ed.*, 19, **1981**, 2255.

Kabalka G. W. and Varma R. S. *Comprehensive Organic Synthesis*, Eds.; Pergamon: Oxford, Vol. 8, **1991**, p 363.

Kailani M. H. and Sung C. S. P., *Macromolecules*, 31, **1998a**, 5771.

Kailani M. H. and Sung C. S. P., *Macromolecules*, 31, **1998b**, 5779.

Kailani M. H., Sung C. S. P. and Huang S. J., *Macromolecules*, 25, **1992**, 3751.

Kakimoto M.-A., Yoneyama M. and Imai Y., *J. Polym. Sci. Part A: Polym. Chem.*, 26, **1988**, 149.

Kerres J., Tang C. M. and Graf C., *Ind. Eng. Chem. Res.*, 43, **2004,** 4571.

Kerres J., Ullrich A., Häring T., Baldauf M., Gebhardt U. and Preidel W., *J. New Mat. Electrochem. Systems*., 3, **2000,** 229.

Kerres J., Ullrich A., Meier F. and Haring T., *Solid State Ionics*, 125, **1999,** 243.

Kerres J., Zhang W., Jörissen L. and Gogel V., *J. New. Mat. Electrochem. Systems*, 5, **2002**, 97.

Kharul U. K. and Kulkarni S. S., *Bull. Mater. Sci.*, 17 (6), **1994**, 1071.

Kharul U. K., Kulkarni S. S., Kulkarni M. G., Houde A.Y. and Charati S. G., *Polymer*, 39 (10), **1998**, 2011.

Kim M.-J., Park Y.-I., Youm K.-H. and Lee K.-H., *J. Appl. Polym. Sci.*, 91, **2004**, 3225.

Kim S.-K., Kim T.-H., Jung J.-W. and Lee J.-C., *J. Polym. Sci., Part A: Polym. Chem.*, 50, **2009**, 3495.

Kim T. H., Koros W. J., Husk G. R. and O'brien K. C., *J. Membr. Sci.*, 37, **1988**, 45.

Kim Y. J., Glass T. E., Lyle G. D. and McGrath J. E., *Macromolecules*, 26, **1993**, 1344.

Kim Y.-H., Ahn S.-K., Kim H. S. and Kwon S.-K., *J. Polym. Sci., Part A: Polym. Chem.*, 40, **2002**, 4288.

Kim Y.-H., Kim H.-S. and Kwon S.-K., *Macromolecules*, 38, **2005**, 7950.

Kingston B. H. M., Garey J. J. and Hellwig W. B, *Anal. Chem.*, 41 (1), **1969**, 86.

Klaren Cornelis H. J. and Krak H., *U. S. Pat*., 3756984, **1973**.

Koros W. J. and Fleming G. K., *J. Membr. Sci.*, 83, **1993**, l.

Koros W. J. and Mahajan R., *J. Membr. Sci.*, 175, **2000**, 181.

Koros W. J., Fleming G. K., Jordan S. M., Kim T. H. and Hoehn H. H., *Prog. Polym. Sci.*, 13, **1988**, 339.

Korshak V. V., Rusanov A. L., *Izv Akad Nauk SSSr Ser Khim*, 10, **1969,** 2418.

Korshak V. V., Rusanov A. L., *J. Macromol. Sci.: Part C: Polym. Rev.*, 21, 2, **1981**, 272.

Kosmala B. and Schauer J., *J. Appld. Polym. Sci.*, 85, **2002**, 1118.

Koton M. M., Kudryavtsev V. V. and Svetlichny V. M., *Polyimides: Synthesis, Characterization and Applications* 1 & 2. Ed. Mittal K. L., Plenum, New York, **1984**.

Kreuer K. D., Peddison S. J., Spohr E. and Schuster M., *Chem. Rev.* **2004**, 104, 4637.

Kreuz J. A., Endrey A. L., Gay F. P. and Sroog C. E., *J. Polym. Sci., Part A-1*: 4, **1966**, 2607.

Kulkarni M., Potrekar R., Kulkarni R. A. and Vernekar S. P., *J. Polym. Sci., Part A: Polym. Chem.*, 46, **2008**, 5776.

Kulkarni S. S., *Bull. Mater. Sci.*, 17 (7), **1994**, 1307.

Kumar D., *J. Polym. Sci., Polym. Chem. Ed*., 19, **1981**, 795.

Kumbharkar S. C., Islam Md. N., Potrekar R. A. and Kharul U. K., *Polymer*, 50, **2009**, 1403.

Kumbharkar S. C., Karadkar P. B. and Kharul U.K.., *J. Membr. Sci.*, 286, **2006**, 161.

Kuzenetsove A. A., *High Perform. Polym.*, 12, **2000**, 445.

Langsam M. and Burgoyne W.F., *J. Polym. Sci., Part A: Polym. Chem.*, 31, **1993**, 909.

Lau K. S. Y. and Dougherty T. K., *U. S. Pat*., 4827054, **1989**.

Lavrov S. V., Ardashnikov A. Ya., Kardash I. Ye. and Pravednikov A. N., *Polym. Sci., USSR*, 19, 5, **1977**, 1212.

Lavrov S. V., Talankina O. B., Vorob'ev V. D., Izumnikov A. L., Kardash I. E. and Pravednikov A. N., *Polym. Sci. USSR (Engl Transl.)*, 22, **1980**, 2069.

LeBlanc O. H., Ward W. J., Matson S. L. and Kimura S. G., *J. Membr. Sci.*, 6, **1980**, 339.

Lee C. W., Kwak S. M. and Yoon T. H., *Polymer*, 47, **2006**, 4140.

Lee C., Sundar S., Kwon J. Han H., *J. Polym. Sci., Part A: Polym. Chem.*, 42, **2004**,3612.

Lee H.-Y. and An M., *Bull. Korean Chem. Soc*., 25, 11, **2004**, 1717.

Lee J. K. and Kerres J., *J. Membr. Sci*, 294, **2007**, 75.

Lee S., Lee J. G., Lee H. and Choe S., *Macromolecules*, 32 , **1999** , 5961.

Lee Y. J., Gungor A., Yoon T. H., McGrath J. E. *The Journal of Adhesion*, 55, 1, **1995**, 165.

Li N., Cui Z., Zhang S. and Li S., *J. Polym. Sci. Part A: Polym. Chem.*, 46, **2008,** 2820.

Li N., Cui Z., Zhang S. and Xing W., *J. Membr. Sci*, 295, **2007c**, 148.

Li N., Cui Z., Zhang S., Li S. and Zhang F., *J. Power Sources*, 172, **2007b,** 511.

Li Q., He R. H., Jensen J. O., Bjerrum N. J., *Chem. Mater.*, **2003**, 15, 4896.

Li Q., He R., Berg R.W., Hjuler H. A. and Bjerrum N. J., *Solid State Ionics*, 168, **2004**, 177.

Li Q., Hjuler H.A., Bjerrum N. J., *J. Appl. Electrochem.*, 31, **2001**, 773.

Li Q., Jensen J. O., Savinell R. F. and Bjerrum N. J., *Prog. Polym. Sci.*, 34, **2009**, 449.

Li W., Zhang S., Chen G. and Zhang Q., *Polymer*, 48, **2007a**, 3082.

Li X.-G., Huang M.-R., Duan W. and Yang Y.-L., *Chem. Rev.*, 102, **2002**, 2925.

Li Y., Ding M. and Xu J., *Macromol. Chem. Phys.*, 198, **1997**, 2769.

Li Y., Wang X., Ding M. and Xu J., *J. Appl. Polym. Sci.*, 61, **1996,** 741.

Liaw D.-J., Huang C.-C. and Chen W.-H., *Polymer*, 47, **2006**, 2337.

Liaw D.-J., Liaw B.-Y., Hus P.-N. and Hwang C.-Y., *Chem. Mater.*, 13, **2001**, 1811.

Lin C. H., Cai S. X., Leu T. S., Hwang T. Y. and Lee H. H., *J. Polym. Sci. Part A: Polym. Chem.*, 44, **2006**, 3454.

Lin W.-H., Vora R. H. and Chung T.-S., *J. Polym. Sci., Part B: Polym. Phys.*, 38, **2000**, 2703.

Liou G.-S., *J. Polym. Sci. Part A: Polym. Chem.*, 36, **1998**, 1937.

Liu B., Hu W., Matsumoto T., Jiang Z. and Ando S., *J. Polym. Sci. Part A: Polym. Chem.*, 43, **2005**, 3018.

Liu B., Robertson G. P., Kim D. S., Guiver M. D., Hu W. and Jiang Z., *Macromolecules*, 40, **2007**, 1934.

Liu S. L., Wang R., Liu Y., Chng M. L. and Chung T. S., *Polymer*, 42, **2001**, 8847.

Liu Y., Pan C., Ding M. and Xu J., *Polym. Int*., 48, **1999**, 832.

Lobato J., Canizares P., Rodrigo M. A., Linares J. J. and Aguilar J. A., *J. Membr. Sci*., 306, **2007**, 47.

Lundberg D. and Phillips R. R., *J. Polym. Sci.: Polym. Phys. Ed.*, 20, **1982**, 1143.

Lv J., Wang K. Y. and Chung T. S., *J. Membr. Sci.*, 310, **2008**, 557.

Ma Y., *Ph. D. Dissertation*, Case Western Reserve University, USA, **2004b**.

Ma Y., Wainright J., Litt M. and Savinella R., *J. Electrochemical Soc.*, 151 (1)**, 2004**, A8.

MacFarlane D. R., Pringle J. M., Johansson K. M., Forsyth S. A. and Forsyth M., *Chem. Commun.*, **2006**, 1905.

Mackenize G. F., *U. S. Pat*., 2861995, **1958**.

Mader J., Xiao L., Schmidt T. J. and Benicewicz B. C., *Adv. Polym. Sci.*, 216, **2008**, 63.

March J., "*Advnced Organic Chemistry: Reactions, Mechanisms and Structure*", 3rd edn., Wiley Eastern Ltd., New Delhi, **1992**.

Marestin C., Gebel G., Diat O. and Mercier R., *Adv. Polym. Sci.*, 216, **2008**, 185.

Mathew J. S., *Ph. D. Dissertation*, University of Pune, Pune, India, **2001**.

Matsumoto K. and Xu P., *J. Appl. Polym. Sci.*, 47, **1993c,** 1951.

Matsumoto K. and Xu P., *J. Membr. Sci.*, 81, **1993b**, 23.

Matsumoto K., Xu P. and Nishikimi T., *J. Membr. Sci.*, 81, **1993a**, 15.

Matsuyama H., Terada A., Nakagawara T., Kitamura Y. and Teramoto M., *J. Membr. Sci.*, 163, **1999**, 221.

Matsuyama H., Teramoto M. and Iwai K., *J. Membr. Sci.*, 93, **1994**, 237.

Matsuyama H., Teramoto M., Sakakura H. and Iwai K., *J. Membr. Sci.*, 117, **1996**, 251.

Mauritz K. A. and Moore R. B., *Chem. Rev.*, 104, **2004**, 4535.

McBride R.B. and McKinley D.L., *Chem. Eng. Prog.*, 61, **1965**, 81.

McHattie J. S., Koros W. J. and Paul D.R., *Polymer*, 32, **1991**, 840.

McHattie J. S., Koros W. J. and Paul D.R., *Polymer*, 33, **1992**, 1701.

Mi Y., Stern S. A. and Trohalaki S., *J. Membr. Sci.*, 77, **1993**, 41.

Mikroyannidis J. A. and Tsivgoulis G. M., *J. Polym. Sci., Part A: Polym. Chem.*, 37, **1999a**, 3646.

Mikroyannidis J. A., *Polymer*, 40, **1999b**, 3107.

Mitchell G. R. and Windle A. H., *Polymer*, 25, **1984**, 906.

Mittal K.L., *Polyimides and Other High Temperature Polymers: Synthesis, Characterization and Applications*, Vol. 1, VSP publication, Netherlands, **2001**.

Miyatake K., Zhou H., Matsuo T., Uchida H. and Watanabe M.., *Chem. Commun.*, **2003**, 368.

Miyatake K., Zhou H., Matsuo T., Uchida H. and Watanabe M., *Macromolecules*, 37, **2004,** 4961.

Morikawa A., Furukawa T. and Moriyama Y., *High Perform. Polym.*, 18, **2006**, 593.

Morikawa A., Furukawa T. and Moriyama Y., *Polym. J*., 37, 10, **2005**, 759.

Morton R. C., Mangroo D. and Gerber G. E., *Can. J. Chem.*, 66, **1988**, 1701.

Muhlbauer H. G., *U. S. Pat*., 3394186, **1968**.

Muruganandam N., Koros W. J. and Paul D. R., *J. Polym. Sci., Part B: Polym. Phys.*, 25, **1987**, 1999.

Musto P., Karasz F. E. and MacKnight W. J., *Polymer*, 30, **1989,** 1012.

Musto P., Karasz F. E. and MacKnight W. J., *Polymer*, 34 (14), **1993,** 2934.

Nakamoto H., Noda A., Hayamizu K., Hayashi S., Hamaguchi H. and Watanabe H., *J. Phys. Chem. C.*, 111 (3), **2007**, 1541.

Nakashima T., *Topics in Current Chemistry*, 139, **1987**, 57.

Nakayama T., Watari T., Tanaka K., Kita H. and Okamoto K., *Trans. Mater. Res. Soc. Jpn.*, 28, **2003**, 777.

Nelson A., Guerra G., Williams D. J., Karasz F. E., MacKnight W. J., *J. Appl. Polym. Sci.*, 36, **1988**, 243.

Niedrach L. W., Fuel cell, *U.S. Patent 3,134,697*, General Electric Corporation, **1964**.

Noda A., Susan A. B. H., Kudo K., Mitsushima S., Hayamizu K. and Watanabe M., *J. Phys. Chem. B.*, 107, **2003**, 4024.

Nunes S.P. and Peinemann K.V., "*Membrane Technology in Chemical Industry*", Wiley-VCH, **2001**.

Okamoto K. I., Yasugi N., Kawabata T., Tanaka K. and Kita H., *Chem. Lett.*, **1996**, 613.

Orwoll R. A., Clair T. L. St., Dobbs K. D., *J. Polym. Sci., Polym. Phys. Ed*., 19, **1981**, 1385.

Peinemann K -V. and Nunes S. P., *Membranes for Energy Conversion, Vol. 2, WILEY-VCH Verlag GmbH & Co. KGaA*, Weinheim, **2008**.

Pellegrino J. and Kang Y. S., *J. Membr. Sci.*, 99, **1995**, 163.

Pellegrino J. J., Nassimbene R. and Noble R. D., *Gas Sep. and Purf.*, 2, **1988**,126.

Penner S. S., *Energy*, 31, **2006**, 33.

Perry M. L. and Fuller T. F., *J. Electrochem. Soc.,* 149,7, **2002**, S59.

Pine S. H., *Organic Chemistry*, 5th Ed., McGraw-Hill Book Company, New York, United States, **1987**.

Pinnau I., He Z. and Morisato A., *J. Membr. Sci.*, 241, **2004**, 363.

Pixton M. R. and Paul D. R., *Macromolecules*, 28, **1995**, 8277.

Potrekar R. A., Kulkarni M. P., Kulkarni R. A. and Vernekar S. P., *J. Polym. Sci., Part A: Polym. Chem.*, 47, **2009b**, 2289.

Potrekar R. A., *Ph. D. Dissertation*, University of Pune, Pune, India, **2009a**.

Pu H., Liu Q., Qiao L. and Yang Z., *Polym. Eng. Sci.*, 45**,** 10, **2005**, 1395.

Qiao K. and Yokoyama C., *Chem. Lett.*, 33, 4, **2004**, 472.

Qiu Z. and Zhang S., *Polymer*, 46, **2005**, 1693.

Qiu Z., Chen G., Zhang Q. and Zhang S., *Eur. Polym. J.*, 43, **2007**, 194.

Qiu Z., Wang J., Zhang Q., Zhang S., Ding M., Gao L., *Polymer*, 47, **2006**, 8444.

Quinn R. and Laciak D. V., *J. Membr. Sci.*, 131, **1997a**, 49.

Quinn R., Laciak D. V. and Pez Z. P., *J. Membr. Sci.*, 104, **1995**, 139.

Quinn R., Laciak D. V. and Pez Z. P., *J. Membr. Sci.*, 131, **1997b**, 61.

Radmard B. and Dadmun M. D., *Polymer*, 42, **2001**, 1591.

Rancourt J. D. and Taylor L .T., *Macromolecules*, 20, **1987**,790.

Ren L., Fu W., Luo Y., Lu H., Jia D., Shen J., Pang B. and Ko T. M., *J. Appl. Polym. Sci.*, 91, **2004**, 2295.

Reynolds G. A., *J. Am. Chem. Soc*., 73, **1951**, 4996.

Rikukawa M. and Sanui K., *Prog. Polym. Sci.*, 25, **2000**, 1463.

Robeson L. M., Burgoyne W. F., Langsam M., Savoca A. C. and Tien C. F., *Polymer*, 35, **1994,** 4970.

Robeson L. M., *J. Membr. Sci.*, 320, **2008**, 390.

Robeson L. M., *J. Membr. Sci.*, 62, **1991,** 165.

Robeson L.M. and Matzner M., *U. S. Pat*., 4380598, **1983**.

Rodgers M., Sang Y. and Holdcroft S., *Eur. Polym. J.*, 42, **2006**, 1075.

Roziere J. and Jones D. J., *Annu. Rev. Mater. Res.*, 33, **2003**, 503.

Rusanov A. L., *Adv. Polym. Sci.,* 111, **1994**, 115.

Rusanov A. L., Likhatchev D., Kostoglodov P. V., Müllen K. and Klapper M ., *Adv. Polym. Sci.,* 179, **2005**, 83.

Rylander P. N., "*Catalytic hydrogenation over Platinum Metals*", Academic Press, New York, **1967**, 168.

Saegusa Y., Horikiri M. and Nakurmura S., *Macrom. Chem. and Phys.*, 198 (2), **1997**, 619.

Sartori G. and Maggi R., *Advances in Friedal-Crafts Acylation Reactions: Catalytic and Green Processes*, **2009**, CRC press, Taylor and Francis Group, Boca Raton, FL.

Savard O., Peckham T. J., Yang Y. and Holdcroft S., *Polymer*, 49, **2008**, 4949.

Schmidhauser J. C. and Longley K. L., *J. Appl. Polym. Sci.*, 39, **1990,** 2083.

Scholes C.A., Kentish S.E. and Stevens G.W., *Recent Patents on Chem. Eng.*, 1, **2008**, 52.

Scriven Eric F. V. and Turnbull K., *Chem. Rev.*, 88, 2, **1988**, 297.

Sek D., Pijet P. and Wanic A., *Polymer*, 33 (1), **1992,** 190.

Sek D., Wanic A. and Schab-Balcerzak E., *J. Polym. Sci. Part A: Polym. Chem.*, 33, **1995**, 547.

Shao L., Chung T.-S., Goh S. H. and Pramoda K. P., *J. Membr. Sci.*, 267, **2005**, 78.

Shin C. K., Maier G. and Scherer G. G., *J. Membr. Sci*., 245, **2004**, 163.

Shingate R. D., *Ph D. Dissertation*, University of Pune, Pune, India, **2006**.

Silverstein R. M. and Webter F. X., *Spectroscopic Identification of Organic Compounds*, 6th edition, Wiley India Pvt. Ltd., New Delhi-110002, **2006**.

Sivanandaiah K. M., Gurusiddappa S. and Gowda D. C., *Indian J. Chem*., 24B, 11, **1985**, 1185.

Souzy R. and Ameduri B., *Prog. Polym. Sci.*, 30, **2005**, 644.

Spiliopoulos I. K. and Mikroyannidis J. A., *Polymer*, 38 (11), **1997**, 2733.

Spiliopoulos I. K., Mikroyannidis J. A. and Tsivgoulis G. M., *Macromolecules*, 31, **1998**, 522.

Sroog C. E., Endrey A. L., Abramo S. V., Berr C. E., Edwards W. M. and Olivier K. L., *J. Polym. Sci., Part A*, 3, **1965**, 1373.

Sroog C. E., *Prog. Polym. Sci.*, 16, **1991**, 561.

St. Clair T. L., St. Clair A. K., Smith E. N., *Polym. Prep.*,17, **1976**, 359.

Stern S. A., Vaidyanathan R. and Pratt J. R., *J. Membr. Sci.*, 49, **1990**, 1.

Stern S. A., Liu Y., Feld W. A., *J. Polym. Sci., Part B: Polym. Phy.*, 31, **1993**, 939.

Stern S. A., Mi Y., Yamamoto H. and Clair A. K. St., *J. Polym. Sci., Part B: Polym. Phy.*, 27, **1989**, 1887.

Subbaraman R., Ghassemi H. and Zawodzinski Jr., T. A., *J. Am. Chem. Soc*. 129, **2007**, 2238.

Takahashi T., Tanase S., Yamamoto O. and Yamauchi S., *J. Solid State Chemistry*, 17, **1976**, 353.

Takekoshi T., *Adv. Polym. Sci.*, 94, **1990**, 1.

Tamai S., Kamada J., Goto K. and Yamaguchi A., *High Perform. Polym.*, 13, **2001**, 173.

Tamai S., Yamaguchi A. and Ohta M., *Polymer*, 37 (16), **1996**, 3683.

Tanaka K., Kita H., Okano M. and Okamoto K.-I., *Polymer*, 33 (3), **1992a**, 585.

Tanaka K., Okano M., Toshino H., Kita H. and Okamoto K.-I., *J. Polym. Sci., Part B: Polym. Phys.*, 30, **1992b**, 907.

Tanaka K., Osada Y., Kita H. and Okamoto K.-I., *J. Polym. Sci., Part B: Polym. Phy.*, 33, **1995**, 1907.

Tang J., Tang H., Sun W., Radosz M. and Shen Y., *J. Polym. Sci. Part A: Polym. Chem.*, 43, **2005**, 5477.

Tiwari P., Kumar R., Maulik P. R. and Misra A. K., *Eur. J. Org. Chem.*, **2005**, 4265.

Tseng P., Lee J. and Friley P., *Energy*, 30, **2005**, 2703.

Tsuda Y., Kawauchi T., Hiyoshi N. and Mataka S., *Polym. J.*, 32 (7), **2000**, 594.

Tsujita Y., *Prog. Polym. Sci*., 28, **2003**, 1337.

Ueda M., Nakamura K., Tanaka K., Kita H. and Okamoto K., *Sensors and Actuators B,* 127, **2007,** 463.

Ueda M., Toyato H., Ouchi T., Sugiyama J.-I, Yonetake K., Masuko T. and Teramoto T. *J. Polym. Sci., Part A: Polym. Chem.*, 31, **1993**, 853.

Van Krevelen D. W., *Properties of Polymers*, Elsevier Science B. V.: Amsterdam, The Netherlands, **1997**.

Volksen W., *Adv. Polym. Sci.*, 117, **1994**, 111.

Vygodskii Ya. S., Spirina T. N., Nechayev P. P., Chudina L. I., Zaikov G. Ye., Korshak V. V., and Vinogradova S. V., *Polym. Sci. USSR*, 19(7), **1977**, 1738.

Wainright J. S., Wang J., Weng D., Savinell R. F. and Litt M., *J. Electrochem Soc.*, 142, **1995**, L121.

Wang D-A., *Adv. Polym. Sci.*, 209, **2007a**, 179.

Wang F., Chen T. and Xu J., *Macromol. Chem. Phys.*, 199, **1998,** 1421.

Wang J. T., Savinell R. F., Wainright J., Litt M. and Yu H., *Electrochimica Acta.*, 41, 2, **1996**, 193.

Wang P., Liu B. and Zheng S., *J. Macromol. Sci., Part B: Physics*, 47, **2008**, 800.

Wang Y., Goh S. H. and Chung T. S., *Polymer*, 48, **2007b**, 2901.

Wang Y.-C., Huang S.-H., Hu C.-C., Li C.-L., Lee K.-R., Liaw D.-J. and Lai J.-Y., *J. Membr. Sci.*, 248, **2005**, 15.

Wenzel M., Ballauff M. and Wegner G., *Makromol. Chem.*, 188, **1987**, 2865.

Wilks B. R., Won J. C., Ludovice P. J., Rezac M. E., Meakin P. and Hill A. J., *J. Polym. Sci., Part B: Polym. Phy.*, 44, **2006**, 215.

Williams R. A., *U. S. Pat.*, 3398195, **1968**.

Wind J. D., Staudt-Bickel C., Paul D. R. and Koros W. J., *Macromolecules*, 36, **2003**, 1882.

Wrasidlo W., *Macromolecules*, 4, **1971**, 642.

Wright S. E., *Renew. Energy*, 29, **2004**, 179.

Wu S., Qiu Z., Zhang S., Yang X., Yang F. and Li Z., *Polymer*, 47, **2006**, 6993.

Wycisk R., Lee J. K. and Pintauro P. N., *J. Electrochem. Soc.*, 152 (5), **2005,** A892.

Xiao S., Huang Robert Y. M. and Feng X., *Polymer*, 48, **2007**, 5355.

Xiao Y., Low B. T., Hosseini S. S., Chung T. S. and Paul D. R., *Prog. Polym. Sci*., 34, **2009**, 561.

Xing D. and Kerres J., *J. New Mat. Electro. Syst.*, 9, **2006**, 51.

Xing O. and Savadogo O., *Electrochem. Comm.*, 2, **2000**, 697.

Xu J. W., Chng M. L., Chung T. S., He C. B. and Wang R., *Polymer,* 44, **2003**, 4715.

Yamaguchi T., Boetje L. M., Koval C. A., Noble R. D. and Bowman C. N., *Ind. Eng. Chem. Res.*, 34, **1995**, 4071.

Yamamoto H., Mi Y., Stern S. A. and Clair A. K. St., *J. Polym. Sci., Part B*: *Polym. Phy.*, 28, **1990**, 2291.

Yang C.-P. and Chen W.-T., *Macromolecules*, 26, **1993**, 4865.

Yang C.-P. and Hsiao F.-Z., *J. Polym. Sci., Part A: Polym. Chem.*, 42, **2004a**, 2272.

Yang C.-P. and Lin J.-H., *J. Polym. Sci., Part A: Polym. Chem.*, 32, **1994**, 423.

Yang C.-P., Hsiao F.-Z. and Hsu M-F., *J. Polym. Sci., Part A: Polym. Chem.*, 40, **2002**, 524.

Yang C.-P., Su Y.-Y. and Wu K.-L., *J. Polym. Sci., Part A: Polym. Chem.*, 42, **2004b**, 424.

Yang S.-J., Lee C., Jang W., Kwon J., Sundar S. and Han H., *J. Polym. Sci. Part B: Polym. Phys.*, 42, **2004c**, 4293.

Yasuda T., Miyatake K., Hirai M., Nanasawa M. and Watanabe M., *J. Poly. Sci.: Part A: Poly. Chem.*, 43, **2005**, 4439.

Yin Y., Chen S., Guo X., Fang J., Tanaka K., Kita H. and Okamoto K., *High Perform. Polym.*, 18, **2006b**, 617.

Yin Y., Fang J., Watari T., Tanaka K., Kita H. and Okamoto K. I., *J. Mater. Chem.*, 14, **2004**, 1062.

Yin Y., Yamada O., Tanaka K. and Okamoto K.-I., *Polym. J.*, 38 (3), **2006a**, 197.

Yu J.-W. and Sung C. S. P., *Macromolecules*, 30, **1997**, 1845

Zaidi S. M. J., Chen S. F., Mikhailenko S. D. and Kaliaguine S., *J. New Mater. Electrochem. Syst.*, 3, **2000**, 27.

Zhang H., Li X., Zhao C., Fu T., Shi Y. and Na H., *J. Membr. Sci.*, 308, **2008**, 66.

Zhang Q., Chen G. and Zhang S., *Polymer*, 48, **2007**, 2250.

Zhang Y., Wang Z., Wang S. C., *Desalination*, 145, **2002**, 385.

Zhao C, Wang Z., Bi D., Lin H., Shao K., Fu T., Zhong S. and Na H., *Polymer*, 48, **2007**, 3090.

Zhou Z., Li S., Zhang Y., Liu M. and Li W., *J. Am. Chem. Soc.*, 127, **2005**, 10824.

Zolandz L. R. and Fleming G. K., *Membrane Handbook*, Ho W.S.W., Sirkar K.K. (eds.) van Nostrand Reinhold, **1992**.

Zou J. and Winston Ho W. S., *J. Membr. Sci.*, 286, **2006**, 310.

Zubkov V. A., Koton M. M., Kudryavtsev V. V. and Svetlichnyi V. M., *J. Organic Chem. of the USSR*, 17 (8), **1981**, 1501.

List of Publications

- **S. S. Kothawade**, M. P. Kulkarni, U. K. Kharul, A.S. Patil, S. P. Vernekar, "Synthesis, Characterization and Gas Permeability of Aromatic Polyimides Containing Pendant Phenoxy Group" *J. Appl. Polym. Sci.*, 108, **2008**, 3881.
- **S. S. Kothawade**, U. K. Kharul, K. Vijayamohanan, S. P. Vernekar, "Novel polyimides containing pendant sulfophenoxy group as membrane material for polymer electrolyte fuel cell (PEFC) and gas permeation" *to be communicated.*
- **S. S. Kothawade**, S. P. Vernekar, U. K. Kharul, "Structure–gas permeability co-relationship in aromatic polyimides having alkyl substituted pendant phenoxy group" *to be communicated.*
- **S. S. Kothawade**, U. K. Kharul, K. Vijayamohanan, S. P. Vernekar, "Blend membranes based on side-chain-type sulfonated polyimide and polybenzimidazole (PBI) for polymer electrolyte fuel cell (PEFC) and gas permeation" *to be communicated.*
- **S. S. Kothawade**, N. Ramgir, T. Gopakumar, U. K. Kharul, K. Vijayamohanan, S. P. Vernekar, "An improved surface functionalized polymer electrolyte membrane for planar fuel cells" *to be communicated*.

Presentations in conferences

- **S. S. Kothawade**, N. S. Ramgir, M. P. Kulkarni, R. A. Potrekar, S. P. Vernekar, K. Vijayamohanan, A Paper titled *"Comparison of surface functionalized HDPE, block Copolymers of Styrene- Propylene-Butadiene and PVDF polymer Membranes for Planar Fuel Cell Applications"* presented in National Seminar on Fuel-to-Fuel Cells, Indian Institute of Chemical Technology, December 4-5, **2003**, Hyderabad, Andhra Pradesh, India.
- **S. S. Kothawade**, N. S. Ramgir, S. P. Vernekar, K. Vijayamohanan, A Paper titled *"Temperature dependent impedance studies of Nafion-117 membrane for PEMFC applications"* presented in National seminar on Membrane Science and Technology: Challenges and Opportunities, February 12-13, **2004**, Regional Research Laboratory, Jorhat, Assam, India.
- **S. S. Kothawade**, N. Ramgir, B. Kakade, A. B. Gaikwad, S.P.Vernekar, I. S. Mulla, K. Vijayamohanan, A poster titled "*Temperature Dependent Impedance Studies of Nafion-117 and Sulfonated Polyimide Membranes for PEMFC Applications"* presented in National Seminar on Fuel cells-Materials, Systems and Accessories Sept. 25-26, **2003**, Ambernath (MS), India.
- **S. S. Kothawade**, M. P. Kulkarni, U. K. Kharul, A.S. Patil, S. P. Vernekar, A poster titled *"Synthesis, Characterization and Gas Permeability of Aromatic Polyimides Containing Pendant Phenoxy Group"* presented in 'MACRO 2006' December 17-20, **2006**, held at National Chemical Laboratory, Pune, India.